

SYNTHESIS, CHARACTERIZATION AND APPLICATION OF BIOPOLYMERIC HYDROGELS IN DRUG DELIVERY

**A Thesis Submitted
for the Degree of**

DOCTOR OF PHILOSOPHY

by

**Priyanka Meena
(2K19/PHDAC/02)**

Under the supervision of

**Supervisor
Prof. Sudhir G. Warkar
Professor
Department of Applied Chemistry
Delhi Technological University**

**Co-supervisor
Dr. Poonam Singh
Assistant Professor
Department of Applied Chemistry
Delhi Technological University**



**To the
Department of Applied Chemistry**

**DELHI TECHNOLOGICAL UNIVERSITY
(Formerly Delhi College of Engineering)
Shahbad Daulatpur, Main Bawana Road, Delhi-110042, India**

December, 2024

ACKNOWLEDGEMENTS

I would like to extend my deepest gratitude to all the individuals who have supported me throughout my PhD journey. First and foremost, I am grateful to my supervisor, **Prof. Sudhir G. Warkar** and co-supervisor, **Dr. Poonam Singh**, for their exceptional guidance, endless patience, and unwavering support. I am genuinely grateful for the time and effort you have dedicated to this research.

I am grateful to **Prof. Prateek Sharma**, Honourable Vice-Chancellor, Delhi Technological University, and **Prof. Anil Kumar**, Head, Department of Applied Chemistry, DTU, for providing the facilities to conduct this research. I would also like to express my gratitude to all faculty members of the Department of Applied Chemistry, DTU, for their valuable support.

I am also deeply appreciative to my SRC and DRC committee members, whose expertise and thoughtful suggestions greatly enhanced the quality of this work. I also thank all the technical and non-technical staff of the Department of Chemistry for their endless help whenever required.

I sincerely thank the Council of Scientific and Industrial Research (CSIR) for providing me with financial support to carry out this research.

I would like to thank my friends and fellow researchers at DTU, especially **Ms. Pooja**, for her support and encouragement during my PhD journey.

I express my heartfelt admiration for my parents, **Mr. Ramesh Chandra Meena** and **Mrs. Urmila Meena**, my brother-in-law, **Mr. Jugal** and my siblings, **Mrs. Ritu**, **Mr. Rupesh**, **Ms. Neha** for their support and blessing throughout my PhD journey. Above all, I am grateful to Almighty God for providing me with wisdom and strength to embrace and overcome the challenges in my life.

Priyanka Meena



DELHI TECHNOLOGICAL UNIVERSITY

(Formerly Delhi College of Engineering)

Shahbad Daultapur, Main Bawana Road, Delhi-42

CANDIDATE'S DECLARATION

I **Priyanka Meena** hereby certify that the work which is being presented in the thesis entitled “**Synthesis, Characterization and Application of Biopolymeric Hydrogels in Drug Delivery**” in partial fulfillment of the requirement for the award of the **Degree of Doctor of Philosophy**, submitted in the Department of Applied Chemistry, Delhi Technological University is an authentic record of my own work carried out during the period from 19/07/2019 to 8/11/2024 under the supervision of **Prof. Sudhir G. Warkar**, Professor, Department of Applied Chemistry, DTU and co-supervision of **Dr. Poonam Singh**, Assistant Professor, Department of Applied Chemistry, DTU.

The matter presented in the thesis has not been submitted by me for the award of any other degree of this or any other Institute.

Candidate's Signature

This is to certify that the student has incorporated all the corrections suggested by the examiners in the thesis and the statement made by the candidate is correct to the best of our knowledge.

Signature of Supervisor (s)

Signature of External Examiner



DELHI TECHNOLOGICAL UNIVERSITY

(Formerly Delhi College of Engineering)

Shahbad Daultpur, Main Bawana Road, Delhi-42

CERTIFICATE BY THE SUPERVISOR(s)

Certified that **Priyanka Meena (2K19/PHDAC/02)** has carried out her search work presented in this thesis entitled “**Synthesis, Characterization and Application of Biopolymeric Hydrogels in Drug Delivery**” for the award of **Doctor of Philosophy** from Department of Applied Chemistry, Delhi Technological University, Delhi, under our supervision. The thesis embodies the results of original work, and studies are carried out by the student herself, and the contents of the thesis do not form the basis for the award of any other degree to the candidate or to anybody else from this or any other University/Institution.

Prof. Sudhir G. Warkar

Supervisor

Professor

Department of Applied Chemistry

Delhi Technological University

Dr. Poonam Singh

Co-supervisor

Assistant Professor

Department of Applied Chemistry

Delhi Technological University

Date:

ABSTRACT

The increasing demand for targeted and controlled drug delivery systems has led to significant interest in the development of biopolymer-based hydrogels, which offer a versatile and biocompatible platform for enhancing therapeutic efficacy and minimizing side effects. This thesis focused on the synthesis and characterization of biopolymer-based hydrogels, with emphasis on their drug delivery applications. Different characterization techniques, i.e., Fourier Transform- Infrared spectroscopy (FTIR), Powder X-ray Diffraction (PXRD) and Scanning electron microscopy (SEM), were used for the detailed characterization of all synthesized hydrogels. The carboxymethyl tamarind kernel gum/polyvinylpyrrolidone/polyacrylamide (CMTKG/PVP/PAM) hydrogel was synthesized via free radical mechanism and its potential for diclofenac sodium (DS) release was studied. The presence of PVP was found to enhance the drug entrapment efficiency (65.54%) of the CMTKG/PVP/PAM hydrogel. The synthesized DS-loaded CMTKG/PVP/PAM hydrogel demonstrated the targeted delivery of DS in the colon (pH 7.4). The research then proceeds with the development of another novel hydrogel with xanthan gum (XG) as a biopolymer, focusing on the delivery of an ibuprofen drug. The addition of PVP enhances the hydrogel properties, such as gel fraction (91.88%), swelling (1100%), porosity (78.35), drug loading (21.38%), and drug release (80.2%). Moreover, the hydrogels based on β -cyclodextrin (β -CD), CMTKG and PAM were developed using polyethylene glycol diacrylate as a cross-linker. The synthesized β -CD/PAM/CMTKG hydrogel showed controlled and prolonged indomethacin release (62.49 %) upon the incorporation of β -CD into the polymeric matrix. The thesis further explored the hydrogel microspheres based on tragacanth gum, β -CD and sodium alginate (TG/ β -CD/SA) and studied its potential in the release of aspirin. The physical crosslinking technique, i.e. ionic gelation, has been employed for the fabrication of the TG/ β -CD/SA hydrogel microsphere. The resulting hydrogel microsphere demonstrated controlled drug release (59.9%), complete degradability (100%) and non-toxic (87.9% cell viability) behavior. Moreover, the structural integrity of TG/ β -CD/SA hydrogel was confirmed

by FTIR and PXRD analysis. Lastly, the research focused on the development of a nanocomposite hydrogel microsphere for curcumin delivery. The synthesized CMTKG/SA/copper oxide nanocomposite hydrogel revealed a slow and prolonged release profile (52.3%) for curcumin, due to addition of copper oxide nanoparticle into the hydrogel matrix. Overall, this thesis highlights the synthesis, characterization and potential of biopolymer-based hydrogels in hydrophobic drug delivery. Their non-toxic and pH-sensitive properties demonstrate their ability to provide a biocompatible and targeted drug delivery system, effectively enhancing the therapeutic efficacy of hydrophobic drugs.

TABLE OF CONTENTS

ACKNOWLEDGEMENTS	ii
CANDIDATE’S DECLARATION	iii
CERTIFICATE BY THE SUPERVISOR(s)	iv
ABSTRACT	v
LIST OF FIGURES	xiv
LIST OF TABLES	xviii
LIST OF SYMBOLS AND ABBREVIATIONS	xix
CHAPTER 1	1
INTRODUCTION AND LITERATURE SURVEY	1
1.1 Introduction	1
1.1.1 Smart or Intelligent Hydrogel	2
1.1.2 Swelling mechanism	5
1.1.3 Applications of Hydrogel.....	6
1.1.4 Drug Release Mechanism	7
1.1.5. Kinetic Modelling of Drug Release	9
1.2 Literature Survey.....	12
1.2.1 Biopolymers-based hydrogels.....	12
1.2.2 Different routes of drug administration using biopolymer-based hydrogel	21
1.2.3 Biopolymer-based hydrogels for hydrophobic drug delivery	28
1.3 Conclusion and Research Gap.....	31
1.4 Research Objectives	32
1.5 REFERENCES.....	33
CHAPTER 2	49
FABRICATION AND CHARACTERIZATION OF CARBOXYMETHYL TAMARIND KERNEL GUM-BASED HYDROGEL FOR THE RELEASE OF DICLOFENAC SODIUM	49
2.1 Introduction	49
2.2 Experimental Section	52

2.2.1 Materials	52
2.2.2 Synthesis of CMTKG/PVP/PAM hydrogel and DS-loaded hydrogels	53
2.2.3 Characterization	55
2.2.4 Swelling studies	55
2.2.5 Sol-Gel analysis	55
2.2.6 Porosity	56
2.2.7 Drug Loading and Drug Entrapment Efficiency.....	56
2.2.8 In vitro DS release study.....	57
2.2.9 Release kinetics studies	58
2.2.10 Cytotoxicity	58
2.2.11 Degradation.....	59
2.3 Results and Discussions	59
2.3.1 Mechanistic pathway followed for the formation of DS-loaded CMTKG/PVP/PAM hydrogel.....	59
2.3.2 Characterization	61
2.3.3 Swelling Studies	64
2.3.4 Sol-Gel Analysis	67
2.3.5 Porosity	68
2.3.6 Drug Loading and Entrapment Efficiency.....	69
2.3.7 In vitro DS release study.....	70
2.3.8 Release kinetics studies	71
2.3.9 Cytotoxicity	73
2.3.10 Degradation.....	75
2.4 Conclusion.....	75
2.5 REFERENCES.....	76
CHAPTER 3	83
DEVELOPMENT AND ASSESSMENT OF XANTHAN GUM-BASED HYDROGEL AS A POTENTIAL CARRIER FOR A HYDROPHOBIC DRUG IBUPROFEN	83
3.1 Introduction	83
3.2 Experimental Section	85
3.2.1 Materials	85

3.2.3 Characterization	87
3.2.4 Swelling studies	87
3.2.5 Sol-Gel analysis	88
3.2.6 Porosity Measurement	88
3.2.7 Ibuprofen Loading and Entrapment Efficiency	89
3.2.8 In vitro ibuprofen release studies	90
3.2.9 Kinetic Modelling	90
3.2.10 Cytotoxicity	91
3.2.11 Degradation.....	91
3.3 Result and Discussion	92
3.3.1 Mechanistic pathway of ibuprofen-loaded XG/PAM/PVP hydrogel formation.....	92
3.3.2 Characterization	93
3.3.3 Swelling studies	96
3.3.4 Sol-Gel analysis	100
3.3.5 Porosity Measurement	101
3.3.6 Ibuprofen Loading and Entrapment Efficiency	102
3.3.7 In vitro ibuprofen release studies.....	103
3.3.8 Kinetic Modelling.....	104
3.3.9 Cytotoxicity	106
3.3.10 Degradation.....	107
3.4 Conclusion.....	108
3.5 REFERENCES.....	109
CHAPTER 4	115
SYNTHESIS AND CHARACTERIZATION OF POLYETHYLENE GLYCOL DIACRYLATE-CROSSLINKED β-CYCLODEXTRIN-BASED HYDROGEL FOR EFFICIENT DELIVERY OF HYDROPHOBIC DRUG INDOMETHACIN	115
4.1 Introduction	115
4.2 Experimental Section	117
4.2.1 Materials	117
4.2.2 Synthesis of PAM/CMTKG and β -CD/PAM/CMTKG hydrogels.....	118

4.2.3 Characterization	119
4.2.4 Swelling analysis	119
4.2.5 Sol-Gel analysis	120
4.2.6 Porosity	120
4.2.7 Indomethacin Loading and Entrapment Efficiency	121
4.2.8 In vitro indomethacin release study	121
4.2.9 Kinetic Modelling	122
4.2.10 Cytotoxicity	122
4.2.11 Degradation.....	123
4.3 Result and Discussion	123
4.3.1 Mechanism of β -CD/PAM/CMTKG and indomethacin-loaded β -CD/PAM/CMTKG hydrogel synthesis	123
4.3.2 Characterization	125
4.3.3 Swelling studies	128
4.3.4 Sol-Gel Analysis	129
4.3.5 Porosity	130
4.3.6 Indomethacin Loading and Entrapment Efficiency	130
4.3.7 In vitro indomethacin release analysis.....	131
4.3.8 Kinetic Modelling	132
4.3.9 Cytotoxicity	134
4.3.10 Degradation.....	135
4.4 Conclusion.....	136
4.5 REFERENCES.....	137
CHAPTER 5	141
FABRICATION AND ASSESSMENT OF CALCIUM-CROSSLINKED TRAGACANTH GUM-BASED HYDROGEL MICROSPHERE FOR ASPIRIN RELEASE	141
5.1 Introduction	141
5.2 Experimental Section	144
5.2.1 Materials	144
5.2.2 Synthesis of TG/SA and TG/ β -CD/SA hydrogels	144
5.2.3 Characterization	145

5.2.4 Swelling studies	146
5.2.5 Sol-Gel analysis	146
5.2.6 Porosity	147
5.2.7 Aspirin Loading and Entrapment Efficiency	147
5.2.8 In vitro aspirin release studies	148
5.2.9 Kinetic Modelling	149
5.2.10 Cytotoxicity Analysis	149
5.2.11 Degradation studies.....	149
5.3 Result and Discussion	150
5.3.1 Mechanism of TG/ β -CD/SA microspheres and aspirin-loaded TG/ β - CD/SA hydrogel microspheres formation	150
5.3.2 Characterization	151
5.3.3 Swelling studies	155
5.3.4 Sol-Gel analysis	158
5.3.5 Porosity	159
5.3.6 Aspirin Loading and Entrapment Efficiency	159
5.3.7 In vitro aspirin release study	160
5.3.8 Kinetic Modelling	162
5.3.9 Cytotoxicity Analysis	164
5.3.10 Degradation studies.....	165
5.4 Conclusion.....	166
5.5 REFERENCES.....	167
CHAPTER 6	175
SYNTHESIS AND CHARACTERIZATION OF COPPER OXIDE NANOPARTICLE-INCORPORATED HYDROGEL MICROSPHERES PREPARED VIA IONOTROPIC GELATION TECHNIQUE FOR DELIVERY OF CURCUMIN	175
6.1 Introduction	175
6.2 Experimental Section	177
6.2.1 Materials	177
6.2.2 Synthesis of CuO Nps.....	177
6.2.3 Synthesis of CMTKG/SA and CMTKG/SA/CuO nanocomposite hydrogel microspheres	178

6.2.4 Characterization	179
6.2.5 Swelling studies	180
6.2.6 Sol-Gel analysis	180
6.2.7 Porosity	181
6.2.8 Curcumin Loading and Entrapment Efficiency	181
6.2.9 In vitro curcumin release analysis	182
6.2.10 Kinetic Modelling	183
6.2.11 Anti-bacterial Assay	183
6.2.12 Cytotoxicity	184
6.2.13 Degradation studies.....	184
6.3 Result and Discussion	185
6.3.1 Mechanism for the synthesis of CMTKG/SA/CuO and curcumin-loaded CMTKG/SA/CuO nanocomposite hydrogel microsphere	185
6.3.2 Characterization	186
6.3.3 Swelling studies	192
6.3.4 Sol-Gel analysis	193
6.3.5 Porosity	194
6.3.6 Curcumin Loading and Entrapment Efficiency	195
6.3.7 In vitro curcumin release analysis	195
6.3.8 Kinetic Modelling	197
6.3.9 Anti-bacterial Assay	198
6.3.10 Cytotoxicity	199
6.3.11 Degradation.....	201
6.4 Conclusion.....	202
6.5. REFERENCE	202
CHAPTER 7	209
CONCLUSION, FUTURE SCOPE AND SOCIAL IMPACT	209
7.1 Conclusion.....	209
7.2 Future Prospects	210
7.3 Social Impact.....	211

LIST OF PUBLICATIONS AND THEIR PROOFS	213
PLAGIARISM VERIFICATION	218
CURRICULUM VITAE	220

LIST OF FIGURES

Fig. 1.1 Schematic representation of the physical and chemical cross-linked hydrogel	2
Fig. 1.2 Applications of hydrogels in various fields	7
Fig. 1.3 (a) Diffusion-controlled via (I) Reservoir, (II) Matrix, (b) Swelling-controlled, and (c) Chemically-controlled	9
Fig. 1.4 Properties of Biopolymers	13
Fig. 1.5 Different routes of drug administration using biopolymers-based hydrogel ..	22
Fig. 2.1 Pictorial representation of the fabrication of DS-loaded CMTKG/PVP/PAM hydrogel.....	54
Fig. 2.2 Proposed mechanism for synthesis of DS-loaded CMTKG/PVP/PAM.....	60
Fig. 2.3 PXRD pattern of DS, CMTKG/PVP/PAM hydrogel (A-15), DS-loaded CMTKG/PVP/PAM hydrogel (A-5)	61
Fig. 2.4 SEM image of (a) CMTKG/PVP/PAM hydrogel, (b) DS-loaded CMTKG/PVP/PAM hydrogel.....	62
Fig. 2.5 ATR-FTIR spectrum of (a) CMTKG, (b) AM, (c) MBA, (d) CMTKG/PVP/PAM hydrogel, and (e) DS-loaded CMTKG/PVP/PAM hydrogel, and (f) DS.....	63
Fig. 2.6 Impact of the (a) CMTKG, (b) KPS, (c) MBA on swelling and (d) equilibrium swelling of A-5 hydrogel in pH 1.2 and 7.4 with respect to time	66
Fig. 2.7 Swelling plot of (a) DS-loaded CMTKG/PAM (A-14) hydrogel and (b) CMTKG/ PVP/PAM hydrogel (A-5) hydrogel in pH 1.2 and 7.4	67
Fig. 2.8 Sol-Gel studies of synthesized formulations of DS-loaded CMTKG/PVP/PAM hydrogel.....	68
Fig. 2.9 Porosity studies of synthesized DS-loaded CMTKG/PVP/PAM hydrogels ..	69
Fig. 2.10 Cumulative drug release curve for (a) DS-loaded CMTKG/PAM hydrogel and (b) DS-loaded CMTKG/PVP/PAM hydrogel in pH 7.4 and 1.2.....	71
Fig. 2.11 DS release kinetic plot at (a) pH 7.4 and (b) 1.2	73
Fig. 2.12 Cytotoxicity profile for DS-loaded CMTKG/PVP/PAM hydrogel (A-5)..	74
Fig. 2.13 Microscopic images of HCT-116 cells treated with (a) control (b) 0.78 $\mu\text{g/ml}$, (c) 1.56 $\mu\text{g/ml}$, (d) 3.125 $\mu\text{g/ml}$ and (e) 6.25 $\mu\text{g/ml}$ of DS-loaded CMTKG/PVP/PAM hydrogel.....	74
Fig. 2.14 Degradation profile for DS-loaded CMTKG/PVP/PAM hydrogel	75
Fig. 3.1 Schematic illustration of the fabrication of XG/PAM/PVP-based hydrogel ..	86
Fig. 3.2 Mechanism for Ibuprofen-loaded XG/PAM/PVP hydrogel.....	93
Fig. 3.3 PXRD plot of Ibuprofen, XG/PAM hydrogel, XG/PAM/PVP hydrogel, and Ibuprofen-loaded XG/PAM/PVP hydrogel.....	94
Fig. 3.4 SEM micrographs of (a) XG/PAM/PVP hydrogel and (b) Ibuprofen-loaded XG/PAM/PVP hydrogel	95

Fig. 3.5 ATR-FTIR spectra of MBA, XG/PAM hydrogel, XG/PAM/PVP hydrogel, and Ibuprofen-loaded XG/PAM/PVP hydrogel	96
Fig. 3.6 Influence of the (a) XG, (b) KPS, and (c) MBA on the swelling of the hydrogel.....	99
Fig. 3.7 Swelling studies of (a) XG/PAM hydrogel and (b) XG/PAM/PVP hydrogel in pH 7.4. and 1.2.....	99
Fig. 3.8 Sol-Gel studies of all fabricated XG/PAM/PVP hydrogels and XG/PAM hydrogel.....	101
Fig. 3.9 Porosity plot of all fabricated XG/PAM/PVP hydrogels and XG/PAM hydrogel.....	102
Fig. 3.10 Cumulative ibuprofen release from ibuprofen-loaded (a) XG/PAM hydrogel, (b) XG/PAM/PVP hydrogel pH 7.4 and 1.2.....	104
Fig. 3.11 Kinetic modelling profile of ibuprofen-loaded XG/PAM/PVP hydrogel	105
Fig. 3.12 Cytotoxicity plot for ibuprofen-loaded XG/PAM/PVP hydrogel	106
Fig. 3.13 Optical Microscope images of HCT-116 cells treated with (a) control (b) 0.78 $\mu\text{g/ml}$, (c) 1.56 $\mu\text{g/ml}$, (d) 3.125 $\mu\text{g/ml}$ and (e) 6.25 $\mu\text{g/ml}$ of ibuprofen-loaded XG/PAM/PVP hydrogel	107
Fig. 3.14 Degradation profile for ibuprofen-loaded XG/PAM/PVP hydrogel	108
Fig. 4.1 Schematic illustration of the β -CD/PAM/CMTKG hydrogel fabrication ..	118
Fig. 4.2 Mechanism for indomethacin-loaded β -CD/PAM/CMTKG hydrogel synthesis	124
Fig. 4.3 PXRD of β -CD/PAM/CMTKG hydrogel (W-1) and indomethacin-loaded β -CD/PAM/CMTKG hydrogel.....	125
Fig. 4.4 SEM micrographs of (a) β -CD/PAM/CMTKG and (b) indomethacin-loaded β -CD/PAM/CMTKG hydrogels.....	126
Fig. 4.5 ATR-FTIR spectra of (a) PEGDA, (b) Indomethacin, (c) β -CD/PAM/CMTKG hydrogel, and (d) indomethacin-loaded β -CD/PAM/CMTKG hydrogel.....	127
Fig. 4.6 (a) Effect of the PEGDA on the equilibrium swelling (%) and (b) Rate of swelling of W-1 hydrogel with respect to time.....	129
Fig. 4.7 Sol-Gel analysis plot for all fabricated β -CD/PAM/CMTKG hydrogels...	129
Fig. 4.8 Porosity plot for all formulated β -CD/PAM/CMTKG hydrogels	130
Fig. 4.9 Indomethacin release profiles for indomethacin-loaded (a) PAM/CMTKG hydrogel and (b) β -CD/PAM/CMTKG hydrogel at pH 1.2 and 7.4	132
Fig. 4.10 Release kinetic plot indomethacin-loaded β -CD/PAM/CMTKG hydrogel	133
Fig. 4.11 Cytotoxicity plot for indomethacin-loaded β -CD/PAM/CMTKG hydrogel	134
Fig. 4.12 Optical microscopic images of HCT-116 cells treated with (a) control (b) 0.78 $\mu\text{g/ml}$, (c) 1.56 $\mu\text{g/ml}$, (d) 3.125 $\mu\text{g/ml}$ and (e) 6.25 $\mu\text{g/ml}$ of indomethacin-loaded β -CD/PAM/CMTKG hydrogel.....	135

Fig. 4.13 Degradation curve for indomethacin-loaded β -CD/PAM/CMTKG hydrogel	136
Fig. 5.1 Illustration of the TG/ β -CD/SA hydrogel microsphere synthesis	145
Fig. 5.2 Mechanism for aspirin-loaded TG/ β -CD/SA hydrogel microsphere	151
Fig. 5.3 ATR-FTIR spectrum of β -CD, TG, SA, TG/SA hydrogel microsphere, TG/ β -CD/SA hydrogel microsphere, and Aspirin-loaded TG/ β -CD/SA hydrogel microsphere	153
Fig. 5.4 PXRD of TG/SA hydrogel, TG/ β -CD/SA hydrogel microsphere, and aspirin-loaded TG/ β -CD/SA hydrogel microsphere	154
Fig. 5.5 SEM images of (a, b) TG/ β -CD/SA and (c, d) Aspirin-loaded TG/ β -CD/SA hydrogel microsphere.....	155
Fig. 5.6 Effect of the (a) TG, (b) SA, and (c) β -CD on the equilibrium swelling of the hydrogel microsphere.....	157
Fig. 5.7 Swelling analysis of (a) TG/SA and (b) TG/ β -CD/SA hydrogel microsphere	157
Fig. 5.8 Sol-Gel analysis of all TG/ β -CD/SA hydrogel microspheres and TG/SA hydrogel microspheres	158
Fig. 5.9 Porosity plot for all synthesized hydrogels	159
Fig. 5.10 Release profile of aspirin-loaded (a) TG/SA hydrogel microsphere and (b) TG/ β -CD/SA hydrogel microsphere in pH 1.2 and 7.4	161
Fig. 5.11 Plot of zero Order kinetic model for aspirin-loaded TG/ β -CD/SA hydrogel microsphere	163
Fig. 5.12 Cytotoxicity profile of aspirin-loaded TG/ β -CD/SA hydrogel microspheres	164
Fig. 5.13 Inverted phase microscopic images of HCT-116 cells treated with (a) control (b) 50 μ g/ml, (c) 100 μ g/ml, (d) 200 μ g/ml, (e) 500 μ g/ml and (f) 1000 μ g/ml of aspirin-loaded TG/ β -CD/SA hydrogel microspheres	165
Fig. 5.14 Degradation profile of aspirin-loaded TG/ β -CD/SA hydrogel microsphere	166
Fig. 6.1 Depiction of the synthesis of CMTKG/SA/CuO nanocomposite hydrogel microspheres	179
Fig. 6.2 Mechanism for curcumin-loaded CMTKG/SA/CuO nanocomposite hydrogel microsphere synthesis	186
Fig. 6.3 ATR-FTIR spectra of curcumin, SA, CuO Nps, CMTKG/SA/CuO and curcumin-loaded CMTKG/SA/CuO nanocomposite hydrogel microspheres.....	188
Fig. 6.4 PXRD of (a) CuO Nps, (b) Curcumin, (c) CMTKG/SA (B-5), (d) CMTKG/SA/CuO (B-4) and (e) Curcumin-loaded CMTKG/SA/CuO nanocomposite	190
Fig. 6.5 SEM images of (a, b) CuO Nps at different magnifications, (c) CMTKG/SA/CuO and (d) curcumin-loaded CMTKG/SA/CuO hydrogel	191
Fig. 6.6 TEM Images of CuO Nps at 100 nm and 20 nm magnification.....	191

Fig. 6.7 Impact of the CuO Nps on the swelling of the CMTKG/SA/CuO nanocomposite hydrogel microspheres	193
Fig. 6.8 Swelling studies of (a) CMTKG/SA and (b) CMTKG/SA/CuO nanocomposite hydrogel microsphere at pH 7.4 and pH 1.2	193
Fig. 6.9 Sol-Gel fraction studies of all CMTKG/SA/CuO hydrogel microsphere ..	194
Fig. 6.10 Porosity analysis studies of all CMTKG/SA/CuO hydrogel microsphere	194
Fig. 6.11 Drug Release plot of curcumin-loaded (a) CMTKG/SA and (b) CMTKG/SA/CuO nanocomposite hydrogel microsphere	196
Fig. 6.12 Plot of Higuchi model for CMTKG/SA/CuO nanocomposite hydrogel microsphere	198
Fig. 6.13 Anti-bacterial profile of CuO Nps and Curcumin-loaded CMTKG/SA/CuO nanocomposite hydrogel microspheres	199
Fig. 6.14 Cytotoxicity plot of CMTKG/SA/CuO nanocomposite hydrogel	200
Fig. 6.15 Microscopic images of HCT-116 cells treated with (a) control (b) 0.78 $\mu\text{g/ml}$, (c) 1.56 $\mu\text{g/ml}$, (d) 3.125 $\mu\text{g/ml}$ and (e) 6.25 $\mu\text{g/ml}$ of CMTKG/SA/CuO nanocomposite hydrogel microsphere.....	200
Fig. 6.16 Degradation curve of curcumin-loaded CMTKG/SA/CuO nanocomposite hydrogel microsphere.....	201

LIST OF TABLES

Table 1.1 Overview of biopolymer-based hydrogels with application in drug delivery	20
Table 1.2 Drug delivery using biopolymer-based hydrogels via different routes.....	26
Table 2.1 Amounts of reagents required in the synthesis of the hydrogels.....	54
Table 2.2 DL% and DEE% of DS-loaded CMTKG/PAM and DS-loaded CMTKG/PVP/PAM hydrogels	70
Table 2.3 Kinetic modelling data for DS-loaded CMTKG/PVP/PAM hydrogel.....	72
Table 3.1 Quantities of reagents used for the synthesis of the hydrogels	87
Table 3.2 Drug loading and drug entrapment efficiency of Ibuprofen-loaded XG/PAM hydrogel and Ibuprofen-loaded XG/PAM/PVP hydrogel	104
Table 3.3 Kinetic modelling data of ibuprofen-loaded XG/PAM/PVP hydrogel ...	106
Table 4.1 Compositions of CMTKG-based hydrogels.....	120
Table 4.2 Indomethacin loading and entrapment efficiency values for β -CD/PAM/CMTKG and PAM/CMTKG hydrogel.....	132
Table 4.3 Regression coefficient (R^2) data for indomethacin-loaded	134
Table 5.1 Different formulations of TG-based hydrogels with required reagent....	146
Table 5.2 Formulations along with their corresponding drug loading (%) and drug entrapment efficiency (%).....	161
Table 5.3 Kinetic Modelling assessment of aspirin-loaded TG/ β -CD/SA hydrogel	164
Table 6.1 Various TG-based nanocomposite hydrogel microspheres with varying compositions	180
Table 6.2 Drug loading and drug entrapment efficiency of CMTKG/SA and CMTKG/SA/CuO nanocomposite hydrogel	196
Table 6.3 Kinetic modelling data of CMTKG/SA/CuO nanocomposite hydrogel .	198

LIST OF SYMBOLS AND ABBREVIATIONS

AM	Acrylamide
ATR-FTIR	Attenuated total reflectance-Fourier transform infrared
M_n	Average Molecular weight
β -CD	β -Cyclodextrin
CaCl_2	Calcium chloride
COO^-	Carboxylate
COOH	Carboxylic acid
CMTKG	Carboxymethyl tamarind kernel gum
CDH	Central drug house
CuO	Copper Oxide
CD	Cyclodextrin
DS	Diclofenac sodium
θ	Diffraction angle
DMSO	Dimethyl sulfoxide
DDS	Drug delivery system
DEE	Drug Encapsulation efficiency
DL	Drug loading
E. coli	Escherichia coli
GI	Gastrointestinal tract
g	Gram
HCl	Hydrogen chloride
OH	Hydroxyl
LCST	Lower critical solution temperature
MBA	Methylenebisacrylamide
μm	Micrometer
ml	Millilitre
MTT	3- [4,5-dimethylthiazol-2-yl]-2,5 diphenyl tetrazolium bromide
MW	Molecular weight

nm	Nanometer
Nps	Nanoparticle
NSAID	Nonsteroidal anti-inflammatory drug
PBS	Phosphate buffer saline
PAM	Polyacrylamide
PEGDA	Poly(ethylene glycol) diacrylate
PNIPAM	Poly (N-isopropyl acrylamide)
PVP	Polyvinyl pyrrolidone
PXRD	Powder X-ray Diffraction
KCl	Potassium chloride
KPS	Potassium per sulphate
R ²	Regression coefficient
SEM	Scanning Electron Microscopy
SA	Sodium Alginate
NaOH	Sodium hydroxide
TKG	Tamarind kernel gum
TG	Tragacanth gum
TEM	Transmission Electron Microscopy
UCST	Upper critical solution temperature
w.r.t.	With respect to
XG	Xanthan Gum

CHAPTER 1

INTRODUCTION AND LITERATURE SURVEY

1.1 Introduction

In the past two decades, numerous traditional drug delivery systems have been developed to enhance the effectiveness and targeting of therapeutic agents. However, increasing attention has been directed toward polymeric drug delivery systems, especially hydrogels, emerging as novel drug delivery systems. These hydrogels basically offer numerous benefits, including biocompatibility, hydrophilicity, controlled drug release, and the ability to provide smart drug delivery solutions. In the year 1955, Wichterle and Lim developed the first cross-linked poly (2-hydroxyethyl methacrylate) hydrogels for biomedical applications. These hydrogels consist of a three-dimensional network of cross-linked polymeric chains capable of holding large amounts of water and other fluids within their porous structure [1-5]. The fluid absorbent behavior of hydrogel is a consequence of the hydrophilic functional groups like $-NH_2$, $-COOH$, $-OH$, $-CONH_2$ etc., present in the polymeric chains [2-3], [6-7]. Moreover, the cross-linking among the polymeric chains results in the swelling of hydrogel instead of their dissolution in fluids [3], [8]. Basically, depending upon the technique employed during the synthesis, hydrogels can be classified into physical and chemical cross-linked hydrogels, as depicted in Fig. 1.1.

Physically cross-linked hydrogels can be made using hydrogen bonding, ionotropic involving interactions such as hydrogen bonding, van der Waals, host-guest interaction, ionic interactions or physical entanglement (2), (9-10). However, chemically crosslinked or permanent hydrogels can be developed using covalent crosslinking of polymeric chains and often by polymerization of end-functionalized macromers [3], [11-12]. The chemical methods used for the synthesis are free radical polymerization, grafting and gamma or electron beam polymerization [2], [13].

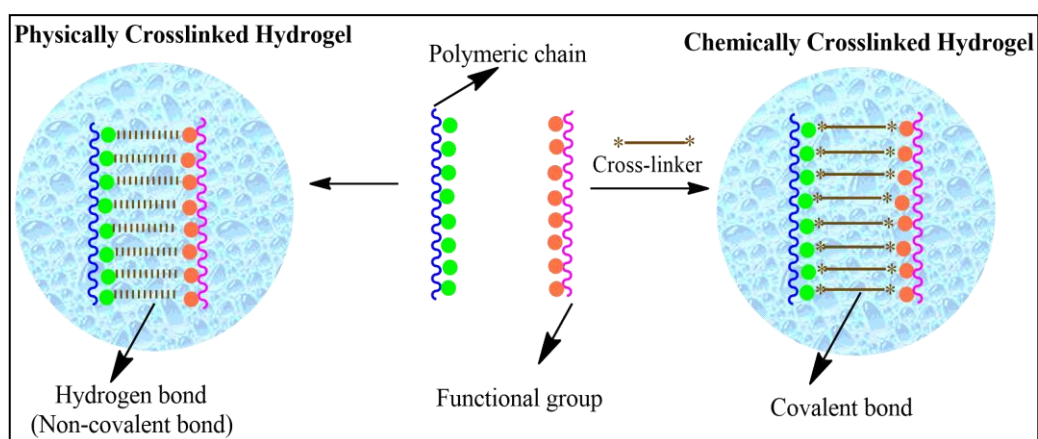


Fig. 1.1 Schematic representation of the physical and chemical cross-linked hydrogel

In addition to the synthesis, they can be further categorized into stimuli or intelligent hydrogel based on their response to external stimuli.

1.1.1 Smart or Intelligent Hydrogel

Smart hydrogels, also known as intelligent or responsive hydrogels, are a special class of hydrogels that can undergo significant and reversible changes in physical

properties or chemical structure in response to external stimuli, i.e., physical stimuli such as temperature, light, electric and magnetic fields or chemical stimuli such as pH, ionic strength and biological stimuli such as enzymes, antigens, and other biomolecules [14-18]. They trigger a wide range of responses such as swelling, shrinking and sol-gel transitions w.r.t stimuli [15-18]. Among these, the pH and temperature-responsive hydrogels are extensively studied [19-21].

1.1.1.1 pH-responsive Hydrogel

pH-responsive hydrogels exhibit significant changes in volume with variations in the pH of the external environment. These hydrogels are typically composed of polymers with acidic or basic functional groups that ionize or deionize depending on the surrounding pH. At low pH, acidic groups (e.g., carboxyl groups) remain protonated, causing the hydrogel to shrink due to hydrogen bonding between the polymer chains. At high pH, these acidic groups deprotonate and become negatively charged, increasing electrostatic repulsion and causing the hydrogel to swell [22-24]. Similarly, for hydrogels with basic groups (e.g., amino groups) at low pH, these groups become positively charged, leading to increased repulsion and swelling. However, at high pH, these groups become neutral, causing the hydrogel to contract. Such hydrogels are particularly useful in drug delivery systems, where they can be designed to release drugs at specific sites within the body, such as the stomach or intestines [25-26], [16]. This targeted release improves the efficacy of the drug and reduces side effects. Various techniques can be utilized to synthesize pH-responsive hydrogels, such as free radical polymerization, graft polymerization, irradiation, etc. For instance, Ashames et al. (2022) developed a pH-responsive hydrogel based on Guar Gum, 2-acrylamido-2-

methylpropanesulfonic acid, and methacrylic acid using a free-radical technique using methylene bisacrylamide (MBA) as a crosslinker for metformin HCl delivery. In this hydrogel, the –COOH groups of methacrylic acid ionize in a slightly basic medium (pH 7.4), leading to increased swelling and drug release at pH 7.4 [27]. Nawaz et al. (2018) also carried out a similar kind of study, i.e., a pH-responsive Gelatin/polyvinyl pyrrolidone hydrogel using graft polymerization technique with glutaraldehyde as crosslinkers [28].

1.1.1.2 Temperature-responsive Hydrogel

Temperature-responsive hydrogels, also known as thermo-responsive hydrogels, undergo a change in their physical and chemical properties in w.r.t temperature variations. These changes typically involve swelling, shrinking and sol-gel transition in the hydrogel network. Thermo-responsive hydrogels can be further categorized into positively, negatively thermo-responsive, and thermally reversible hydrogels.

These classifications relate to their behavior around critical solution temperatures (CST), namely the lower critical solution temperature (LCST) and the upper critical solution temperature (UCST). Positively thermo-sensitive hydrogels, upon cooling below their LCST, are hydrophilic and, hence, can absorb a significant amount of water. However, above the LCST, these hydrogels become hydrophobic, resulting in the expulsion of water and shrinking of the hydrogel. Examples include poly(N-isopropylacrylamide) (PNIPAM) hydrogel, which exhibits an LCST around 32°C. Below this temperature, PNIPAM hydrogels are swollen and hydrated, while above this temperature, they shrink and expel water. This positive-thermo-responsive

hydrogel was useful for the controlled drug release around body temperature [29-31], [16].

Moreover, negatively thermo-sensitive hydrogels swell upon cooling below their UCST. These hydrogels are hydrophobic, meaning they are in a contracted state with limited water absorption. However, above UCST, the hydrogels become hydrophilic, leading to the absorption of water and swelling [22]. They can be tailored for specific industrial processes and environmental applications.

Furthermore, thermally reversible hydrogels are physically crosslinked hydrogels that show sol-gel phase transitions with a change in temperature. They can be used as potential targeted drug carriers that are injected into the body in a liquid state and form a gel if the body temperature rises above CST [16], [32]. Ahsan et al. [33], reported the synthesis of an injectable thermally reversible disulfiram-loaded chitosan hydrogel using a self-assembly method. This thermally reversible hydrogel solution underwent a phase change from a liquid (sol) state to a solid (gel) state rapidly within about 3 minutes.

1.1.2 Swelling mechanism

Swelling can be defined as the transition of material from a glassy state to a rubbery state upon absorption. When the hydrogel comes into contact with water or a biological fluid, the hydrophilic groups present within the polymeric network interact with water molecules, leading to water absorption. The swelling behavior of hydrogels involves the absorption of water into three distinct forms: primary-bound water, secondary-

bound water, and free water. Primary bound water refers to water molecules that directly interact with the hydrophilic sites on the polymer chains, tightly bound to the network. Secondary-bound water is comparatively less tightly bound and interacts with the primary-bound water rather than the polymer chains themselves. However, the free water represents the excess water that occupies the spaces within the expanded polymer network and is not bound to the polymer. Water continues to diffuse into the hydrogel until an equilibrium state is reached. At equilibrium, the rate of water entering the hydrogel is balanced by the rate of water leaving it, resulting in an equilibrium swelling state. Moreover, the extent of swelling depends on the crosslinking density of the hydrogel. A lower crosslinking density allows more water to penetrate and increase swelling, whereas a higher crosslinking density restricts water uptake [11].

1.1.3 Applications of Hydrogel

Hydrogels have a wide range of applications in various fields, such as agriculture, energy storage, biosensors, water treatment, food packaging, tissue engineering, implants, and scaffolds, as depicted in Fig. 1.2 [11], [34]. Among these, drug delivery is one of the most interesting and widely explored applications. Over the past few decades, hydrogel-based drug delivery systems have gained attention due to their remarkable properties such as flexibility, porosity, bio-degradability, and bio-compatibility [35].

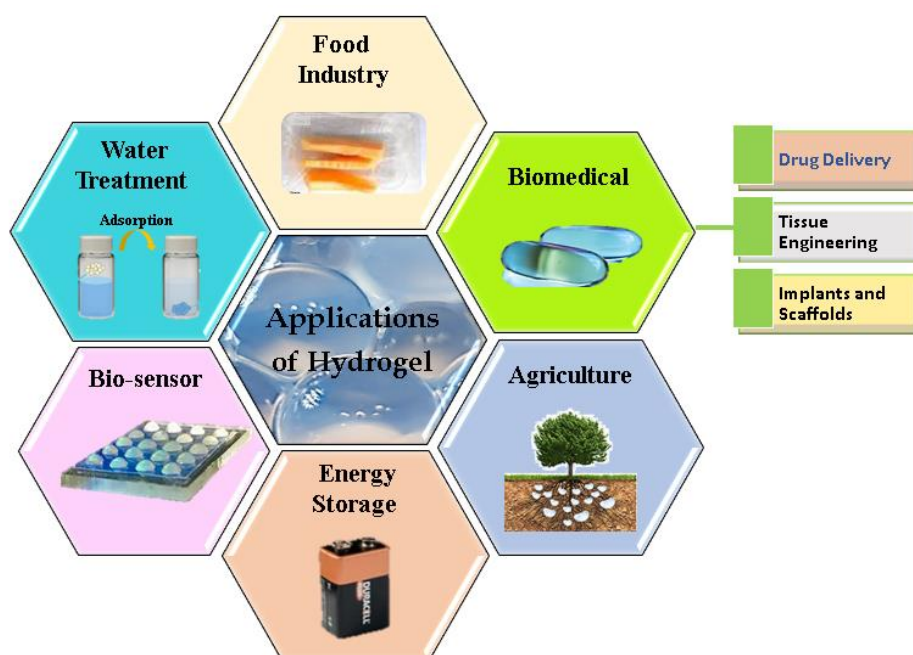


Fig. 1.2 Applications of hydrogels in various fields

1.1.4 Drug Release Mechanism

Drug release from the hydrogel matrix typically occurs via diffusion, swelling, enzymatic or hydrolytic cleavage of polymer chains or a combination of these processes (Fig. 1.3).

1.1.4.1 Diffusion-controlled drug release

Diffusion-controlled drug release relies on the movement of drug molecules from the hydrogel matrix (higher concentration) into the surrounding fluid (lower concentration), driven by a concentration gradient. It utilises Fick's diffusion theory to explain the release mechanism of the drug from the hydrogel. Diffusion-controlled release can be further categorized as a reservoir and matrix system. For reservoir drug delivery systems, the core-containing drug molecules are surrounded by a hydrogel

matrix, and drug release is governed by the first law of Fickian diffusion. However, for matrix drug delivery systems, drug molecules are uniformly distributed throughout the hydrogel, and drug release typically obeys the second law of Fickian diffusion. In a diffusion-controlled release, the diffusion of drug molecules through the polymer matrix is the rate-limiting step. Moreover, the rate of diffusion depends on the size of the drug molecules and the pore size of the hydrogel [1],[3].

1.1.4.2 Swelling-controlled drug release

Swelling involves the hydrogel's transition from a glassy (rigid state) to a rubbery (flexible state), driven by water absorption. This transition expands the polymer network, allowing trapped drug molecules to be released in a controlled manner. The extent of swelling depends on hydrogel composition, crosslinking density, and external environmental conditions such as pH, temperature, etc. In solely swelling-controlled drug release, the swelling of the hydrogel is the rate-limiting step [1],[3].

1.1.4.3 Chemically-controlled drug release

In chemically-controlled drug release, the hydrogel matrix itself degrades over time, either through enzymatic or hydrolysis cleavage of the network. As the polymeric network breaks down, the drug is gradually released from the matrix. However, in chemically-controlled drug release, the polymeric network cleavage is the rate-limiting step[3].

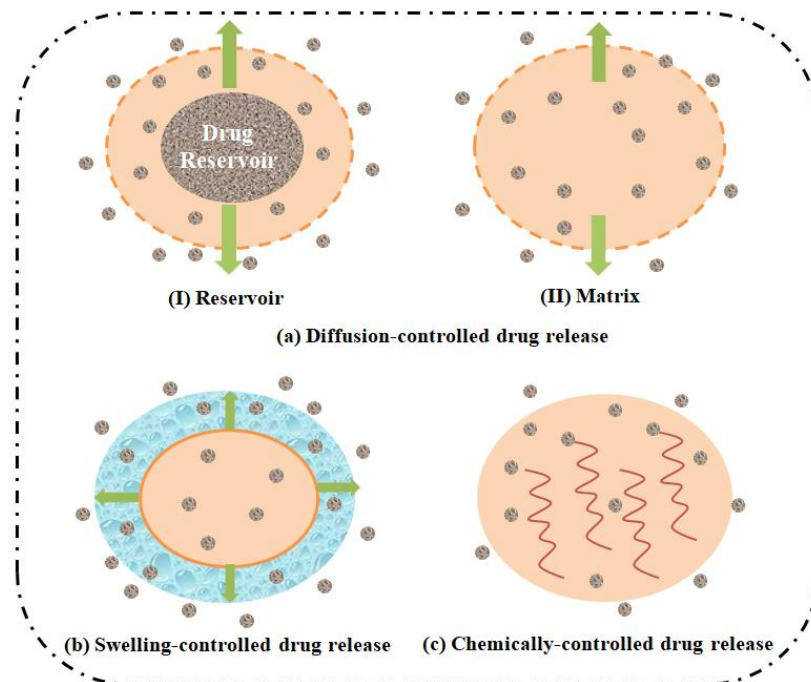


Fig. 1.3 (a) Diffusion-controlled via (I) Reservoir, (II) Matrix, (b) Swelling-controlled, and (c) Chemically-controlled

1.1.5. Kinetic Modelling of Drug Release

Several kinetic models have been utilized nowadays to predict whether it's swelling-controlled, diffusion-controlled, or chemically-controlled drug release. Some commonly employed mathematical models include Korsmeyer-Peppas, Higuchi, Hixson-Crowell, Zero-order and First-order models.

1.1.5.1 Korsmeyer-Peppas Model

It is the semi-empirical model used to describe drug release from the polymeric matrix, mainly when the drug release involves multiple processes. The Eqn. (1.1) for this model is computed as below.

$$\frac{M_t}{M_\infty} = k \cdot t^n \quad (1.1)$$

where k is the release constant, n is the release exponent, M_t is the amount of drug released at time t , M_∞ is the amount of drug loaded.

Moreover, based on n values, the drug release mechanism is determined as follows:

- I. If $n < 0.5$, it indicates Fickian diffusion, which means drug release is diffusion-controlled (36).
- II. If $0.5 \leq n < 0.89$, it signifies non-fickian or anomalous transport, which means drug release occurs by a combination of diffusion and swelling (37).
- III. If $n = 0.89$, it represents case-II transport, meaning drug release follows a swelling-controlled mechanism.
- IV. If $n > 0.89$, it denotes super case-II transport, indicating erosion of the polymer matrix [18], [38-40].

1.1.5.2 Higuchi Model

This model is based on Fickian diffusion and describes drug release from a matrix as a square root of a time-dependent process. It is suitable for polymeric systems where drug release is solely controlled by diffusion through the polymeric matrix. The Eqn. (1.2) for this model is given below.

$$\frac{M_t}{M_\infty} = k_H \cdot t^{1/2} \quad (1.2)$$

where M_t is the amount of drug released at time t , M_∞ represent the amount of drug loaded, and k_H is the Higuchi release constant [18], [38].

1.1.5.3 Hixson-Crowell Model

The Hixson-Crowell model is commonly applicable to the system where the surface or bulk erosion of the dosage forms is the primary mechanism of drug release. The model assumes that the rate of drug release is proportional to the surface area of the system. Hence, as the surface area reduces, a decrease in the dissolution & release rate is observed. The Eqn. (1.3) for this model is given below.

$$M_t^{1/3} - M_\infty^{1/3} = k_{HX} \cdot t \quad (1.3)$$

here, M_t indicates the amount of drug released at time t , M_∞ signify the amount of drug loaded, and k_{HX} is the Hixson-Crowell release constant [38].

1.1.5.4 Zero-Order Model

The zero-order drug release kinetic model describes a drug release mechanism where the drug is released at a constant rate, independent of its concentration. In this model, the amount of drug released over time remains consistent, meaning the drug is delivered at a uniform rate throughout the entire release period. This type of release is particularly desirable in drug delivery systems because it ensures a steady concentration of the drug in the bloodstream, leading to more predictable therapeutic effects. The zero-order release kinetic can be expressed by the Eqn. (1.4) below.

$$M_t = M_\infty + k_0 \cdot t \quad (1.4)$$

here, M_t is defined as the amount of drug released at time t , M_∞ represent the total amount of drugs loaded, and k_0 is the zero-order release constant [18], [38].

1.1.5.5 First-Order Model

According to the first-order model, the drug release rate is directly proportional to the drug concentration remaining in the polymeric system. This means that as the amount of drug in the system decreases, the rate at which the drug is released also decreases. This model suggests that a higher concentration of the drug will be released faster initially, but as the drug gets depleted in a system with time, the drug release rate also slows down. The first-order release kinetic Eqn. (1.5) is expressed as below.

$$\text{Log}M_t = \text{Log}M_\infty + \frac{k_1 t}{2.303} \quad (1.5)$$

where M_t represents the amount of drug released at time t , M_∞ indicates the amount of drug loaded, and k_1 is the first-order release constant [18], [38].

1.2 Literature Survey

1.2.1 Biopolymer-based hydrogel

Biopolymer-based hydrogel are receiving much interest nowadays in biomedical applications due to their non-toxicity, biodegradability and biocompatibility (Figure 4.4) [41-44]. Biopolymers can be broadly categorized into natural, semi-synthetic and synthetic biopolymers. Nature biopolymers are directly produced by living organisms, including plants, animals, and microorganisms [45-48]. Examples include proteins

(silk and gelatin), polysaccharides (chitosan and sodium alginate), and nucleic acids (DNA and RNA) [46-51].

Moreover, semi-synthetic biopolymers are synthesized by chemically modifying natural biopolymers. These modifications are often performed to enhance specific properties such as pH-sensitivity, swelling, or controlled release. Examples include carboxymethyl cellulose and carboxymethyl tamarind kernel gum [3], [46-47], [52]. On the other hand, synthetic biopolymers are synthesized from natural monomeric units through polymerization processes. Examples of synthetic biopolymers include polylactic acid and polycaprolactone, which are used in drug delivery systems, tissue engineering, and other medical applications due to their controlled degradation rates and tunable properties [46-47].

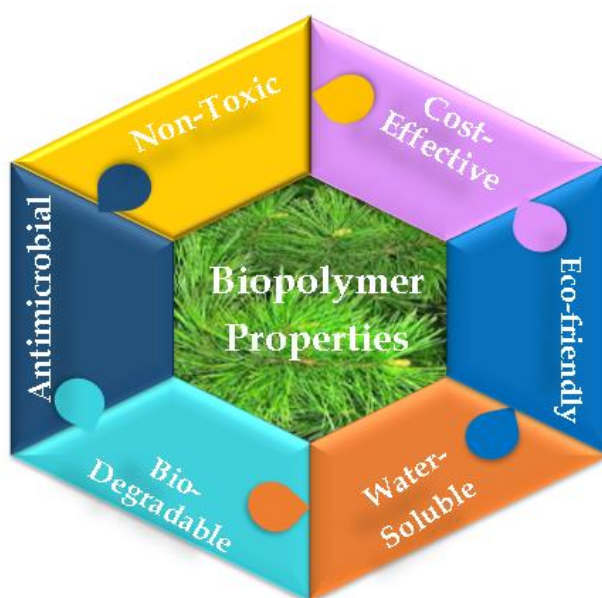


Fig. 1.4 Properties of Biopolymers

The most commonly studied biopolymer-based drug delivery systems are polysaccharide and protein-based systems. Table 1.1 enlists the existing reported literature on biopolymer-based hydrogels utilized in drug delivery.

Basically, polysaccharides are complex carbohydrates composed of long chains of monosaccharide units bonded together by glycosidic linkages [53-54]. Polysaccharides are diverse in their structure and function, making them essential components in various biomedical applications. Furthermore, proteins are composed of long chains of amino acids linked by peptide bonds, forming polypeptide chains that fold into specific three-dimensional structures. These structures determine the protein's function and are classified into four levels: primary, secondary, tertiary, and quaternary. The primary structure is the unique sequence of amino acids in a polypeptide chain, which is determined by the genetic code. The secondary structure involves the local folding of the polypeptide chain into structures such as alpha-helices and beta-sheets. The tertiary structure refers to the overall three-dimensional shape of a single polypeptide chain formed by interactions between the side chains (R groups) of the amino acids. Lastly, the quaternary structure arises when two or more polypeptide chains (subunits) interact to form a functional protein complex. Not all proteins have a quaternary structure; it is only present in proteins composed of multiple subunits. Proteins are essential for virtually every process in a living organism, highlighting their importance in the biomedical field [54].

1.2.1.1 Chitosan

Chitosan is a cationic polysaccharide obtained from the de-acetylation of chitin. The

degree of de-acetylation and molecular weight of chitosan directly influences its solubility, viscosity, and biological behavior. Chitosan hydrogels are, in general, pH-responsive, as they carry a positive amino group that protonates or deprotonates with variations in the pH of the medium. This pH-responsive property makes it highly versatile and suitable for a wide range of applications, including in the fields of biomedical, agriculture, food, and cosmetics field. Moreover, the positive charge of chitosan allows it to adhere to negatively charged mucosal surfaces, making it particularly useful for drug delivery through mucosal routes, such as nasal, ocular, and oral delivery [46], [55]. For instance, Armengol et al. (2024) developed chitosan-maleic acid hydrogel for ocular delivery of Dexamethasone, which demonstrates excellent mucoadhesiveness and antimicrobial activity against *E. coli* [56].

1.2.1.2 Carboxymethyl tamarind kernel Gum

Carboxymethyl tamarind kernel gum (CMTKG) is a modified polysaccharide derived from tamarind kernel gum, a natural gum obtained from the seeds of the tamarind tree (*Tamarindus indica*). The modification process involves carboxymethylation, which introduces carboxymethyl groups into the polysaccharide backbone. This modification increases its solubility in water and introduces functional groups that can interact with a wide range of drug molecules. The molar ratios of galactose, xylose, and glucose in CMTKG are 1:2:3. CMTKG-based hydrogel exhibits high swelling capacity under aqueous environments, allowing for sustained release of encapsulated drugs over time [57-58]. Owing to its pH-sensitive nature, CMTKG swells more in alkaline pH conditions than in acidic pH, making it an ideal candidate for site-specific drug

delivery [59]. For instance, Jana et al. (2016) synthesized a CMTKG/gelatin-based hydrogel that exhibited a higher aceclofenac release rate at pH 6.8 compared to pH 1.2 [60].

1.2.1.3 Sodium Alginate

Sodium alginate is a naturally occurring polysaccharide extracted from the cell walls of brown seaweed. It consists of two types of monomers, β -D-mannuronic acid (M) and α -L-glucuronic acid (G), which are arranged in varying sequences [54], [61-65]. Sodium alginate-based hydrogels have emerged as a promising material in drug delivery systems due to their unique ability to encapsulate and release therapeutic agents in a controlled manner [54]. These hydrogels are typically formed by the ionic crosslinking of sodium alginate with divalent cations, such as Fe^{2+} , Ca^{2+} , Ba^{2+} , etc. The gelation process, known as the ionotropic gelation technique, occurs when sodium alginate interacts with Ca^{2+} , triggering a crosslinking reaction between the G-blocks of the polymer chains, resulting in the formation of a stable, three-dimensional polymeric network [54], [61], [66-67]. For instance, Akalin et al. (2023) synthesized an alginate/sodium carboxymethyl cellulose hydrogel using FeCl_3 as a crosslinker and employed it for the pH-dependent release of propranolol hydrochloride [67]. The gelling property, along with its biocompatibility, non-toxicity, and ease of use, has made sodium alginate-based hydrogel a versatile material in various other industries, including food, textile, cosmetics and agricultural [66].

1.2.1.4 Tragacanth Gum

Tragacanth gum is a polysaccharide obtained from the sap of the *Astragalus* species,

particularly *Astragalus gummifer*. It primarily consists of two main components: tragacanthin and bassorin. Tragacanthin is a water-soluble component that forms a viscous solution, while bassorin is a water-insoluble component that contributes to the swellable gel-like properties of the gum. Tragacanth gum is known for its excellent thickening, emulsifying, and stabilizing properties. Tragacanth gum-based hydrogels offer several remarkable properties, including muco-adhesiveness, high swelling capacity, controlled release, and biocompatibility, which make them an ideal material for drug delivery applications. Tragacanth gum-based hydrogels are utilized to deliver a wide range of therapeutic agents, including peptides, proteins, and small molecules. For example, Cikrikci et al. (2018) fabricated an alginate-gum tragacanth hydrogel using the ionotropic gelation technique, which delivered the insulin in a pH-dependent manner [68]. The hydrogel matrix provides a protective environment for sensitive drugs, shielding them from enzymatic or hydrolytic degradation [69-70].

1.2.1.5 Xanthan Gum

Xanthan gum is an anionic polysaccharide produced by the bacterium *Xanthomonas campestris* through a fermentation process [71-72]. It contains glucuronic acid and pyruvic acid groups in its side chains. It is widely used as a thickening, stabilizing, and emulsifying agent in various industries, including food, cosmetics, and pharmaceuticals. It is non-toxic, non-irritating, biodegradable and biocompatible, making it valuable in the pharmaceutical industry for applications in drug delivery, wound healing, and other therapeutic formulations [72]. For example, Suhail et al.

(2023) reported the colon-targeted release of atomoxetine HCl using xanthan gum-pluronic F-127 hydrogels [73].

1.2.1.6 Silk

Silk, particularly silk fibroin derived from the *Bombyx mori* silkworm, has emerged as a promising material in drug delivery due to its unique properties such as biocompatibility, biodegradability, and mechanical robustness [74-75]. The protein-based nature of silk fibroin allows for versatile processing into various forms, including films, hydrogels, nanoparticles, and fibers, each offering different advantages for drug delivery applications. Silk protein-based hydrogels are gaining attention in drug delivery systems mainly in tissue regeneration and wound healing. Derived from natural silk proteins, such as fibroin, these hydrogels exhibit outstanding biocompatibility and biodegradability, oxygen and water permeability making them effective for medical applications [76]. Silk-based hydrogel has highly organized beta-sheet structures with hydrogen-bonded arrangements that give silk its remarkable strength and stability. The mechanical strength of silk proteins contributes to hydrogels with significant elasticity and durability, crucial for maintaining structural integrity during drug delivery [75-79]. Moreover, silk fibroin based hydrogel can retain moisture and form protective barrier, creating optimal environment for wound healing and reducing the risk of infection. For instance, Singh et al. (2023), synthesized a vancomycin-loaded silk fibroin hydrogel. This hydrogel demonstrated excellent

wound healing properties, effective antibacterial activity, and a controlled release profile of the antibiotic vancomycin [76].

1.2.1.7 Gelatin

Gelatin is a biopolymer obtained by hydrolyzing collagen, which makes it inherently biocompatible and biodegradable [80-83]. Due to these properties, gelatin-based hydrogels offer a versatile platform for drug delivery. However, pure gelatin-based hydrogel faces challenges such as poor mechanical strength, low thermal stability, and degradation in gastrointestinal fluid. To address these issues, different crosslinking techniques have been employed nowadays [84]. For instance, Yan et al. (2023) crosslinked gelatin hydrogel with oxidized dextran of varying molecular weights. The finding revealed that higher molecular weight oxidized dextran improved thermal and mechanical stability, reduced porosity, and allowed for controlled curcumin release [84]. Additionally, the gelatin-based hydrogels can be further modified by incorporating nanoparticles, for tunable drug release rates, which is particularly useful in drug delivery application [81-82]. For example, Rahmani et al (2022), developed a nanocomposite hydrogel based on gelatin, polyvinyl alcohol, boric acid, gum arabic aldehyde and graphene oxide. This hydrogel exhibits excellent mechanical strength, self-healing properties, pH responsive swelling behavior and controlled release of rivastigmine drug [51].

Table 1.1 Overview of biopolymer-based hydrogels with application in drug delivery

Hydrogel	Technique	Model Drug	Highlights	Ref.
Tragacanth gum-cl-(polyvinyl alcohol-co-poly(2-acrylamido-2-methylpropane sulfonic acid))	Co-polymerization	Methotrexate	Demonstrates excellent haemo-compatibility & muco-adhesivity, and is non-thrombogenic in nature.	[85]
Xanthan gum/starch/polyacrylic acid	Microwave irradiation	Paracetamol and aspirin	Non-cytotoxic to COS-7 cells and bio-compatible, exhibiting minimal hemolysis.	[86]
Chitosan-g-poly(acrylamide-co-acrylic acid)	Free-radical polymerization	Tenofovir disoproxil fumarate	Exhibits non-toxicity against HeLa cell lines	[12]
Polyvinyl alcohol/Gelatin	Gamma irradiation and Freeze-thaw	Metformin HCl	Higher gelatin concentration leads to reduced drug release.	[81]
Sodium alginate-co-poly(2-acrylamido-2-methyl propane sulphonic acid)	Free-radical polymerization	Diclofenac sodium	Sustained pH-dependent release of diclofenac sodium for 24 hr.	[87]

Carboxymethyl sago pulp/Chitosan	Electron-beam irradiation	Diclofenac sodium	Showed antimicrobial activities against both gram-negative and gram-positive bacteria.	[88]
Carboxymethyl tamarind kernel gum/PVA	Citric acid crosslinking	Moxifloxacin	Sustained release of moxifloxacin for 24 h.	[89]
Carboxymethyl tamarind kernel gum	Citric acid crosslinking	Metronidazole	Hydrogel swelling decreases with an increase in the quantity of CMTKG and citric acid.	[90]
Poly(N-Isopropylacrylamide) /Chitosan/Polyvinyl Alcohol	Gamma irradiation and Freeze-thaw	Metformin HCl	Demonstrate pH-dependent and temperature-dependent sustained drug release.	[91]

1.2.2 Different routes of drug administration using biopolymer-based hydrogel

Biopolymer-based hydrogels, due to their unique properties such as high water content, biocompatibility, and tunable drug release, serve as versatile carriers for drug delivery across various routes of administration, as illustrated in Fig. 1.5. Table 1.2

discusses the different routes of administration where hydrogels are used effectively used for drug delivery.



Fig. 1.5 Different routes of drug administration using biopolymer-based hydrogel

1.2.2.1 Oral Drug Delivery

Oral drug delivery is a widely used and convenient method for administering a wide range of hydrophobic and hydrophilic drugs. It involves the administration of drugs in various forms, such as tablets, capsules, or liquid solutions, which are then absorbed through the gastrointestinal (GI) tract into the bloodstream. This route of administration is favored for its ease of use, non-invasiveness, and patient compliance. Biopolymer-based hydrogels offer several advantages for oral drug delivery, including controlled release, improved bioavailability, and targeted delivery

Another benefit of hydrogels as an oral delivery carrier is their ability to protect drugs from degradation in the acidic environment of the stomach [3], [92], [17]. Moreover, particularly pH-sensitive hydrogels respond to changes in the pH of the GI tract, making them ideal for oral drug delivery. For example, an anionic chondroitin sulfate-co-poly(acrylic acid) hydrogel can remain almost intact in the acidic environment of the stomach and only release the drug when it reaches the more neutral pH of the intestines, targeting the release site more effectively [40]. Additionally, biopolymer-based hydrogels as oral drug carriers improve the solubility of poorly water-soluble drugs, enhancing their absorption and effectiveness. Moreover, certain hydrogels possess mucoadhesive properties, allowing them to adhere to the mucosal lining of the GI tract. This prolongs the residence time of the drug at the absorption site, potentially improving drug absorption and bioavailability [3], [1].

1.2.2.2 Parental Drug Delivery

The parenteral drug delivery approach is favoured for its ability to bypass the first-pass metabolism in the liver and digestive system, ensuring that drugs are delivered directly into the bloodstream or specific tissues, which enhances bioavailability and drug therapeutic effect. Common conventional parental drug delivery methods include intravenous (IV) injections, subcutaneous injections and intramuscular injections, leading to immediate or rapid drug release (93). This typically provides a short duration of action, often requiring frequent dosing. However, in biopolymer-based hydrogel, the drug molecules are embedded within a biocompatible polymeric matrix, which gradually releases the drug over time as it degrades or responds to

environmental triggers (e.g., pH, temperature). Moreover, thermo-responsive hydrogels are most commonly studied hydrogel for injectable formulations because they can be administered in a liquid form and, undergo gelation upon exposure to the body temperature and slowly release the drug over time. Additionally, modified chitosan-based hydrogels are frequently studied for their potential in parental drug delivery (94). Hence, biopolymer-based hydrogel as a parenteral drug delivery provides sustained, controlled release, improved drug stability, and greater patient comfort, making it ideal for long-term treatments and reducing the frequency of administration [3].

1.2.2.3 Ocular Drug Delivery

Biopolymer-based hydrogel systems for ocular drug delivery present a highly promising approach to treat various eye conditions due to their unique properties. Hydrogels are highly hydrophilic, which allows them to maintain high water content, closely mimicking the natural state of the eye [17], [92], [11]. This ensures minimal irritation and good compatibility with ocular tissues. The eye's natural barriers, such as tear turnover and corneal epithelial tight junctions, limit drug absorption. The mucoadhesive properties of hydrogels can improve drug retention time on the ocular surface and provide controlled release within intraocular tissues, such as the vitreous cavity and aqueous humor. Biopolymer-based hydrogels are particularly effective for delivering drugs to the anterior segment of the eye, including treatments for conditions like conjunctivitis, keratitis, and corneal ulcers [92]. Additionally, most ocular medications are administered as conventional eye drops. However, a significant

portion of these medicines enters systemic circulation through conjunctival absorption into the nasal cavity, resulting in only a small portion of the drugs being effectively utilized. These eye drops typically have a short contact time with the eye, often washed away by tears within minutes, leading to a need for frequent administration. Moreover, it provides an initial burst of drug release, often resulting in an increase in drug concentration followed by a rapid decline. However, biopolymer-based hydrogel contact lenses can retain drugs on the ocular surface for extended periods, providing a sustained release of drugs. This prolonged retention time enhances drug absorption and efficacy [11], [17]. Gelatin-based hydrogels are commonly used for the delivery of a variety of drug molecules to the eye [95].

1.2.2.4 Transdermal Drug Delivery

Transdermal drug delivery systems offer a non-invasive method of administering medications through the skin, providing a controlled and sustained release of drugs into the systemic circulation. This approach avoids first-pass metabolism by the liver, which can degrade drugs before they reach their target [96-97], [2]. It relies on the diffusion of drugs across the skin's layers, primarily the stratum corneum, which is the outermost barrier [92], [98]. Conventional transdermal drug delivery systems are not able to deliver larger or more complex drugs effectively due to the skin's barrier properties. Generally, the outer layer of the skin (stratum corneum) can act as a significant obstacle to drug penetration. Moreover, the adhesives used in conventional transdermal patches can sometimes cause skin irritation or allergic reactions, especially with prolonged use. However, biopolymer-based hydrogel films are used as

patches for transdermal drug delivery, which provides several advantages over conventional delivery material. These systems consist of hydrophilic polymer networks capable of retaining significant amounts of water, creating a moist environment that enhances drug permeability through the skin [3]. Biopolymer-based hydrogel patches are adhesive patches that can be directly applied to the skin, adhering comfortably and controlled release of the drug over a specified period [92]. These patches are beneficial for conditions such as pain management, insulin delivery, nicotine delivery for smoking cessation, etc. Moreover, hydrogel films can be combined with microneedles to create advanced transdermal delivery systems. These hydrogel microneedle patches enhance transdermal delivery by creating microchannels in the skin, allowing drugs to bypass the stratum corneum and reach deeper skin layers for more effective absorption. This method is minimally invasive and can improve the delivery of larger molecules or vaccines [9]. Hyaluronic acid-based hydrogels have been extensively investigated for transdermal drug delivery [99]. Moreover, the biopolymer-based hydrogel provides a hydrated environment that can improve drug solubility and release [100].

Table 1.2 Drug delivery using biopolymer-based hydrogels via different routes

Hydrogel	Delivery Route	Drug	Key Aspect	Ref.
Xanthan Gum /chitosan/ 2-acrylamido-2-methylpropane sulfonic acid	Oral	Acyclovir	Controlled acyclovir release for 24 hr.	[101]

Acacia gum/ polyvinylpyrrolidone /carbopol	Transdermal	Moxifloxacin	The film demonstrates non-hemolytic, antioxidant, and mucoadhesive properties.	[102]
γ -cyclodextrin	Ocular	Josamycin	Exhibit 4-fold higher drug loading efficiency compared to dextran hydrogels.	[103]
Chitosan-co-poly(N-isopropyl-acrylamide)	Parental	Loxoprofen	Released the drug in a controlled manner at pH 7.4 and 37 °C.	[104]
Tragacanth Gum/polyvinyl alcohol/polyvinyl pyrrolidone	Transdermal	Lidocaine	It revealed excellent blood compatibility, water vapor and oxygen permeability.	[105]
Aspartic acid/alginate acid-co-poly(acrylic acid)	Oral	Ibuprofen	Increased drug release was noted at alkaline pH.	[106]
Tamarind kernel Gum/ β -cyclodextrin co-poly (methacrylate)	Oral	Acyclovir	It displayed no indications of pathology or necrosis	[107]
Chitosan-PNIPAm	Parental	Loxoprofen	Achieved controlled drug release at a higher temperature (37°C) and pH 7.4.	[104]

Carboxymethyl cellulose/poly (ethylene glycol)	Transdermal	Ketoconazole	Grafted PEG significantly slowed the release of Ketoconazole.	[108]
--	-------------	--------------	---	-------

1.2.3 Biopolymer-based hydrogels for hydrophobic drug delivery

Biopolymer-based hydrogels are mainly utilized for the delivery of hydrophilic drugs, as their polymer matrices are typically hydrophilic, making them less compatible with hydrophobic drugs as well as poor water-soluble drug [109]. Thus, hydrophobic drugs exhibit low loading and release capacity within the hydrogel matrix. To address this limitation, one approach is to incorporate hydrophobic components into the hydrogel matrix to improve compatibility with hydrophobic drug [110].

1.2.3.1 Thermosensitive Block Co-polymeric hydrogel

Physical hydrogels, particularly thermosensitive block co-polymeric hydrogels, are ideal for the controlled delivery of hydrophobic drugs [111]. These biopolymer-based hydrogels are often composed of triblock or diblock copolymer matrix. The most common triblock hydrogel is fabricated with poly(ethylene glycol) (PEG) as the hydrophilic segment [112] and hydrophobic blocks arranged as ABA or BAB. PEG provides high water solubility and biocompatibility through micelle formation [113], [57], while the hydrophobic blocks increase drug loading capacity. For instance, polylactic acid-polyethylene glycol-polylactic acid triblock hydrogel was synthesized for ibuprofen delivery. The drug release was observed to be slow and prolonged compared to the commercial ibuprofen tablet [114].

1.2.3.2 Complex formation

Cyclodextrins (CDs) are widely used for complexing hydrophobic molecules due to their unique structure, which has a hydrophobic cavity in its interior and a hydrophilic exterior. These cyclic oligosaccharides, composed of 6, 7, or 8 glucose units (α , β , γ -CD), enhance the solubility of hydrophobic drugs by forming inclusion complexes [115]. The inclusion complex is basically a type of supramolecular structure formed when a drug molecule (guest) is encapsulated within the cavity of a CD molecule (host) through an interaction called host-guest interaction. CDs are often combined with chemical crosslinkers like epichlorohydrin (EP), methylene bisacrylamide, or diisocyanates to synthesize hydrogels to deliver drug molecules. These hydrogels are particularly useful for delivering poorly soluble drugs, enhancing their bioavailability, and providing sustained or targeted drug delivery. For instance, β -CD-grafted chitosan/glycerophosphate was synthesized for sustained release of hydrophobic drug curcumin. The study revealed that β -CD improved both the solubility and bioavailability of curcumin [116].

1.2.3.3 Amphiphilic hydrogel

One way to introduce hydrophobic domains into a biopolymer-based hydrogel network is by chemically cross-linking hydrophobic polymer or monomers with a hydrophilic polymer, creating amphiphilic hydrogels. Moreover, this can also be achieved using hydrophobic crosslinkers. Free-radical polymerization is often employed to synthesize such hydrogels [110]. A study by Das et al (2014) reported the synthesis of an amphiphilic hydrogel composed of hydrophobic polylactic acid and

hydrophilic dextrin using methylene bisacrylamide as a crosslinker via free-radical polymerization. The findings revealed that the incorporation of poly(lactic acid) onto the dextrin backbone effectively sustained the release of the hydrophobic drug ornidazole [117].

1.2.3.4 Nanocomposite

Biopolymer-based hydrogel nanocomposites are advanced materials composed of a hydrogel matrix integrated with nanoparticles [118]. Incorporating nanoparticles into hydrogel structures is an effective way to introduce hydrophobic depots [110]. Moreover, the high surface area and porosity of nanoparticles allow them to carry a larger quantity of drugs within the hydrogel, improving the overall drug loading capacity of the system [17]. Several types of nanoparticles, such as metallic nanoparticles, polymeric nanoparticles, liposomes, carbon-based nanoparticles, and silica nanoparticles, can be used in biopolymer-based hydrogel nanocomposites. The introduction of nanoparticles into a hydrogel matrix can be achieved through various methods, such as physical crosslinking and chemical crosslinking [119-120]. In physical crosslinking, the pre-synthesized nanoparticles are mixed with the hydrogel precursor solution before the gelation process. However, in chemical cross-linking, the nanoparticles with functional groups can be chemically bonded to the polymer chains of the hydrogel, creating a strong and stable composite structure [121]. When nanoparticles are embedded within this hydrogel matrix, the resulting nanocomposite has properties of both hydrogels and nanoparticles, such as biocompatibility, flexibility, high water content, enhanced mechanical strength,

targeted delivery, and controlled drug release [118]. For example, sodium alginate/ carboxymethyl chitosan-zinc oxide hydrogel nanocomposite was reported for oral delivery of diclofenac sodium. It was found that incorporating nanoparticles slowed and sustained the drug release [122]. Similarly, oxidized starch-copper oxide (CuO) hydrogel nanocomposite was reported for oral delivery of naproxen. It was observed that naproxen loading efficiency increases with the rise in the CuO nanoparticle concentration [123].

1.3 Conclusion and Research Gap

Biopolymer-based hydrogels have shown significant potential in drug delivery by offering unique advantages such as biocompatibility and biodegradability. Recent advancements in hydrogel-based drug delivery systems, such as smart hydrogel and nanocomposite hydrogels, have led to improved control over drug release, enhanced stability, and targeted drug delivery, making them highly efficient for various therapeutic applications. Moreover, biopolymer-based hydrogels have shown great potential in drug delivery applications, primarily for hydrophilic drugs due to the hydrophilic nature of most hydrogels. However, this property restricts their efficiency in loading and delivering hydrophobic drugs, resulting in limited literature on their application in this area. To address this limitation, this thesis work has focused on fabricating novel biopolymer-based hydrogels specifically designed for the delivery of hydrophobic and sparingly water-soluble drugs.

Moreover, CMTKG, TG, and XG are pH-sensitive, non-toxic, and biodegradable biopolymers, making them an ideal candidate for the synthesis of drug delivery

systems. Despite these favorable properties, there is limited literature existing on the synthesis of hydrogels using these biopolymers, and their potential applications in drug delivery have not been fully explored. Thus, the current thesis works focused on the development of novel hydrogels based on CMTKG, TG and XG and their application in drug delivery.

Additionally, β -CD was used for its ability to encapsulate hydrophobic drug molecules. Its amphiphilic structure, with a hydrophobic interior and a hydrophilic exterior, allows it to effectively entrap hydrophobic drugs, thereby improving their loading efficiency. However, to the best of our knowledge, β -CD incorporated CMTKG and TG-based hydrogels have not yet been synthesized. The introduction of β -CD into biopolymer-based matrices could lead to the development of hydrogels capable of efficiently delivering poor hydrophobic drugs. This innovative approach could potentially overcome the current limitations associated with hydrophobic drug delivery using conventional hydrophilic hydrogel matrices.

1.4 Research Objectives

To address the research gaps identified in the literature, the following objectives have been established:

- I. To synthesize various biopolymer-based hydrogels.
- II. To characterized the synthesized hydrogels using techniques such as Fourier Transform Infrared Spectroscopy (FTIR), Scanning Electron Microscopy (SEM) etc.
- III. To conduct the swelling studies of synthesized hydrogel in different pH media.

- IV. To perform the loading of various drugs into the hydrogel matrix.
- V. To conduct drug release experiments with drug-loaded hydrogel at different pH.
- VI. To perform the kinetic modelling of drug released data of synthesized hydrogel matrix.

1.5 REFERENCES

1. Narayanaswamy R, Torchilin VP (2019) Hydrogels and their applications in targeted drug delivery. *Molecules* 24:603. <https://doi.org/10.3390/molecules24030603>
2. Bharskar GR (2020) A review on hydrogel. *World journal of pharmacy and pharmaceutical sciences* 9:1288–1298. <https://doi.org/10.20959/wjpps20207-16602>
3. Ghasemiyeh P, Mohammadi-Samani S (2019) Hydrogels as Drug Delivery Systems; Pros and Cons. *Trends in Pharmaceutical Sciences* 5:7–24. <https://doi.org/10.30476/TIPS.2019.81604.1002>
4. Chatterjee S, Hui PC leung (2019) Review of stimuli-responsive polymers in drug delivery and textile application. *Molecules* 24. <https://doi.org/10.3390/molecules24142547>
5. Amiri M, Khazaeli P, Salehabadi A, Salavati-Niasari M (2021) Hydrogel beads-based nanocomposites in novel drug delivery platforms: Recent trends and developments. *Advances in Colloid and Interface Science* 288:102316. <https://doi.org/10.1016/j.cis.2020.102316>
6. Musa H, Yahaya S (2022) Polyacrylamide hydrogels for application in oral drug delivery. *Nigerian Journal of Scientific Research* 20.

7. Sennakesavan G, Mostakhdemin M, Dkhar LK, et al (2020) Acrylic acid/acrylamide based hydrogels and its properties - A review. *Polymer Degradation and Stability* 180:109308. <https://doi.org/10.1016/j.polymdegradstab.2020.109308>
8. Kamini, Puri D (2024) Hydrogel-based drug delivery systems - a review. *Polymer-Plastics Technology and Materials* 1–24. <https://doi.org/10.1080/25740881.2024.2369670>
9. Dreiss CA (2020) Hydrogel design strategies for drug delivery. *Current Opinion in Colloid and Interface Science* 48:1–17. <https://doi.org/10.1016/j.cocis.2020.02.001>
10. Ghawanmeh AA, Ali GAM, Algarni H, et al (2019) Graphene oxide-based hydrogels as a nanocarrier for anticancer drug delivery. *Nano Research* 12:973–990. <https://doi.org/10.1007/s12274-019-2300-4>
11. Kasai RD, Radhika D, Archana S, et al (2023) A review on hydrogels classification and recent developments in biomedical applications. *International Journal of Polymeric Materials and Polymeric Biomaterials* 72:1059–1069. <https://doi.org/10.1080/00914037.2022.2075872>
12. Safari JB, Bapolisi AM, Krause RWM (2021) Development of pH-sensitive chitosan-g-poly (Acrylamide-co-acrylic acid) hydrogel for controlled drug delivery of tenofovir disoproxil fumarate. *Polymers* 13. <https://doi.org/10.3390/polym13203571>
13. El Sayed MM (2023) Production of Polymer Hydrogel Composites and Their Applications. *Journal of Polymers and the Environment* 31:2855–2879. <https://doi.org/10.1007/s10924-023-02796-z>
14. Thippeswamy M, Ganjeenahalli Puttagiddappa M, Thippaiah D, Satyanarayan ND (2021) Poly(acrylamide-co-acrylic acid) synthesized, moxifloxacin drug-loaded hydrogel: Characterization and evaluation studies. *Journal of Applied Pharmaceutical Science*. <https://doi.org/10.7324/JAPS.2021.1101205>

15. Ho TC, Chang CC, Chan HP, et al (2022) Hydrogels: Properties and Applications in Biomedicine. *Molecules* 27:1–29. <https://doi.org/10.3390/molecules27092902>
16. Sikdar P, Uddin MM, Dip TM, et al (2021) Recent advances in the synthesis of smart hydrogels. *Materials Advances* 2:4532–4573. <https://doi.org/10.1039/d1ma00193k>
17. Jacob S, Nair AB, Shah J, et al (2021) Emerging role of hydrogels in drug delivery systems, tissue engineering and wound management. *Pharmaceutics* 13. <https://doi.org/10.3390/pharmaceutics13030357>
18. Qureshi D, Nayak SK, Maji S, et al (2019) Environment sensitive hydrogels for drug delivery applications. *European Polymer Journal* 120:109220. <https://doi.org/10.1016/j.eurpolymj.2019.109220>
19. Ghumman SA, Noreen S, Hameed H, et al (2022) Synthesis of pH-Sensitive Cross-Linked Basil Seed Gum/Acrylic Acid Hydrogels by Free Radical Copolymerization Technique for Sustained Delivery of Captopril. *Gels* 8. <https://doi.org/10.3390/gels8050291>
20. Bai X, Bao Z, Bi S, et al (2018) Chitosan-Based Thermo/pH Double Sensitive Hydrogel for Controlled Drug Delivery. *Macromolecular Bioscience* 18:1–12. <https://doi.org/10.1002/mabi.201700305>
21. Meena P, Singh P, Warkar SG (2024) Fabrication and evaluation of stimuli-sensitive xanthan gum-based hydrogel as a potential carrier for a hydrophobic drug ibuprofen. *Colloid and Polymer Science* 302:377–391. <https://doi.org/10.1007/s00396-023-05198-8>
22. Mehta P, Sharma M, Devi M (2023) Hydrogels: An overview of its classifications, properties, and applications. *Journal of the Mechanical Behavior of Biomedical Materials* 147:106145. <https://doi.org/10.1016/j.jmbbm.2023.106145>

23. Bordbar-Khiabani A, Gasik M (2022) Smart Hydrogels for Advanced Drug Delivery Systems. *International Journal of Molecular Sciences* 23. <https://doi.org/10.3390/ijms23073665>
24. Aji Z, Maarouf M, Khattab A, Ghazal H (2020) Synthesis of pH-responsive hydrogel based on PVP grafted with crotonic acid for controlled drug delivery. *Radiation Physics and Chemistry* 170:108612. <https://doi.org/10.1016/j.radphyschem.2019.108612>
25. Tulain UR, Ahmad M, Rashid A, et al (2018) Fabrication of pH-Responsive Hydrogel and Its In Vitro and In Vivo Evaluation. *Advances in Polymer Technology* 37:290–304. <https://doi.org/10.1002/adv.21668>
26. Sharpe LA, Daily AM, Horava SD, Peppas NA (2014) Therapeutic applications of hydrogels in oral drug delivery. *Expert Opin Drug Delivery* 11:901–915. <https://doi.org/10.1517/17425247.2014.902047>
27. Ashames A, Ullah K, Al-Tabakha M, et al (2022) Development, characterization and In-vitro evaluation of guar gum based new polymeric matrices for controlled delivery using metformin HCl as model drug. *PLoS ONE* 17. <https://doi.org/10.1371/journal.pone.0271623>
28. Nawaz S, Khan S, Farooq U, et al (2018) Biocompatible hydrogels for the controlled delivery of anti-hypertensive agent: Development, characterization and in vitro evaluation. *Designed Monomers and Polymers* 21:18–32. <https://doi.org/10.1080/15685551.2018.1445416>
29. Fan R, Cheng Y, Wang R, et al (2022) Thermosensitive Hydrogels and Advances in Their Application in Disease Therapy 14:2379. <https://doi.org/10.3390/polym14122379>
30. Oral N, Basal G (2023) The effects of crosslinker ratio and photoinitiator type on the properties of pnipam hydrogel. *Journal of Polymer Research* 30:1–11. <https://doi.org/10.1007/s10965-022-03419-2>

31. Thirupathi K, Phan TTV, Santhamoorthy M, et al (2022) pH and Thermoresponsive PNIPAm-co-Polyacrylamide Hydrogel for Dual Stimuli-Responsive Controlled Drug Delivery. *Polymers* 15:167. <https://doi.org/10.3390/polym15010167>
32. Luo Y, Lu C, Zhang X, Zhan S (2023) Poly(N-isopropylacrylamide-co-maleic acid)/acylated chitosan thermosensitive hydrogels: preparation and properties. *Iranian Polymer Journal* 32:1189–1197. <https://doi.org/10.1007/s13726-023-01199-0>
33. Ahsan A, Farooq MA, Parveen A (2020) Thermosensitive chitosan-based injectable hydrogel as an efficient anticancer drug carrier. *ACS Omega* 5:20450–20460. <https://doi.org/10.1021/acsomega.0c02548>
34. Jing Z, Xu A, Liang YQ, et al (2019) Biodegradable poly(acrylic acid-co-acrylamide)/ poly(vinyl alcohol) double network hydrogels with tunable mechanics and high self-healing performance. *Polymers* 11. <https://doi.org/10.3390/polym11060952>
35. Sun S, Cui Y, Yuan B, et al (2023) Drug delivery systems based on polyethylene glycol hydrogels for enhanced bone regeneration. *Frontiers in Bioengineering and Biotechnology* 11:1–17. <https://doi.org/10.3389/fbioe.2023.1117647>
36. Jafari Jezeh A, Entezam M, Haghirsadat BF, et al (2023) Liposomal Nanocarriers-Loaded Poly(vinyl alcohol) (PVA)/Poly(ethylene glycol) (PEG) Hydrogels: Physico-mechanical Properties and Drug Release. *Journal of Polymers and the Environment* 31:5110–5125. <https://doi.org/10.1007/s10924-023-02932-9>
37. Jin X, Wei CX, Wu CW, Zhang W (2022) Customized Hydrogel for Sustained Release of Highly Water-Soluble Drugs. *ACS Omega* 7:8493–8497. <https://doi.org/10.1021/acsomega.1c06106>

38. Vigata M, Meinert C, Hutmacher DW, Bock N (2020) Hydrogels as drug delivery systems: A review of current characterization and evaluation techniques. *Pharmaceutics* 12:1–45. <https://doi.org/10.3390/pharmaceutics12121188>
39. Bhattacharyya R, Chowdhury P (2021) Hydrogels of Acryloyl guar gum-g-(acrylic acid-co-3sulfopropylacrylate) for high-performance adsorption and release of gentamicin sulphate. *Journal of Polymer Research* 28. <https://doi.org/10.1007/s10965-021-02633-8>
40. Suhail M, Wu PC, Minhas MU (2021) Development and characterization of pH-sensitive chondroitin sulfate-co-poly(acrylic acid) hydrogels for controlled release of diclofenac sodium. *Journal of Saudi Chemical Society* 25:101212. <https://doi.org/10.1016/j.jscs.2021.101212>
41. Munim SA, Raza ZA (2019) Poly(lactic acid) based hydrogels: formation, characteristics and biomedical applications. *Journal of Porous Materials* 26:881–901. <https://doi.org/10.1007/s10934-018-0687-z>
42. Balodhi D, Khushbu, Warkar SG, et al (2021) Natural carbohydrate gums based hydrogels. *Indian Journal of Chemical Technology* 28:262–273. <https://doi.org/10.56042/ijct.v28i3.44596>
43. Raza MA, Park SH (2020) Irradiated Ch/GG/PVP-based stimuli-responsive hydrogels for controlled drug release. *Journal of Applied Polymer Science* 137:49041. <https://doi.org/10.1002/app.49041>
44. Deng Y, Chen J, Huang J, et al (2020) Preparation and characterization of cellulose/flaxseed gum composite hydrogel and its hemostatic and wound healing functions evaluation. *Cellulose* 27:3971–3988. <https://doi.org/10.1007/s10570-020-03055-3>
45. Varghese SA, Rangappa SM, Siengchin S, Parameswaranpillai J (2019) Natural polymers and the hydrogels prepared from them. Elsevier Inc. 17-47.

46. Biswas MC, Jony B, Nandy PK, et al (2022) Recent Advancement of Biopolymers and Their Potential Biomedical Applications. *Journal of Polymers and the Environment* 30:51–74. <https://doi.org/10.1007/s10924-021-02199-y>
47. Baranwal J, Barse B, Fais A, et al (2022) Biopolymer: A Sustainable Material for Food and Medical Applications. *Polymers* 14. <https://doi.org/10.3390/polym14050983>
48. Thang NH, Chien TB, Cuong DX (2023) Polymer-Based Hydrogels Applied in Drug Delivery: An Overview. *Gels* 9:1–38. <https://doi.org/10.3390/gels9070523>
49. Shin Y, Kim D, Hu Y, Kim Y et al (2021) pH-Responsive Succinoglycan-Carboxymethyl Cellulose Hydrogels with Highly Improved Mechanical Strength for Controlled Drug Delivery Systems. *polymers*
50. Far BF, Naimi-Jamal MR, Safaei M, et al (2022) A Review on Biomedical Application of Polysaccharide-Based Hydrogels with a Focus on Drug Delivery Systems. *Polymers* 14:1–26. <https://doi.org/10.3390/polym14245432>
51. Rahmani S, Olad A, Rahmani Z (2022) Preparation of self-healable nanocomposite hydrogel based on Gum Arabic/gelatin and graphene oxide: study of drug delivery behavior. *Polymer Bulletin* 80:4117–4138. <https://doi.org/10.1007/s00289-022-04247-6>
52. Meena P, Singh P, Warkar SG (2023) Development and assessment of carboxymethyl tamarind kernel gum-based pH-responsive hydrogel for release of diclofenac sodium. *European Polymer Journal* 197:112340. <https://doi.org/10.1016/j.eurpolymj.2023.112340>
53. Sung YK (2020) Recent advances in polymeric drug delivery systems. *Biomaterials Research* 24. <https://doi.org/10.1186/s40824-020-00190-7>
54. Mahmood A, Patel D, Hickson B, et al (2022) Recent Progress in Biopolymer-Based Hydrogel Materials for Biomedical Applications. *International Journal*

- of Molecular Sciences 23. <https://doi.org/10.3390/ijms23031415>
55. Ways TMM, Lau WM, Khutoryanskiy V V. (2018) Chitosan and its derivatives for application in mucoadhesive drug delivery systems. *Polymers* 10. <https://doi.org/10.3390/polym10030267>
 56. Sanchez Armengol E, Grassiri B, Piras AM, et al (2024) Ocular antibacterial chitosan-maleic acid hydrogels: In vitro and in vivo studies for a promising approach with enhanced mucoadhesion. *International Journal of Biological Macromolecules* 254:127939. <https://doi.org/10.1016/j.ijbiomac.2023.127939>
 57. Kajal, Kumar R, Meena P, Warkar SG (2023) Development and characterization of pH-responsive CMTKG/PAM/PEG hydrogel for oral administration of etophylline. *Colloid and Polymer Science* 301:1313–1323. <https://doi.org/10.1007/s00396-023-05152-8>
 58. Tushar, Saraswat Y, Meena P, Warkar SG (2023) Synthesis and characterization of novel xanthan gum-based pH-sensitive hydrogel for metformin hydrochloride release. *Colloid and Polymer Science* 301:1147-1158. <https://doi.org/10.1007/s00396-023-05135-9>
 59. Meena P, Singh P, Warkar SG (2023) Fabrication and evaluation of stimuli - sensitive xanthan gum - based hydrogel as a potential carrier for a hydrophobic drug ibuprofen. *Colloid and Polymer Science* 302:377-391. <https://doi.org/10.1007/s00396-023-05198-8>
 60. Jana S, Banerjee A, Sen KK, Maiti S (2016) Gelatin-carboxymethyl tamarind gum biocomposites: In vitro characterization & anti-inflammatory pharmacodynamics. *Materials Science and Engineering C* 69:478–485. <https://doi.org/10.1016/j.msec.2016.07.008>
 61. Li S, Xiaowen Y, Yang Y, et al (2023) Osteogenic and anti-inflammatory effect of the multifunctional bionic hydrogel scaffold loaded with aspirin and nano-hydroxyapatite. *Frontiers in Bioengineering and Biotechnology* 11:1–16. <https://doi.org/10.3389/fbioe.2023.1105248>

62. Cuomo F, Cofelice M, Lopez F (2019) Rheological characterization of hydrogels from alginate-based nanodispersion. *Polymers* 11. <https://doi.org/10.3390/polym11020259>
63. Özakar SR, Özakar E (2021) The effect of polymer amount and crosslinker ratio in polymeric hydrogel beads on characterization. *Journal of Research in Pharmacy* 25:653–666. <https://doi.org/10.29228/jrp.57>
64. Afriani K, Sutanti Budikania T (2020) Synthesis and Characterization of Hydrogel of Chitosan-Poly (N-Vinyl-2-Pyrrolidone) (PVP)- Alginate for Ibuprofen Release. *The Journal of Pure and Applied Chemistry Research* 9:201–211. <https://doi.org/10.21776/ub.jpacr.2020.009.03.558>
65. Gao SK, Yin R, Wang XC, et al (2021) Structure characteristics, biochemical properties, and pharmaceutical applications of alginate lyases. *Marine Drugs* 19. <https://doi.org/10.3390/md19110628>
66. Abasalizadeh F, Moghaddam SV, Alizadeh E, et al (2020) Erratum: Alginate-based hydrogels as drug delivery vehicles in cancer treatment and their applications in wound dressing and 3D bioprinting. *Journal of Biological Engineering* 14:1–22. <https://doi.org/10.1186/s13036-020-00239-0>
67. Akalin GO (2023) Alginate/carboxymethylcellulose-based hydrogels as pH-sensitive drug delivery systems: facile production with enhanced degradation, thermal and mechanical properties. *Iranian Polymer Journal* 32:1013–1032. <https://doi.org/10.1007/s13726-023-01182-9>
68. Cikrikci S, Mert B, Oztop MH (2018) Development of pH Sensitive Alginate/Gum Tragacanth Based Hydrogels for Oral Insulin Delivery. *Journal of Agricultural and Food Chemistry* 66:11784–11796. <https://doi.org/10.1021/acs.jafc.8b02525>
69. Mansouri Shirazi N, Eslahi N, Gholipour-Kanani A (2021) Production and Characterization of Keratin/Tragacanth Gum Nanohydrogels for Drug Delivery

- in Medical Textiles. *Frontiers in Materials* 8:1–12. <https://doi.org/10.3389/fmats.2021.720385>
70. Abdi G, Jain M, Patil N, et al (2024) Tragacanth gum-based hydrogels for drug delivery and tissue engineering applications. *Frontiers in Materials* 11:1–21. <https://doi.org/10.3389/fmats.2024.1296399>
 71. Hanna DH, Saad GR (2019) Encapsulation of ciprofloxacin within modified xanthan gum- chitosan based hydrogel for drug delivery. *Bioorganic Chemistry* 84:115–124. <https://doi.org/10.1016/j.bioorg.2018.11.036>
 72. Li L, Zheng X, Pan C, et al (2021) A pH-sensitive and sustained-release oral drug delivery system: The synthesis, characterization, adsorption and release of the xanthan gum-graft-poly(acrylic acid)/GO-DCFP composite hydrogel. *RSC Advances* 11:26229–26240. <https://doi.org/10.1039/d1ra01012c>
 73. Suhail M, Chiu IH, Lai YR, et al (2023) Xanthan-Gum/Pluronic-F-127-Based-Drug-Loaded Polymeric Hydrogels Synthesized by Free Radical Polymerization Technique for Management of Attention-Deficit/Hyperactivity Disorder. *Gels* 9. <https://doi.org/10.3390/gels9080640>
 74. Buwalda SJ (2020) Bio-based composite hydrogels for biomedical applications. *Multifunctional Materials* 3. <https://doi.org/10.1088/2399-7532/ab80d6>
 75. Wani SUD, Zargar MI, Masoodi MH, et al (2022) Silk Fibroin as an Efficient Biomaterial for Drug Delivery, Gene Therapy, and Wound Healing. *International Journal of Molecular Sciences* 23. <https://doi.org/10.3390/ijms232214421>
 76. Singh V, Tripathi DK, Sharma VK, et al (2023) Silk fibroin hydrogel: A novel biopolymer for sustained release of vancomycin drug for diabetic wound healing. *Journal of Molecular Structure* 1286:135548. <https://doi.org/10.1016/j.molstruc.2023.135548>
 77. Xu Z, Tang E, Zhao H (2019) An Environmentally sensitive silk fibroin/chitosan hydrogel and its drug release behaviors. *Polymers*

2019;11:1980.

78. Moin A, Wani SUD, Osmani RA, et al (2021) Formulation, characterization, and cellular toxicity assessment of tamoxifen-loaded silk fibroin nanoparticles in breast cancer. *Drug Delivery* 28:1626–1636. <https://doi.org/10.1080/10717544.2021.1958106>
79. Tomeh MA, Hadianamrei R, Zhao X (2019) Silk Fibroin as a Functional Biomaterial for Drug and Gene Delivery. *Pharmaceutics* 1–22. <https://doi.org/10.3390/pharmaceutics11100494>
80. Naeem F, Khan S, Jalil A, et al (2017) pH Responsive cross-linked polymeric matrices based on natural polymers: Effect of process variables on swelling characterization and drug delivery properties. *BioImpacts* 7:177–192. <https://doi.org/10.15171/bi.2017.21>
81. Hariyanti, Erizal, Mustikarani E, et al (2022) In Vitro Release of Metformin HCl from Polyvinyl Alcohol (PVA) - Gelatin Hydrogels Prepared by Gamma Irradiation. *Atom Indonesia* 48:37–43. <https://doi.org/10.17146/aij.2022.1123>
82. Rafique N, Ahmad M, Minhas MU, et al (2022) Designing gelatin-based swellable hydrogels system for controlled delivery of salbutamol sulphate: characterization and toxicity evaluation. *Polymer Bulletin* 79:4535–4561. <https://doi.org/10.1007/s00289-021-03629-6>
83. Zhao X, Xi Y, Zhang Y, et al (2019) Redox-Sensitive Gelatin/Silica-Aptamer Nanogels for Targeted siRNA Delivery. *Nanoscale Research Letters* 14. <https://doi.org/10.1186/s11671-019-3101-0>
84. Yan S, Wu S, Zhang J, et al (2023) Controlled release of curcumin from gelatin hydrogels by the molecular-weight modulation of an oxidized dextran cross-linker. *Food Chemistry* 418:135966. <https://doi.org/10.1016/j.foodchem.2023.135966>
85. Singh B, Sharma K, Rajneesh, Dutt S (2020) Dietary fiber tragacanth gum based hydrogels for use in drug delivery applications. *Bioactive Carbohydrates and*

- Dietary Fibre 21:100208. <https://doi.org/10.1016/j.bcdf.2019.100208>
86. Sethi S, Saruchi, Kaith BS, et al (2020) Cross-linked xanthan gum–starch hydrogels as promising materials for controlled drug delivery. *Cellulose* 27:4565–4589. <https://doi.org/10.1007/s10570-020-03082-0>
 87. Suhail M, Khan A, Rosenholm JM, et al (2021) Fabrication and characterization of diclofenac sodium loaded hydrogels of sodium alginate as sustained release carrier. *Gels* 7:1–16. <https://doi.org/10.3390/gels7010010>
 88. Tan LS, Tan HL, Deekonda K, et al (2021) Fabrication of radiation cross-linked diclofenac sodium loaded carboxymethyl sago pulp/chitosan hydrogel for enteric and sustained drug delivery. *Carbohydrate Polymer Technologies and Applications* 2:100084. <https://doi.org/10.1016/j.carpta.2021.100084>
 89. Mali KK, Ghorpade VS, Dias RJ, Dhawale SC (2023) Synthesis and characterization of citric acid crosslinked carboxymethyl tamarind gum-polyvinyl alcohol hydrogel films. *International Journal of Biological Macromolecules* 236:123969. <https://doi.org/10.1016/j.ijbiomac.2023.123969>
 90. Badadare R, Mali K K, Dias R (2020) Citric Acid Crosslinked Hydrogel Dressings for Delivery of Metronidazole. *International Journal of Science and Research* 9:995–1005. <https://doi.org/10.21275/SR20514125011>
 91. Barleany DR, Ananta CV, Maulina F, et al (2020) Controlled release of metformin hydrogen chloride from stimuli-responsive hydrogel based on poly(N-Isopropylacrylamide)/Chitosan/Polyvinyl alcohol composite. *International Journal of Technology* 11:511–521. <https://doi.org/10.14716/ijtech.v11i3.2330>
 92. Raeisi A, Farjadian F (2024) Commercial hydrogel product for drug delivery based on route of administration. *Frontiers in Chemistry* 12:1–14. <https://doi.org/10.3389/fchem.2024.1336717>
 93. Adepu S, Seeram R (2021) Controlled Drug Delivery Systems : Current Status and. *Molecules* 26:5905. doi:10.3390/molecules26195905.

94. Maiz-Fernández S, Pérez-Álvarez L, Silván U, et al (2022) Dynamic and Self-Healable Chitosan/Hyaluronic Acid-Based In Situ-Forming Hydrogels. *Gels* 8:477. <https://doi.org/10.3390/gels8080477>
95. Lynch CR, Kondiah PPD, Choonara YE, et al (2020) Hydrogel Biomaterials for Application in Ocular Drug Delivery. *Frontiers in Bioengineering and Biotechnology* 8:1–18. <https://doi.org/10.3389/fbioe.2020.00228>
96. Sami AJ, Khalid M, Jamil T, et al (2018) Formulation of novel chitosan guar gum based hydrogels for sustained drug release of paracetamol. *International Journal of Biological Macromolecules* 108:324–332. <https://doi.org/10.1016/j.ijbiomac.2017.12.008>
97. Wang XH, Su T, Zhao J, et al (2020) Fabrication of polysaccharides-based hydrogel films for transdermal sustained delivery of Ibuprofen. *Cellulose* 27:10277–10292. <https://doi.org/10.1007/s10570-020-03503-0>
98. Yuan N, Xu L, Wang H, et al (2016) Dual Physically Cross-Linked Double Network Hydrogels with High Mechanical Strength, Fatigue Resistance, Notch-Insensitivity, and Self-Healing Properties. *ACS Applied Materials and Interfaces* 8:34034–34044. <https://doi.org/10.1021/acsami.6b12243>
99. Kim MH, Nguyen DT, Kim DD (2022) Recent studies on modulating hyaluronic acid-based hydrogels for controlled drug delivery. *Journal of Pharmaceutical Investigation* 52:397–413. <https://doi.org/10.1007/s40005-022-00568-w>
100. Migdadi EM, Courtenay AJ, Tekko IA, et al (2018) Hydrogel-forming microneedles enhance transdermal delivery of metformin hydrochloride. *Journal of Controlled Release* 285:142–151. <https://doi.org/10.1016/j.jconrel.2018.07.009>
101. Malik NS, Ahmad M, Minhas MU, et al (2020) Chitosan/Xanthan Gum Based Hydrogels as Potential Carrier for an Antiviral Drug: Fabrication,

- Characterization, and Safety Evaluation. *Frontiers in Chemistry* 8:1–16. <https://doi.org/10.3389/fchem.2020.00050>
102. Singh B, Sharma S, Dhiman A (2017) Acacia gum polysaccharide based hydrogel wound dressings: Synthesis, characterization, drug delivery and biomedical properties. *Carbohydrate Polymers* 165:294–303. <https://doi.org/10.1016/j.carbpol.2017.02.039>
 103. Huling J, Oschatz S, Lange H, et al (2024) γ -Cyclodextrin hydrogel for the sustained release of josamycin for potential ocular application. *Drug Delivery* 31. <https://doi.org/10.1080/10717544.2024.2361168>
 104. Ahmad U, Sohail M, Ahmad M, et al (2019) Chitosan based thermosensitive injectable hydrogels for controlled delivery of loxoprofen: development, characterization and in-vivo evaluation. *International Journal of Biological Macromolecules* 129:233–245. <https://doi.org/10.1016/j.ijbiomac.2019.02.031>
 105. Singh B, Varshney L, Francis S, Rajneesh (2017) Synthesis and characterization of tragacanth gum based hydrogels by radiation method for use in wound dressing application. *Radiation Physics and Chemistry* 135:94–105. <https://doi.org/10.1016/j.radphyschem.2017.01.044>
 106. Suhail M, Hsieh YH, Khan A, et al (2021) Preparation and in vitro evaluation of aspartic/alginate based semi-interpenetrating network hydrogels for controlled release of ibuprofen. *Gels* 7:. <https://doi.org/10.3390/gels7020068>
 107. Shafiq K, Mahmood A, Salem-Bekhit MM, et al (2022) Development and Optimization of Tamarind Gum- β -Cyclodextrin-g-Poly(Methacrylate) pH-Responsive Hydrogels for Sustained Delivery of Acyclovir. *Pharmaceuticals* 15. <https://doi.org/10.3390/ph15121527>
 108. Ghorpade VS, Yadav AV, Dias RJ, et al (2018) Citric acid crosslinked carboxymethylcellulose-poly(ethylene glycol) hydrogel films for delivery of poorly soluble drugs. *International Journal of Biological Macromolecules* 118:783–791. <https://doi.org/10.1016/j.ijbiomac.2018.06.142>

109. Mohan A, Santhamoorthy M, Phan TTV, Kim S-C (2024) pNIPAm-Based pH and Thermoresponsive Copolymer Hydrogel for Hydrophobic and Hydrophilic Drug Delivery. *Gels* 10:184. <https://doi.org/10.3390/gels10030184>
110. Larrañeta E, Stewart S, Ervine M, et al (2018) Hydrogels for Hydrophobic Drug Delivery. Classification, Synthesis and Applications. *Journal of Functional Biomaterials* 13:2018. <https://doi.org/10.3390/jfb9010013>
111. Gulhane CA, Parbat AY, Tayade GP, et al (2021) Injectable Hydrogels, a New Drug Delivery System: Mechanism, Application and Future Perspectives. *Gels* 21:313–326
112. Zhao W, Zhu Y, Zhang J, et al (2018) A comprehensive study and comparison of four types of zwitterionic hydrogels. *Journal of Materials Science* 53:13813–13825. <https://doi.org/10.1007/s10853-018-2535-6>
113. Khan R, Zaman M, Salawi A, et al (2022) Synthesis of Chemically Cross-Linked pH-Sensitive Hydrogels for the Sustained Delivery of Ezetimibe. *Gels* 8. <https://doi.org/10.3390/gels8050281>
114. Nguyen TTH, Nguyen LTTN, Ha AC et al (2023) Evaluation of Ibuprofen Prolonged Release of Biomedical PLA-PEG-PLA. *International Journal of Biomaterials*. 2023. doi: 10.1155/2023/5005316
115. Kiran, Tiwari R, Singh VK, et al (2020) Synthesis, characterization of β -CD based novel hydrogels with dual objectives of drug release and dye removal. *Iranian Polymer Journal* 29:615–623. <https://doi.org/10.1007/s13726-020-00826-4>
116. Hao PY, Zhou HY, Ren LJ, et al (2023) Preparation and antibacterial properties of curcumin-loaded cyclodextrin-grafted chitosan hydrogel. *Journal of Sol-Gel Science and Technology* 106:877–894. <https://doi.org/10.1007/s10971-023-06097-8>

117. Das D, Das R, Mandal J, et al (2014) Dextrin crosslinked with poly(lactic acid): A novel hydrogel for controlled drug release application. *Journal of Applied Polymer Science* 131:1–12. <https://doi.org/10.1002/app.40039>
118. Shahid N, Erum A, Zaman M, et al (2021) Ph-responsive nanocomposite based hydrogels for the controlled delivery of ticagrelor; in vitro and in vivo approaches. *International Journal of Nanomedicine* 16:6345–6366. <https://doi.org/10.2147/IJN.S330186>
119. Gholamali I, Hosseini SN, Alipour E (2021) Doxorubicin-loaded oxidized starch/poly (vinyl alcohol)/CuO bio-nanocomposite hydrogels as an anticancer drug carrier agent. *International Journal of Polymeric Materials and Polymeric Biomaterials* 70:967–980. <https://doi.org/10.1080/00914037.2020.1767616>
120. Gholamali I, Alipour E (2020) Carboxymethyl Chitosan/Starch/CuO Nanocomposite Hydrogels for Controlled Release of Amoxicillin. *Regenerative Engineering and Translational Medicine* 6:398–406. <https://doi.org/10.1007/s40883-020-00173-z>
121. Madduma-Bandarage USK, Madihally S V. (2021) Synthetic hydrogels: Synthesis, novel trends, and applications. *Journal of Applied Polymer Science* 138:1–23. <https://doi.org/10.1002/app.50376>
122. Niu B, Jia J, Wang H, et al (2019) In vitro and in vivo release of diclofenac sodium-loaded sodium alginate/carboxymethyl chitosan-ZnO hydrogel beads. *International Journal of Biological Macromolecules* 141:1191–1198. <https://doi.org/10.1016/j.ijbiomac.2019.09.059>
123. Namazi H, Pooresmaeil M, Hasani M (2021) Oxidized starch/CuO bio-nanocomposite hydrogels as an antibacterial and stimuli-responsive agent with potential colon-specific naproxen delivery. *International Journal of Polymeric Materials and Polymeric Biomaterials* 70:1296–1305. <https://doi.org/10.1080/00914037.2020.1798431>

CHAPTER 2

FABRICATION AND CHARACTERIZATION OF CARBOXYMETHYL TAMARIND KERNEL GUM-BASED HYDROGEL FOR THE RELEASE OF DICLOFENAC SODIUM

2.1 Introduction

During recent decades, development of drug delivery systems, particularly those that can respond to environmental stimuli, often referred to as "smart or stimuli delivery vehicles", has garnered significant interest amongst researchers around the world. A drug delivery system (DDS) aims to enhance the release performance of therapeutic agents by improving crucial properties of drugs i.e. solubility, stability, specificity, efficacy, etc [1]. Till date, various materials have been investigated in the field of drug delivery, including nano-scale materials (nano-capsules, dendrimers, nanotubes, nano gels) [2-3], inorganic-based DDS (layer double hydroxide, graphene oxide, metal oxides) [1], [4-5] and bioactive polymers (hyaluronic acid, collagen, etc) [6]. But still the traditional drug delivery systems face several challenges, including poor bioavailability, limited biocompatibility, elevated toxicity, rapid drug release, and insufficient hydrophilicity, leading to lowered drug delivery efficiency. To overcome these challenges associated with use of traditional DDS, controlled drug delivery systems based on hydrogels have been focused owing to their easily tunable properties

during synthesis, followed by controlled release, degradation and efficiency to protect labile drugs [7], [8].

Moreover, one of the most remarkable properties of hydrogel, particularly smart or stimuli-sensitive hydrogels is their ability to change their volume in response to changes in physical and chemical stimuli such as pH, light, magnetic field, temperature, enzyme, ionic strength, etc. The pH is one of the most promising stimulants in drug delivery applications [9], [10]. Numerous research has been carried out in the past few decades to fabricate pH-sensitive hydrogel using various synthetic polymers such as polyethylene glycol [11], polyacrylamide [12], poly (vinyl alcohol) [13], etc.

Polyacrylamide (PAM) is among the most commonly used pH-sensitive polymers in drug delivery applications, known for its non-toxicity and excellent mechanical strength. It contains a cationic amine functional group that either protonates or deprotonates to show variation in swelling with change in pH [12], [14]. However, PAM exhibits several disadvantages, such as lesser biocompatibility, low biodegradability, lesser hydrophilicity, etc. To overcome these limitations of PAM-based hydrogels, researchers have incorporated biopolymers into the drug delivery system [15]. Risbud et al. (2000) fabricated chitosan/PAM hydrogels to control the release of amoxicillin [16]. Raghavendra et al. (2008) developed polyacrylamide - grafted-xanthan hydrogels and studied the transdermal delivery of ketoprofen [17]. The introduction of biopolymers imparts efficient drug release and also enhances the hydrophilicity, biodegradability, and biocompatibility of synthesized hydrogel [9].

An example of such a biopolymer is CMTKG. As mentioned earlier, this water-soluble polymer responds to changes in pH, where the COO^- groups undergo deprotonation or protonation, leading to pH-dependent drug delivery [18], [19], [20-22]. Moreover, hydrogels are commonly utilized for the delivery of hydrophilic drugs due to their hydrophilic nature [23]. To increase the compatibility of hydrophobic drugs with the polymer matrix, either the polymers capable of the formation of inclusion complexes, such as cyclodextrin, are introduced, or various hydrophobic components are incorporated into the hydrogels [25].

PVP is a non-toxic, biocompatible, and pH-sensitive polymer mainly used for drug delivery applications. It is an amphiphilic polymer containing a pyrrolidone ring, C=O, C-N, and CH_2 as a hydrophilic component and an alkyl group as a hydrophobic part. The hydrophobic component of PVP interacts with the hydrophobic drug and increases drug loading capacity. Therefore, PVP is employed to deliver hydrophilic, hydrophobic, as well as sparingly soluble drugs such as amoxicillin [24], acyclovir [25], diclofenac sodium [26], etc. Diclofenac sodium (DS) is a widely used nonsteroidal anti-inflammatory drug (NSAID) known for its effectiveness in relieving pain, reducing inflammation, and lowering fever. It is the sodium salt of o-(2,6-dichloro phenylamino)-phenylacetic acid, and its antipyretic, analgesic, and anti-inflammatory actions help to treat rheumatoid arthritis and osteoarthritis. It works by inhibiting the activity of cyclooxygenase enzymes, which play a crucial role in the synthesis of prostaglandins that mediate inflammation and pain. By blocking these enzymes, diclofenac reduces the levels of prostaglandins, leading to decrease

inflammation and relief from pain. The drug has a relatively short half-life of about 1 to 2 hrs, which means it is quickly metabolized and eliminated from the body. This necessitates multiple dosing throughout the day for effective pain management. As a result, numerous doses of DS are required to provide sustained pharmacological action which causes unfavorable side effects such as ulcers and gastrointestinal bleeding. Therefore, a novel delivery system for DS release is required to decrease the complications and to ensure the site-specific delivery of sparingly-soluble DS drug [27].

Thus, the CMTKG/PVP/PAM-based hydrogel was synthesized and loaded with DS to obtain smart pH-responsive hydrogels for site-specific release of DS. The synthesized hydrogel was characterized using ATR-FTIR, SEM, and PXRD techniques. The impact of amounts of CMTKG, KPS, or MBA on swelling was also examined for all DS-loaded hydrogels using pH 1.2 and 7.4 buffer. A sol-gel fraction study, porosity, degradation and cytotoxicity analysis were performed on the synthesized hydrogel. The work also emphasizes the *in vitro* release of DS to estimate the DS release %. To contemplate the drug release mechanism, various kinetic models like Zero-Order, Hixson-Crowell, Higuchi, Korsmeyer-Peppas, and First-Order were employed. Additionally, all experiments were conducted in triplicate, with the standard deviations shown as error bars in the graphs.

2.2 Experimental Section

2.2.1 Materials

Acrylamide (MW=71.08 g/mol, CDH, New Delhi), Polyvinylpyrrolidone K-30

(MW= 4×10^4 g/mol, CDH, New Delhi), Potassium persulphate (MW=270.30 g/mol, Fischer Scientific, Mumbai), and N, N'-methylenebis(acrylamide) (MW=154.16 g/mol, Merck, Germany), were used as supplied. Carboxymethyl Tamarind Kernel Gum (0.20° of substitution, MW= 9.14×10^5 g/mol) was gratefully provided by Hindustan Gum and Chemicals Ltd., Haryana, India and diclofenac sodium (MW=318.1 g/mol), was provided by Unicare India Pvt Ltd, Noida, India.

2.2.2 Synthesis of CMTKG/PVP/PAM hydrogel and DS-loaded hydrogels

The novel hydrogel based on CMTKG, PVP, and AM was synthesized using a free radical mechanism by employing KPS (initiator) and MBA (cross-linker), shown in Fig. 2.1. The reaction was typically carried out by dissolving the desired quantity of CMTKG, AM, and PVP in distilled water on a magnetic stirrer for 1hr. To the resultant solution, KPS and MBA were added and stirred. Later, the solution was transferred into 20 ml test tubes and placed in a water bath at 60°C for 1 hour. The obtained hydrogel was cut into discs, dried at room temperature, and then in the oven at 60°C till a persistent weight was attained [29]. For the synthesis of DS-loaded hydrogels, during the addition of KPS and MBA, a solution of diclofenac sodium dissolved in ethanol was added to the mixture; the rest of the procedure followed the same as above [30]. Table 2.1 summarizes the exact reagent amounts required for hydrogel synthesis.

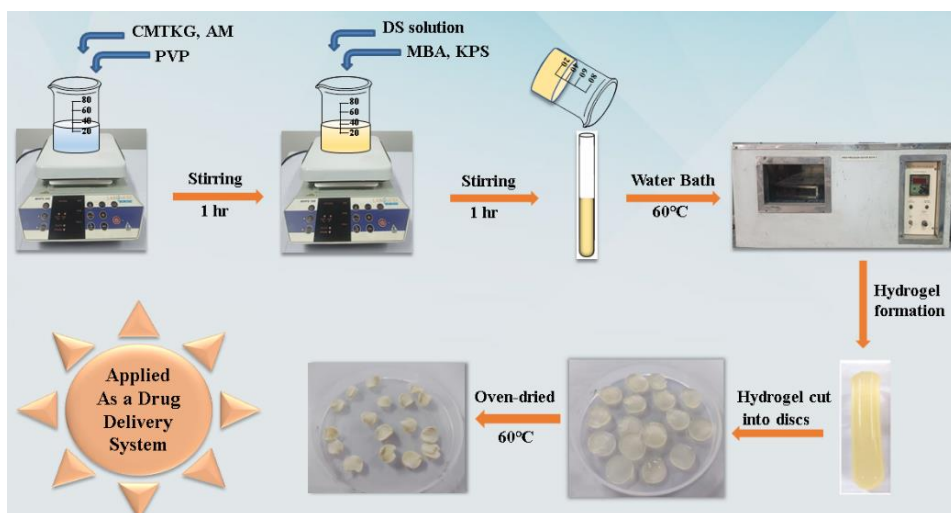


Fig. 2.1 Pictorial representation of the fabrication of DS-loaded CMTKG/PVP/PAM hydrogel

Table 2. 1 Amounts of reagents required in the synthesis of the hydrogels

Sample code	CMTKG (g)	AM (g)	PVP (g)	MBA (mg)	KPS (mg)	DS (mg)
A-1	0.20	2.5	0.1	17	35	50
A-2	0.25	2.5	0.1	17	35	50
A-3	0.30	2.5	0.1	17	35	50
A-4	0.35	2.5	0.1	17	35	50
A-5	0.40	2.5	0.1	17	35	50
A-6	0.40	2.5	0.1	17	45	50
A-7	0.40	2.5	0.1	17	40	50
A-8	0.40	2.5	0.1	17	30	50
A-9	0.40	2.5	0.1	17	25	50
A-10	0.40	2.5	0.1	27	35	50
A-11	0.40	2.5	0.1	37	35	50
A-12	0.40	2.5	0.1	47	35	50
A-13	0.40	2.5	0.1	57	35	50
A-14	0.40	2.5	00	17	35	50
A-15	0.40	2.5	0.1	17	35	0

2.2.3 Characterization

PXRD was recorded using a Bruker D8 diffractometer within the 2θ range of 5-70° using Cu K α radiation. The ATR-FTIR analysis was done by an ATR-FTIR spectrophotometer (Model: PerkinElmer spectrum 2) within the wavenumber range from 450-4000 cm⁻¹. The surface morphology was investigated using SEM (Model: JEOL Japan Mode: JSM 6610LV).

2.2.4 Swelling studies

Gravimetric analysis was carried out to analyse the swelling nature of the prepared DS-loaded hydrogels. First, dried hydrogels were weighed (W_D) and soaked in pH 1.2 and 7.4 buffer solutions. After a regular interval, the swollen hydrogel disc was taken out, surface water was wiped using filter paper, and again, weight (W_S) was noted [27]. The study was carried out in triplicate, and the swelling & equilibrium swelling was computed using the given Eqn. (2.1) and Eqn. (2.2).

$$\text{Swelling (\%)} = \frac{W_S - W_D}{W_D} \times 100 \quad (2.1)$$

$$\text{Equilibrium Swelling (\%)} = \frac{W_E - W_D}{W_D} \times 100 \quad (2.2)$$

Here, W_E refers to the weight of the hydrogel at equilibrium [31].

2.2.5 Sol-Gel analysis

Sol-gel analysis was done to discover the uncross-linked portion of the synthesized DS-loaded hydrogel. A gel is the insoluble cross-linked portion of a hydrogel, and a sol implies the soluble uncross-linked portion of a hydrogel [27]. For this analysis, the dried extracted hydrogel disc was dried at 50°C in an oven till persistent weight

(W_F) was attained [32]. The sol and gel fraction calculation was performed using the following Eqn. (2.3) and Eqn. (2.4).

$$\text{Sol Fraction} = \frac{W_i - W_F}{W_F} \times 100 \quad (2.3)$$

$$\text{Gel fraction} = 100 - \text{Sol fraction} \quad (2.4)$$

2.2.6 Porosity

The porosity of the synthesized hydrogels was evaluated using the solvent displacement method. In this process, pre-weighed dried hydrogel discs (A_i) were submerged in 5 ml of hexane for 2 hr. After immersion, the discs were removed, gently blotted with filter paper, and reweighed (A_f) [33]. The porosity (%) was calculated using Eqn. (2.5).

$$\text{Porosity (\%)} = \frac{A_f - A_i}{\rho V} \times 100 \quad (2.5)$$

Here, ρ represents the density of hexane, and V denotes the volume of the hydrogel disc [34].

2.2.7 Drug Loading and Drug Entrapment Efficiency

The ideal candidate, hydrogel A-5, was selected for drug loading and entrapment studies on account of its highest swelling. The effect of PVP (amphiphilic polymer) on drug loading & entrapment efficiency was established by comparing formulation A-5 (DS-loaded CMTKG/PVP/PAM) that contains PVP to formulation A-14 (DS-loaded CMTKG/PAM) hydrogel, which lacks PVP. The drug loading (DL %) & entrapment efficiency (DEE %) were determined by placing the pre-weighed

hydrogels (0.1 g) into a physiological buffer of pH 7.4 for 24 hr. The solution was withdrawn after 24 hr, and absorbance was noted at 276 nm with a UV-visible spectrophotometer (Model: Cary 300 UV-Vis). The amount of DS was estimated using a calibration curve. The below Eqn. (2.6) and Eqn. (2.7) were used to establish the percent of drug loading and drug entrapment efficiency [35].

$$DL (\%) = \frac{\text{Drug amount in hydrogel}}{\text{Weight of hydrogel disc}} \times 100 \quad (2.6)$$

$$DEE (\%) = \frac{\text{Drug amount in hydrogel}}{\text{Theoretical Drug amount in hydrogel disc}} \times 100 \quad (2.7)$$

2.2.8 In vitro DS release study

In vitro release analysis of DS was accomplished at physiological pH of 7.4 and 1.2 using DS-loaded CMTKG/PVP/PAM and DS-loaded CMTKG/PAM hydrogel to study the impact of the incorporation of PVP on drug release. The release study was done in an orbital incubator shaker by immersing 0.1g of the DS-loaded hydrogel disc into 100 mL buffer of pH 1.2 and 7.4 at 37 °C, respectively [35]. After 1hr, a 3mL sample was extracted, and an equal amount of fresh buffer was made up. Absorbance was recorded on a UV-visible spectrophotometer at λ_{max} 276 nm for pH 7.4 and λ_{max} 274 nm for Ph 1.2. The study was performed in triplicate, and the drug content was evaluated using a calibration curve [36]. The Eqn. (2.8) was employed to calculate the drug release.

$$\text{Cumulative drug release} \left(\frac{M_t}{M_\infty} \right) = \frac{V_t C_t + V_W \sum_{1}^{n-1} C_{t-1}}{M_\infty} \quad (2.8)$$

Here, M_t represents the amount of drug released at time t , M_∞ is the total amount of drug loaded, V_t denotes the total volume of release medium, V_W refer to the volume of solution withdrawn, C_t and C_{t-1} refers to the concentration of solution at time t and $t-1$ [37].

2.2.9 Release kinetics studies

Several mathematical models, such as the Zero-Order, Hixson-Crowell, Higuchi, Korsmeyer-Peppas, and First-Order, were used to identify the drug's release mechanism. The release data were fitted to all the models mentioned above, and regression coefficient (R^2) values were compared. The R^2 value must be closer to 1 for the model to be considered the best-fit model [38].

2.2.10 Cytotoxicity

The effect of DS-loaded CMTKG/PVP/PAM hydrogel (A-5) on the HCT 116 human colon cell line purchased from NCCS Pune, was investigated using the MTT Assay. Cells were seeded at a density of 10,000 cells per well in a 96-well plate containing DMEM medium with 10% FBS and 1% antibiotic solution and incubated at 37 °C with 5% CO₂ for 24 hours. The cells were then exposed to varying hydrogel concentrations (0.78 to 6.25 µg/ml), with control wells containing no hydrogel. After 24-hour incubation, MTT solution was added and incubated for 2 hours. The supernatant was discarded, and the cells were dissolved in 100 µl of DMSO. Absorbance was measured at 540 nm and 660 nm using an Elisa plate reader (iMark, Biorad, USA), and images were taken under an inverted microscope with a 10 MP Aptima CMOS digital camera [39].

The cell viability (%) was calculated using Eqn. (2.9).

$$\text{Cell viability (\%)} = \frac{\text{Total cells} - \text{dead cells}}{\text{Total cells}} \times 100 \quad (2.9)$$

2.2.11 Degradation

Degradation experiments were conducted in a pH 7.4 buffer (simulated intestinal fluid) using an orbital incubator shaker maintained at 37 °C over 20 days. Hydrogel discs were first immersed in the buffer until they reached equilibrium, and their weight was recorded as (A_{IH}). Subsequently, the discs were removed every 2 days, gently blotted with filter paper, weighed as (A_{FH}), and then returned to the buffer [39]. The degradation (%) was calculated using Eqn. (2.10).

$$\text{Degradation (\%)} = \frac{A_{IH} - A_{FH}}{A_{IH}} \times 100 \quad (2.10)$$

2.3 Results and Discussions

2.3.1 Mechanistic pathway followed for the formation of DS-loaded CMTKG/PVP/PAM hydrogel

The details of various combinations (A-1 to A-13) of DS-loaded hydrogels attempted using a variable concentration of CMTKG, KPS, and MBA are given in Table 2.1. Here, KPS was used as an initiator, MBA was used as a cross-linker, and drug DS was loaded into the hydrogel. All the samples were fabricated with a varied amount of CMTKG (A-1 to A-5), KPS (A-6 to A-9), or MBA (A-10 to A-13). The mechanism involved during synthesis for hydrogel formation has been shown in Fig 2.2. In the reaction, at first, the sulphate radical was formed by the decomposition of KPS (initiator) at 60°C, which further leads to the polymerization of AM. While the MBA

acts as a cross-linker, it helps in the formation of a crosslinked polymeric network based on CMTKG, PAM, and PVP. The hydrophobic interaction between the the alkyl group of PVP and the aryl ring of DS, along with hydrogen bonding between the pyrrolidone ring of PVP and DS, results in the synthesis of a tri-dimensional network of DS-loaded CMTKG/PVP/PAM hydrogel.

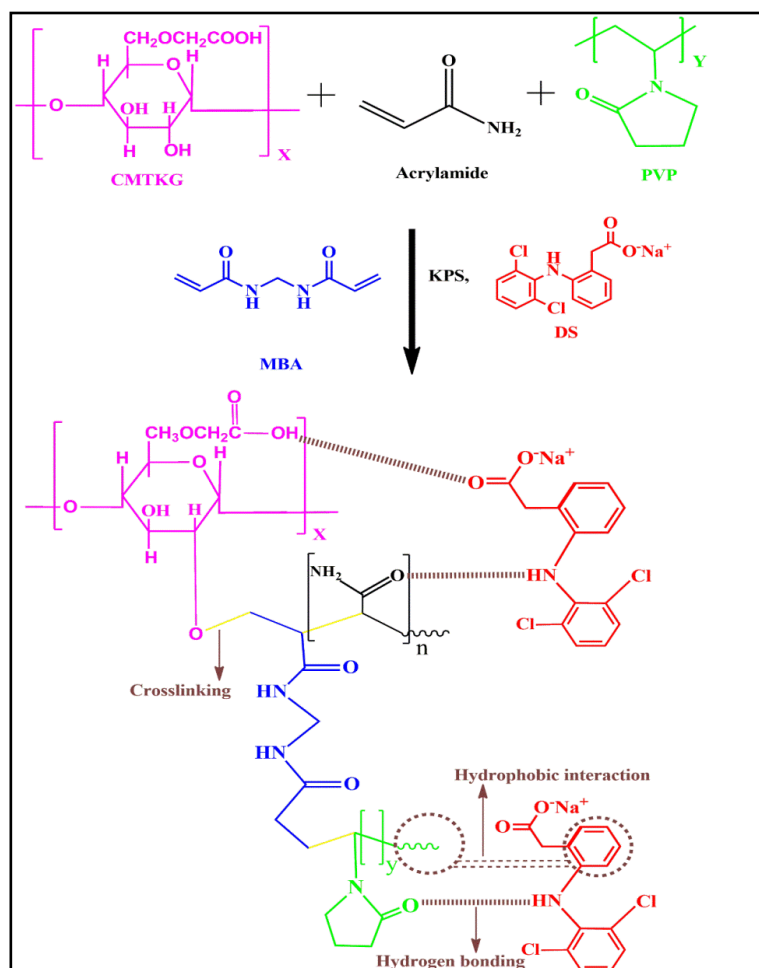


Fig. 2.2 Proposed mechanism for synthesis of DS-loaded CMTKG/PVP/PAM hydrogel

2.3.2 Characterization

PXRD was done to examine the crystallinity nature of hydrogel and the dispersion of the drug into the hydrogel matrix, as shown in Fig. 2.3. DS shows its characteristic peak at 2θ values of 6.2, 6.7, 8.6, 11.3, 15.2, 17.2, 20.3, 27.1, and 37.9. The sharp peaks in the DS reveal the crystallinity nature of the drug. However, the broad peak for CMTKG/PVP/PAM hydrogel indicated that the hydrogel disc was amorphous and showed no long crystallographic order [31]. In the diffractogram of DS-loaded CMTKG/PAM/PVP hydrogel, no characteristic peak of DS was observed, indicating uniform dispersion of DS in polymeric matrices. The increase in peak intensity was observed for DS-loaded hydrogel compared to unloaded hydrogel, which implies that the drug was effectively entrapped within the amorphous hydrogel matrices [27].

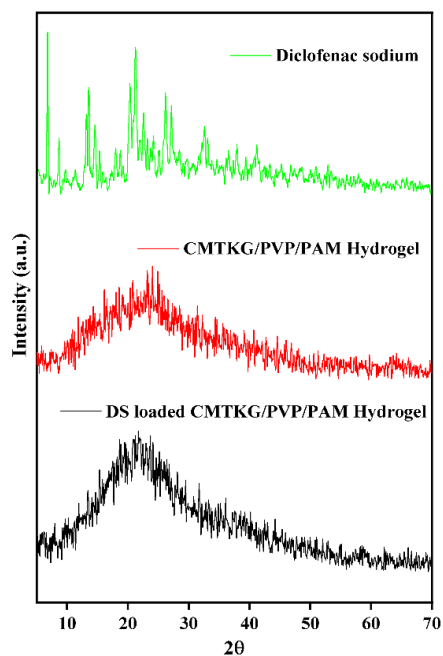


Fig. 2.3 PXRD pattern of DS, CMTKG/PVP/PAM hydrogel (A-15), DS-loaded CMTKG/PVP/PAM hydrogel (A-5)

The SEM images of CMTKG/PVP/PAM (A-15) hydrogel and DS-loaded CMTKG/PVP/PAM (A-5) hydrogel are displayed in Fig. 2.4. The micrographs of CMTKG/PVP/PAM hydrogel reveal uneven surface morphology, and porous structure, indicating good water retention, and drug loading capacity of the hydrogel. However, micrographs of DS-loaded CMTKG/PVP/PAM hydrogel show a smooth surface with fewer pores. Hence, the drug got incorporated into the hydrogel matrix, therefore lesser interstitial void remains in the hydrogel [25].

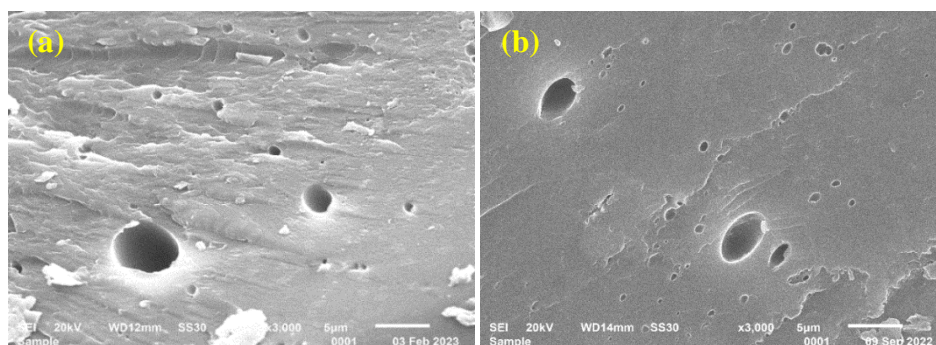


Fig. 2.4 SEM image of (a) CMTKG/PVP/PAM hydrogel, (b) DS-loaded CMTKG/PVP/PAM hydrogel

ATR-FTIR spectrum of CMTKG, AM, MBA, CMTKG/PVP/PAM (A-15), DS-loaded CMTKG/PVP/PAM (A-5) hydrogels and DS are presented in Fig. 2.5. In the FTIR spectra of AM and MBA, the =C-H wagging peaks at 960 cm^{-1} and 989 cm^{-1} , disappeared in both CMTKG/PVP/PAM and DS-loaded CMTKG/PVP/PAM hydrogel, confirming the polymerization and cross-linking [29]. This concludes that crosslinked CMTKG/PVP/PAM hydrogel has been successfully synthesized. In DS-loaded CMTKG/PVP/PAM, the new characteristic peak of DS was noticed at 702 cm^{-1} .

This signifies that the drug was successfully encapsulated into the hydrogel matrix. There was no appearance of additional peaks other than the drug noticed in DS-loaded hydrogel compared to unloaded hydrogel, which concludes that no chemical interaction exists, only physical interaction (hydrogen bonding) took place between the drug and poly network [31].

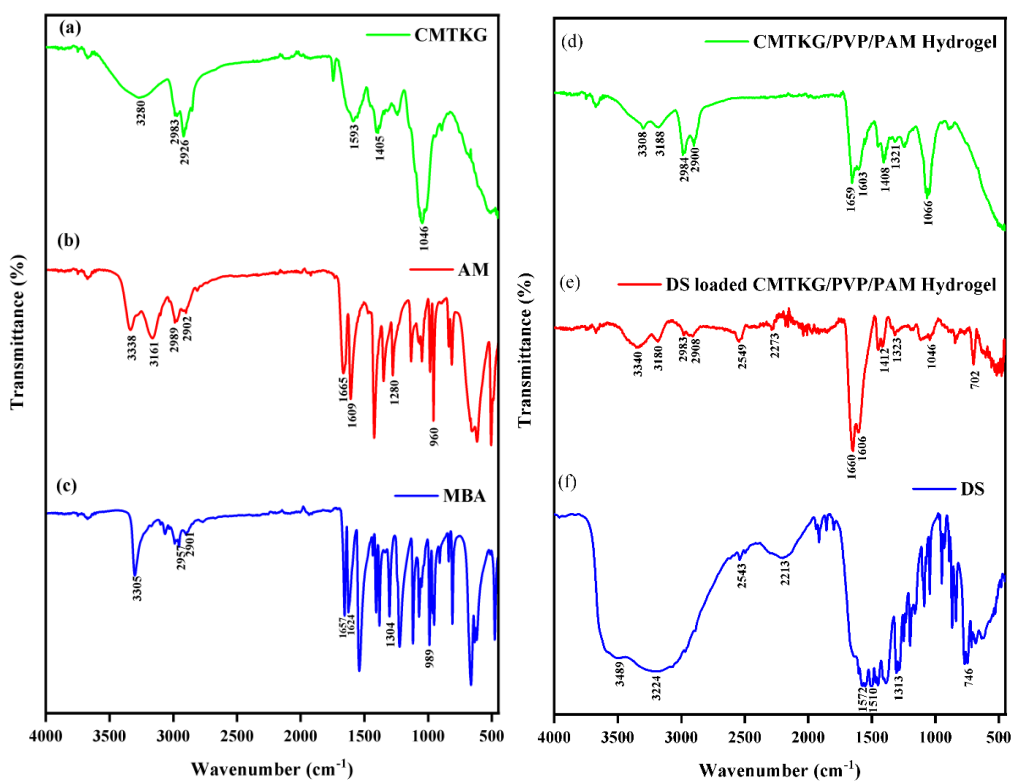


Fig. 2.5 ATR-FTIR spectrum of (a) CMTKG, (b) AM, (c) MBA, (d) CMTKG/PVP/PAM hydrogel, and (e) DS-loaded CMTKG/PVP/PAM hydrogel, and (f) DS

2.3.3 Swelling Studies

The swelling of all DS-loaded hydrogels was examined using pH 1.2 and 7.4 buffers with varying amounts of CMTKG, KPS, or MBA.

2.3.3.1 Impact of biopolymer

The impact of concentrations of the CMTKG (biopolymer) on the swelling is presented in Fig. 2.6 (a). The hydrogel swelling increases with an increase in the amount of CMTKG from 0.2 to 0.4 g. Maximum swelling of about 1128 ± 0.73 % was noticed at pH 7.4, while at pH 1.2, 967 ± 0.65 % swelling was recorded at 0.40 g of CMTKG. This may be associated with a greater number of carboxylate ions as the amount of CMTKG increases. The repulsion of carboxylate ion triggers chain relaxation, and as a consequence, swelling increases. However, attempts were made to process hydrogel with a concentration of CMTKG greater than 0.40 g, but the solution became highly viscous and was challenging to stir [20].

2.3.3.2 Impact of Initiator

Since the maximum swelling was observed at a biopolymer amount of 0.40 g, therefore it was kept constant. At the same time, the impact of altering the KPS concentration is shown in Fig. 2.6 (b). As the KPS amount was elevated, the swelling percentage increased to a certain limit, and later, an increase in the KPS amount led to decreased water absorption capacity. At 35 mg of an initiator, maximum swelling of about 1128 ± 0.73 % was noticed in pH 7.4, while in pH 1.2, 967 ± 0.65 % swelling was reported. For the amount of KPS below 35 mg, the swelling was found to be decreased. This may be the consequence of a large quantity of unreacted soluble monomer,

leading to a weak hydrogel network and reducing the swelling. When the amount of KPS was increased beyond 35 mg, swelling decreased again because of the high collision between the free radicals. It leads to oligomer formation and increased cross-linking density; as a result, swelling decreases [20].

2.3.3.3 Impact of cross-linker

According to Flory's network theory, one of the significant factors that influence hydrogel swelling is cross-linking density. A slight variation in the cross-linker amount causes substantial changes in the swelling percentage, as presented in Fig. 2.6 (c). Maximum swelling of about $1128 \pm 0.73\%$ was noticed at pH 7.4. While at pH 1.2, maximum swelling of about $967 \pm 0.65\%$ was reported at 17 mg of a cross-linker. When the amount of MBA was less than 17 mg, it was found that a jelly-like substance was produced due to a lack of a strong cross-linked network between polymeric chains [20]. The hydrogel swelling ratio decreased when the MBA concentration varied from 17 to 57 mg. A higher cross-linker amount reduces the free space inside the hydrogels and decreases the swelling of the hydrogels. Hence, the resulting rigid structure cannot expand, so water absorption decreases [28].

Moreover, among all the formulations attempted the greater swelling was noticed for A-5 hydrogel having CMTKG (0.40 g), AM (2.5 g), PVP (0.1 g), KPS (35 mg), MBA (17 mg), and DS (50 mg). Additionally, the DS-loaded CMTKG/PVP/PAM hydrogel (A-5) exhibited greater swelling compared to the CMTKG/PAM hydrogel (A-14), shown in Fig. 2.7. This was attributed to the higher number of hydrophilic pyrrolidone rings present in of PVP. Moreover, for all hydrogels, a higher swelling was noticed in

pH 7.4 than in pH 1.2. The greater swelling at alkaline pH is a consequence of the deprotonated carboxylate anion of CMTKG. This leads to anion-anion repulsion between COO^- ion, which further tends to polymeric chain relaxation and more free space, resulting in fluid absorption [40]. At pH 1.2, hydrogen bonding exists between PAM and CMTKG, causing shrinkage of the hydrogel network, thereby decreasing water absorption capacity [31].

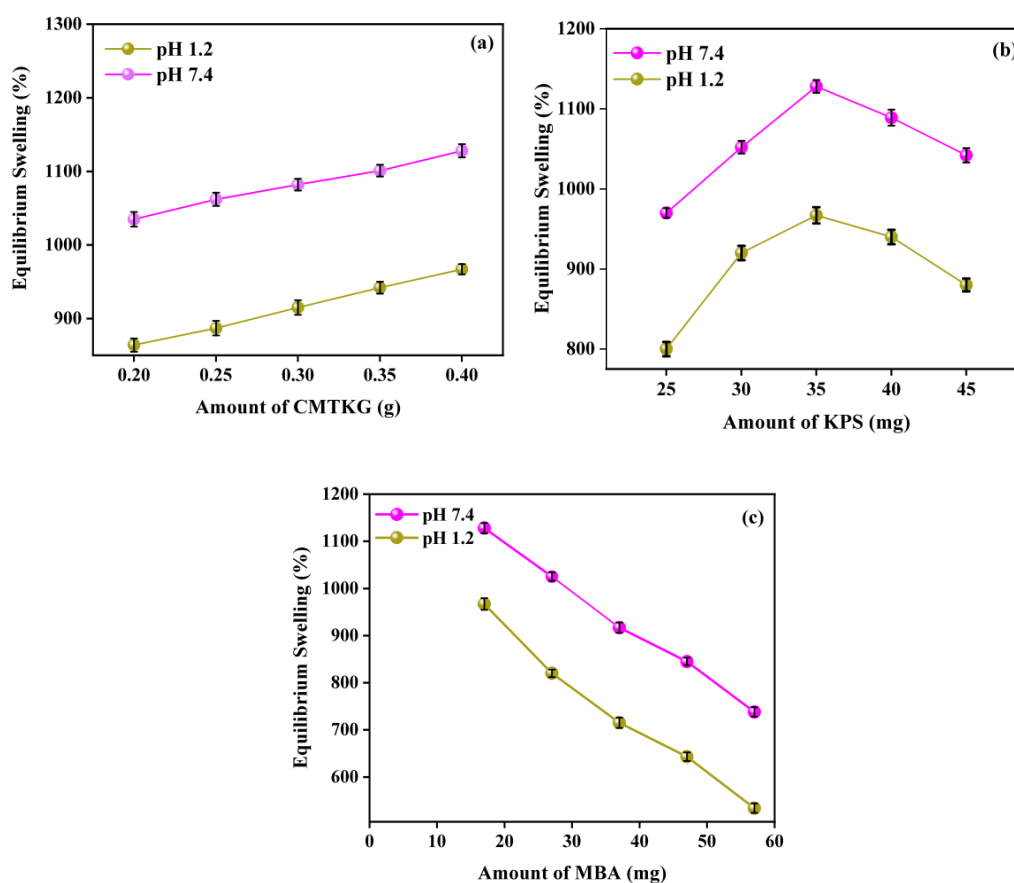


Fig. 2.6 Impact of the (a) CMTKG, (b) KPS, (c) MBA on swelling and (d) equilibrium swelling of A-5 hydrogel in pH 1.2 and 7.4 with respect to time

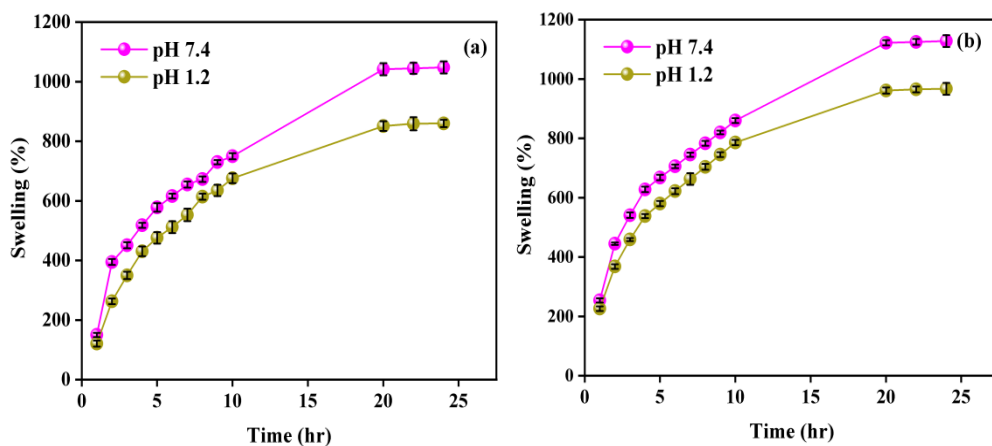


Fig. 2.7 Swelling plot of (a) DS-loaded CMTKG/PAM (A-14) hydrogel and (b) CMTKG/ PVP/PAM hydrogel (A-5) hydrogel in pH 1.2 and 7.4

2.3.4 Sol-Gel Analysis

Sol-gel fraction study for synthesized DS-loaded CMTKG/PVP/PAM hydrogel samples is shown in Fig. 2.8. An increase in gel fraction was noticed, with increases in the amount of CMTKG (A-1 A-2, A-3, A-4, A-5) and KPS (A-8, A-9). This is because as CMTKG increases, more polymer chains containing free radicals increase. As KPS increases, more free radicals are generated, and thus, there are more active sites for crosslinking, so the gel fraction increases. In addition, when KPS was further increased (A-6, A-7), a soluble oligomer chain forms, resulting in a greater sol fraction and a lesser gel fraction. As the concentration of MBA (A-10, A-11, A-12, A-13) increases, crosslinking density increases within the polymeric network, which causes an increase in gel fraction [27].

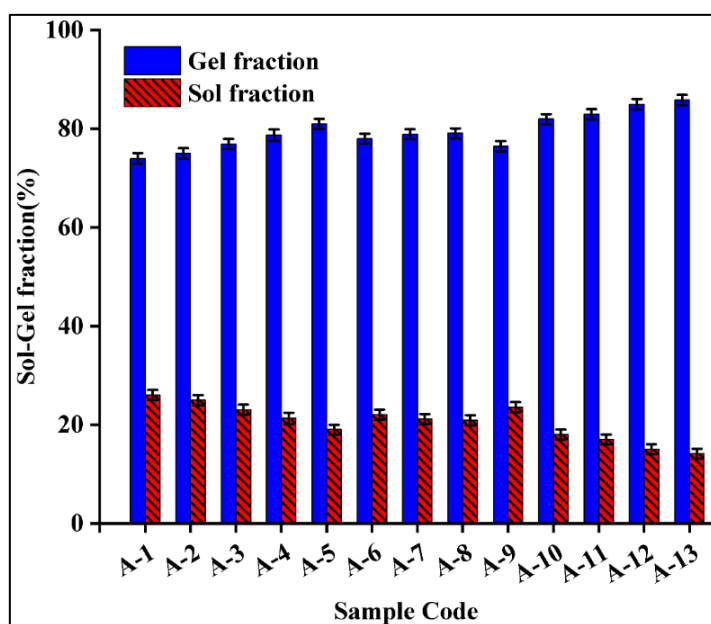


Fig. 2.8 Sol-Gel studies of synthesized formulations of DS-loaded CMTKG/PVP/PAM hydrogel

2.3.5 Porosity

The analysis of the porosity plot (Fig. 2.9) reveals that increasing the CMTKG (A-1 to A-5) leads to greater porosity due to a rise in solution viscosity. This higher viscosity traps bubbles, forming an interconnected network, hence porosity increases. Additionally, as the initiator KPS increases (A-6, A-7), the polymerization increases, creating more voids and enhancing porosity. However, beyond a certain point (A-8, A-9), the rate becomes too fast, leading to increases in short chains, thus crosslinking density increases and porosity decreases. Similarly, increasing the crosslinker MBA (A-10 to A-13) increases crosslinking density, resulting in a denser structure and reduced porosity [41].

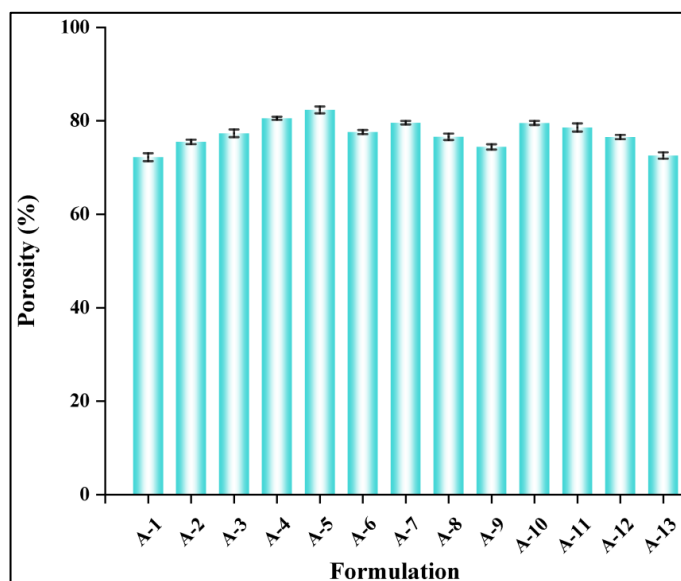


Fig. 2.9 Porosity studies of synthesized DS-loaded CMTKG/PVP/PAM hydrogels

2.3.6 Drug Loading and Entrapment Efficiency

The drug loading (DL%) & drug entrapment efficiency (DEE%) were determined for DS-loaded CMTKG/PAM hydrogel (A-14) and DS-loaded CMTKG/PVP/PAM efficient swelling hydrogel (A-5) as illustrated in Table 2.2. It was noticed that the DS-loaded CMTKG/PVP/PAM hydrogel showed greater DL% and DEE% than the DS-loaded CMTKG/PAM hydrogel. This was due to the hydrophobic-hydrophobic interaction existing among the alkyl group of PVP and the aryl ring of diclofenac sodium in DS-loaded CMTKG/PVP/PAM hydrogel, which enhances the loading of the DS.

Table 2.2 DL% and DEE% of DS-loaded CMTKG/PAM and DS-loaded CMTKG/PVP/PAM hydrogels

Formulation	Hydrogel	DL%	DEE%
A-5	DS-loaded CMTKG/PVP/PAM	20.34 \pm 0.54	65.54 \pm 0.67
A-14	DS-loaded CMTKG/PAM	17.25 \pm 0.8	60.35 \pm 0.39

2.3.7 In vitro DS release study

In vitro release studies were performed for DS-loaded CMTKG/PAM hydrogel (A-14) and DS-loaded CMTKG/PVP/PAM hydrogel (A-5) in a simulated physiological buffer solution of pH 1.2 and 7.4, at 37°C for 24 hr, presented in Fig. 2.10. For both DS-loaded CMTKG/PAM and DS-loaded CMTKG/PVP/PAM hydrogel, the higher percent of DS release was noticed at pH 7.4 because of the deprotonated COO⁻ anion of the CMTKG. Here, anionic-anionic repulsion among the carboxylate group causes an enlargement in network gaps. Therefore, the swelling increases, which leads to rapid diffusion of DS from the polymeric matrix. However, at acidic pH, the carboxylate ion gets protonated, which results in the hydrogen bonding between PAM and CMTKG. As an outcome, shrinkage of the hydrogel took place, resulting in a decrease in swelling % as well as drug release [29]. The maximum DS release was reported to be 66.3 \pm 0.75% in DS-loaded CMTKG/PAM and 87.3 \pm 0.69% in DS-loaded CMTKG/PVP/PAM hydrogel at pH-7.4, while 22.9 \pm 0.62% and 26.3 \pm 0.46% in DS-loaded CMTKG/PAM and DS-loaded CMTKG/PVP/PAM hydrogel at pH-1.2. It was perceived that DS-loaded CMTKG/PVP/PAM hydrogel showed more excellent drug release compared to DS-loaded CMTKG/PAM hydrogel at pH 7.4 and 1.2. This

is due to the greater swelling observed in DS-loaded CMTKG/PVP/PAM hydrogel, which in turn facilitated higher DS release. Hence, it can be concluded that the synthesized CMTKG/PVP/PAM hydrogel can be utilized as an excellent material for the efficient delivery of DS.

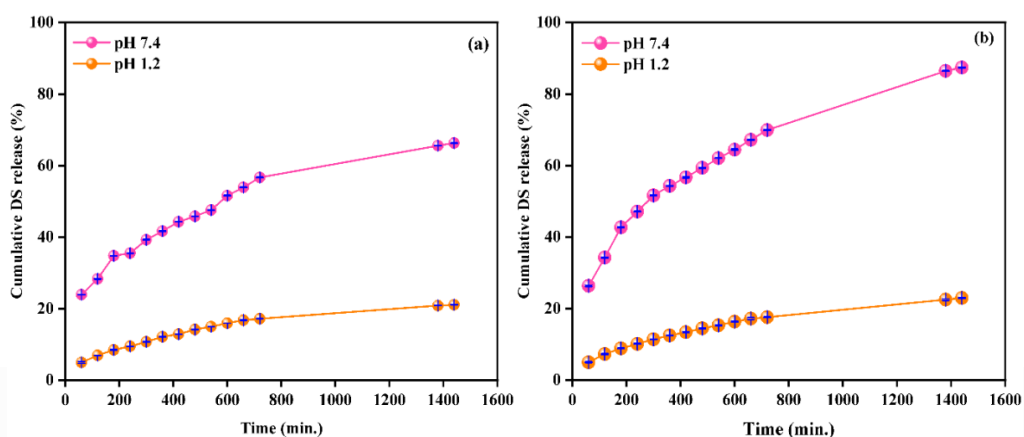


Fig. 2.10 Cumulative drug release curve for (a) DS-loaded CMTKG/PAM hydrogel and (b) DS-loaded CMTKG/PVP/PAM hydrogel in pH 7.4 and 1.2

2.3.8 Release kinetics studies

A higher percentage of drug release was noticed in the case of DS-loaded CMTKG/PVP/PAM hydrogel (A-5) as compared to (A-14) hydrogel. Therefore, kinetic modelling was performed for A-5 hydrogel using Korsmeyer-Peppas, First-order, Higuchi, Zero-order, and Hixson-Crowell models, as presented in Table 2.3. Based on the R^2 value for all the models, the most suitable model to explain the drug release mechanism was selected. The R^2 value for the Korsmeyer-Peppas model was the highest of the other models. The release exponent “n” suggested the type of diffusion. The R^2 value based on the Korsmeyer-Peppas model at pH 1.2 is found to be 0.995, and the diffusion exponent value (n) value is 0.484. In pH 7.4, the R^2 was

0.993, and the n value was 0.397. The kinetic graphs for this model are shown in Fig. 2.11. However, based on the n value, i.e. $n < 0.5$, the diffusion mechanism was observed as Fickian at both pH values, which implies that drug release from the polymeric network is solely diffusion dependent [42-43].

Table 2.3 Kinetic modelling data for DS-loaded CMTKG/PVP/PAM hydrogel

Model	Mechanism	Equation	pH 7.4		pH 1.2		Ref
			k	R ²	k	R ²	
Zero Order	Drug release rate is independent of the drug amount	$M_t = M_\infty + k_0t$	0.061	0.898	0.061	0.911	[34]
Higuchi	Fickian diffusion	$M_t/M_\infty = k_H t^{1/2}$ $k_H = \text{kinetic constant}$	0.079	0.986	0.076	0.990	[30]
First Order	Release rate is directly proportional to the quantity of the drug.	$\text{Log } M_t = \text{Log } M_\infty + \frac{kt}{2.303}$	0.088	0.756	0.082	0.747	[34]
Hixson-Crowell	Erosion	$(M_t)^{1/3} - (M_\infty)^{1/3} = k_{HC}t$ $k_{HC} = \text{Hixson Crowell constant}$	0.098	0.809	0.095	0.810	[34]
Korsmeyer-Peppas	1. Fickian Diffusion ($n < 0.5$) 2. Non-Fickian Diffusion ($0.89 \geq n \geq 0.5$) 3. Case II transport ($n > 0.89$)	$M_t/M_\infty = kt^n$ $k = \text{kinetic constant}$ $n = \text{diffusion exponent}$	0.075	0.993	0.079	0.995	[30]

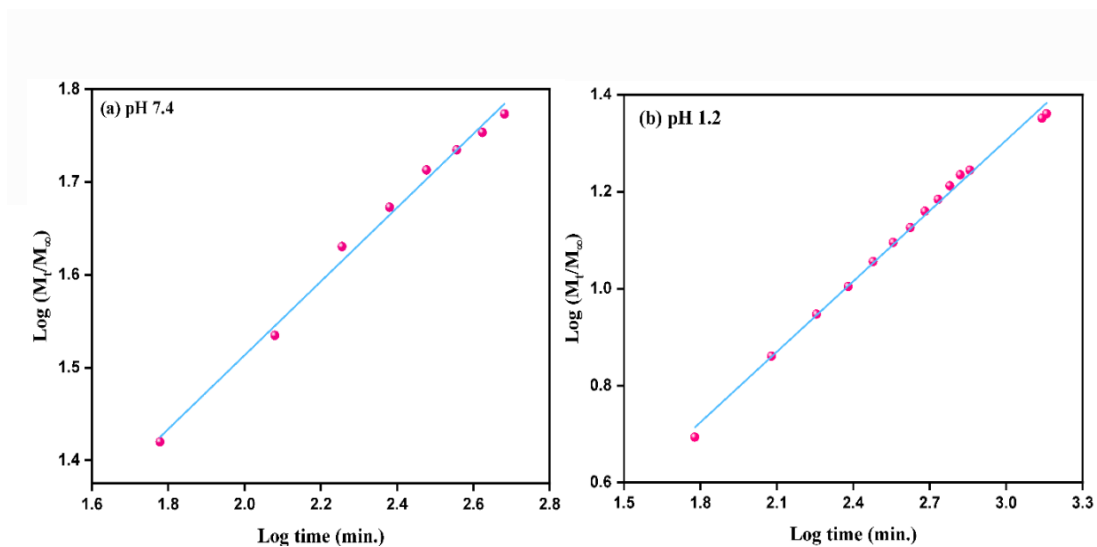


Fig. 2.11 DS release kinetic plot at (a) pH 7.4 and (b) 1.2

2.3.9 Cytotoxicity

Cytotoxicity assessment was carried out against the HCT-116 human colon cell line with different concentrations (0.78, 1.56, 3.125, 6.25 $\mu\text{g/ml}$) of the DS-loaded CMTKG/PVP/PAM hydrogel (A-5), along with a control (without hydrogel), Fig. 2.12. The hydrogel exhibited 77% cell viability at the highest concentration (6.25 $\mu\text{g/mL}$), demonstrating its non-toxic behaviour [39]. Microscopic analysis showed polygonal cell shapes in both the control and hydrogel-treated samples, indicating no significant changes in cell morphology (Fig. 2.13).

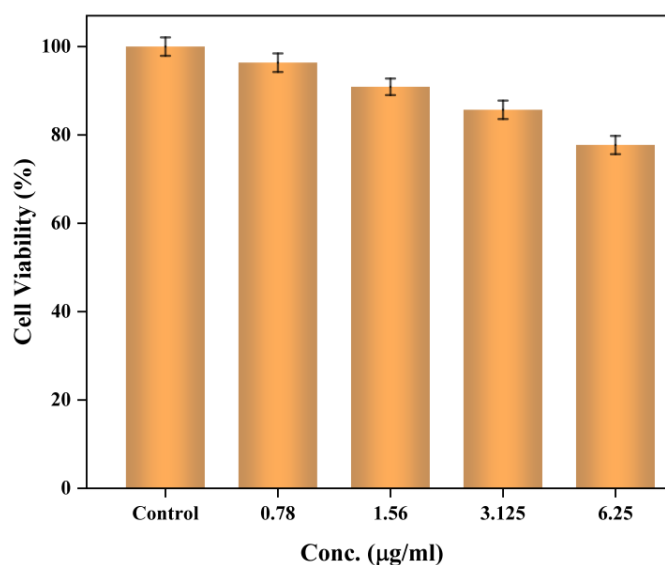


Fig. 2.12 Cytotoxicity profile for DS-loaded CMTKG/PVP/PAM hydrogel (A-5)

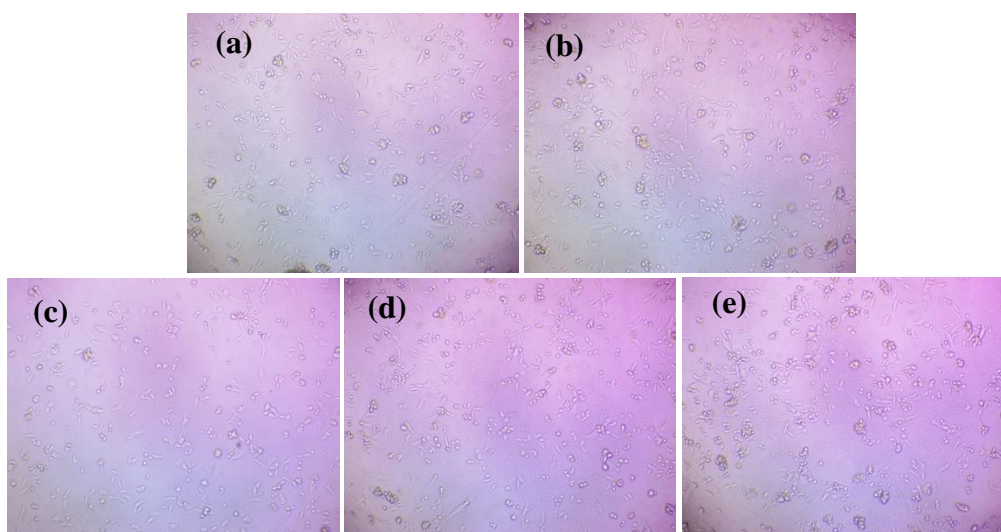


Fig. 2.13 Microscopic images of HCT-116 cells treated with (a) control (b) 0.78 µg/ml, (c) 1.56 µg/ml, (d) 3.125 µg/ml and (e) 6.25 µg/ml of DS-loaded CMTKG/PVP/PAM hydrogel

2.3.10 Degradation

The degradation profile of the synthesized DS-loaded CMTKG/PVP/PAM hydrogel was evaluated in pH 7.4 buffer at 37°C, as shown in Fig. 2.14. Initially, the degradation proceeds gradually for the first 14 days, after which it slows down more significantly. The gradual degradation is due to the strong crosslinked network of the synthesized hydrogel matrix [39].

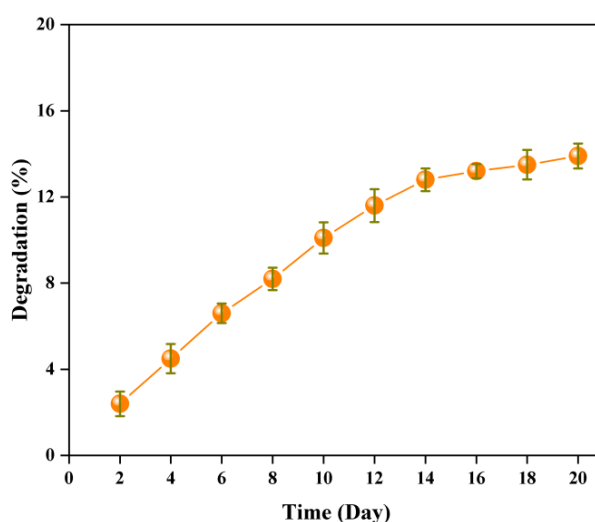


Fig. 2.14 Degradation profile for DS-loaded CMTKG/PVP/PAM hydrogel

2.4 Conclusion

This research work reports the successful synthesis of smart DS-loaded CMTKG/PVP/PAM hydrogel for the release of DS drug. Furthermore, the impact of the concentration of initiator, biopolymer, and crosslinker on the swelling nature of synthesized hydrogel was also studied. The swelling and drug release were examined in alkaline and acidic pH and found to be higher in alkaline conditions, attributed to strong electrostatic repulsion between COO^- anion of the CMTKG. Sol-gel fraction

analysis was conducted using varying amounts of CMTKG, MBA, or KPS and showed an increase in gel fraction with the rise in the amount of reactant. Porosity was found to increase with the KPS amount and decrease with the MBA amount. The effect of the addition of PVP on drug loading and release was also studied. The result indicates that in the presence of PVP, a hydrophobic character imparts in the polymeric matrix, leading to increased drug loading and release capacity. The kinetics of drug release were effectively correlated with the Korsmeyer-Peppas model, suggesting drug release from the hydrogel is purely diffusion-dependent as it follows the Fickian diffusion mechanism. Moreover, synthesized hydrogel showed excellent cell viability against HCT-116 cells. The degradation of synthesized hydrogels at pH 7.4 was also evaluated. The above key findings represents the utilization of DS-loaded CMTKG/PVP/PAM hydrogel as a feasible material for pH-dependent release of DS.

2.5 REFERENCES

1. Bi X, Zhang H, Dou L (2014) Layered double hydroxide-based nanocarriers for drug delivery. *Pharmaceutics* 6:298–332. <https://doi.org/10.3390/pharmaceutics6020298>
2. Md Saquib Hasnain, Syed Anees Ahmed, Saad Alkahtani, Milan Milivojevic, et al (2011) *Biopolymers for drug delivery*. Springer International Publishing
3. Ravi Kiran AVVV, Kusuma Kumari G, Krishnamurthy PT (2020) Carbon nanotubes in drug delivery: Focus on anticancer therapies. *Journal of Drug Delivery Science and Technology* 59:101892. <https://doi.org/10.1016/j.jddst.2020.101892>

4. Liu L, Ma Q, Cao J, et al (2021) Recent progress of graphene oxide-based multifunctional nanomaterials for cancer treatment. *Cancer Nanotechnology* 12:1–31. <https://doi.org/10.1186/s12645-021-00087-7>
5. Senapati S, Mahanta AK, Kumar S, Maiti P (2018) Controlled drug delivery vehicles for cancer treatment and their performance. *Signal Transduction and Targeted Therapy* 3:1–19. <https://doi.org/10.1038/s41392-017-0004-3>
6. How KN, Yap WH, Lim CLH, et al (2020) Hyaluronic Acid-Mediated Drug Delivery System Targeting for Inflammatory Skin Diseases: A Mini Review. *Frontiers in Pharmacology* 11:1–8. <https://doi.org/10.3389/fphar.2020.01105>
7. Gholamali I, Yadollahi M (2021) Bio-nanocomposite Polymer Hydrogels Containing Nanoparticles for Drug Delivery: a Review. *Regenerative Engineering and Translational Medicine* 7:129–146. <https://doi.org/10.1007/s40883-021-00207-0>
8. Ullah F, Othman MBH, Javed F, et al (2015) Classification, processing and application of hydrogels: A review. *Materials Science and Engineering C* 57:414–433. <https://doi.org/10.1016/j.msec.2015.07.053>
9. Munim SA, Raza ZA (2019) Poly(lactic acid) based hydrogels: formation, characteristics and biomedical applications. *Journal of Porous Materials* 26:881–901. <https://doi.org/10.1007/s10934-018-0687-z>
10. Rizwan M, Yahya R, Hassan A, et al (2017) pH sensitive hydrogels in drug delivery: Brief history, properties, swelling, and release mechanism, material selection and applications. *Polymers* 9:137. <https://doi.org/10.3390/polym9040137>
11. Sun S, Cui Y, Yuan B, et al (2023) Drug delivery systems based on polyethylene glycol hydrogels for enhanced bone regeneration. *Frontiers in Bioengineering and Biotechnology* 11:1–17. <https://doi.org/10.3389/fbioe.2023.1117647>

12. Thirupathi K, Phan TTV, Santhamoorthy M, et al (2022) pH and Thermoresponsive PNIPAm-co-Polyacrylamide Hydrogel for Dual Stimuli-Responsive Controlled Drug Delivery. *Polymers* 15:167. <https://doi.org/10.3390/polym15010167>
13. Martínez-Gómez F, Guerrero J, Matsuhiro B, Pavez J (2017) In vitro release of metformin hydrochloride from sodium alginate/polyvinyl alcohol hydrogels. *Carbohydrate Polymers* 155:182–191. <https://doi.org/10.1016/j.carbpol.2016.08.079>
14. Musa H, Yahaya S (2022) Polyacrylamide hydrogels for application in oral drug delivery. *Nigerian Journal of Scientific Research*
15. Nangia S, Warkar SG, Katyal D (2018) A review on environmental applications of chitosan biopolymeric hydrogel based composites. *Journal of Macromolecular Science, Part A: Pure and Applied Chemistry* 55:747–763. <https://doi.org/10.1080/10601325.2018.1526041>
16. Risbud M V., Bhonde RR (2000) Polyacrylamide-chitosan hydrogels: In vitro biocompatibility and sustained antibiotic release studies. *Drug Delivery: Journal of Delivery and Targeting of Therapeutic Agents* 7:69–75. <https://doi.org/10.1080/107175400266623>
17. Kulkarni R, Sa B (2008) Enteric delivery of ketoprofen through functionally modified poly(acrylamide-grafted-xanthan)-based pH-sensitive hydrogel beads: Preparation, in vitro and in vivo evaluation. *Journal of Drug Targeting* 16:167–177. <https://doi.org/10.1080/10611860701792399>
18. Goyal P, Kumar V, Sharma P (2007) Carboxymethylation of Tamarind kernel powder. *Carbohydrate Polymers* 69:251–255. <https://doi.org/10.1016/j.carbpol.2006.10.001>
19. Pal S, Sen G, Mishra S, et al (2008) Carboxymethyl tamarind: Synthesis, characterization and its application as novel drug-delivery agent. *Journal of Applied Polymer Science* 110:392–400. <https://doi.org/10.1002/app.28455>

20. Khushbu, Warkar SG, Kumar A (2019) Synthesis and assessment of carboxymethyl tamarind kernel gum based novel superabsorbent hydrogels for agricultural applications. *Polymer* 182:121823. <https://doi.org/10.1016/j.polymer.2019.121823>
21. Jana S, Banerjee A, Sen KK, Maiti S (2016) Gelatin-carboxymethyl tamarind gum biocomposites: In vitro characterization & anti-inflammatory pharmacodynamics. *Materials Science and Engineering C* 69:478–485. <https://doi.org/10.1016/j.msec.2016.07.008>
22. Mali K, Dhawale S, Dias RJ, Ghorpade V (2019) Delivery of drugs using tamarind gum and modified tamarind gum: A review. *Bulletin of Faculty of Pharmacy, Cairo University* 57:1–24. <https://doi.org/10.21608/BFPC.2019.47260>
23. Larrañeta E, Stewart S, Ervine M (2018) Hydrogels for Hydrophobic Drug Delivery. Classification, Synthesis and Applications. *Journal of Functional Biomaterials* 13:2018
24. Ekici S and Saraydin D (2007) Interpenetrating polymeric network hydrogels for potential gastrointestinal. *Polym Int* 56:1371–1377. <https://doi.org/10.1002/pi.2271>
25. Shoukat H, Pervaiz F, Noreen S, et al (2020) Fabrication and evaluation studies of novel polyvinylpyrrolidone and 2-acrylamido-2-methylpropane sulphonic acid-based crosslinked matrices for controlled release of acyclovir. *Polymer Bulletin* 77:1869–1891. <https://doi.org/10.1007/s00289-019-02837-5>
26. Nayak AK, Khatua S, Hasnain MS, Sen KK (2011) Development of diclofenac sodium-loaded alginate-PVP K 30 microbeads using central composite design. *DARU, Journal of Pharmaceutical Sciences* 19:356–366
27. Suhail M, Khan A, Rosenholm JM, et al (2021) Fabrication and characterization of diclofenac sodium loaded hydrogels of sodium alginate as sustained release carrier. *Gels* 7:1–16. <https://doi.org/10.3390/gels7010010>

28. Hosseinzadeh H (2010) Controlled release of diclofenac sodium from pH-responsive carrageenan-g-poly(acrylic acid) superabsorbent hydrogel. *Journal of Chemical Sciences* 122:651–659. <https://doi.org/10.1007/s12039-010-0100-1>
29. Wei QB, Fu F, Zhang YQ, et al (2014) PH-responsive CMC/PAM/PVP semi-IPN hydrogels for theophylline drug release. *Journal of Polymer Research* 21:453. <https://doi.org/10.1007/s10965-014-0453-0>
30. Khushbu, Warkar SG, Thombare N (2022) Controlled release and release kinetics studies of boron through the functional formulation of carboxymethyl tamarind kernel gum-based superabsorbent hydrogel. *Polymer Bulletin* 79:2287–2303. <https://doi.org/10.1007/s00289-021-03634-9>
31. Tan LS, Tan HL, Deekonda K, et al (2021) Fabrication of radiation cross-linked diclofenac sodium loaded carboxymethyl sago pulp/chitosan hydrogel for enteric and sustained drug delivery. *Carbohydrate Polymer Technologies and Applications* 2:100084. <https://doi.org/10.1016/j.carpta.2021.100084>
32. Nawaz S, Khan S, Farooq U, et al (2018) Biocompatible hydrogels for the controlled delivery of anti-hypertensive agent: Development, characterization and in vitro evaluation. *Designed Monomers and Polymers* 21:18–32. <https://doi.org/10.1080/15685551.2018.1445416>
33. Kalantari K, Mostafavi E, Saleh B, et al (2020) Chitosan/PVA hydrogels incorporated with green synthesized cerium oxide nanoparticles for wound healing applications. *European Polymer Journal* 134:109853. <https://doi.org/10.1016/j.eurpolymj.2020.109853>
34. Suhail M, Chiu IH, Hung MC, et al (2022) In Vitro Evaluation of Smart and pH-Sensitive Chondroitin Sulfate/Sodium Polystyrene Sulfonate Hydrogels for Controlled Drug Delivery. *Gels* 8:1–18. <https://doi.org/10.3390/gels8070406>

35. Niu B, Jia J, Wang H, et al (2019) In vitro and in vivo release of diclofenac sodium-loaded sodium alginate/carboxymethyl chitosan-ZnO hydrogel beads. *International Journal of Biological Macromolecules* 141:1191–1198. <https://doi.org/10.1016/j.ijbiomac.2019.09.059>
36. Jana S, Sharma R, Maiti S, Sen KK (2016) Interpenetrating hydrogels of O-carboxymethyl Tamarind gum and alginate for monitoring delivery of acyclovir. *International Journal of Biological Macromolecules* 92:1034–1039. <https://doi.org/10.1016/j.ijbiomac.2016.08.017>
37. Hu Y, Dong X, Ke L, et al (2017) Polysaccharides/mesoporous silica nanoparticles hybrid composite hydrogel beads for sustained drug delivery. *Journal of Materials Science* 52:3095–3109. <https://doi.org/10.1007/s10853-016-0597-x>
38. Varahala Setti ML, Ratna JV (2009) Preparation and evaluation of controlled release tablets of carvedilol. *Asian Journal of Pharmaceutics* 3:252–256. <https://doi.org/10.4103/0973-8398.56307>
39. Kumar J, Purwar R (2024) Self-Healing Biocompatible Injectable Hydrogel Based on Multialdehyde *Moringa oleifera*. *ChemistrySelect* 9:e202400309
40. Mali KK, Dhawale SC, Dias RJ (2017) Synthesis and characterization of hydrogel films of carboxymethyl tamarind gum using citric acid. *International Journal of Biological Macromolecules* 105:463–470. <https://doi.org/10.1016/j.ijbiomac.2017.07.058>
41. Soltani B, Nabipour H, Ahmadi Nasab N (2018) Fabrication, controlled release, and kinetic studies of indomethacin—layered zinc hydroxide nanohybrid and its effect on the viability of HFFF2. *Journal of Dispersion Science and Technology* 39:1200–1207. <https://doi.org/10.1080/01932691.2017.1388178>
42. Ghumman SA, Noreen S, Hameed H, et al (2022) Synthesis of pH-Sensitive Cross-Linked Basil Seed Gum/Acrylic Acid Hydrogels by Free Radical Copolymerization Technique for Sustained Delivery of Captopril. *Gels* 8.

<https://doi.org/10.3390/gels8050291>

43. Suhail M, Chiu IH, Lai YR, et al (2023) Xanthan-Gum/Pluronic-F-127-Based-Drug-Loaded Polymeric Hydrogels Synthesized by Free Radical Polymerization Technique for Management of Attention-Deficit/Hyperactivity Disorder. *Gels* 9. <https://doi.org/10.3390/gels9080640>

CHAPTER 3

DEVELOPMENT AND ASSESSMENT OF XANTHAN GUM-BASED HYDROGEL AS A POTENTIAL CARRIER FOR A HYDROPHOBIC DRUG IBUPROFEN

3.1 Introduction

Ibuprofen (2-(4-(2-methylpropyl)phenyl) propionic acid), is widely used as a nonsteroidal anti-inflammatory drug known for its effectiveness in the reduction of pain, inflammation, and fever. It has poor solubility, high permeability, and limited bioavailability [1-2]. Moreover, the half-life of ibuprofen is approximately 2 to 4 hours. This relatively short half-life means that ibuprofen needs to be taken multiple times in a day so as to maintain pain relief or anti-inflammatory [3-4]. This can cause side effects, including gastrointestinal issues such as stomach irritation, nausea, or heartburn. Therefore, the development of a novel biopolymer-based hydrogel is necessary to minimize adverse effects and achieve extended delivery, thereby enhancing therapeutic efficacy [5].

Xanthan gum (XG) is one such biopolymer produced through the fermentation of carbohydrates by the bacterium *Xanthomonas campestris* [6-8]. The primary structure of this naturally occurring polysaccharide is composed of the side chain of

glucuronic acid and pyruvic acid [9]. It is widely used in the pharmaceutical industry as a binder in tablet formulations and as a thickener in liquid medications, ensuring uniform distribution of active ingredients. XG-based hydrogels have garnered significant attention in drug delivery systems due to their unique properties, including hydrophilicity, tunable release rate and biocompatibility [10-11]. Moreover, due to its pH-responsive nature, these hydrogels provide a controlled and sustained release of therapeutic agents, making them ideal for various biomedical applications.

Additionally, these biopolymer-based hydrogels can also protect drugs from degradation, enzymatic activity, and harsh physiological conditions, leading to enhanced drug stability and bioavailability [12-18]. However, extensive research is currently focused on the development of hybrid hydrogels that combine synthetic and biopolymers. Moreover, among synthetic polymers utilized for the fabrication of hybrid hydrogels, PAM and PVP have received considerable attention in drug delivery applications due to their non-toxic nature. Additionally, PVP-based hydrogels are widely utilized for delivering both hydrophobic and hydrophilic drugs [19-26].

Thus, in present work, pH-sensitive XG/PAM and XG/PAM/PVP-based hydrogels were developed for the release of ibuprofen drug. Ibuprofen was loaded into the fabricated hydrogel using an ex-situ technique. The addition of PVP was implemented to enhance the loading capacity of the hydrophobic drug (ibuprofen). To confirm the synthesis, surface morphology and crystalline nature, the hydrogels were characterized using ATR-FTIR, SEM, and PXRD techniques. The swelling behavior of the developed hydrogels was analyzed at pH 1.2 and

7.4. Sol-gel, porosity, degradation and cytotoxicity studies were also conducted for synthesized hydrogels. The study mainly focused on estimating the percentage of ibuprofen release through the *in vitro* release method. To elucidate the drug release mechanism, several kinetic models, such as First-Order, Higuchi, Hixson-Crowell, Korsmeyer-Peppas, and Zero-Order, were used. To ensure accuracy, all experiments were done in triplicate, and standard deviations are shown as error bars in the graphs.

3.2 Experimental Section

3.2.1 Materials

N, N'-methylene bis(acrylamide) (MW=154.16 g/mol, Merck, Germany), Polyvinylpyrrolidone K-30 (MW=4 ×10⁴ g/mol, CDH, New Delhi), Potassium persulphate (MW=270.30g/mol, Fischer Scientific, Mumbai, India), Acrylamide (MW=71.08 g/mol, CDH, New Delhi), and Xanthan Gum (MW=2 ×10⁶ g/mol, s d fine chem. Ltd., Mumbai, India) were used as obtained. Ibuprofen (MW=206.2 g/mol) was courteously provided by Unicare India Pvt Ltd, Noida, India.

3.2.2 Fabrication of XG/PAM hydrogel and XG/PAM/PVP hydrogels

The fabrication of XG/PAM hydrogel (U-1) and series of XG/PAM/PVP hydrogels (U-2 to U-11), with the varied composition of the initiator KPS (25-40 mg), crosslinker MBA (15-30 mg) and biopolymer XG (0.02-0.05 g) were carried out via free radical polymerization. Table 3.1 details the specific amount of MBA, XG, PVP, KPS and acrylamide (AM) utilized during the fabrication of hydrogels. For the synthesis of XG/PAM hydrogel (U-1), the first fixed amount of XG and AM were dissolved in

distilled water, followed by continuous stirring on a magnetic stirrer for 1 hour. Secondly, KPS and MBA in requisite amounts were added while stirring for an additional 1hr to ensure complete mixing. Then, the mixture was carefully poured into glass test tubes and transferred to a water bath maintained at 60°C. After 1 hour, the tubes were removed from the water bath, and the hydrogel was extracted from the tubes and cut into discs. The obtained hydrogels were then washed with distilled water to remove unreacted chemicals and impurities, if any. Finally, the obtained hydrogel was dried in an oven at 60°C until a consistent weight was achieved [23], [27].

For the synthesis of a series of XG/PAM/PVP hydrogels (U-2 to U-11), an additional polymer PVP was also introduced simultaneously during the addition of XG and AM, while the rest of the procedure remained the same as outlined above, as presented in Fig. 3.1 [37].

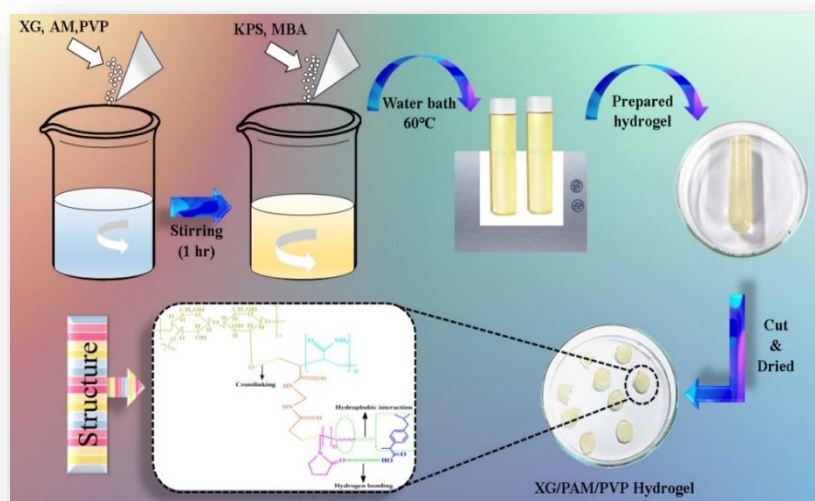


Fig. 3.1 Schematic illustration of the fabrication of XG/PAM/PVP-based hydrogel

Table 3.1 Composition of reagents used for the synthesis of the hydrogels

Formulation	XG (g)	AM (g)	PVP (g)	MBA (mg)	KPS (mg)
U-1	0.05	2.2	00	15	35
U-2	0.02	2.2	0.12	15	35
U-3	0.03	2.2	0.12	15	35
U-4	0.04	2.2	0.12	15	35
U-5	0.05	2.2	0.12	15	35
U-6	0.05	2.2	0.12	15	25
U-7	0.05	2.2	0.12	15	30
U-8	0.05	2.2	0.12	15	40
U-9	0.05	2.2	0.12	20	35
U10	0.05	2.2	0.12	25	35
U-11	0.05	2.2	0.12	30	35

3.2.3 Characterization

The PXRD measurements were done using a Bruker D8 diffractometer, with Cu K α radiation ($\lambda = 1.5418 \text{ \AA}$), over a 2θ of $5-70^\circ$ using a Gobel mirror. The ATR-FTIR spectra were recorded using an ATR-FTIR spectrophotometer (Model: PerkinElmer spectrum 2) within a range of $450-4000 \text{ cm}^{-1}$. The surface morphology was examined via SEM (Model: JEOL Japan Mode: JSM 6610LV).

3.2.4 Swelling studies

To investigate the swelling behavior of the XG/PAM hydrogel and all XG/PAM/PVP hydrogels, gravimetric analysis was conducted. Initially, the pre-dried hydrogels were precisely weighed (M_d) and immersed in an HCl-KCl buffer (pH 1.2) and phosphate

buffer saline (pH 7.4) for a duration of 24 hr. At intervals of 1 hour, the swollen hydrogel discs were carefully extracted and gently blotted with filter paper to eliminate any adhered liquid droplets on the surface. The swelled hydrogels were then weighed again (M_s) and dipped back in the buffer solutions [17], [28]. The entire study was conducted in triplicate to ensure reliability, and the swelling ratio was determined using the provided Eqn. (3.1).

$$\text{Swelling (\%)} = \frac{M_s - M_d}{M_d} \times 100 \quad (3.1)$$

Additionally, to determine the equilibrium swelling, the weight M_s was replaced by M_f , which represents the weight of the hydrogel at equilibrium when fully swollen.

3.2.5 Sol-Gel analysis

To investigate the uncrosslinked part of the XG/PAM hydrogel and all fabricated XG/PAM/PVP-based hydrogels, a sol-gel analysis was conducted. Dried hydrogels were weighed (M_i) and dipped in distilled water for 48 hr with stirring at room temperature. Subsequently, the extracted swollen hydrogel discs were subjected to oven drying at 45°C till a consistent weight (M_e) was reached [29-30]. The sol and gel fraction was quantitatively assessed using the below Eqn. (3.2) and Eqn. (3.3).

$$\text{Sol Fraction (\%)} = \frac{M_i - M_e}{M_e} \times 100 \quad (3.2)$$

$$\text{Gel fraction (\%)} = 100 - \text{Sol fraction} \quad (3.3)$$

3.2.6 Porosity Measurement

The porosity analysis of all fabricated hydrogels was performed using the solvent displacement method. The initial weighed dry hydrogel discs (M_i) were placed in 5 ml

of hexane overnight. After 2 hr, the hydrogel discs were taken out from the hexane, extra liquid on their surfaces was removed by blotting with filter paper, and the weight of the final dry hydrogel discs (M_f) was recorded. To calculate the porosity of the hydrogel discs, the below Eqn. (3.4) was used:

$$\text{Porosity (\%)} = \frac{M_i - M_f}{\rho V} \times 100 \quad (3.4)$$

Here, ρ denotes the density of hexane, and V denotes the volume of the hydrogel disc [32], [31].

3.2.7 Ibuprofen Loading and Entrapment Efficiency

Among all the formulated XG/PAM/PVP-based hydrogels, the optimized XG/PAM/PVP (U-5) hydrogel demonstrated the highest swelling capacity. Therefore, drug loading was carried out on this specific formulation, and it was selected for comparison with the control XG/PAM (U-1) hydrogel, which does not contain PVP. To assess the drug loading and encapsulation efficiency of ibuprofen-loaded XG/PAM and XG/PAM/PVP hydrogel, the weight method was employed. The fixed amount of dried hydrogel discs (M_i) were immersed in 100 ml of pH 7.4 buffer solution containing 50 mg of the ibuprofen, which represent as M_D , for a period of 24 hr at room temperature. After the designated time, the hydrogel discs were carefully removed from the buffer solution and kept in the oven at 40°C until a constant weight (M_f) was reached [33-36]. The below-mentioned Eqn. (3.5) and Eqn. (3.6) were utilized to find out the drug loading (DL%) and drug encapsulation efficiency (DEE%)

$$DL (\%) = \frac{M_f - M_i}{M_i} \times 100 \quad (3.5)$$

$$DEE (\%) = \frac{M_f - M_i}{M_D} \times 100 \quad (3.6)$$

3.2.8 In vitro ibuprofen release studies

An *in vitro* release study of ibuprofen was conducted using ibuprofen-loaded XG/PAM hydrogel and Ibuprofen-loaded XG/PAM/PVP hydrogel in an orbital incubator shaker maintained at 37°C. The fixed amount of the ibuprofen-loaded hydrogel discs was dipped in 100 mL of pH 1.2 and 7.4 buffer solutions [36]. The 3mL aliquot was collected from each buffer solution at regular time intervals (1hr), and an equal volume of fresh buffer solutions was added to ensure constant volume. The sample was analysed using a UV- visible spectrophotometer (Model: Cary 300 UV-Vis), recording the absorbance at the λ_{\max} 223 nm for pH 7.4 and λ_{\max} 221 nm for pH 1.2. The ibuprofen amount in the released samples was determined via a calibration curve of the drug [37]. The Eqn. (3.7) was used to determine the drug release.

$$\text{Cumulative drug release} \left(\frac{M_t}{M_\infty} \right) = \frac{V_t C_t + V_B \sum_{1}^{n-1} C_{t-1}}{M_\infty} \quad (3.7)$$

where, V_W is the volume of buffer solution withdrawn at time t, M_t is the amount of drug released at time t, M_∞ is the amount of drug loaded, V_B is the total volume of release medium, C_t and C_{t-1} is the concentration of solution at time t and t-1.

3.2.9 Kinetic Modelling

Various mathematical models, such as First-Order, Zero-Order, Higuchi, Hixson-

Crowell and Korsmeyer-Peppas were employed to elucidate the drug release mechanism. The release data acquired from the *in-vitro* studies were fitted to each of these models. The goodness of fit was assessed by comparing the Regression coefficient (R^2) values associated with each model. The model exhibiting an R^2 value close to 1 is termed the most suitable and best-fitted model for describing the drug release mechanism [38].

3.2.10 Cytotoxicity

The effect of DS-loaded CMTKG/PVP/PAM hydrogel (A-5) on the HCT 116 human colon cell line purchased from NCCS Pune was investigated using the MTT Assay. Cells were seeded at a density of 10,000 cells per well in a 96-well plate containing DMEM medium with 10% FBS and 1% antibiotic solution and incubated at 37°C with 5% CO₂ for 24 hours. The hydrogel was initially immersed in phosphate buffer saline and stirred. Then, the cells were then exposed to varying hydrogel concentrations (0.78 to 6.25 µg/ml), with control wells containing no hydrogel. After 24-hour incubation, MTT solution was added and incubated for 2 hours. The supernatant was discarded, and the cells were dissolved in 100 µl of DMSO. Absorbance was measured at 540 nm and 660 nm using an Elisa plate reader (iMark, Biorad, USA), and images were taken under an inverted microscope with a 10 MP Aptima CMOS digital camera [39].

3.2.11 Degradation

Degradation experiments were conducted in a pH 7.4 buffer (simulated intestinal fluid) using an orbital incubator shaker maintained at 37°C for 18 days. Hydrogel discs were first immersed in the buffer until they reached equilibrium, and their weight was

recorded as (M_{IH}). Subsequently, the discs were removed every 2 days, gently blotted with filter paper, weighed as (M_{FH}), and then returned to the buffer [39]. The degradation (%) was calculated using Eqn. (3.8).

$$\text{Degradation (\%)} = \frac{M_{IH} - M_{FH}}{M_{IH}} \times 100 \quad (3.8)$$

3.3 Result and Discussion

3.3.1 Mechanistic pathway of ibuprofen-loaded XG/PAM/PVP hydrogel

formation

In the synthesis of all ibuprofen-loaded XG/PAM/PVP hydrogels using a free radical mechanism, KPS (initiator) and MBA (crosslinker) played a key role. Fig. 3.2 depicts the proposed mechanism of the hydrogel fabrication. At 60°C, the KPS decomposes, releasing sulfate radicals. The highly reactive radicals initiate the polymerization of acrylamide monomers by breaking the vinyl double bond of the acrylamide and generating the free radical on the acrylamide. This sulfate radical also abstracts a hydrogen atom from XG and PVP and generates a reactive free radical. To introduce cross-links and form a three-dimensional network, a cross-linking agent (MBA) was added. The MBA molecules consist of two reactive ends that react with active radical sites of XG, PAM and PVP. This results in the formation of covalent bonds between the polymeric chains, leading to the formation of a crosslinked network structure of XG/PAM/PVP hydrogel. Moreover, in ibuprofen-loaded XG/PAM/PVP hydrogel, the hydrophobic interaction exists between the alkyl group of PVP and the aryl ring of Ibuprofen, as well as the formation of hydrogen bonds between the -O atom of pyrrolidone ring of PVP and -OH of Ibuprofen took place [40], [24]

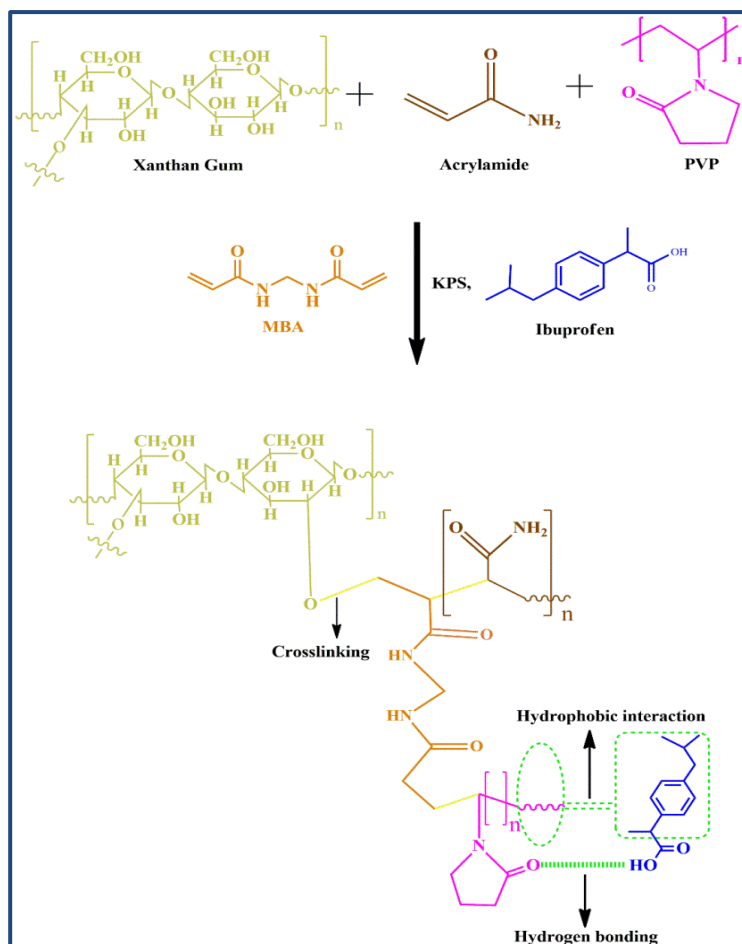


Fig. 3. 2 Mechanism for Ibuprofen-loaded XG/PAM/PVP hydrogel

3.3.2 Characterization

PXRD analysis was employed to analyze both the crystallinity of the hydrogel and the distribution of the drug within the polymeric matrix, as depicted in Fig. 3.3. In the PXRD pattern of ibuprofen, the characteristic peaks corresponding to ibuprofen were observed at 2θ values of 6.1, 12.3, 16.7, 20.1, 22.4 and 27.5° [2]. The distinct and well-defined peaks of ibuprofen indicated its crystalline nature [28]. While the broad peaks observed in the XG/PAM/PVP (U-5) and XG/PAM (U-1) hydrogel diffractograms suggested that the hydrogel matrix lacked a well-defined crystalline

structure, however exhibited amorphous characteristics. Moreover, in the Ibuprofen-loaded XG/PAM/PVP hydrogel, the peaks of Ibuprofen were absent.

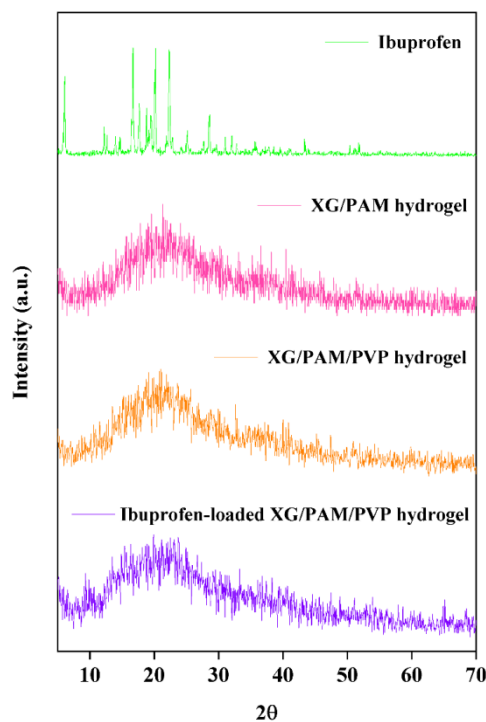


Fig. 3.3 PXRD pattern of Ibuprofen, XG/PAM, XG/PAM/PVP, and Ibuprofen-loaded XG/PAM/PVP hydrogel

SEM micrographs of XG/PAM/PVP (U-5) and Ibuprofen-loaded XG/PAM/PVP hydrogel are depicted in Fig. 3.4. The XG/PAM/PVP hydrogel exhibits an irregular surface morphology and a porous structure, revealing the hydrogel's favorable fluid retention and drug loading capacity. Moreover, the micrographs of Ibuprofen-loaded XG/PAM/PVP hydrogel display a little smooth surface with fewer visible pores as compared to the unloaded hydrogel. This observation suggests that the ibuprofen has successfully been encapsulated into the hydrogel matrix, resulting in reduced interstitial voids within the hydrogel structure [42].

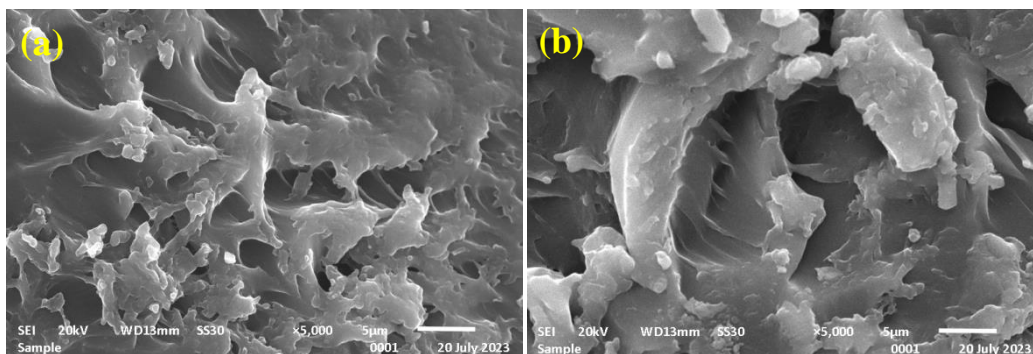


Fig. 3.4 SEM micrographs of (a) XG/PAM/PVP and (b) Ibuprofen-loaded XG/PAM/PVP hydrogel

The ATR-FTIR spectra of MBA, XG/PAM hydrogel (U-1), XG/PAM/PVP (U-5) hydrogel, and Ibuprofen-loaded XG/PAM/PVP hydrogel are illustrated in Fig. 3.5. In the ATR-FTIR spectrum of MBA, the peaks at 1304 cm^{-1} corresponding to C-N stretch shifted to 1319 cm^{-1} , 1320 cm^{-1} , 1319 cm^{-1} in XG/PAM, XG/PAM/PVP and Ibuprofen-loaded XG/PAM/PVP hydrogel respectively, due to cross-linking. Moreover, the peak representing the C=C stretch shifted to 1649 cm^{-1} , 1647 cm^{-1} , and 1648 cm^{-1} in XG/PAM, XG/PAM/PVP and Ibuprofen-loaded XG/PAM/PVP hydrogel respectively, confirming the cross-linking. These results provide confirmation of the successful synthesis of crosslinked XG/PAM/PVP hydrogel [40]. The XG/PAM/PVP hydrogel exhibited almost identical spectra to XG/PAM hydrogel due to the overlapping of the characteristic peaks (C=O, N-H, C-H) of PVP with PAM, resulting in no additional visible peaks upon the addition of PVP. Only changes in intensity and little shifts in wave number due to the interaction of PVP were observed. In the case

of Ibuprofen-loaded XG/PAM/PVP hydrogel, no new peaks appeared or disappeared as compared to the spectra of unloaded XG/PAM/PVP hydrogel. This observation suggests the absence of chemical interaction, rather, only a physical interaction, such as hydrogen bonding, occurred between the ibuprofen and hydrogel [28].

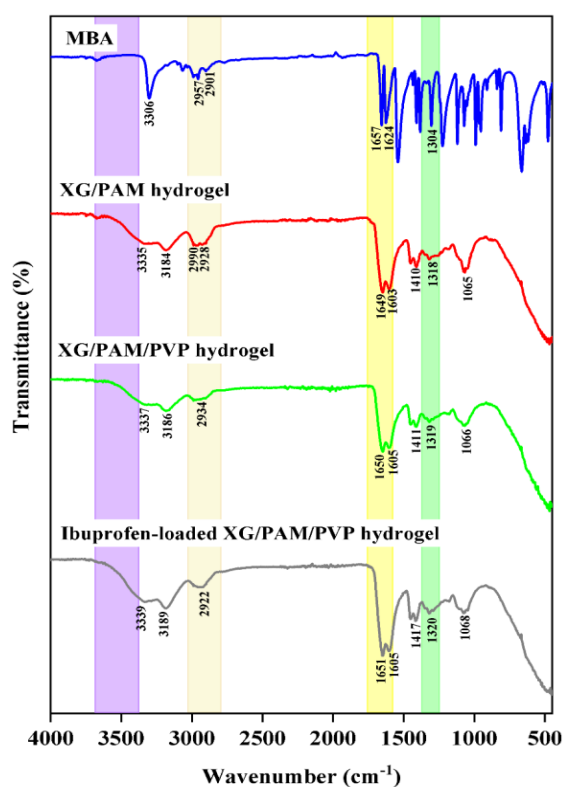


Fig. 3.5 ATR-FTIR spectra of MBA, XG/PAM hydrogel, XG/PAM/PVP hydrogel, and Ibuprofen-loaded XG/PAM/PVP hydrogel

3.3.3 Swelling studies

The swelling of hydrogel was influenced by the amount of the biopolymer, initiator and crosslinker, as depicted in Fig. 3.6.

3.3.3.1 Influence of biopolymer

The impact of varying XG amounts (U-2 to U-5 formulation) on the equilibrium swelling was illustrated in Fig. 3.6 (a). The swelling ratio of hydrogels rises as the amount of XG increases from 0.02 g to 0.05 g. Notably, the highest swelling, 1100.31%, was observed at pH 7.4. However, at pH 1.2, a swelling of 997.75% was noticed when using 0.05 g of XG. This can be attributed to an increase in hydrophilicity as the XG quantity increases. As the XG content rises, the number of hydrophilic groups such as -OH attached to XG, also increases, consequently, high swelling is observed. Furthermore, a solution with an XG amount exceeding 0.05 g faced challenges due to the resulting highly viscous solution, rendering stirring difficult. Hence, the formation of hydrogel with XG above 0.05 g was not attempted [17], [40].

3.3.3.2 Influence of Initiator

The highest swelling occurred with 0.05 g of XG, hence this value amount of XG was kept constant in all the attempted formulations and the effect of varying KPS (initiator) concentration (U-6 to U-8) on swelling is observed, as depicted in Fig. 3.6 (b). At a KPS amount of 35 mg, the highest swelling of approximately $1100.31 \pm 0.58\%$ occurred at pH 7.4, whereas pH 1.2 exhibited a swelling of $997.75 \pm 0.84\%$. The swelling was noted to rise as the amount of KPS increased from 25 mg to 35 mg, and subsequently, it decreased beyond 35 mg. The initial rise in swelling could be linked to a higher number of free radicals along the polymeric chain, leading to more polymerization and greater swelling. However, the decrease in swelling results from the biomolecular collision, which took place as the reaction rate increased, which

increased the crosslinking density and decreased swelling [17].

3.3.3.3 Influence of Crosslinker

The influence of crosslinker amount (U-9 to U-11) on the swelling was examined. As depicted in Fig. 3.6 (c), a higher MBA amount yields greater swelling. The increased crosslinker amount from 15 mg to 30 mg reduces the available space between the polymeric chains. Consequently, the resulting highly rigid crosslinked network cannot expand, and hence, swelling decreases [17].

In all the formulations, it was noticed that the hydrogel exhibited greater swelling at pH 7.4 in comparison to pH 1.2. This can be attributed to the deprotonation of the COOH group present in XG in the pH 7.4 buffer solution. The repulsion took place between the deprotonated COO⁻ ions, resulting in chain relaxation, which generates additional free space within the polymeric network, and consequently, the hydrogel exhibited more swelling [43]. On the other hand, the presence of hydrogen bonding interactions among PAM, PVP, and XG at pH 1.2 causes the hydrogel to shrink, resulting in a lesser swelling compared to the alkaline pH [28].

In comparison of the XG/PAM/PVP (U-5) hydrogel to XG/PAM (U-1) hydrogel, the XG/PAM/PVP (U-5) hydrogel shows notably higher swelling, as observed in Fig. 3.7. It is primarily attributed to the presence of PVP, an amphiphilic polymer containing hydrophilic moieties such as C=O and C-N, responsible for promoting greater swelling.

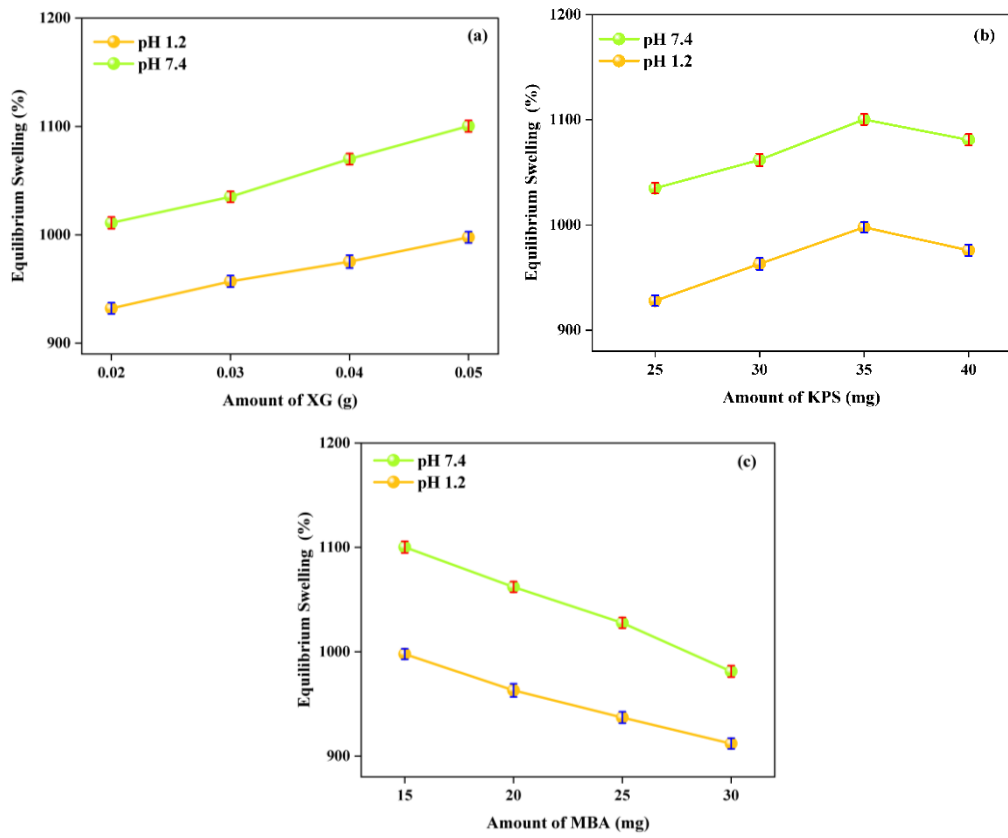


Fig. 3.6 Influence of the (a) XG, (b) KPS, and (c) MBA on the swelling of the hydrogel

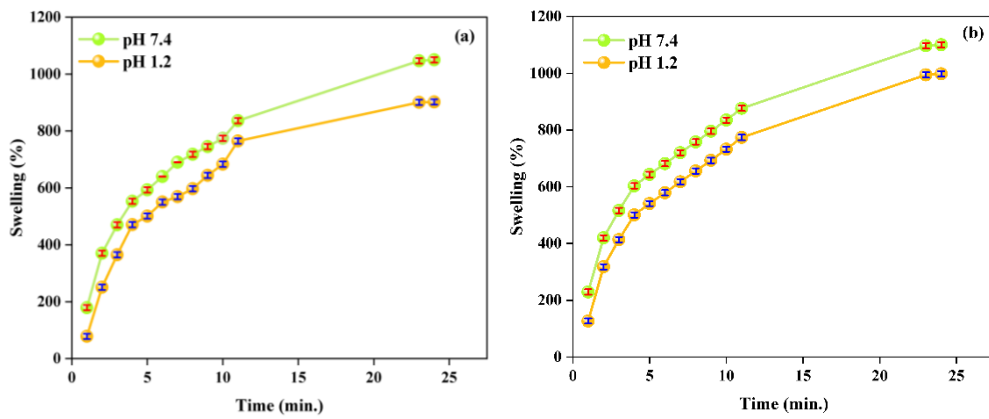


Fig. 3.7 Swelling studies of (a) XG/PAM hydrogel and (b) XG/PAM/PVP hydrogel in pH 7.4. and 1.2

3.3.4 Sol-Gel analysis

The gel fraction and sol fraction for all fabricated hydrogels are illustrated in Fig. 3.8. As the amount of XG (U-2 to U-5) and KPS (U-6, U-7) increases, a noticeable rise in gel fraction was observed. This was attributed to the generation of a higher number of free radicals, leading to a greater number of active sites available for crosslinking. Consequently, the crosslinking density within the polymer network rises, resulting in an increase in gel fraction. However, the further increase in the concentration of KPS (U-8), prompts the generation of soluble chains (oligomer) instead of interconnected crosslinked networks, consequently, the gel fraction decreases. Moreover, the rise in MBA amount (U-9, U-10, U-11) increases crosslinking within the polymeric chain, which corresponds to a rise in gel fraction.

In a comparison of XG/PAM/PVP (U-5) hydrogel with XG/PAM (U-1) hydrogel, the result shows that an addition of polymer (PVP) results in a decrease of the sol fraction and an increase of the gel fraction. This can be attributed to the presence of higher concentrations of polymer chains containing free radicals during the incorporation of PVP. Consequently, numerous active sites for crosslinking are generated, leading to more crosslinked parts, subsequently increasing the gel portion. However, as the gel fraction increases, the sol fraction decreases due to their inverse relationship [44].

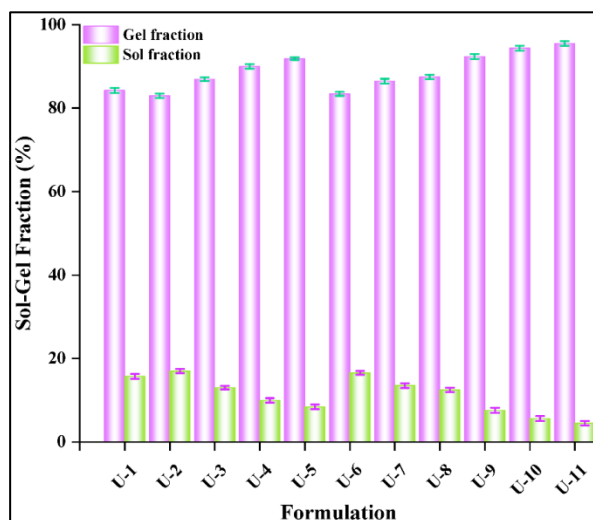


Fig. 3.8 Sol-Gel studies of all fabricated XG/PAM/PVP hydrogels and XG/PAM hydrogel

3.3.5 Porosity Measurement

The analysis of the porosity (Fig 3.9) illustrates that as the amount of the biopolymer XG (U-2 to U-5) is increased, porosity also increases due to the rise in solution viscosity. The presence of a viscous solution effectively hinders the escape of bubbles, leading to the formation of an interconnected network and consequently contributing to the observed increase in porosity. Furthermore, initially, on increasing the initiator, KPS (U-6, U-7), more radicals are generated, leading to a higher polymerization rate. This rapid polymerization results in the generation of more void within the hydrogel structure, thus increasing porosity. However, with further increases in KPS (U-8), the polymerization rate becomes too fast. This causes polymer chains to crosslink too quickly, leading to denser and less porous structures hence porosity decreases. Moreover, increasing the amount of crosslinker, MBA (U-9 to U-11), the entanglement between the polymeric chain of XG, PVP, and PAM increases, resulting in a denser

structure and lesser porosity [45]. The XG/PAM hydrogel (U-1) exhibits lower porosity in comparison to the XG/PAM/PVP hydrogel (U-5). This revealed that the addition of PVP, enhances the viscosity of the solution, resulting in the entrapment of bubbles, consequently, porosity increases [30].

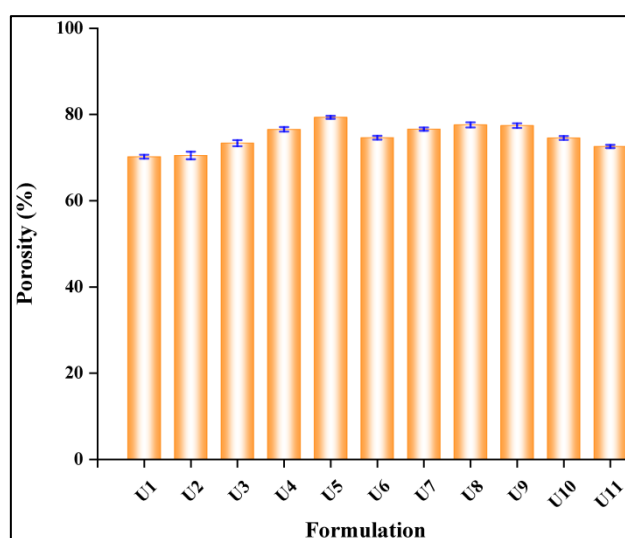


Fig. 3.9 Porosity plot of all fabricated XG/PAM/PVP hydrogels and XG/PAM hydrogel

3.3.6 Ibuprofen Loading and Entrapment Efficiency

The ibuprofen loading (DL%) and entrapment efficiency (DEE%) were calculated as per equations (5) and (6), respectively, for Ibuprofen-loaded XG/PAM hydrogel and Ibuprofen-loaded XG/PAM/PVP hydrogel, and their data displayed in Table 3.2. Notably, Ibuprofen-loaded XG/PAM/PVP hydrogel exhibited higher DL% and DEE% values than Ibuprofen-loaded XG/PAM hydrogel. This can be attributed to the hydrophobic interaction between the alkyl group of PVP and the aryl ring of Ibuprofen, responsible for increasing the loading of hydrophobic drug ibuprofen in XG/PAM/PVP hydrogel [24].

Table 3.2 Drug loading and drug entrapment efficiency of Ibuprofen-loaded XG/PAM hydrogel and Ibuprofen-loaded XG/PAM/PVP hydrogel

Sample code	Hydrogel	Drug Loading (%)	Drug Entrapment Efficiency (%)
U-1	XG/PAM	16.53±0.76	55.42±0.59
U-5	XG/PAM/PVP	21.38±0.88	62.27±0.74

3.3.7 In vitro ibuprofen release studies

The *in vitro* release analysis was conducted for Ibuprofen-loaded XG/PAM hydrogel and Ibuprofen-loaded XG/PAM/PVP hydrogel, as shown in Fig. 3.10. The Ibuprofen-loaded XG/PAM/PVP hydrogel possess higher drug release (%) than Ibuprofen-loaded XG/PAM hydrogel due to higher swelling that observed in the XG/PAM/PVP hydrogel. This notable difference was mainly due to the addition of the PVP, which consists of hydrophilic constituents such as C=O and C-N groups, which increases the swelling, as a result, drug release also increases. The Ibuprofen release percentages were 69.3% and 80.2% in XG/PAM and XG/PAM/PVP hydrogel at pH 7.4, respectively, while 17.6% and 20.6% in XG/PAM and XG/PAM/PVP hydrogel at pH 1.2 respectively.

For both formulations, the Ibuprofen release was higher at pH 7.4 due to deprotonation of carboxylic acid (-COOH) present in XG, leading to anionic repulsion between COO⁻ anion, causing polymeric network expansion, increased swelling, consequently higher drug release. However, at pH 1.2, -COOH group protonation led to hydrogel bonding between XG, PAM and PVP, as a result, hydrogel shrinks, hence lesser

swelling and reduced drug release [23]. Hence, fabricated XG/PAM/PVP hydrogel exhibits good potential for sustained release of hydrophobic drug ibuprofen at pH 7.4.

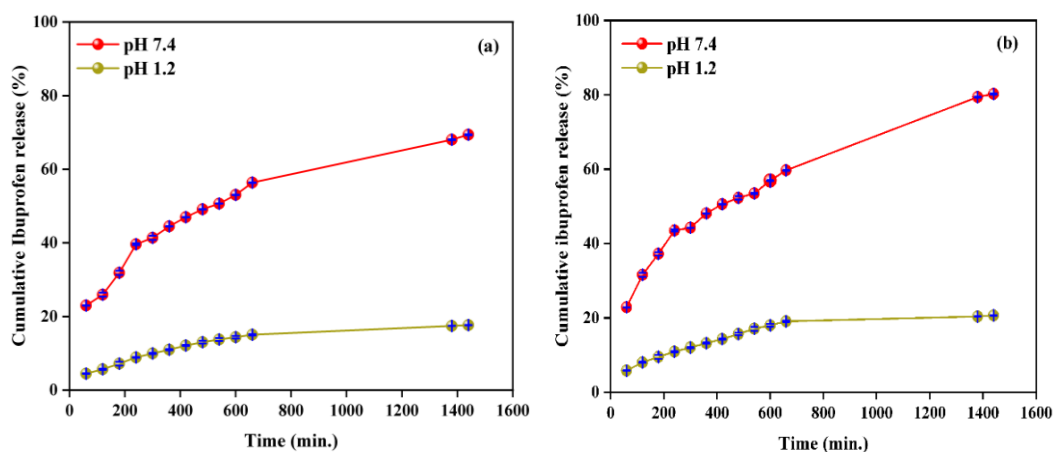


Fig. 3.10 Cumulative ibuprofen release from ibuprofen-loaded (a) XG/PAM

hydrogel, (b) XG/PAM/PVP hydrogel pH 7.4 and 1.2

3.3.8 Kinetic Modelling

Different kinetic models were utilized to analyze the release data and understand the mechanism of drug release from ibuprofen-loaded XG/PAM/PVP hydrogel, as observed in Table 3.3. Among the First-Order, Hixson-Crowell, Zero-Order, Higuchi, and Korsmeyer-Peppas models, the Korsmeyer-Peppas model exhibited the highest R^2 value for both hydrogels formulation, as given in Table 4. In ibuprofen-loaded XG/PAM/PVP hydrogel, the diffusion mechanism was determined to be Fickian with n values as 0.4480 and 0.4160 at pH 1.2 and 7.4, respectively (Fig. 3.11). The Fickian diffusion indicates that drug release from the hydrogel via a diffusion process.

Table 3.3 Kinetic modelling data of ibuprofen-loaded XG/PAM/PVP hydrogel

Model	Equation	pH 7.4		pH 1.2		Ref.
		k	R ²	k	R ²	
Zero Order	$M_t = M_\infty + k_0t$	0.053	0.925	0.067	0.756	[10]
Higuchi	$M_t/M_\infty = k_H t^{1/2}$ $k_H = \text{kinetic constant}$	0.064	0.961	0.079	0.898	[10]
First Order	$\text{Log } M_t = \text{Log } M_\infty + \frac{kt}{2.303}$ $k = \text{First order rate constant}$	0.058	0.778	0.054	0.642	[44]
Hixson-Crowell	$(M_t)^{1/3} - (M_\infty)^{1/3} = k_{HX}t$ $k_{HX} = \text{Hixson Crowell constant}$	0.074	0.835	0.074	0.683	[10]
Korsmeyer-Peppas	$M_t/M_\infty = kt^n$ $k = \text{kinetic constant}$ $n = \text{diffusion exponent}$	0.066	0.985	0.059	0.973	[44]

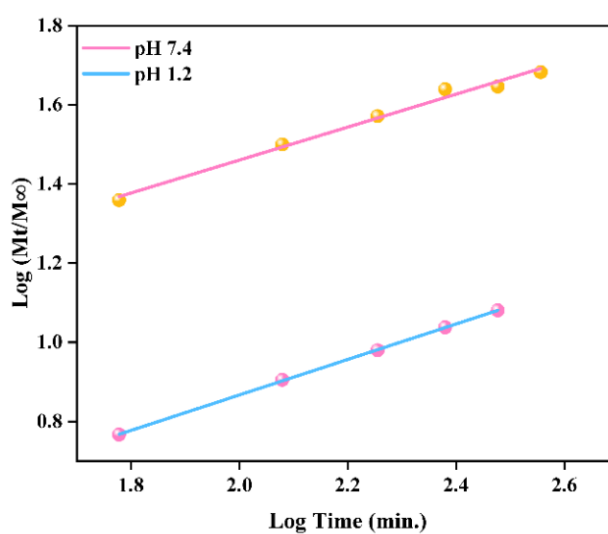


Fig. 3.11 Kinetic modelling profile of ibuprofen-loaded XG/PAM/PVP hydrogel

3.3.9 Cytotoxicity

Cytotoxicity was evaluated using the HCT-116 human colon cell line with various concentrations (0.78, 1.56, 3.125, and 6.25 $\mu\text{g/ml}$) of the ibuprofen-loaded XG/PAM/PVP hydrogel and a control (without hydrogel), as depicted in Fig. 3.12. At the highest concentration, the hydrogel demonstrated 75% cell viability, indicating its non-toxic and biocompatible properties [39]. Optical Microscopic images revealed polygonal cell shapes in both the control and hydrogel-treated samples, showing no significant alterations in cell morphology, as seen in Fig. 3.13.

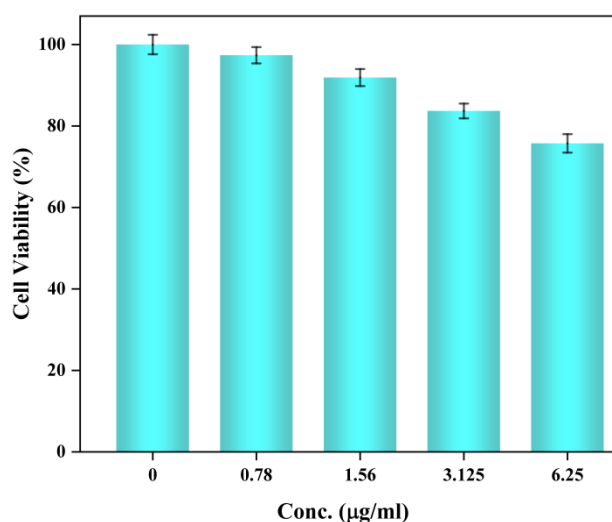


Fig. 3.12 Cytotoxicity plot for ibuprofen-loaded XG/PAM/PVP hydrogel

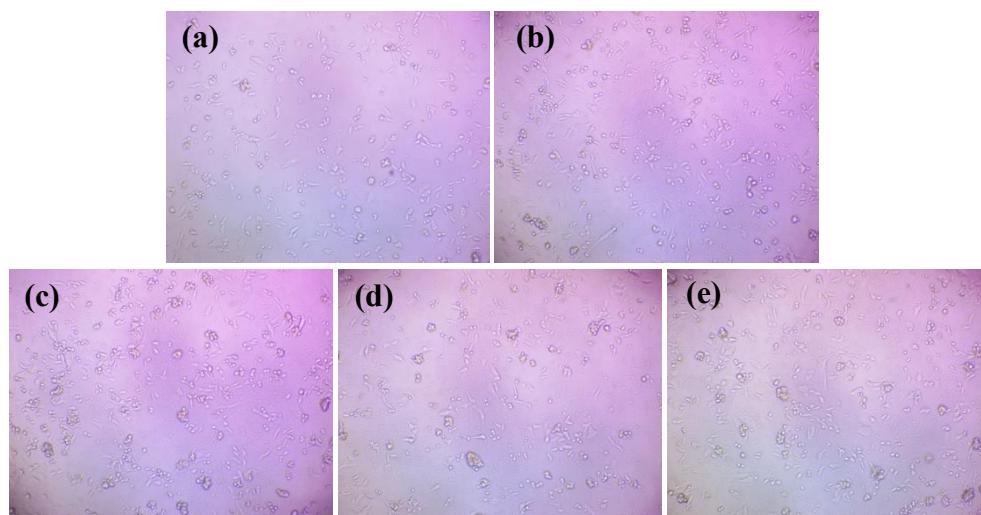


Fig. 3.13 Optical Microscope images of HCT-116 cells treated with (a) control (b) 0.78 µg/ml, (c) 1.56 µg/ml, (d) 3.125 µg/ml and (e) 6.25 µg/ml ibuprofen-loaded XG/PAM/PVP hydrogel

3.3.10 Degradation

The degradation of the fabricated ibuprofen-loaded XG/PAM/PVP hydrogel was assessed in a pH 7.4 buffer solution at 37°C for 18 days, as illustrated in Fig. 3.14. The results indicate a gradual degradation process during the first 12 days, after that the degradation becomes more slow. This gradual degradation can be attributed to the crosslinking present in the polymeric network [39].

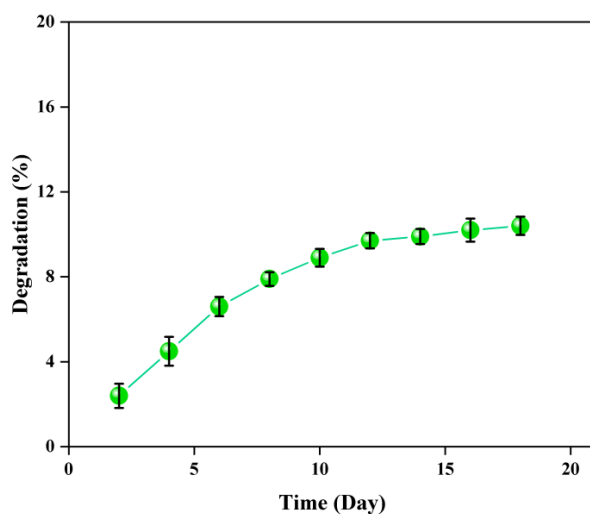


Fig. 3.14 Degradation profile for ibuprofen-loaded XG/PAM/PVP hydrogel

3.4 Conclusion

In the present work, XG-based hydrogels were successfully formulated using a free radical mechanism. The hydrogel exhibited excellent swelling properties and was consequently employed as an effective carrier for delivering the hydrophobic drug ibuprofen. The introduction of PVP in hydrogel results in an increase in the percentage of gel fraction, swelling, porosity, and drug loading efficiency, with XG/PAM/PVP showing higher drug loading efficiency than XG/PAM hydrogel. The XG/PAM/PVP hydrogel possesses high swelling and drug release at pH 7.4, in comparison to pH 1.2. Hence, it is suitable for targeted drug delivery in the colon region of the gastrointestinal tract. Moreover, the drug release mechanism for ibuprofen-loaded XG/PAM/PVP hydrogels was determined to be non-Fickian at both pH (1.2 and 7.4). Additionally, the cytotoxicity evaluation demonstrated non-toxic effects on the HCT-116 cell line. In conclusion, the synthesized pH-sensitive hydrogel acts as a potential carrier for the efficient delivery of ibuprofen.

3.5 REFERENCES

1. Nguyen HT, Nguyen LT, Ha AC, Huynh PD (2023) Evaluation of Ibuprofen Prolonged Release of Biomedical PLA-PEG-PLA Hydrogel via Degradation Mechanism. 2023. <https://doi.org/10.1155/2023/5005316>
2. Shinde AK et al (2019) Enhancement Solubility and Dissolution Rate of Paracetamol and Ibuprofen By Coamorphous Particles Using Microwave Technique. *Asian Journal of Pharmaceutical and Clinical Research* 12:155–162. <https://doi.org/10.22159/ajpcr.2019.v12i11.34589>
3. Sami AJ et al (2018) Sustained Release of Ibuprofen by a Novel Formulated Hydrogel Containing Molecular Pharmaceutics & Organic Process Research Sustained Release of Ibuprofen by a Novel Formulated Hydrogel Containing Graphene Oxide. *Molecular Pharmaceutics & Organic Process Research* 6:1000143. <https://doi.org/10.4172/2329-9053.1000143>
4. Wang XH, Su T, Zhao J, et al (2020) Fabrication of polysaccharides-based hydrogel films for transdermal sustained delivery of Ibuprofen. *Cellulose* 27:10277–10292. <https://doi.org/10.1007/s10570-020-03503-0>
5. Suhail M, Hsieh YH, Khan A, et al (2021) Preparation and in vitro evaluation of aspartic/alginate acid based semi-interpenetrating network hydrogels for controlled release of ibuprofen. *Gels* 7. <https://doi.org/10.3390/gels7020068>
6. Kulkarni R V, Sa B (2008) Evaluation of pH-sensitivity and drug release characteristics of (Polyacrylamide-Grafted-Xanthan)-carboxymethyl cellulose-based pH-sensitive interpenetrating network hydrogel beads. *Drug Development and Industrial Pharmacy* 34:1406–1414. <https://doi.org/10.1080/03639040802130079>
7. Hanna DH, Saad GR (2019) Encapsulation of ciprofloxacin within modified xanthan gum- chitosan based hydrogel for drug delivery. *Bioorganic Chemistry* 84:115–124. <https://doi.org/10.1016/j.bioorg.2018.11.036>

8. Sethi S, Saruchi, Kaith BS, et al (2020) Cross-linked xanthan gum–starch hydrogels as promising materials for controlled drug delivery. *Cellulose* 27:4565–4589. <https://doi.org/10.1007/s10570-020-03082-0>
9. Malik NS, Ahmad M, Minhas MU, et al (2020) Chitosan/Xanthan Gum Based Hydrogels as Potential Carrier for an Antiviral Drug: Fabrication, Characterization, and Safety Evaluation. *Frontiers in Chemistry* 8:1–16. <https://doi.org/10.3389/fchem.2020.00050>
10. Tushar, Saraswat Y, Meena P, Sudhir G. Warkar (2023) Synthesis and characterization of novel xanthan gum - based pH - sensitive hydrogel for metformin hydrochloride release. *Colloid and Polymer Science* 301:1147-1158. <https://doi.org/10.1007/s00396-023-05135-9>
11. Bhattacharyya R, Chowdhury P (2021) Hydrogels of Acryloyl guar gum-g-(acrylic acid-co-3sulfopropylacrylate) for high-performance adsorption and release of gentamicin sulphate. *Journal of Polymer Research* 28. <https://doi.org/10.1007/s10965-021-02633-8>
12. Sutar PB, Mishra RK, Pal K, Banthia AK (2008) Development of pH sensitive polyacrylamide grafted pectin hydrogel for controlled drug delivery system. *Journal of Materials Science: Materials in Medicine* 19:2247–2253. <https://doi.org/10.1007/s10856-007-3162-y>
13. Reddy PRS, Rao KM, Rao KSVK, et al (2014) Synthesis of alginate based silver nanocomposite hydrogels for biomedical applications. *Macromolecular Research* 22:832–842. <https://doi.org/10.1007/s13233-014-2117-7>
14. Rizwan M, Yahya R, Hassan A, et al (2017) pH sensitive hydrogels in drug delivery: Brief history, properties, swelling, and release mechanism, material selection and applications. *Polymers* 9. <https://doi.org/10.3390/polym9040137>
15. Ahmad U, Sohail M, Ahmad M, et al (2019) Chitosan based thermosensitive injectable hydrogels for controlled delivery of loxoprofen: development, characterization and in-vivo evaluation. *International Journal of Biological*

- Macromolecules 129:233–245. <https://doi.org/10.1016/j.ijbiomac.2019.02.031>
16. Munim SA, Raza ZA (2019) Poly(lactic acid) based hydrogels: formation, characteristics and biomedical applications. *Journal of Porous Materials* 26:881–901. <https://doi.org/10.1007/s10934-018-0687-z>
 17. Hosseinzadeh H (2010) Controlled release of diclofenac sodium from pH-responsive carrageenan-g-poly(acrylic acid) superabsorbent hydrogel. *Journal of Chemical Sciences* 122:651–659. <https://doi.org/10.1007/s12039-010-0100-1>
 18. García-Verdugo KF, Ramírez-Irigoyen AJ, Castillo-Ortega M, et al (2022) A pH/Temperature-Sensitive s-IPN Based on Poly(vinyl alcohol), Poly(vinyl methyl ether-alt-maleic acid) and Poly(vinyl methyl ether) Prepared by Autoclaving. *Macromolecular Research* 30:353–364. <https://doi.org/10.1007/s13233-022-0044-6>
 19. Raza MA, Park SH (2020) Irradiated Ch/GG/PVP-based stimuli-responsive hydrogels for controlled drug release. *Journal of Applied Polymer Science* 137. <https://doi.org/10.1002/app.49041>
 20. Thirupathi K, Phan TTV, Santhamoorthy M, et al (2022) pH and Thermoresponsive PNIPAm-co-Polyacrylamide Hydrogel for Dual Stimuli-Responsive Controlled Drug Delivery. *Polymers* 15:167. <https://doi.org/10.3390/polym15010167>
 21. Martinez-Ruvalcabal A et al (2009) Swelling characterization and drug delivery kinetics of polyacrylamide-co-itaconic acid/chitosan hydrogels. *Express Polymer Letters* 3:25–32. <https://doi.org/10.3144/expresspolymlett.2009.5>
 22. Musa H, Yahaya S (2022) Polyacrylamide hydrogels for application in oral drug delivery. *Nigerian Journal of Scientific Research*
 23. Wei QB, Fu F, Zhang YQ, et al (2014) PH-responsive CMC/PAM/PVP semi-IPN hydrogels for theophylline drug release. *Journal of Polymer Research* 21:453. <https://doi.org/10.1007/s10965-014-0453-0>

24. Meena P, Singh P, Warkar SG (2023) Development and assessment of carboxymethyl tamarind kernel gum-based pH-responsive hydrogel for release of diclofenac sodium. *European Polymer Journal* 197:112340. <https://doi.org/10.1016/j.eurpolymj.2023.112340>
25. Lim DK, Cui MH, Nam JM (2011) Highly stable, amphiphilic DNA-encoded nanoparticle conjugates for DNA encoding/decoding applications. *Journal of Materials Chemistry* 21:9467–9470. <https://doi.org/10.1039/c1jm11150g>
26. Afriani K, Sutanti Budikania T (2020) Synthesis and Characterization of Hydrogel of Chitosan-Poly (N-Vinyl-2-Pyrrolidone) (PVP)- Alginate for Ibuprofen Release. *The Journal of Pure and Applied Chemistry Research* 9:201–211. <https://doi.org/10.21776/ub.jpacr.2020.009.03.558>
27. Chauhan D, Kumar A, Warkar SG (2022) Synthesis, characterization and metal ions sensing applications of meta-benziporphodimethene-embedded polyacrylamide/carboxymethyl guar gum polymeric hydrogels in water. *Environmental Technology* 43:991–1002. <https://doi.org/10.1080/09593330.2020.1812730>
28. Tan LS, Tan HL, Deekonda K, et al (2021) Fabrication of radiation cross-linked diclofenac sodium loaded carboxymethyl sago pulp/chitosan hydrogel for enteric and sustained drug delivery. *Carbohydrate Polymer Technologies and Applications* 2:100084. <https://doi.org/10.1016/j.carpta.2021.100084>
29. Rahmani S, Olad A, Rahmani Z (2022) Preparation of self-healable nanocomposite hydrogel based on Gum Arabic/gelatin and graphene oxide: study of drug delivery behavior. *Polymer Bulletin* 80:4117–4138. <https://doi.org/10.1007/s00289-022-04247-6>
30. Naeem F et al (2017) pH Responsive cross-linked polymeric matrices based on natural polymers: Effect of process variables on swelling characterization and drug delivery properties. *BioImpacts* 7:177–192. <https://doi.org/10.15171/bi.2017.21>

31. Kalantari K, Mostafavi E, Saleh B, et al (2020) Chitosan/PVA hydrogels incorporated with green synthesized cerium oxide nanoparticles for wound healing applications. *European Polymer Journal* 134:109853. <https://doi.org/10.1016/j.eurpoly.2020.109853>
32. Khan R, Zaman M, Salawi A, et al (2022) Synthesis of Chemically Cross-Linked pH-Sensitive Hydrogels for the Sustained Delivery of Ezetimibe. *Gels* 8. <https://doi.org/10.3390/gels8050281>
33. Safari JB, Bapolisi AM, Krause RWM (2021) Development of pH-sensitive chitosan-g-poly (Acrylamide-co-acrylic acid) hydrogel for controlled drug delivery of tenofovir disoproxil fumarate. *Polymers* 13. <https://doi.org/10.3390/polym13203571>
34. Rashid H, Ahmad M, Minhas MU, et al (2015) Synthesis and characterization of poly(hydroxyethyl methacrylate-co-methacrylic acid) cross linked polymeric network for the delivery of analgesic agent. *Journal of the Chemical Society of Pakistan* 37:999–1007
35. Tulain UR, Ahmad M, Rashid A, et al (2018) Fabrication of pH-Responsive Hydrogel and Its In Vitro and In Vivo Evaluation. *Advances in Polymer Technology* 37:290–304. <https://doi.org/10.1002/adv.21668>
36. Niu B, Jia J, Wang H, et al (2019) In vitro and in vivo release of diclofenac sodium-loaded sodium alginate/carboxymethyl chitosan-ZnO hydrogel beads. *International Journal of Biological Macromolecules* 141:1191–1198. <https://doi.org/10.1016/j.ijbiomac.2019.09.059>
37. Jana S, Sharma R, Maiti S, Sen KK (2016) Interpenetrating hydrogels of O-carboxymethyl Tamarind gum and alginate for monitoring delivery of acyclovir. *International Journal of Biological Macromolecules* 92:1034–1039. <https://doi.org/10.1016/j.ijbiomac.2016.08.017>
38. Varahala Setti ML, Ratna JV (2009) Preparation and evaluation of controlled release tablets of carvedilol. *Asian Journal of Pharmaceutics* 3:252–256.

<https://doi.org/10.4103/0973-8398.56307>

39. Kumar J, Purwar R (2024) Self-Healing Biocompatible Injectable Hydrogel Based on Multialdehyde Moringa oleifera. *ChemistrySelect* 9:e202400309
40. Malik R, Warkar SG, Saxena R (2023) Carboxy-methyl tamarind kernel gum based bio-hydrogel for sustainable agronomy. *Materials Today Communications* 35:105473. <https://doi.org/10.1016/j.mtcomm.2023.105473>
41. Elzayat EM, Abdel-Rahman AA, Ahmed SM, et al (2016) Studying the impact of formulation and processing parameters on the release characteristics from hydroxypropyl methylcellulose matrix tablets of diclofenac. *Acta Poloniae Pharmaceutica - Drug Research* 73:439–452
42. Ekici S, Saraydin D (2007) Interpenetrating polymeric network hydrogels for potential gastrointestinal. *Polym Int* 56:1371–1377. <https://doi.org/10.1002/pi.2271>
43. Mali KK, Dhawale SC, Dias RJ (2017) Synthesis and characterization of hydrogel films of carboxymethyl tamarind gum using citric acid. *International Journal of Biological Macromolecules* 105:463–470. <https://doi.org/10.1016/j.ijbiomac.2017.07.058>
44. Suhail M, Khan A, Rosenholm JM, et al (2021) Fabrication and characterization of diclofenac sodium loaded hydrogels of sodium alginate as sustained release carrier. *Gels* 7:1–16. <https://doi.org/10.3390/gels7010010>
45. Nawaz S, Khan S, Farooq U, et al (2018) Biocompatible hydrogels for the controlled delivery of anti-hypertensive agent: Development, characterization and in vitro evaluation. *Designed Monomers and Polymers* 21:18–32. <https://doi.org/10.1080/15685551.2018.1445416>
46. Goonoo N, Bhaw-Luximon A, Ujoodha R, et al (2014) Naltrexone: A review of existing sustained drug delivery systems and emerging nano-based systems. *Journal of Controlled Release* 183:154–166. <https://doi.org/10.1016/j.jconrel.2014.03.046>

CHAPTER 4

SYNTHESIS AND CHARACTERIZATION OF POLYETHYLENE GLYCOL DIACRYLATE-CROSSLINKED β -CYCLODEXTRIN-BASED HYDROGEL FOR EFFICIENT DELIVERY OF HYDROPHOBIC DRUG INDOMETHACIN

4.1 Introduction

The development of the next generation of drugs has fueled a growing interest in advanced drug delivery systems [1]. Unlike traditional drug delivery systems (DDS), which result in a quick spike followed by a decline over time in the bloodstream, controlled drug delivery systems aims to provide a consistent delivery rate. Among these DDS, hydrogels have gained prominent attention for their unique properties, including their ability to swell in response to environmental stimuli and their sensitivity to pH variations. This characteristic enables them to provide sustained drug release, enhancing therapeutic efficacy while minimizing side effects [2].

Nowadays, natural biopolymer-based pH-sensitive hydrogels, particularly those derived from polysaccharides such as sodium alginate, chitosan, CMTKG, etc, have gained interest due to their good biodegradability, and biocompatibility [1], [3-6].

Moreover, the combination of natural polymers with synthetic polymers like polyacrylamide (PAM) has also garnered significant attention in recent times.[7]. Considerable research has been reported on PAM-based hydrogels for hydrophilic drug delivery [8-10]. For instance, Chen et al. (2022) reported the synthesis of alendronate hydrochloride-loaded polyacrylamide/carboxymethyl cellulose hydrogel [11]. However, exploration in the realm of hydrophobic drugs has been relatively limited. Furthermore, existing studies on hydrogel-based hydrophobic drug delivery still face challenges, including difficulty in achieving targeted delivery. For example, Sarfraz et al. (2017) developed β -cyclodextrin-g-poly(2-acrylamido-2-methylpropane sulfonic acid) hydrogel for delivery of the hydrophobic drug indomethacin. Although the finding revealed that 27-36% indomethacin was released at pH 1.2, this non-targeted high release in the stomach can lead to gastric irritation [12]. Thereby, this study seeks to address this research gap by developing a pH-responsive hydrogel matrix and investigating the impact of beta-cyclodextrin (β -CD) on the controlled release of the hydrophobic drug indomethacin.

The β -CD has a truncated cone-like structure with seven glucose units, having a hydrophobic inner cavity and a hydrophilic outer surface, demonstrating significant potential in forming inclusion host-guest complexes with numerous hydrophobic guest (drug molecules), such as aspirin, indomethacin, etc [13-14]. This property enables β -CD to enhance the loading of hydrophobic drugs such as indomethacin, thereby extending their therapeutic efficacy.

Indomethacin, classified as a non-steroidal anti-inflammatory drug, finds extensive use in addressing chronic pain and inflammatory conditions, including rheumatoid and osteoarthritis [15]. However, its shorter half-life necessitates repeated dosing, which can lead to serious health issues.

Thus, in the present study, the efforts are directed toward the synthesis of a hydrogel based on β -CD, CMTKG, and PAM via the free radical mechanism for controlled indomethacin release. The fabricated hydrogels were characterized using ATR-FTIR, PXRD, and SEM techniques. Sol-gel fraction, swelling and porosity were investigated for all the synthesized hydrogels. Furthermore, the drug release mechanism was explored using various mathematical models, including Hixson-Crowell, Korsmeyer-Peppas, First-Order, Zero-Order, and Higuchi. Moreover, degradability and cytotoxicity studies have been conducted for the synthesized hydrogel. Additionally, all experiments were performed in triplicate, with the standard deviations shown as error bars in the graphs.

4.2 Experimental Section

4.2.1 Materials

β -Cyclodextrin (MW=1134.98 g/mol, CDH, New Delhi, India), Acrylamide (MW=71.08 g/mol, Fischer Scientific, Mumbai, India), Poly(ethylene glycol diacrylate) ($M_n = 2000$ g/mol, Sigma Aldrich, India), potassium persulfate (MW=270.30 g/mol, Fischer Scientific, Mumbai, India), and indomethacin (MW=357.78 g/mol, Unicare India Pvt Ltd, Noida, India) were used as obtained.

CMTKG (0.20° of substitution, MW=9.14 ×10⁵ g/mol) was courteously gifted by Hindustan Gum Pvt Ltd, Haryana, India.

4.2.2 Synthesis of PAM/CMTKG and β-CD/PAM/CMTKG hydrogels

The series of β-CD/PAM/CMTKG hydrogels (W-1 to W-4) with varied quantities of the PEGDA (1.5-3 ml) were fabricated using a free radical mechanism, as displayed in Table 4.1. For the fabrication of β-CD/PAM/CMTKG hydrogels, a specific quantity of CMTKG, β-CD, and AM was dissolved in distilled water and stirred for 30 min (Fig. 4.1). To the above solution, the fixed amount of KPS and PEGDA were added and again stirred for 30 min. Then, the solution was poured into the test tubes and placed inside the water bath, set at 60°C for 1 h. Finally, the developed hydrogel was extracted from the test tube, cut into slices, and oven-dried at 55°C for 48 h [16].

For the fabrication of control (PAM/CMTKG hydrogel) (W-5), the procedure was the same as the one described above, with modification that β-CD was not added.

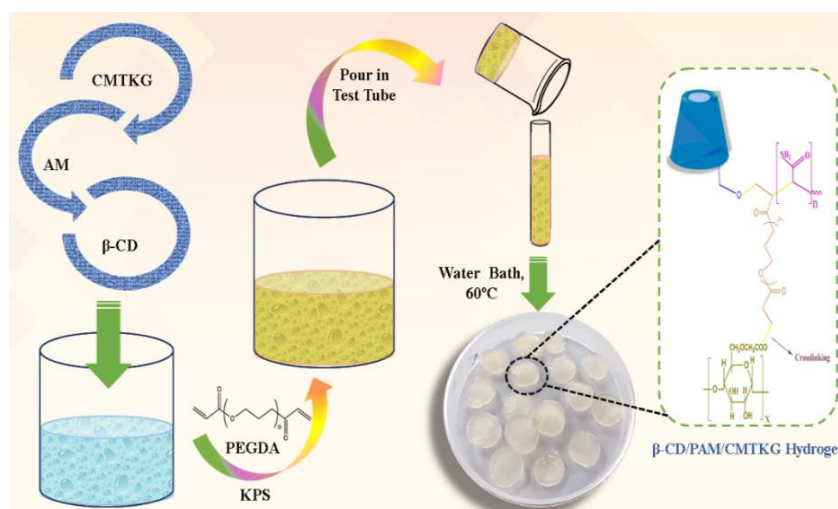


Fig. 4.1 Schematic illustration of the β-CD/PAM/CMTKG hydrogel fabrication

Table 4.1 Compositions of CMTKG-based hydrogels

Sample Code	CMTKG (g)	β-CD (g)	AM (g)	PEGDA (ml)
W-1	0.1	0.1	2	1.5
W-2	0.1	0.1	2	2.0
W-3	0.1	0.1	2	2.5
W-4	0.1	0.1	2	3.0
W-5	0.1	0	2	2.5

4.2.3 Characterization

PXRD measurements were performed via a Bruker D8 Discover Diffractometer utilizing Cu K α radiation ($\lambda = 1.5418 \text{ \AA}$), within 2θ range of $5\text{-}70^\circ$. The ATR-FTIR spectra were captured with a Nicolet iS50 FTIR Tri-detector spectrometer within the wavenumber range from $450\text{-}4000 \text{ cm}^{-1}$. The micrographic images were captured using SEM (Model: JEOL Japan Mode: JSM 6610LV).

4.2.4 Swelling analysis

A swelling assessment was carried out for all synthesized hydrogels in both HCl-KCl buffer (pH 1.2) and phosphate buffer saline (pH 7.4) for 24 h, using gravimetric analysis. In the study, a specific amount (M_{DH}) of dried hydrogels was placed into the buffer solution. At time interval (1 h), the hydrogels were taken out from the solutions, carefully dried using a filter paper, and reweighed (M_{SH}). The given Eqn. (4.1) was applied for the calculation of swelling [17].

$$\text{Swelling (\%)} = \frac{M_{SH} - M_{DH}}{M_{DH}} \times 100 \quad (4.1)$$

Moreover, at time t , when hydrogel reaches equilibrium, its swelling is termed as equilibrium swelling %, calculated using the same formula

4.2.5 Sol-Gel analysis

To analyze the non-crosslinked (sol) and crosslinked (gel) components of the developed hydrogels, a sol-gel analysis was performed. Initially, the dried hydrogel weight was measured (M_i) and then immersed in distilled water for 24 h. Then, the hydrogel was subjected to drying in the oven at 50°C until a constant weight (M_e) was reached. The sol and gel fraction (%) was assessed by utilizing the given Eqn. (4.2) and Eqn. (4.3) [2].

$$\text{Sol Fraction (\%)} = \frac{M_i - M_e}{M_e} \times 100 \quad (4.2)$$

$$\text{Gel fraction (\%)} = 100 - \text{Sol fraction} \quad (4.3)$$

4.2.6 Porosity

The porosity evaluation for all the synthesized hydrogels was carried out using the solvent displacement technique. Initially, the weighed dried hydrogel disc (W_i) was immersed in 5 ml of hexane for 1 h. Then, the hydrogel discs were extracted from the hexane, the disc was wiped with filter paper, and weight (W_f) was noted [18]. The porosity of the hydrogel discs was determined using the given Eqn. (4.4).

$$\text{Porosity (\%)} = \frac{W_f - W_i}{\rho V} \times 100 \quad (4.4)$$

where, ρ represents hexane density (0.659 g/ml), while V corresponds to the volume of the cylindrical hydrogel disk, calculated using the formula $V = \pi r^2 h$, where 'r' is

the radius and 'h' is the height of the disk, quantified using a vernier calliper [19].

4.2.7 Indomethacin Loading and Entrapment Efficiency

Out of all the fabricated formulations, the hydrogel (W-1) was selected for the drug loading due to its highest swelling capacity. The drug loading and entrapment efficiency of β -CD/PAM/CMTKG hydrogel (with β -CD) and control PAM/CMTKG hydrogel (without β -CD) (W-5) was examined using a weight method. The specified amount of hydrogel disc (M_{UH}) was immersed into a 100 ml buffer solution with a pH of 7.4 containing 75 mg of the indomethacin, which represent as M_D for 24 h. Afterwards, a hydrogel disc was taken out and oven-dried at 60°C, and weight (M_{LH}) was noted. The DL% and DEE% were determined using the Eqn.(4.5) and Eqn.(4.6) [20].

$$DL (\%) = \frac{M_{LH} - M_{UH}}{M_{UH}} \times 100 \quad (4.5)$$

$$DEE (\%) = \frac{M_{LH} - M_{UH}}{M_D} \times 100 \quad (4.6)$$

4.2.8 In vitro indomethacin release study

To investigate the release of indomethacin from the hydrogel, a precise amount of indomethacin-loaded hydrogel disc was immersed in 100 mL of each pH 1.2 buffer solution and pH 7.4 till equilibrium was achieved. The solutions were agitated at 200 rpm and 37°C in an orbital incubator shaker. To keep the volume constant, 3 mL of released medium was withdrawn and replaced with fresh buffer every hour for up to 24 h. The withdrawn solution was diluted with ethanol, and absorbance of the released

drug in the medium was quantified using a UV-visible spectrophotometer (Cary 300 UV-Vis model) at the λ_{\max} 318 nm for pH 1.2 and λ_{\max} 320 nm for pH 7.4 solution [19]. The drug content was determined by utilizing the standard calibration curve of indomethacin. The Eqn. (4.7) was used to calculate drug release.

$$\text{Cumulative drug release } \left(\frac{M_t}{M_\infty} \right) = \frac{V_t C_t + V_W \sum_1^{n-1} C_{t-1}}{M_\infty} \quad (4.7)$$

Here, M_t is the amount of drug released at time t, M_∞ is the amount of drug loaded, V_t is the total volume of release medium, V_W is the volume of solution withdrawn, C_t and C_{t-1} are the concentration of solution at time t and t-1 [21].

4.2.9 Kinetic Modelling

Different mathematical models, such as the Hixson-Crowell, Korsmeyer-Peppas, First-Order, Zero-Order, and Higuchi, were employed to analyse the drug release mechanism. The evaluation of regression coefficient (R^2) values was conducted for each model. The model exhibiting an R^2 value closest to 1 was identified as the most suitable model for the description of the drug release mechanism [22], [23].

4.2.10 Cytotoxicity

The impact of indomethacin-loaded β -CD/PAM/CMTKG hydrogel on the HCT 116 human colon cell line, obtained from NCCS Pune, was examined through the MTT Assay. Cells were initially seeded at a density of 10,000 cells per well in a 96-well plate in DMEM medium, supplemented with 10% FBS and 1% antibiotic solution, at 37°C with 5% CO₂ for 24 hours. Following this, the cells were subjected to various concentrations (0.78 to 6.25 μ g/ml) of the hydrogel, while a solution with no hydrogel

was designated as the control. After 24-hour incubation, MTT Solution was introduced and allowed to incubate for 2 hours. Subsequently, the supernatant was removed, and the cell layer was dissolved in 100 μ l of Dimethyl Sulfoxide. To evaluate cell viability, absorbance readings were taken at 540 nm and 660 nm using an Elisa plate reader (iMark, Biorad, USA). Furthermore, images were captured under an inverted microscope (Olympus ek2).

4.2.11 Degradation

Degradation experiments were executed in a pH 7.4 buffer, employing an orbital incubator shaker set at 37°C. The hydrogel disc was immersed in buffer until it achieved complete swelling and was then weighed (W_{IH}). Subsequently, every hour, the hydrogel discs were taken out, wiped with filter paper, weighed (W_{FH}), and then dipped back into the buffer solution. The degradation (%) was computed using the following Eqn. (4.8) [24],[25].

$$\text{Degradation (\%)} = \frac{W_{IH} - W_{FH}}{W_{IH}} \times 100 \quad (4.8)$$

4.3 Result and Discussion

4.3.1 Mechanism of β -CD/PAM/CMTKG and indomethacin-loaded β -CD/PAM/CMTKG hydrogel synthesis

Several β -CD/PAM/CMTKG hydrogels (W-1 to W4) were synthesized through the free radical mechanism, employing KPS as an initiator and PEGDA as a crosslinker. Initially, the thermal decomposition of KPS at 60°C produces a sulphate radical, triggering the polymerization of acrylamide (AM) to form polyacrylamide and

simultaneously generating radicals on CMTKG & β -CD. PEGDA acts as a crosslinker, fostering the formation of a crosslinked polymeric network by establishing covalent bonds between CMTKG, PAM, and β -CD (hydrophilic exterior), leading to the fabrication of a three-dimensional β -CD/PAM/CMTKG hydrogel [14], [26].

In indomethacin-loaded β -CD/PAM/CMTKG hydrogels, β -CD (guest) hydrophobic interior forms a host-guest complex with indomethacin (guest) entrapped in its cavity, enhancing drug loading and enabling a slow & controlled release over time. Fig. 4.2 outlines the mechanism involved in the synthesis of the indomethacin-loaded β -CD/PAM/CMTKG hydrogel [27].

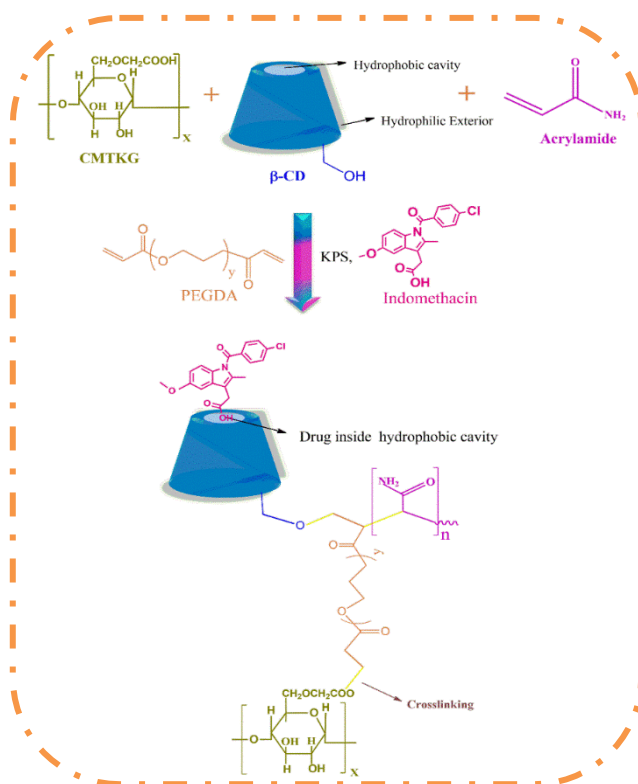


Fig. 4.2 Mechanism for indomethacin-loaded β -CD/PAM/CMTKG hydrogel synthesis

4.3.2 Characterization

PXRD was done to investigate the crystalline or amorphous nature of the material. The PXRD pattern of indomethacin displayed sharp peaks at 2θ values of 12.9° , 18.2° , 19.3° , 28° , and 39.8° , revealing its high crystallinity. The broad peak observed in the β -CD/PAM/CMTKG and indomethacin-loaded β -CD/PAM/CMTKG hydrogel indicates their amorphous structure (Fig. 4.3). Additionally, in the indomethacin-loaded β -CD/PAM/CMTKG hydrogel, no extra peaks attributable to indomethacin (drug) were detected, implying a homogeneous dispersion of indomethacin within the hydrogel matrix [28].

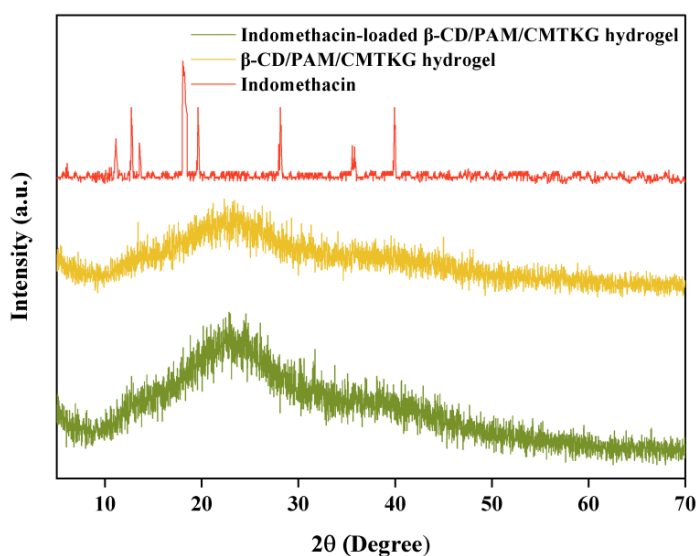


Fig. 4.3 PXRD pattern of β -CD/PAM/CMTKG hydrogel (W-1) and indomethacin-loaded β -CD/PAM/CMTKG hydrogel

SEM micrographs of β -CD/PAM/CMTKG hydrogel (W-1) and indomethacin-loaded β -CD/PAM/CMTKG hydrogel are presented in Fig. 4.5. The β -CD/PAM/CMTKG hydrogel exhibited a highly porous surface, emphasizing its capacity for swelling and drug loading. Additionally, the surface morphology analysis of the indomethacin-loaded β -CD/PAM/CMTKG hydrogel displayed a very low porous surface. Thus, it suggests that indomethacin has been successfully encapsulated within the polymer network, resulting in a decrease in the free void in hydrogel [2].

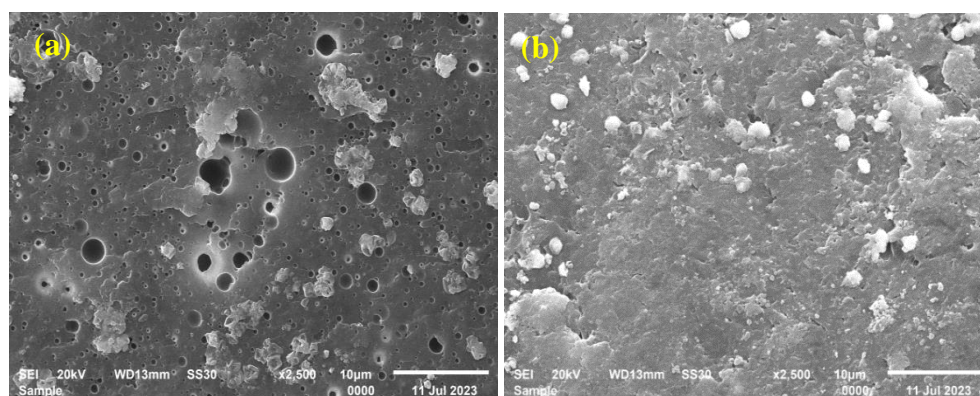


Fig. 4.4 SEM micrographs of (a) β -CD/PAM/CMTKG and (b) indomethacin-loaded β -CD/PAM/CMTKG hydrogels

The ATR-FTIR spectra of the PEGDA, indomethacin, β -CD/PAM/CMTKG hydrogel (W-1), and indomethacin-loaded β -CD/PAM/CMTKG hydrogel, are depicted in Fig. 4.4. The C=C stretch at 1646 cm^{-1} in PEGDA shifted to lower wavenumbers (1602 cm^{-1} and 1603 cm^{-1}) in β -CD/PAM/CMTKG hydrogel, and indomethacin-loaded β -CD/PAM/CMTKG hydrogel respectively, indicating crosslinking. Furthermore, the C=O peak shifted to higher wavenumbers (1668 cm^{-1} and 1665 cm^{-1}) in β -CD/PAM/CMTKG and indomethacin-loaded β -CD/PAM/CMTKG hydrogels,

indicates a reduction in conjugation and hence, confirming polymerization of AM [29]. Additionally, in indomethacin-loaded β -CD/PAM/CMTKG hydrogel, no new peaks emerged other than drug compared to β -CD/PAM/CMTKG hydrogel, suggesting a weak physical interaction (hydrogen bonding) between indomethacin (drug) and the hydrogel [26].

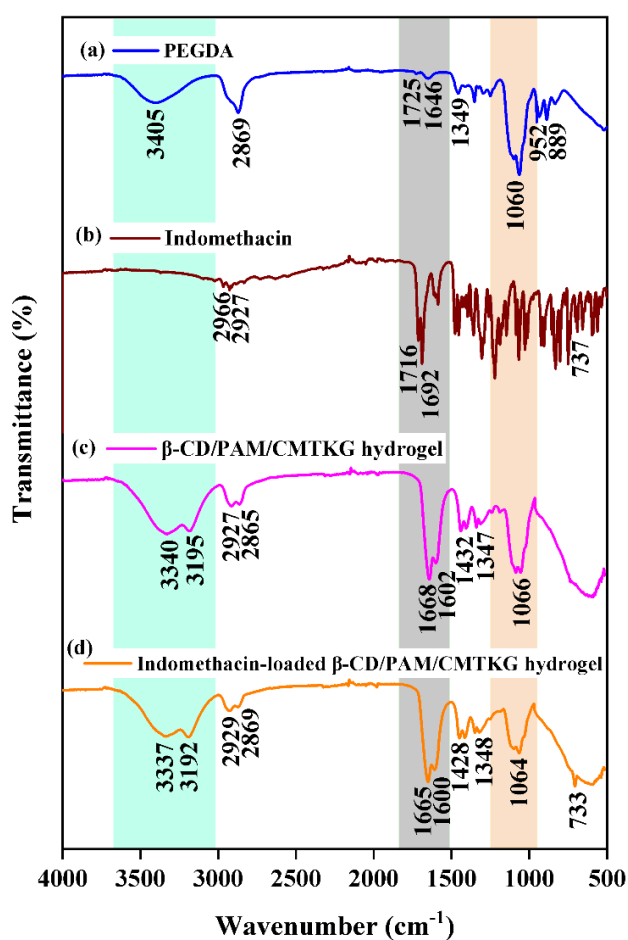


Fig. 4.5 ATR-FTIR spectra of (a) PEGDA, (b) Indomethacin, (c) β -CD/PAM/CMTKG hydrogel, and (d) indomethacin-loaded β -CD/PAM/CMTKG hydrogel

4.3.3 Swelling studies

The swelling behavior of hydrogels is affected by different PEGDA concentrations (W-1 to W-4), as shown in Fig. 4.6(a). It was observed that with an increase in PEGDA concentration (1.5-3 ml), a decrease in equilibrium swelling ratio occurs. The increased PEGDA content contributes to an increased crosslinking density, thus reducing the available free space for fluid absorption, resulting in diminished swelling [29]. The formulation W-1, containing 1.5 ml of PEGDA, exhibits maximum swelling of $1000.27 \% \pm 0.42$ at pH 7.4, with a recorded swelling of $750.21 \% \pm 0.32$ at pH 1.2. A notable difference in swelling was observed in pH 7.4 and 1.2 buffer solutions, as shown in Fig. 4.6(b). This phenomenon is attributed to the deprotonation of the carboxylic acid (COOH) within CMTKG at pH 7.4. Under this condition, electrostatic repulsion occurs between the deprotonated COO^- ions, leading to network expansion and, consequently, more available space for fluid absorption, leading to increased swelling. While, at pH 1.2, the carboxyl groups may remain in their un-ionized state, so there is no network expansion, resulting in a lower swelling compared to that observed at pH 7.4 [6].

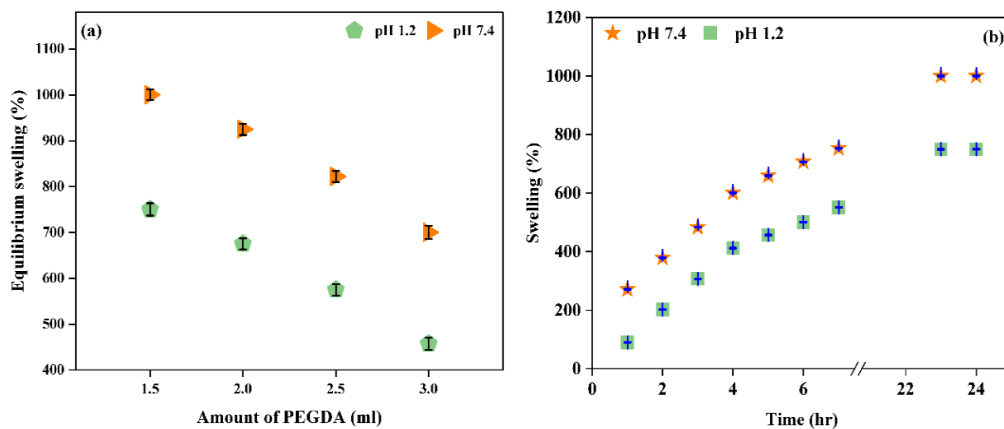


Fig. 4.6 (a) Effect of the PEGDA on the equilibrium swelling (%) and (b) Rate of swelling of W-1 hydrogel with respect to time

4.3.4 Sol-Gel Analysis

The sol-gel analysis for the fabricated hydrogels is illustrated in Fig. 4.7. As the quantities of PEGDA (W-1 to W-4) increased, a significant increase in crosslinking density was observed. Consequently, more crosslinking within the hydrogel leads to a more compact structure and an increase in the insoluble gel part [30].

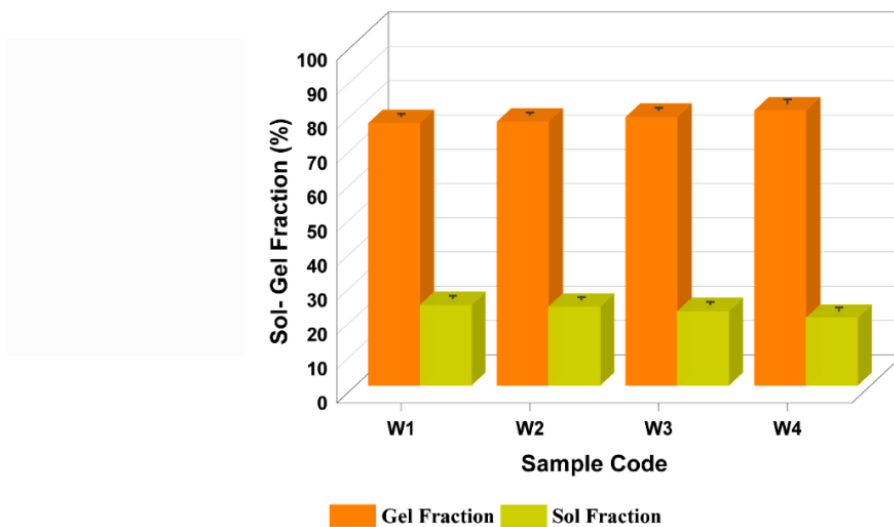


Fig. 4.7 Sol-Gel analysis plot for all fabricated β -CD/PAM/CMTKG hydrogels

4.3.5 Porosity

The porosity profile reveals that an increase in the quantity of the crosslinker PEGDA (W-1 to W-4) leads to a corresponding decrease in porosity, as presented in Fig. 4.8. This phenomenon arises from an increase in the entanglement and crosslinking between the polymeric chains of CMTKG, β -CD, and PAM, creating a denser structure and consequently, reduced porosity [22].

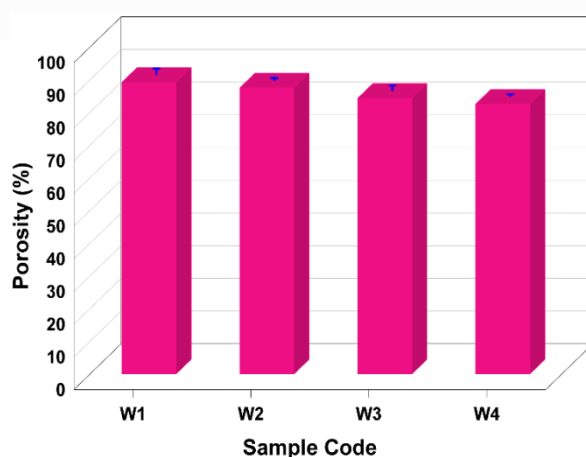


Fig. 4.8 Porosity plot for all formulated β -CD/PAM/CMTKG hydrogels

4.3.6 Indomethacin Loading and Entrapment Efficiency

The β -CD/PAM/CMTKG and PAM/CMTKG hydrogels were evaluated for drug loading and drug entrapment efficiency, and the corresponding values are detailed in Table 4.2. The β -CD/PAM/CMTKG hydrogel shows a significant increase in both drug loading and drug entrapment efficiency when compared to the PAM/CMTKG hydrogel. This is attributed to β -CD, which entrapped the hydrophobic indomethacin drug within its hydrophobic cavity, thus enhancing the loading and entrapment efficiency of β -CD/PAM/CMTKG hydrogel [27].

Table 4.2 Indomethacin loading and entrapment efficiency values for β -CD/PAM/CMTKG and PAM/CMTKG hydrogel

Sample Code	Hydrogel	Drug Loading (%)	Drug Entrapment Efficiency (%)
W-1	β -CD/PAM/CMTKG	25.84 \pm 0.54	79.89 \pm 0.49
W-5	PAM/CMTKG	20.36 \pm 0.73	72.36 \pm 0.57

4.3.7 In vitro indomethacin release analysis

In vitro release analysis was conducted for indomethacin-loaded PAM/CMTKG hydrogel and indomethacin-loaded β -CD/PAM/CMTKG hydrogel. The indomethacin-loaded β -CD/PAM/CMTKG hydrogel exhibited lesser drug release in comparison to the indomethacin-loaded PAM/CMTKG hydrogel, as depicted in Fig. 4.9. This is attributed to the hydrophobic cavity of β -CD, which is responsible for entrapping indomethacin inside the cavity and lowering down its release from the hydrogel [27]. At pH 7.4, the maximum release of indomethacin from PAM/CMTKG and β -CD/PAM/CMTKG hydrogels was noted as 73.53 \pm 0.47% and 62.49 \pm 0.77%, respectively. However, at pH 1.2, the maximum indomethacin release (%) for PAM/CMTKG and β -CD/PAM/CMTKG hydrogels were 18.99 \pm 0.59% and 16.34 \pm 0.67%, respectively. Indomethacin release was significantly higher in both hydrogels at pH 7.4 compared to pH 1.2. The increased release at pH 7.4 is attributed to higher swelling (as discussed in the swelling section), facilitating greater diffusion of indomethacin from the hydrogel [13]. Therefore, the β -CD/PAM/CMTKG hydrogel shows the potential to facilitate the better-controlled release of indomethacin.

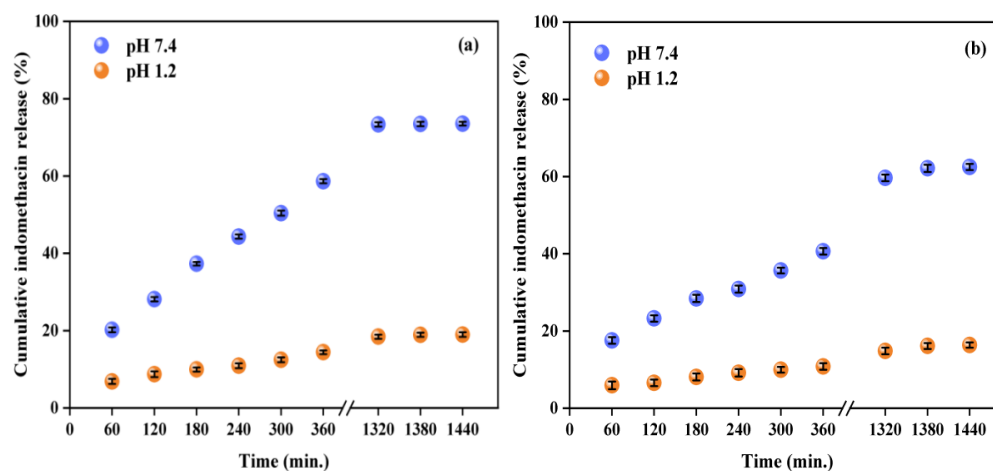


Fig. 4.9 Indomethacin release profiles for indomethacin-loaded (a) PAM/CMTKG hydrogel and (b) β -CD/PAM/CMTKG hydrogel at pH 1.2 and 7.4

4.3.8 Kinetic Modelling

The correlation coefficients (R^2) of various models were compared to assess the release mechanism of indomethacin from indomethacin-loaded β -CD/PAM/CMTKG hydrogel (Table 4.3). For indomethacin-loaded β -CD/PAM/CMTKG hydrogel, the Higuchi model demonstrated the highest R^2 value, indicating the best fit to describe the drug release mechanism (Fig. 4.10). According to the Higuchi model, drug release predominantly occurs through Fickian diffusion. Fickian diffusion occurs when drug molecules move through the hydrogel due to a concentration gradient. This movement is governed by the diffusion principle, where drug molecules move from regions of higher concentration (i.e., hydrogel) to areas of lower concentration (i.e., surrounding buffer solution) [7].

Table 4.3 Regression coefficient (R^2) data for indomethacin-loaded β -CD/PAM/CMTKG hydrogel

Model	Equation	pH 7.4		pH 1.2		Ref.
		K	R^2	R^2	K	
Hixson-Crowell	$(M_t)^{1/3} - (M_\infty)^{1/3} = k_{HX} \cdot t$ k_{HX} =Hixson Crowell constant	0.068	0.947	0.963	0.095	[3]
First Order	$\text{Log } M_t = \text{Log } M_\infty + \frac{kt}{2.303}$ k =First order rate constant	0.079	0.929	0.948	0.067	[16]
Korsmeyer-Peppas	$M_t/M_\infty = kt^n$ k = kinetic constant n = diffusion exponent	0.085	0.978	0.975	0.065	[19]
Zero Order	$M_t = M_\infty + k_0t$	0.095	0.972	0.967	0.073	[7]
Higuchi	$M_t/M_\infty = k_{HG} \cdot t^{1/2}$ k_{HG} = kinetic constant	0.076	0.980	0.982	0.064	[19]

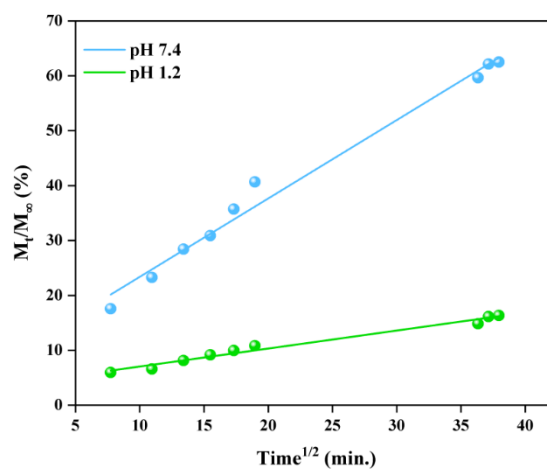


Fig. 4.10 Release kinetic plot indomethacin-loaded β -CD/PAM/CMTKG hydrogel

4.3.9 Cytotoxicity

The evaluation of cytotoxicity is important for ensuring the biocompatibility of fabricated hydrogel intended for biomedical applications. The analysis was performed for the different concentrations (0.78, 1.56, 3.125, 6.25 $\mu\text{g/ml}$) of synthesized indomethacin-loaded $\beta\text{-CD/PAM/CMTKG}$ hydrogel and a control (without hydrogel), against the HCT-116 human colon cell line (Fig. 4.11). The fabricated indomethacin-loaded $\beta\text{-CD/PAM/CMTKG}$ hydrogel shows 79% cell viability at the highest concentration (6.25 $\mu\text{g/mL}$), highlighting the non-toxic behaviour of synthesized matrix. This result was observed due to the inherent biocompatibility of CMTKG and $\beta\text{-CD}$ present in the hydrogel [14]. Additionally, microscopic examination of HCT-116 cells revealed polygonal-shaped cells and similar cell density in control and hydrogel-treated cell lines, signifying no change in cell shape and very little impact on the cell viability induced by the synthesized hydrogel (Fig. 4.12).

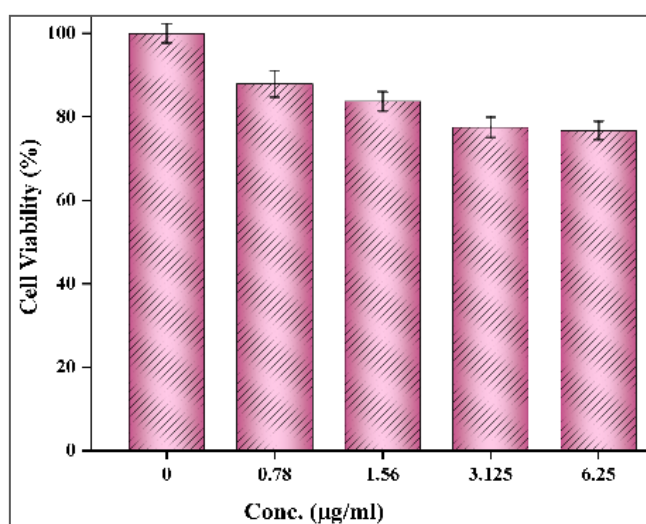


Fig. 4.11 Cytotoxicity plot for indomethacin-loaded $\beta\text{-CD/PAM/CMTKG}$ hydrogel

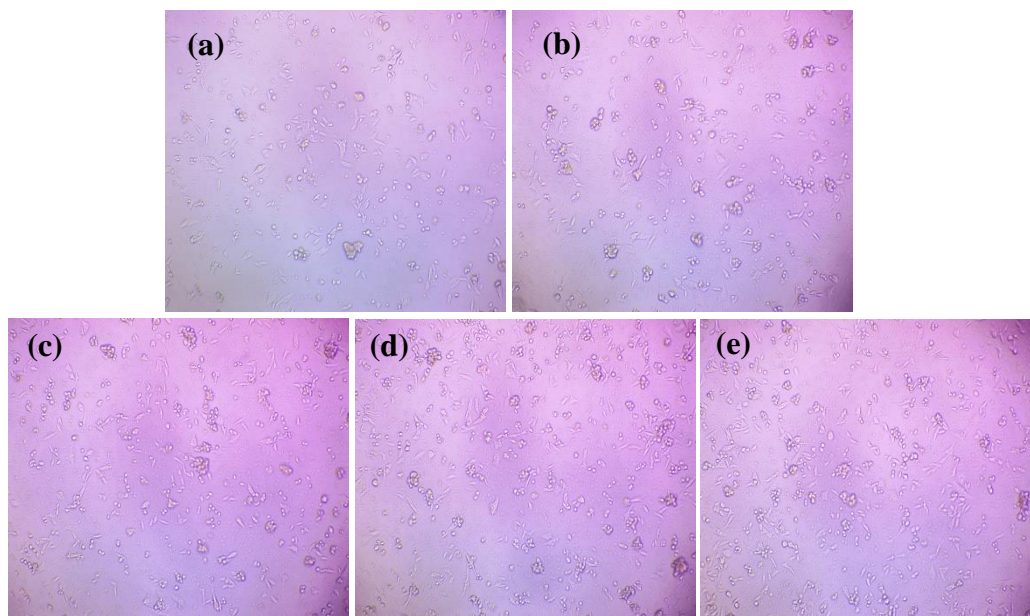


Fig. 4.12 Optical microscopic images of HCT-116 cells treated with (a) control (b) 0.78 µg/ml, (c) 1.56 µg/ml, (d) 3.125 µg/ml and (e) 6.25 µg/ml of indomethacin-loaded β -CD/PAM/CMTKG hydrogel

4.3.10 Degradation

The biodegradability of materials plays a pivotal role in facilitating their effectiveness and versatility in various biomedical applications. The degradation profile of the synthesized indomethacin-loaded β -CD/PAM/CMTKG hydrogel, depicted in Fig. 4.13, reveals degradation attributed to the breakdown of glycosidic (C-O-C) linkages, which led to complete degradation (100%) within 10 days. Thus, this remarkable degradability highlights the potential of this fabricated indomethacin-loaded β -CD/PAM/CMTKG hydrogel for safe and effective drug delivery applications.

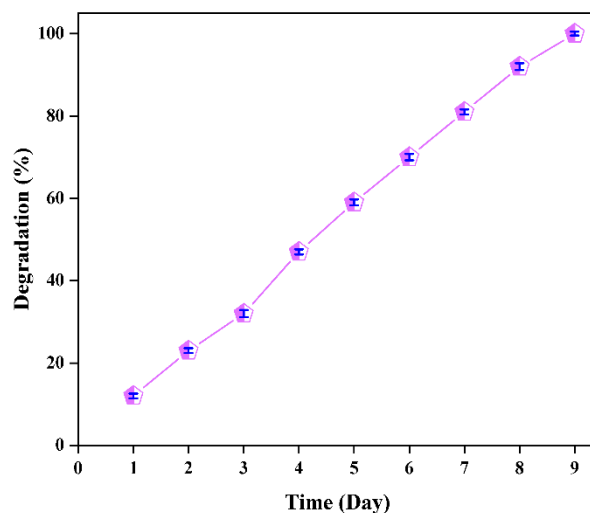


Fig. 4.13 Degradation curve for indomethacin-loaded β -CD/PAM/CMTKG hydrogel

4.4 Conclusion

In this work, CMTKG, β -CD, and PAM-based hydrogels were successfully synthesized for controlled indomethacin release. The concentration of PEGDA was observed to impact the porosity (%), gel fraction (%) and swelling behavior of the hydrogel. The addition of β -CD revealed an increase in drug loading and entrapment efficiency, with the drug release data fitting a Higuchi model. Remarkably, hydrogel exhibited higher release (62.49%) at pH 7.4, making it ideal for targeted drug delivery to the colon. Importantly, the synthesized hydrogel degrades completely (100%) within 10 days and exhibits no cytotoxicity against HCT-116 human colon cell lines. Consequently, the synthesized indomethacin-loaded β -CD/PAM/CMTKG hydrogel demonstrates non-toxicity and exhibits pH-responsive properties, emphasizing its potential for the controlled release of the hydrophobic drug indomethacin.

4.5 REFERENCES

1. Kong WQ, Gao CD, Hu SF, et al (2017) Xylan-modified-based hydrogels with temperature/pH dual sensitivity and controllable drug delivery behavior. *Materials* 10. <https://doi.org/10.3390/ma10030304>
2. Naeem F, Khan S, Jalil A, Ranjha NM, Riaz A, Haider MS, Sarwar S, Saher F, Afzal S (2017) pH Responsive cross-linked polymeric matrices based on natural polymers: Effect of process variables on swelling characterization and drug delivery properties. *BioImpacts* 7:177–192. <https://doi.org/10.15171/bi.2017.21>
3. Thirupathi K, Phan TTV, Santhamoorthy M, et al (2022) pH and Thermoresponsive PNIPAm-co-Polyacrylamide Hydrogel for Dual Stimuli-Responsive Controlled Drug Delivery. *Polymers* 15:167. <https://doi.org/10.3390/polym15010167>
4. Raza MA, Park SH (2020) Irradiated Ch/GG/PVP-based stimuli-responsive hydrogels for controlled drug release. *Journal of Applied Polymer Science* 137. <https://doi.org/10.1002/app.49041>
5. Mali KK, Dhawale SC, Dias RJ, et al (2017) Interpenetrating networks of carboxymethyl tamarind gum and chitosan for sustained delivery of aceclofenac. *Marmara Pharmaceutical Journal* 21:771–782. <https://doi.org/10.12991/mpj.2017.20>
6. Jana S, Sharma R, Maiti S, Sen KK (2016) Interpenetrating hydrogels of O-carboxymethyl Tamarind gum and alginate for monitoring delivery of acyclovir. *International Journal of Biological Macromolecules* 92:1034–1039. <https://doi.org/10.1016/j.ijbiomac.2016.08.017>
7. Meena P, Singh P, Warkar SG (2023) Development and assessment of carboxymethyl tamarind kernel gum-based pH-responsive hydrogel for release of diclofenac sodium. *European Polymer Journal* 197:112340. <https://doi.org>

/10.1016/j.eurpolymj.2023.112340

8. Xu X, Gu Z, Chen X, et al (2019) An injectable and thermosensitive hydrogel: Promoting periodontal regeneration by controlled-release of aspirin and erythropoietin. *Acta Biomaterialia* 86:235–246. <https://doi.org/10.1016/j.actbio.2019.01.001>
9. Li S, Xiaowen Y, Yang Y, et al (2023) Osteogenic and anti-inflammatory effect of the multifunctional bionic hydrogel scaffold loaded with aspirin and nano-hydroxyapatite. *Frontiers in Bioengineering and Biotechnology* 11:1–16. <https://doi.org/10.3389/fbioe.2023.1105248>
10. Sethi S, Saruchi, Kaith BS, et al (2020) Cross-linked xanthan gum–starch hydrogels as promising materials for controlled drug delivery. *Cellulose* 27:4565–4589. <https://doi.org/10.1007/s10570-020-03082-0>
11. Chen ZY, Gao S, Zhou RB, et al (2022) Dual-crosslinked networks of superior stretchability and toughness polyacrylamide-carboxymethylcellulose hydrogel for delivery of alendronate. *Materials and Design* 217:110627. <https://doi.org/10.1016/j.matdes.2022.110627>
12. Sarfraz RM, Ahmad M, Mahmood A, et al (2017) Development of β -cyclodextrin-based hydrogel microparticles for solubility enhancement of rosuvastatin: An in vitro and in vivo evaluation. *Drug Design, Development and Therapy* 11:3083–3096. <https://doi.org/10.2147/DDDT.S143712>
13. Malik NS, Ahmad M, Minhas MU (2017) Cross-linked β -cyclodextrin and carboxymethyl cellulose hydrogels for controlled drug delivery of acyclovir. *PLoS ONE* 12:1–17. <https://doi.org/10.1371/journal.pone.0172727>
14. Zakaria AF, Kamaruzaman S, Abdul Rahman N, Yahaya N (2022) Sodium Alginate/ β -Cyclodextrin Reinforced Carbon Nanotubes Hydrogel as Alternative Adsorbent for Nickel(II) Metal Ion Removal. *Polymers* 14:5524. <https://doi.org/10.3390/polym14245524>

15. Yuan M, Niu J, Xiao Q, et al (2022) Hyaluronan-modified transfersomes based hydrogel for enhanced transdermal delivery of indomethacin. *Drug Delivery* 29:1232–1242. <https://doi.org/10.1080/10717544.2022.2053761>
16. Tushar, Saraswat Y, Meena P, Sudhir G. Warkar (2023) Synthesis and characterization of novel xanthan gum - based pH - sensitive hydrogel for metformin hydrochloride release. *Colloid and Polymer Science*. <https://doi.org/10.1007/s00396-023-05135-9>
17. Gholamali I, Asnaashariisfahani M, Alipour E, Sepahi AA (2020) In-situ synthesized carboxymethyl chitosan/poly(vinyl alcohol) bio-nanocomposite hydrogels containing nanoparticles with drug-delivery properties. *Bulletin of Materials Science* 43:. <https://doi.org/10.1007/s12034-020-02231-2>
18. Kalantari K, Mostafavi E, Saleh B, et al (2020) Chitosan/PVA hydrogels incorporated with green synthesized cerium oxide nanoparticles for wound healing applications. *European Polymer Journal* 134:109853. <https://doi.org/10.1016/j.eurpolymj.2020.109853>
19. Suhail M, Chiu IH, Hung MC, et al (2022) In Vitro Evaluation of Smart and pH-Sensitive Chondroitin Sulfate/Sodium Polystyrene Sulfonate Hydrogels for Controlled Drug Delivery. *Gels* 8:1–18. <https://doi.org/10.3390/gels8070406>
20. Niu B, Jia J, Wang H, et al (2019) In vitro and in vivo release of diclofenac sodium-loaded sodium alginate/carboxymethyl chitosan-ZnO hydrogel beads. *International Journal of Biological Macromolecules* 141:1191–1198. <https://doi.org/10.1016/j.ijbiomac.2019.09.059>
21. Hu Y, Dong X, Ke L, et al (2017) Polysaccharides/mesoporous silica nanoparticles hybrid composite hydrogel beads for sustained drug delivery. *Journal of Materials Science* 52:3095–3109. <https://doi.org/10.1007/s10853-016-0597-x>

22. Suhail M, Wu PC, Minhas MU (2021) Development and characterization of pH-sensitive chondroitin sulfate-co-poly(acrylic acid) hydrogels for controlled release of diclofenac sodium. *Journal of Saudi Chemical Society* 25:101212. <https://doi.org/10.1016/j.jscs.2021.101212>
23. Khushbu, Warkar SG, Thombare N (2022) Controlled release and release kinetics studies of boron through the functional formulation of carboxymethyl tamarind kernel gum-based superabsorbent hydrogel. *Polymer Bulletin* 79:2287–2303. <https://doi.org/10.1007/s00289-021-03634-9>
24. Raza MA, Park SH (2020) Irradiated Ch/GG/PVP-based stimuli-responsive hydrogels for controlled drug release. *Journal of Applied Polymer Science* 137:49041. <https://doi.org/10.1002/app.49041>
25. Jing Z, Xu A, Liang YQ, et al (2019) Biodegradable poly(acrylic acid-co-acrylamide)/ poly(vinyl alcohol) double network hydrogels with tunable mechanics and high self-healing performance. *Polymers* 11. <https://doi.org/10.3390/polym11060952>
26. Rani I, Warkar SG, Kumar A (2023) Nano ZnO embedded poly (ethylene glycol) diacrylate cross-linked carboxymethyl tamarind kernel gum (CMTKG)/poly (sodium acrylate) composite hydrogels for oral delivery of ciprofloxacin drug and their antibacterial properties. *Materials Today Communications* 35:105635. <https://doi.org/10.1016/j.mtcomm.2023.105635>
27. Liu C, Zhang Z, Liu X, et al (2013) Gelatin-based hydrogels with β -cyclodextrin as a dual functional component for enhanced drug loading and controlled release. *RSC Advances* 3:25041–25049. <https://doi.org/10.1039/c3ra42532k>
28. Kiran, Tiwari R, Singh VK, et al (2020) Synthesis, characterization of β -CD based novel hydrogels with dual objectives of drug release and dye removal. *Iranian Polymer Journal* 29:615–623. <https://doi.org/10.1007/s13726-020-00826-4>

CHAPTER 5

FABRICATION AND ASSESSMENT OF CALCIUM-CROSSLINKED TRAGACANTH GUM-BASED HYDROGEL MICROSPHERE FOR ASPIRIN RELEASE

5.1 Introduction

In past decades, hydrogels have become a versatile candidate in drug delivery owing to their numerous advantages, such as controlled drug delivery, biocompatibility, and ease of administration [1-3]. Extensive research has been dedicated to the development of controlled oral drug delivery systems, particularly using hydrogel microspheres. These microspheres, which range in size from 1 to 1000 μm , offer several benefits, including customizable shapes, high surface area, efficient drug loading, and potential for structural modification. These properties make hydrogel microspheres promising options in the field of pharmaceutical sciences [4-6].

Moreover, hydrogel materials based on biopolymers like sodium alginate [6], β -cyclodextrin [7], chitosan [8] etc., are naturally occurring, non-toxic, biocompatible, and biodegradable [9]. These features make them better alternatives over synthetic hydrogel, as their excellent biodegradability lowers the risk of adverse effects after

hydrogel administration and enhances patient safety.

One such example of a biopolymer is sodium alginate (SA), found in the cell walls of various classes of brown algae [10-12]. SA comprises repetitive units of two monosaccharides: D-mannuronic acid and L-guluronic acid. The physical crosslinking technique (ionotropic gelation), commonly used for the preparation of alginate-based hydrogel, involves the crosslinking of polyelectrolytes (alginate, pectin, etc.) and oppositely charged ions (Ca^{2+} , Mg^{2+} etc) [13-16]. An advantage of this method is its preference for the utilization of natural, biocompatible, and biodegradable polymers. Moreover, opting for physical cross-linkers over chemical ones, such as glutaraldehyde, eliminates potential toxicity and unwanted effects [17].

Tragacanth gum (TG) is another highly branched biopolymer obtained from the sap of the Astragalus plant [18]. TG has gained attention as a promising material in drug delivery due to its excellent hydrophilicity, biocompatibility, biodegradability, non-toxicity, and cost-effectiveness [19]. However, TG and SA stand out as an excellent biopolymer for drug delivery due to their non-toxic, pH-sensitive, and biodegradable nature. They do have limitations, such as burst drug release. To address this issue, our study explored the combination of SA and TG with β -cyclodextrin.

β -cyclodextrin (β -CD) is a cyclic oligosaccharide composed of seven glucose units joined together through α -1,4-glycosidic linkage. It has a truncated cone-like structure with a hydrophobic inner cavity and a hydrophilic exterior [7]. The host-guest interaction occurs between the hydrophobic cavity of the host β -CD and the guest molecule (drug). This interaction enables β -CD to increase the loading of hydrophobic drugs such as aspirin,

ibuprofen and controlled their release, thus minimizing the chance of burst release [20].

Aspirin, also called acetylsalicylic acid, is a non-steroidal anti-inflammatory drug mainly utilized to treat pain, arthritis, and fever and decrease heart attacks and stroke risk [21-22]. Due to its shorter half-life, frequent dosing is required, which ultimately leads to several side effects [23], [10]. Moreover, available research on aspirin often lacks targeted delivery, leading to serious health issues like gastric ulcers, stomach pain, vomiting, etc. For instance, Sethi et al. (2020) fabricated XG/starch/poly (acrylic acid) hydrogel for the delivery of aspirin. However, the result demonstrated that almost 50% of the drug was released at pH 1.2. This non-targeted delivery in the stomach can cause gastric irritation and other problems [24].

Therefore, in the current study, attempts have been made toward the fabrication of novel hydrogel microspheres based on TG, SA, and β -CD for the pH-dependent targeted of aspirin using the ionotropic gelation technique. The synthesized microspheres were characterized using ATR-FTIR, PXRD, and SEM techniques. The swelling behavior of all TG-based microspheres was examined at pH values of 1.2 and 7.4. The impact of β -CD on aspirin loading capacity within the microsphere was also investigated and found to be more efficient in TG/ β -CD/SA compared to TG/SA microspheres. A sol-gel fraction, porosity, degradation, and cytotoxicity analysis was conducted for the hydrogel microspheres. Furthermore, the drug release mechanism was studied by employing mathematical release models such as Hixson-Crowell, Korsmeyer-Peppas, First-Order, Zero-Order, and Higuchi. Moreover, all experiments

were carried out three times, with the standard deviations shown as error bars in the plot.

5.2 Experimental Section

5.2.1 Materials

β -Cyclodextrin (MW=1134.98 g/mol, CDH, New Delhi, India), Calcium chloride (MW=110.98 g/mol, Fischer Scientific, Mumbai, India), Sodium alginate (MW= 1.65×10^5 g/mol, Qualikems Lifesciences Pvt. Ltd., Gujarat, India), Tragacanth Gum (MW= 8.4×10^5 g/mol, CDH, New Delhi, India), and aspirin (MW=180.16 g/mol, Unicare India Pvt Ltd, Noida, India) were used as purchased.

5.2.2 Synthesis of TG/SA and TG/ β -CD/SA hydrogels

The TG/SA microsphere (Y-1) and various series of TG/ β -CD/SA hydrogels (Y-2 to Y-11) with varying amounts of the SA (0.7-1 g), TG (0.1-0.4 g) and β -CD (0.03-0.06 g) were synthesized using an ionotropic-gelation technique having CaCl_2 as a crosslinker, as detailed in Table 5.1. For the synthesis of the TG/SA hydrogel (Y-1), continuous stirring for 1 hr was carried out. The solution of TG and SA was then added dropwise, using a syringe, in an aqueous solution containing CaCl_2 . The resulting solution was left undisturbed overnight, after which the obtained microspheres were filtered and oven-dried at 40°C for 48 hours [16]. For fabricating a series of TG/ β -CD/SA hydrogel firstly, a predetermined amount of TG and SA were dissolved in distilled water with microspheres (Y-2 to Y-11), the desired amount of β -CD was incorporated during the addition of TG and SA, as depicted in Fig. 5.1. The remaining steps followed the same protocol as outlined above [16].

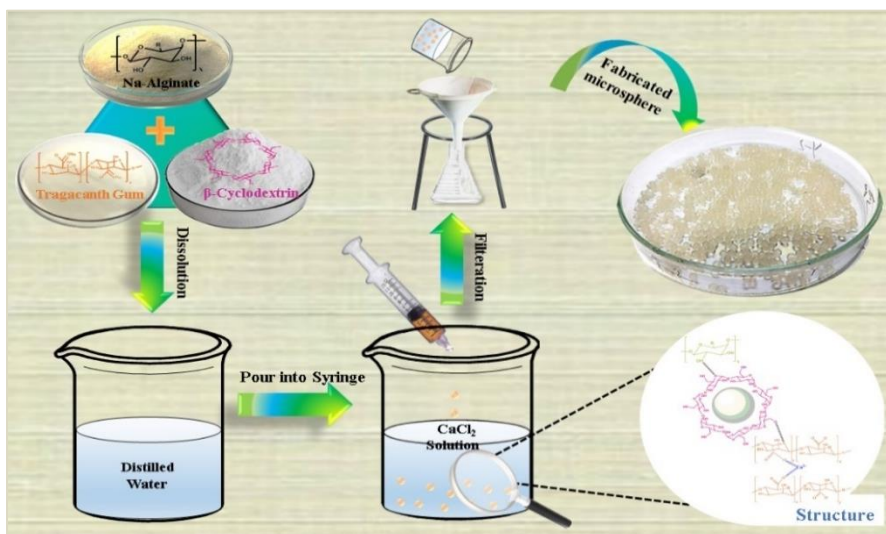


Fig. 5.1 Illustration of the TG/β-CD/SA hydrogel microsphere synthesis

Table 5.1 Different formulations of TG-based hydrogels with required reagent

Sample Code	TG (g)	SA (g)	β-CD (g)
Y-1	0.4	1.0	00
Y-2	0.1	1.0	0.06
Y-3	0.2	1.0	0.06
Y-4	0.3	1.0	0.06
Y-5	0.4	1.0	0.06
Y-6	0.4	0.7	0.06
Y-7	0.4	0.8	0.06
Y-8	0.4	0.9	0.06
Y-9	0.4	1.0	0.03
Y-10	0.4	1.0	0.04
Y-11	0.4	1.0	0.05

5.2.3 Characterization

PXRD analysis was done using a Bruker D8 Discover Diffractometer with Cu K α radiation ($\lambda = 1.5418 \text{ \AA}$) in the 2θ range from $5-70^\circ$. ATR-FTIR spectra were recorded using

a Nicolet iS50 FTIR Tri-detector spectrometer in the wavenumber range of 450-4000 cm^{-1} . The surface morphology was analysed through SEM (Model: JEOL Japan Model: JSM 6610LV).

5.2.4 Swelling studies

Swelling experiments were performed for all fabricated microspheres in simulated gastric fluid (pH 1.2) and intestinal fluid (pH 7.4). A 0.1 g (W_{DH}) of pre-dried microspheres was dipped in the respective buffer solution. After a predetermined period (1 hour), the microspheres were taken out from the buffer solutions, dried with filter paper, and then weighed (W_{SH}) again. This process was repeated constantly for 8 hours, and the complete study was implemented in triplicate [1]. The swelling (%) was determined using the given Eqn. (5.1) [25].

$$\text{Swelling (\%)} = \frac{W_{\text{SH}} - W_{\text{DH}}}{W_{\text{DH}}} \times 100 \quad (5.1)$$

Moreover, W_{SH} is replaced with W_{EH} for the calculation of equilibrium swelling, which corresponds to the weight of the hydrogel at equilibrium (maximum swelling).

5.2.5 Sol-Gel analysis

For calculating the non-crosslinked portion (sol part) and crosslinked portion (gel part) for the formulated microspheres, a sol-gel analysis was performed. Initially, the dried microsphere was weighed (W_i) and swelled in distilled water for 8 h. Afterward, the swollen hydrogel microsphere was dried at 40°C in the oven till a stable weight (W_e) was achieved [26]. The complete analysis was executed three times, and the given equation Eqn. (5.2) and Eqn. (5.3) was used to analyze the sol-gel fraction [27]:

$$\text{Sol Fraction (\%)} = \frac{W_i - W_e}{W_e} \times 100 \quad (5.2)$$

$$\text{Gel fraction (\%)} = 100 - \text{Sol fraction} \quad (5.3)$$

5.2.6 Porosity

The porosity of all synthesized hydrogel microspheres was evaluated using the solvent displacement method. First, the dried hydrogel microsphere was weighed (A_i) and then immersed in 5 ml of hexane for one hour. After extraction from the hexane, the microsphere was gently wiped with filter paper, and its final weight (A_f) was recorded [28-29]. The porosity of the hydrogel discs was calculated using the given Eqn. (5.4).

$$\text{Porosity (\%)} = \frac{A_f - A_i}{\rho V} \times 100 \quad (5.4)$$

Here, ρ denotes the density of hexane, and V is the volume of the hydrogel microsphere.

5.2.7 Aspirin Loading and Entrapment Efficiency

Among all the formulations synthesized, the hydrogel microsphere (Y-5) offers a higher degree of swelling and, therefore, the formulation Y-5 was considered suitable for drug loading. The drug loading behavior of microspheres with β -CD (TG/ β -CD/SA) and without β -CD (TG/SA) was compared. The drug loading was carried out through the swelling equilibrium method. The pre-determined amount of hydrogel microspheres (W_{UH}) was placed into a 100 ml drug solution comprised of a mixture of ethanol and pH 7.4 buffer solution (40:60), containing 80 mg aspirin, which represent as W_D and left undisturbed for 8 hr. Thereafter, hydrogel microsphere was taken out and oven-dried at 40°C, and weight (W_{DLH}) was noted. The given Eqn.(5.5), Eqn.(5.6) were

employed to calculate the drug loading (DL%) and drug entrapment efficiency (DEE%) [16].

$$DL (\%) = \frac{W_{LH} - W_{UH}}{W_{UH}} \times 100 \quad (5.5)$$

$$DEE (\%) = \frac{W_{LH} - W_{UH}}{W_D} \times 100 \quad (5.6)$$

5.2.8 In vitro aspirin release studies

To examine the aspirin release from the hydrogel microspheres, a specific quantity of the aspirin-loaded microspheres was dipped in 100 mL buffer solutions of pH 7.4 and 1.2. These solutions were then kept within an orbital incubator shaker at 37°C. To ensure the volume of the medium remained constant throughout the measurements, 3 mL of the released medium was extracted every 1 hour up to 8 h and replaced with 3 mL fresh buffer solutions. The withdrawn samples were diluted with ethanol, and absorbance of the released drug in the medium was found using a UV-visible spectrophotometer (Model: Cary 300 UV-Vis), measuring absorbance at λ_{\max} 228 nm for pH 7.4 and λ_{\max} 226 nm for pH 1.2. The drug amount was found using the calibration curve of aspirin. The drug release was calculated using Eqn. (5.7).

$$\text{Cumulative drug release} \left(\frac{M_t}{M_\infty} \right) = \frac{V_t C_t + V_W \sum_1^{n-1} C_{t-1}}{M_\infty} \quad (5.7)$$

Here, M_t represent the amount of drug released at time t, M_∞ is the total amount of drug loaded, V_t is the total volume of release medium, V_W is the volume of solution withdrawn, C_t and C_{t-1} denotes the concentration of drug solution at time t and t-1, respectively [30].

5.2.9 Kinetic Modelling

Various mathematical models (i.e., Hixson-Crowell, Korsmeyer-Peppas, First-Order, Zero-Order, and Higuchi models) were applied to drug release data to gain insights into the drug release mechanism. The regression coefficient (R^2) values corresponding to each model were examined. The model that demonstrated an R^2 value closest to 1 was deemed the best model for describing the release mechanism effectively [1], [31].

5.2.10 Cytotoxicity Analysis

The cytotoxicity of aspirin-loaded TG/ β -CD/SA hydrogel microspheres on the HCT 116 human colon cell line, sourced from NCCS Pune, was evaluated via MTT Assay. Cells were seeded at 10,000 cells per well in a 96-well plate and cultured in DMEM medium supplemented with 10% FBS and 1% antibiotic solution at 37°C with 5% CO₂ for 24 hours. Then, cells were exposed to varying concentrations (50, 100, 200, 500, 1000 μ g/ml) of the hydrogel microsphere, while wells without hydrogel serve as control. After further 24-hour incubation, MTT Solution was added and incubated for an additional 2 hours. Subsequently, the supernatant was discarded, and the cell layer was dissolved in 100 μ l of Dimethyl Sulfoxide. Absorbance readings at 540 and 660 nm were taken using an Elisa plate reader (iMark, Biorad, USA) to assess cell viability. Images were also captured under an inverted microscope (Olympus ek2) using a 10 MP Aptima CMOS digital camera (AmScope).

5.2.11 Degradation studies

Degradation experiments were carried out using a phosphate buffer solution (PBS) with a pH of 7.4 (simulated intestinal fluid) in an orbital incubator shaker (80 rpm) at

37°C. Initially, the dried hydrogel disc was soaked in PBS until fully swollen and then weighed (W_i). After that, the hydrogel discs were removed every hour, blotted with filter paper, weighed (W_d), and then immersed again in the buffer. The process continued until the discs were completely degraded, and the degradation (%) was calculated using the following Eqn. (5.8) [32], [33].

$$\text{Degradation (\%)} = \frac{W_i - W_d}{W_i} \times 100 \quad (5.8)$$

5.3 Result and Discussion

5.3.1 Mechanism of TG/ β -CD/SA microspheres and aspirin-loaded TG/ β -CD/SA hydrogel microspheres formation

A series of TG/ β -CD/SA hydrogel microspheres were developed via the ion gelation technique (physical crosslinking method) using CaCl_2 as a cross-linker. The divalent positively charged calcium ions (Ca^{2+}) bind to the two negatively charged oxygen ions (O^-) present within the alginate chain, resulting in the ionic crosslinking of alginate molecules and the formation of a stable cage-like network. Moreover, β -CD is an amphiphilic polymer consisting of a hydrophilic exterior and a hydrophobic cavity within its interior. While hydrogen bonds formed through interactions between the oxygen (-O) atom on its hydrophilic surface and the -OH groups of SA and TG, leading to the development of a three-dimensional TG/ β -CD/SA network.

On the other hand, in the aspirin-loaded TG/ β -CD/SA microsphere, the hydrophobic interior of β -CD functions as a host molecule. It encapsulates aspirin within its hydrophobic cavity, resulting in a substantial increase in drug loading capacity and

facilitating slow as well as controlled release of the aspirin over time. Fig. 5.2 shows the probable mechanism of the aspirin-loaded hydrogel microspheres.

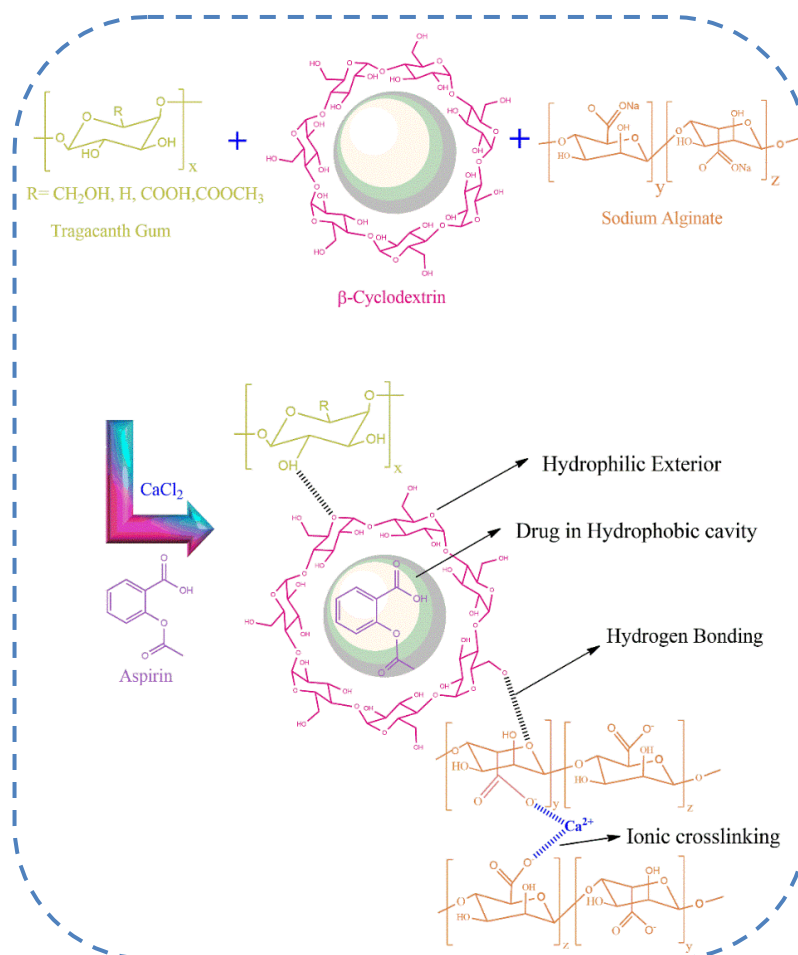


Fig. 5.2 Mechanism for aspirin-loaded TG/ β -CD/SA hydrogel microspheres

5.3.2 Characterization

The ATR-FTIR spectrum of TG/SA (Y-1), TG/ β -CD/SA (Y-5), and aspirin-loaded TG/ β -CD/SA hydrogel are represented in Fig. 5.3. The -OH band at 3365 cm^{-1} of SA shifted towards lower wavenumber of 3356 cm^{-1} , 3354 cm^{-1} and 3351 cm^{-1} in TG/SA, TG/ β -CD/SA, and aspirin-loaded TG/ β -CD/SA hydrogel respectively. This noticeable shift is attributed to the hydrogen bonding among the hydroxyl groups (-OH) of TG

and SA with those present on β -CD [34]. The shift towards lower wavenumber confirmed the occurrence of physical crosslinking (hydrogen bonding) between polymeric chains within the microsphere. Furthermore, the band at 1594 cm^{-1} , due to the presence of the C=O peak of SA, shifted towards higher wavenumbers of 1712 cm^{-1} , 1718 cm^{-1} , and 1717 cm^{-1} in the TG/SA, TG/ β -CD/SA, and aspirin-loaded TG/ β -CD/SA hydrogel respectively. This shift revealed a strong interaction between calcium ions (Ca^{2+}) and the C=O group of SA. The interaction among the C=O group of SA and Ca^{2+} , as well as the H-bonding interaction, results in the development of a hydrogel network [34]. The TG/ β -CD/SA hydrogel displayed nearly identical spectrum to the TG/SA hydrogel, primarily because the characteristic peaks (O-H, C-H) of β -CD overlapped with those of TG and SA. Consequently, no discernible new peaks emerged upon the introduction of β -CD. The observed differences were mainly in peak intensity and slight shifts in wave numbers, reflecting the interactions between the β -CD and the existing components.

On comparing FTIR spectra of aspirin-loaded TG/ β -CD/SA and TG/ β -CD/SA hydrogel, the shifting in wavenumber and increase in the intensity of $-\text{OH}$, C=O, C-H, COO^- and C-O-C peak was observed, confirming the successful loading of drug into the hydrogel matrix [12]. Moreover, the FTIR spectrum of the aspirin-loaded TG/ β -CD/SA hydrogel and TG/ β -CD/SA was almost similar. There was no additional characteristic peak of the drug observed in the FTIR spectrum of aspirin-loaded TG/ β -CD/SA hydrogel microspheres. This confirmed that the aspirin is encapsulated within the hydrophobic cavity of β -CD. A similar result was reported by Hao et al. (2023),

where the FTIR spectrum of curcumin-loaded β -CD/chitosan/ α , β -glycerophosphate hydrogel closely resembled that of the β -CD/chitosan/ α , β -glycerophosphate hydrogel. The characteristic peaks of curcumin were not observed, leading to the conclusion that curcumin was encapsulated within the β -CD cavity and dispersed throughout the hydrogel matrix [35].

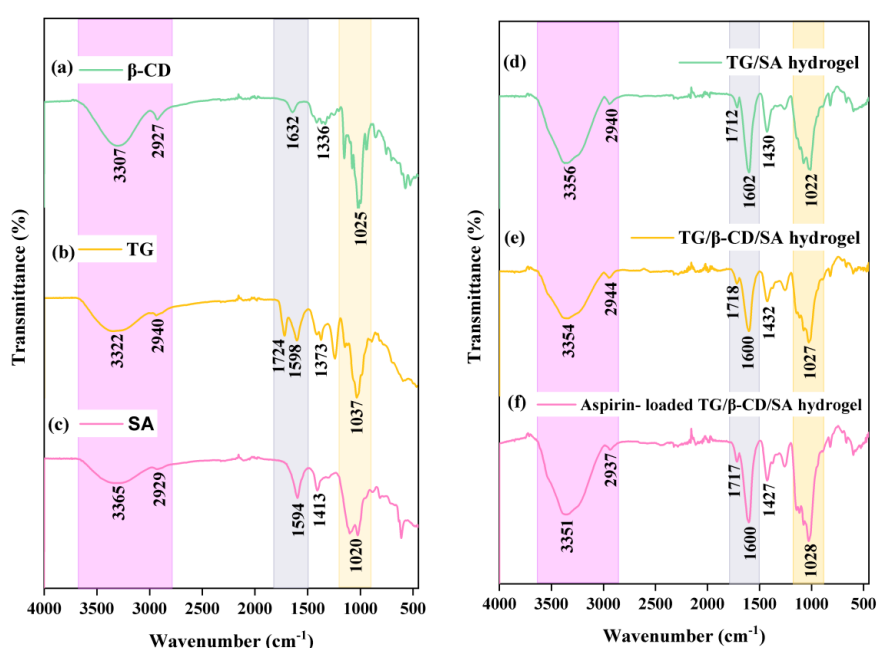


Fig. 5.3 ATR-FTIR spectrum of β -CD, TG, SA, TG/SA, TG/ β -CD/SA, and aspirin-loaded TG/ β -CD/SA hydrogel microsphere

PXRD was carried out to examine the crystalline nature and verify the drug distribution within the hydrogel network, as illustrated in Fig. 5.4. The broad nature of peak at 2θ values of 12.56° , 12.41° and 12.62° in the TG/SA (Y-1), TG/ β -CD/SA (Y-5) and aspirin-loaded TG/ β -CD/SA hydrogel microspheres indicates that the hydrogel microspheres possess an amorphous structure. Furthermore, in the aspirin-loaded TG/ β -CD/SA hydrogel, no additional sharp peaks due to the presence of aspirin were

observed. This suggested that aspirin was uniformly dispersed within the microsphere [36], [7]. Similar results were reported by Li et al. (2023), where the peaks of aspirin disappeared upon its incorporation into the hydrogel matrix [10].

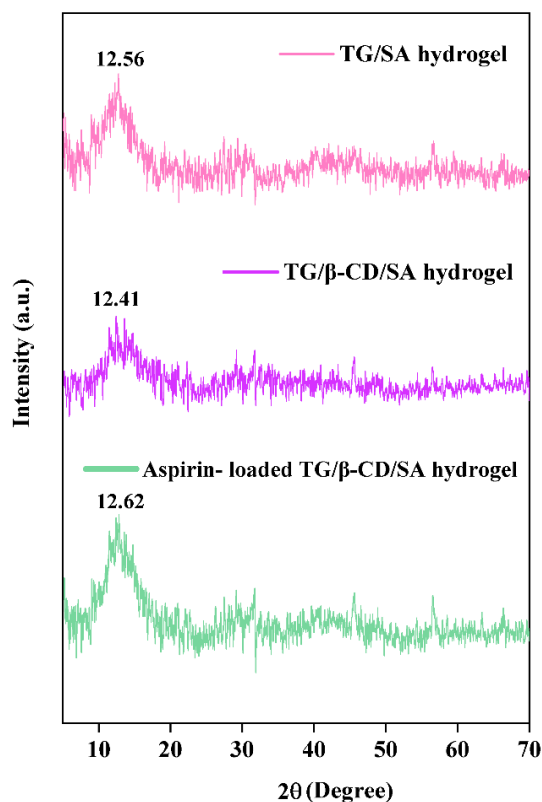


Fig. 5.4 PXR D of TG/SA hydrogel, TG/β-CD/SA hydrogel microsphere, and aspirin-loaded TG/β-CD/SA hydrogel microsphere

The surface morphology of TG/β-CD/SA (Y-5) and aspirin-loaded TG/β-CD/SA hydrogel are presented in Fig. 5.5. The TG/β-CD/SA hydrogel possesses a rough surface with a spherical and micro-porous structure, highlighting the hydrogel swelling and drug loading efficiency [9]. Furthermore, the SEM image of the aspirin-loaded TG/β-CD/SA microsphere reveals a little smoother, spherical surface with no visible pores. This result indicates that the aspirin has been effectively entrapped within the

polymeric matrix, leading to a reduction in the void within the microsphere. Additionally, the diameter of hydrogel microspheres was determined using SEM with Image J software, which was found to be 901 μm for the TG/ β -CD/SA hydrogel and 928 μm for the aspirin-loaded TG/ β -CD/SA hydrogel. These measurements confirm that the synthesized beads are indeed microspheres. Notably, the larger size of the loaded microsphere implies that the presence of the drug leads to an enlargement in microsphere size, likely due to the surface being covered with aspirin crystals [37].

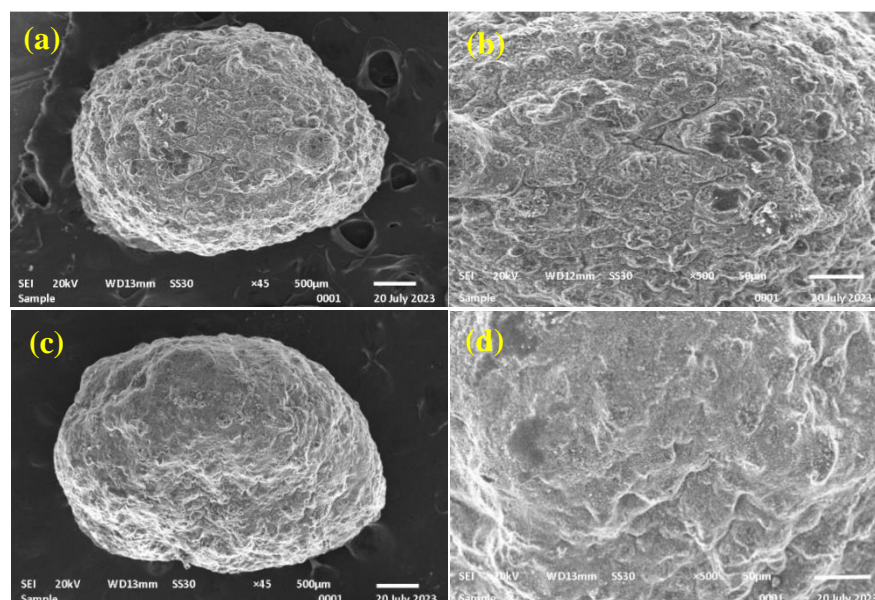


Fig. 5.5 SEM images of (a, b) TG/ β -CD/SA and (c, d) Aspirin-loaded TG/ β -CD/SA hydrogel microsphere

5.3.3 Swelling studies

The effect of varying the TG (Y-2 to Y-5), SA (Y-6 to Y-8), and β -CD (Y-9 to Y-11) on the equilibrium swelling behaviour of microspheres are shown in Fig. 5.6, respectively. The swelling of the microspheres was found to be highly dependent on

the quantities of the TG, SA, and β -CD present in the microspheres. The equilibrium swelling of TG/SA/ β -CD microspheres tends to increase, with an increase in the concentration of TG (0.1 g - 0.4 g), SA (0.7 g- 1 g), and β -CD (0.03 g- 0.06 g), reaching maxima at pH 7.4 ($1709.63 \pm 0.92\%$) and pH 1.2 ($158.96 \pm 0.96\%$). This increase is assigned to the hydrophilic nature of the hydrogels since more hydrophilic groups (-OH, COOH) become available with an increase in polymer content [7], [38]. However, this behaviour was observed only at a certain concentration since a further increase in polymer content results in high viscosity, making stirring tedious and hindering attempts to form microspheres. For all the formulations attempted, a noticeable difference in swelling was observed at pH 7.4 and 1.2. This is related to the deprotonation of the COOH group within TG at pH 7.4. At pH 7.4, electrostatic repulsion occurred between the deprotonated COO⁻ ions, leading to expansion of the network and swelling increases. However, at pH 1.2, the COOH groups of TG bind to the oxygen atom of β -CD through hydrogen bonding interactions, causing the hydrogel to contract and resulting in reduced swelling compared to pH 7.4 [34]. Similar results were observed by Suhail et al. [38], where sodium alginate-co-poly(2-acrylamido-2-methyl propane sulphonic acid) hydrogel demonstrates higher swelling at pH 7.4 compared to pH 1.2. On comparing the swelling behaviour of TG/ β -CD/SA (Y-5) with the TG/SA (Y-1) hydrogel, it was evident that the TG/ β -CD/SA (Y-5) microsphere exhibits higher swelling capacity, as depicted in Fig. 5.7. This pronounced swelling behaviour is ascribed to the introduction of an amphiphilic polymer (β -CD) with hydrophilic moieties (-OH), which enhances the swelling capacity [39]. The TG/ β -CD/SA hydrogel microsphere displays a swelling of $1709.63 \pm 0.92\%$ and $158.96 \pm$

0.96% at pH 7.4 and 1.2. Meanwhile, the TG/SA microspheres demonstrate an equilibrium swelling of 1603.16% and 128.73% at pH 7.4 and 1.2, respectively.

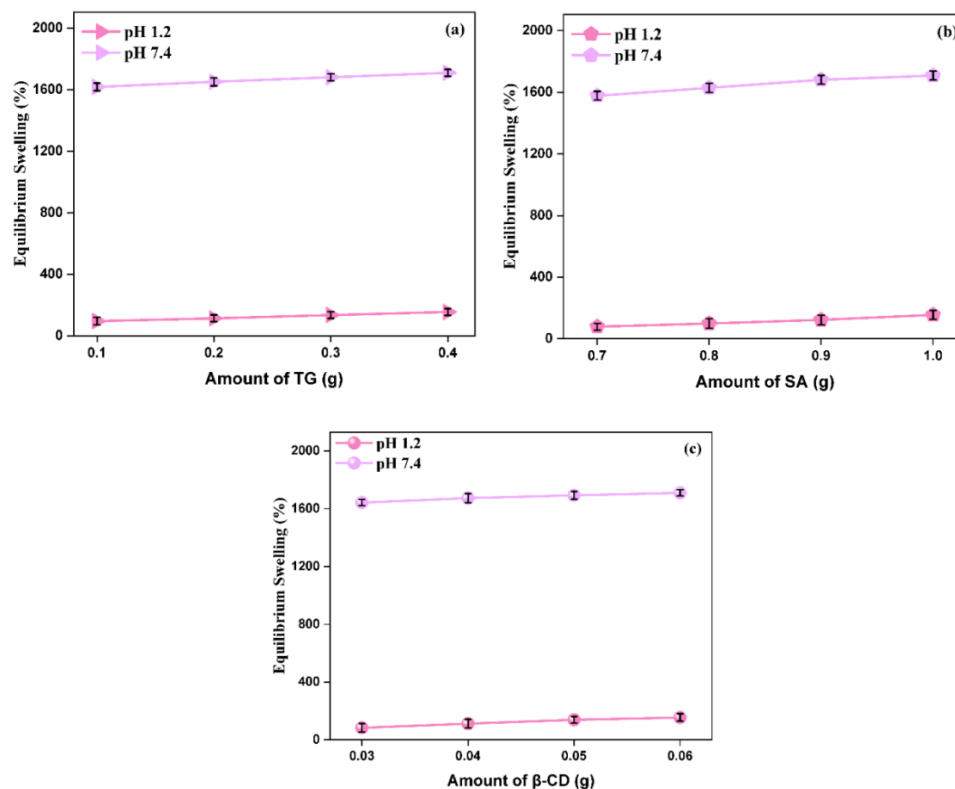


Fig. 5.6 Effect of the (a) TG, (b) SA, and (c) β -CD on the equilibrium swelling of the hydrogel microsphere

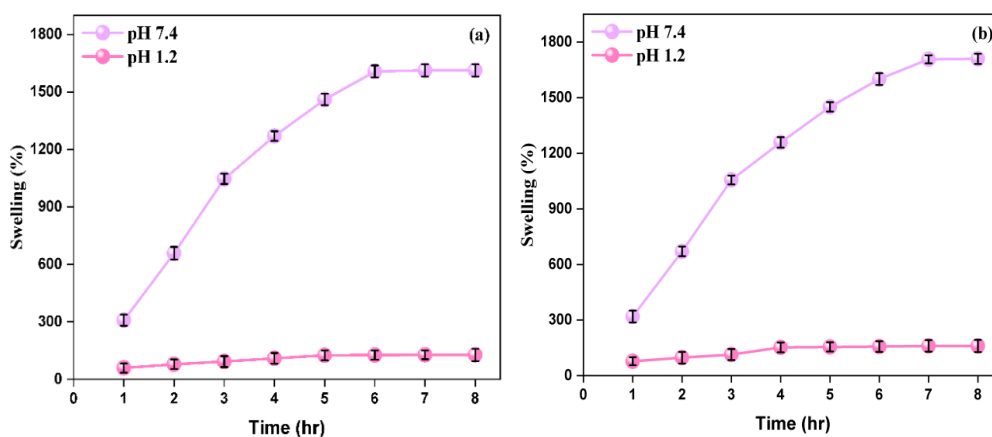


Fig. 5.7 Swelling analysis of (a) TG/SA and (b) TG/ β -CD/SA hydrogel microsphere

5.3.4 Sol-Gel analysis

The sol-gel analysis for the prepared microspheres is presented in Fig. 5.8. It was noticeable that as the quantities of TG (Y-2 to Y-5), SA (Y-6 to Y-8), and β -CD (Y-9 to Y-11) increased, there was a considerable increase in the gel fraction as well. This increase in gel fraction is correlated with the presence of a more significant number of free radical-containing polymeric chains, resulting in an increased number of active sites available for cross-linking. Subsequently, the crosslinking density within the microsphere is raised, resulting in an increase in the gel fraction. Moreover, the comparison of gel fractions between the TG/ β -CD/SA (Y-5) hydrogel and the TG/ β -CD hydrogel microsphere (Y-1) reveals an increased gel fraction, owing to the addition of β -CD. This increase is primarily associated with the more significant number of polymeric chains, which is responsible for an increased cross-linking density within the hydrogel and, hence, gel fraction [38].

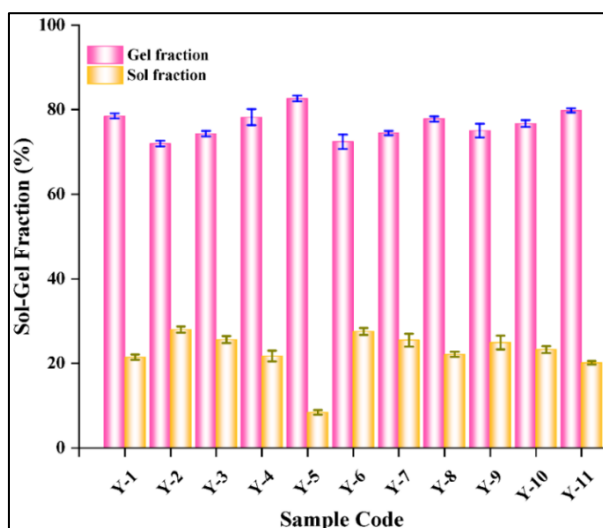


Fig. 5.8 Sol-Gel analysis of all TG/ β -CD/SA hydrogel microspheres and TG/SA hydrogel microspheres

5.3.5 Porosity

The porosity profile reveals that an increase in the quantity of the TG, SA, and β -CD leads to a corresponding increase in porosity, as presented in Fig. 5.8. The porosity result indicates that an increase in the amounts of TG, SA, and β -CD results in a corresponding rise in porosity, as shown in Fig. 5.9. This is attributed to the increased viscosity of the solution, which traps bubbles and increases the number of voids, thereby enhancing porosity. Furthermore, the TG/ β -CD/SA (Y-5) hydrogel and the TG/ β -CD hydrogel microsphere (Y-1) exhibit greater porosity due to the incorporation of β -CD. This is likely due to the increased viscosity of the solution, which helps capture bubbles and create more pores within the structure [40].

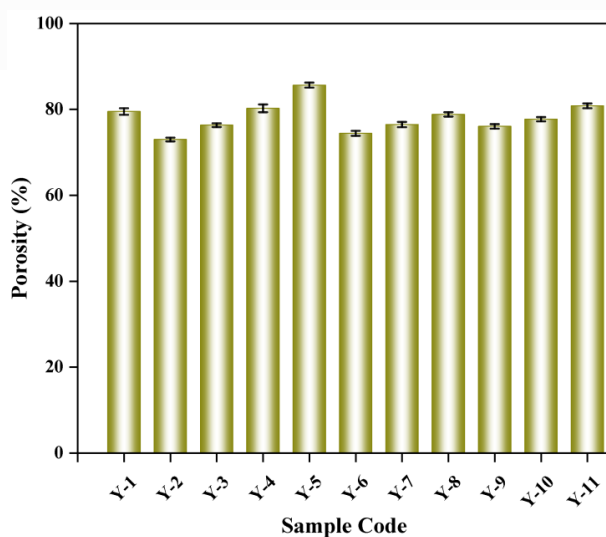


Fig. 5.9 Porosity plot for all synthesized hydrogels

5.3.6 Aspirin Loading and Entrapment Efficiency

The drug loading percentage (DL%) and drug entrapment efficiency percentage (DEE%) were ascertained for the aspirin-loaded TG/SA microsphere and aspirin-loaded TG/ β -CD/SA microsphere, as presented in Table 5.2. Remarkably, aspirin-

loaded TG/ β -CD/SA hydrogel possesses a high amount of drug-loaded DL% and DEE% values compared to aspirin-loaded TG/SA microsphere. This enhancement can be ascribed to the presence of β -CD, which encapsulates the hydrophobic drug aspirin within its hydrophobic cavity, thereby increasing the loading and entrapment of the aspirin in the TG/ β -CD/SA microsphere [20].

Table 5.2 Formulations along with their corresponding drug loading (%) and drug entrapment efficiency (%)

Sample Code	Hydrogel microsphere	Drug Loading (DL%)	Drug Entrapment Efficiency (DEE%)
Y-1	TG/SA	16.2 \pm 0.66	54 \pm 0.55
Y-5	TG/ β -CD/SA	19 \pm 0.85	63.33 \pm 0.49

5.3.7 In vitro aspirin release study

The *in vitro* release analysis was performed for the aspirin-loaded TG/SA microsphere and aspirin-loaded TG/ β -CD/SA microsphere. Notably, as shown in Fig. 5.10, the aspirin-loaded TG/ β -CD/SA microsphere exhibited a lower drug release when compared to the aspirin-loaded TG/SA microsphere. This slower and controlled release of aspirin from the aspirin-loaded TG/ β -CD/SA microsphere can be primarily ascribed to the presence of β -CD, which forms a complex with the aspirin through its hydrophobic cavity and consequently retards the release of aspirin from the microsphere [20]. The maximum aspirin release was observed as 70.9 \pm 0.67% and 59.9 \pm 0.57% in TG/SA and TG/ β -CD/SA microspheres at pH 7.4, respectively, while 23.1 \pm 0.74% and 17.1 \pm 0.83% in TG/SA and TG/ β -CD/SA microspheres at pH 1.2.

In both microspheres, aspirin release was significantly greater at pH 7.4 compared to pH 1.2. This enhancement at pH 7.4 can be attributed to the higher swelling of the microspheres, as discussed in the swelling section, which, in turn, increases the diffusion of the drug. However, at pH 1.2, the hydrogel experiences shrinkage, resulting in reduced swelling and consequently slowing down the diffusion of the drug from the microspheres[39], [41]. Similarly, Rehman et al. (2021) synthesized sodium alginate hydrogel beads, showing around 99% diclofenac sodium drug release at pH 7.4 in 4 hr [42]. However, in our study, the introduction of β -CD resulted in a slow and prolonged drug release (59.9%) for 8 hr, thus minimizing the repeated dosage condition. This is attributed to the ability of β -CD to encapsulate the drug within its cavity, leading to prolonged release. Hence, the synthesized TG/ β -CD/SA microsphere demonstrates promise for slow and prolonged release of the hydrophobic drug aspirin at pH 7.4.

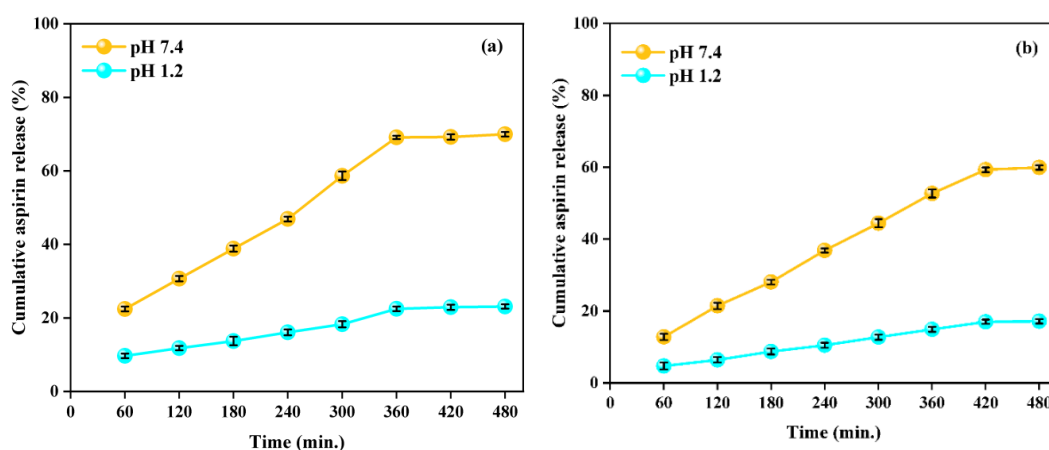


Fig. 5.10 Release profile of aspirin-loaded (a) TG/SA hydrogel microsphere and (b) TG/ β -CD/SA hydrogel microsphere in pH 1.2 and 7.4

5.3.8 Kinetic Modelling

The correlation coefficients (R^2) values for different models like Hixson-Crowell, First-Order, Korsmeyer-Peppas, Zero-Order, and Higuchi were compared to determine which model provided the best description of the release mechanism of aspirin from aspirin-loaded TG/ β -CD/SA microsphere, as illustrated in Table 5.3. In the case of aspirin-loaded TG/ β -CD/SA microsphere, the zero-order model was discovered to be the best-fit model for drug release kinetic at both pH values (Fig. 5.11). Moreover, it was observed that the R^2 value for the Korsmeyer-Peppas model is also closer to 1, with an n value of 0.5273 at pH 7.4 and 0.5182 at pH 1.2. Hence, the best fit of the zero-order model indicates that the release of the drug from the microsphere follows a controlled release pattern throughout the in vitro release analysis, and the Korsmeyer-Peppas model suggests the non-fickian mechanism of drug release [41]. The release exponent (n) value determined from the Korsmeyer-Peppas model was 0.5232 at pH 7.4 and 0.5172 at pH 1.2. This n value ($n \geq 0.5$) indicates that the drug release from the microsphere followed a non-fickian diffusion mechanism. In this mechanism, both drug diffusion and the relaxation of the polymer contribute to the release process [43].

Table 5.3 Kinetic Modelling assessment of aspirin-loaded TG/ β -CD/SA hydrogel

Model	Equation	pH 7.4		pH 1.2		Ref.
		R ²	k	R ²	k	
Hixson-Crowell	$(M_t)^{1/3} - (M_\infty)^{1/3} = k_{HX}t$ k _{HX} =Hixson Crowell constant	0.925	0.063	0.967	0.056	[44]
First Order	$\text{Log } M_t = \text{Log } M_\infty + \frac{kt}{2.303}$ k=First order rate constant	0.899	0.073	0.947	0.048	[44]
Korsmeyer–Peppas	$M_t/M_\infty = kt^n$ k = kinetic constant n = diffusion exponent	0.980	0.057	0.985	0.073	[2]
Zero Order	$M_t = M_\infty + k_0t$	0.983	0.068	0.986	0.062	[45]
Higuchi	$M_t/M_\infty = k_H t^{1/2}$ k _H = kinetic constant	0.961	0.091	0.960	0.092	[31], [46]

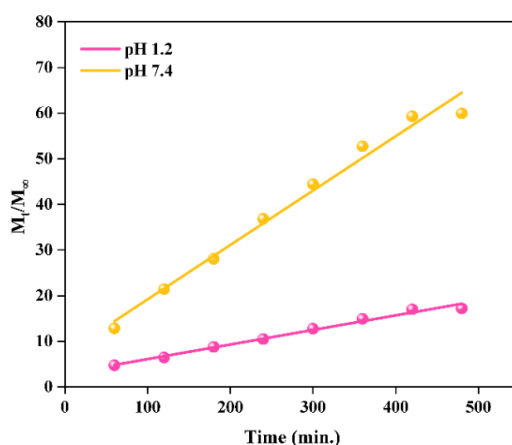


Fig. 5.11 Plot of zero Order kinetic model for aspirin-loaded TG/ β -CD/SA hydrogel microspheres

5.3.9 Cytotoxicity Analysis

Cytotoxicity examination is crucial to ensure the safety of synthesized hydrogel microspheres for drug delivery application. The cytocompatibility assessment of various concentrations (50, 100, 200, 500, 1000 $\mu\text{g/ml}$) of synthesized aspirin-loaded TG/ β -CD/SA hydrogel microspheres and control (without hydrogel) was carried out against HCT-116 human colon cell line (Fig. 5.12). The chosen concentrations were based on the previous study reported by Jitendra et al. (2024). Notably, even at a higher sample concentration (1000 $\mu\text{g/mL}$), the synthesized aspirin-loaded TG/ β -CD/SA hydrogel microspheres exhibit 87.9% cell viability, revealing its biocompatibility and non-toxic nature. This is attributed to the biocompatible nature of TG and SA biopolymers within the hydrogel microsphere [47-49]. Furthermore, the microscopic images of HCT-116 cells (Fig. 5.13) demonstrate a polygonal morphology and almost similar cell density in both control and hydrogel-treated cells at varying concentrations, indicating no huge alteration in cell shape and cell viability by the synthesized hydrogel.

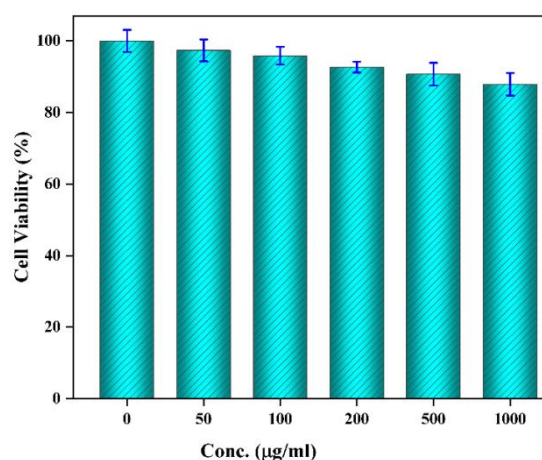


Fig. 5.12 Cytotoxicity profile of aspirin-loaded TG/ β -CD/SA hydrogel microspheres

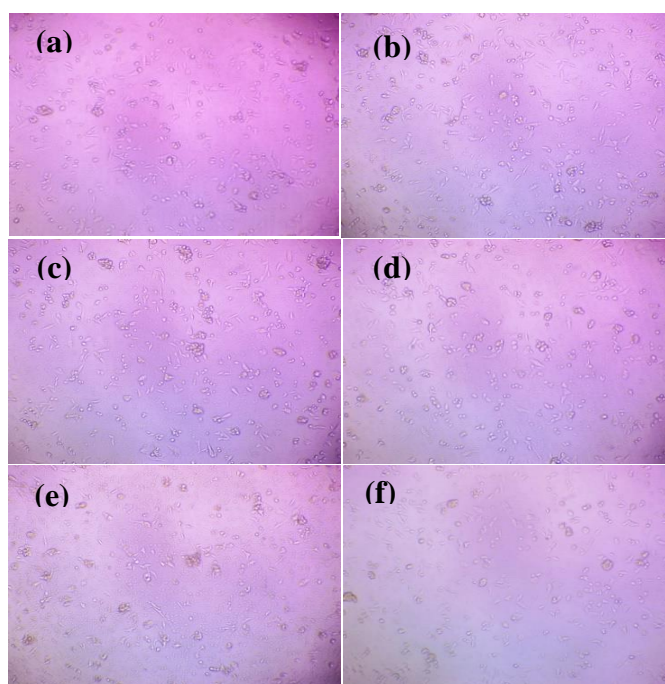


Fig. 5.13 Inverted phase microscopic images of HCT-116 cells treated with (a) control (b) 50 $\mu\text{g/ml}$, (c) 100 $\mu\text{g/ml}$, (d) 200 $\mu\text{g/ml}$, (e) 500 $\mu\text{g/ml}$ and (f) 1000 $\mu\text{g/ml}$ of aspirin-loaded TG/ β -CD/SA hydrogel microspheres

5.3.10 Degradation studies

The degradability of biomaterials plays a crucial role in biomedical applications. The degradability assessment, as illustrated in Fig. 5.14, provides valuable insights into the stability of the synthesized aspirin-loaded TG/ β -CD/SA hydrogel. The degradation occurred in two stages, beginning with a rapid profile followed by slow degradation. The rapid degradation was observed within the first 8 hours due to the cleavage of weak hydrogen bonds between TG, β -CD, and SA chains of hydrogel [32], [51-52]. Following this period, slow degradation of the hydrogels could be observed till 12 hours, likely due to the breakdown of glycosidic (C-O-C) linkages within the TG

structure. It's observed that the synthesized aspirin-loaded TG/ β -CD/SA hydrogel microsphere achieves complete degradation, reaching 100%. Hence, this degradable carrier provides a better option for safe drug delivery.

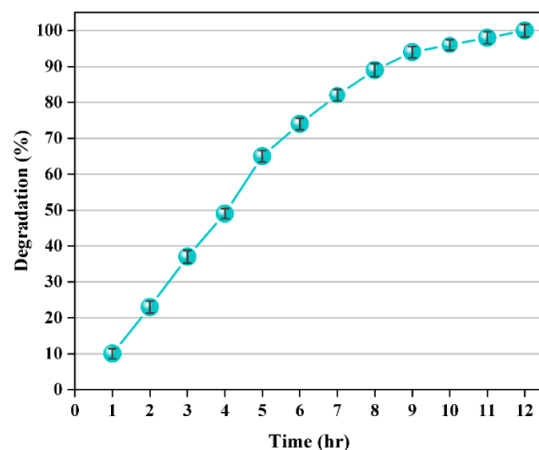


Fig. 5.14 Degradation profile of aspirin-loaded TG/ β -CD/SA hydrogel microsphere

5.4 Conclusion

In this study, we have successfully fabricated hydrogel microspheres based on TG, SA, β -CD, and their role as efficient carriers for the controlled release of the hydrophobic drug aspirin was studied. The gel fraction and swelling behaviour of the microspheres were found to be dependent upon the concentrations of β -CD, SA, and TG. Furthermore, the introduction of β -CD into the TG/ β -CD/SA microsphere shows high drug loading (19%) and drug entrapment efficiency (63.33%) compared to the TG/SA microsphere. This is attributed to the entrapment of aspirin within the hydrophobic cavities of β -CD, which improves the loading of aspirin within the microspheres. Also, it retards the release of aspirin from the microspheres, resulting in

a controlled release pattern (zero order kinetic) at pH 1.2 and 7.4 in TG/ β -CD/SA microsphere. The TG/ β -CD/SA microsphere demonstrated higher drug release at pH 7.4 (59.9 %), in contrast to pH 1.2 (17.1 %), rendering them well-suited for targeted drug delivery within the colon region of the gastrointestinal tract. The developed hydrogel microsphere degrades completely in PBS and shows no cytotoxicity against HCT-116 human colon cell lines. Thus, we successfully provide a solution for the controlled and targeted delivery of aspirin, by developing a pH-sensitive TG/ β -CD/SA hydrogel microsphere, highlighting the potential for oral drug delivery.

5.5 REFERENCES

1. Suhail M, Wu PC, Minhas MU (2021) Development and characterization of pH-sensitive chondroitin sulfate-co-poly(acrylic acid) hydrogels for controlled release of diclofenac sodium. *Journal of Saudi Chemical Society* 25:101212. <https://doi.org/10.1016/j.jscs.2021.101212>
2. Tushar, Saraswat Y, Meena P, Warkar SG (2023) Synthesis and characterization of novel xanthan gum-based pH-sensitive hydrogel for metformin hydrochloride release. *Colloid and Polymer Science* 301: 1147-1158. <https://doi.org/10.1007/s00396-023-05135-9>
3. Meena P, Singh P, Warkar SG (2023) Development and assessment of carboxymethyl tamarind kernel gum-based pH-responsive hydrogel for release of diclofenac sodium. *European Polymer Journal* 197:112340. <https://doi.org/10.1016/j.eurpolymj.2023.112340>
4. Lin F, Li Y, Cui W (2023) Injectable hydrogel microspheres in cartilage repair. *Biomedical Technology* 1:18–29. <https://doi.org/10.1016/j.bmt.2022.11.002>
5. Lengyel M, Kállai-Szabó N, Antal V, et al (2019) Microparticles, microspheres, and microcapsules for advanced drug delivery. *Scientia Pharmaceutica* 87. <https://doi.org/10.3390/scipharm87030020>

6. Abasalizadeh F, Moghaddam SV, Alizadeh E, et al (2020) Alginate-based hydrogels as drug delivery vehicles in cancer treatment and their applications in wound dressing and 3D bioprinting. *Journal of Biological Engineering* 14:1–22. <https://doi.org/10.1186/s13036-020-00239-0>
7. Kiran, Tiwari R, Singh VK, et al (2020) Synthesis, characterization of β -CD based novel hydrogels with dual objectives of drug release and dye removal. *Iranian Polymer Journal* 29:615–623. <https://doi.org/10.1007/s13726-020-00826-4>
8. Kumar PTS, Praveen G, Raj M, et al (2014) Flexible, micro-porous chitosan-gelatin hydrogel/nanofibrin composite bandages for treating burn wounds. *RSC Advances* 4:65081–65087. <https://doi.org/10.1039/c4ra11969j>
9. Zakaria AF, Kamaruzaman S, Abdul Rahman N, Yahaya N (2022) Sodium Alginate/ β -Cyclodextrin Reinforced Carbon Nanotubes Hydrogel as Alternative Adsorbent for Nickel(II) Metal Ion Removal. *Polymers* 14. <https://doi.org/10.3390/polym14245524>
10. Li S, Xiaowen Y, Yang Y, et al (2023) Osteogenic and anti-inflammatory effect of the multifunctional bionic hydrogel scaffold loaded with aspirin and nano-hydroxyapatite. *Frontiers in Bioengineering and Biotechnology* 11:1–16. <https://doi.org/10.3389/fbioe.2023.1105248>
11. Qureshi MAUR, Arshad N, Rasool A, et al (2024) Kappa-carrageenan and sodium alginate-based pH-responsive hydrogels for controlled release of methotrexate. *Royal Society Open Science* 11. <https://doi.org/10.1098/rsos.231952>
12. Atta R, Ata S, Islam A, et al (2020) Kinetics and controlled release of lidocaine from novel carrageenan and alginate-based blend hydrogels Kinetics and controlled release of lidocaine from novel carrageenan and alginate-based blend hydrogels. *International Journal of Biological Macromolecules* 147:67–78. <https://doi.org/10.1016/j.ijbiomac.2020.01.073>

13. Mandal S, Senthil Kumar S, Krishnamoorthy B, Basu SK (2010) Development and evaluation of calcium alginate beads prepared by sequential and simultaneous methods. *Brazilian Journal of Pharmaceutical Sciences* 46:785–793. <https://doi.org/10.1590/S1984-82502010000400021>
14. Martínez-Gómez F, Guerrero J, Matsuhira B, Pavez J (2017) In vitro release of metformin hydrochloride from sodium alginate/polyvinyl alcohol hydrogels. *Carbohydrate Polymers* 155:182–191. <https://doi.org/10.1016/j.carbpol.2016.08.079>
15. Nayak AK, Khatua S, Hasnain MS, Sen KK (2011) Development of diclofenac sodium-loaded alginate-PVP K 30 microbeads using central composite design. *DARU, Journal of Pharmaceutical Sciences* 19:356–366
16. Niu B, Jia J, Wang H, et al (2019) In vitro and in vivo release of diclofenac sodium-loaded sodium alginate/carboxymethyl chitosan-ZnO hydrogel beads. *International Journal of Biological Macromolecules* 141:1191–1198. <https://doi.org/10.1016/j.ijbiomac.2019.09.059>
17. Sevinç Özakar R, Özakar E (2021) The effect of polymer amount and crosslinker ratio in polymeric hydrogel beads on characterization. *Journal of Research in Pharmacy* 25:653–666. <https://doi.org/10.29228/jrp.57>
18. Mansouri Shirazi N, Eslahi N, Gholipour-Kanani A (2021) Production and Characterization of Keratin/Tragacanth Gum Nanohydrogels for Drug Delivery in Medical Textiles. *Frontiers in Materials* 8:1–12. <https://doi.org/10.3389/fmats.2021.720385>
19. Cikrikci S, Mert B, Oztop MH (2018) Development of pH Sensitive Alginate/Gum Tragacanth Based Hydrogels for Oral Insulin Delivery. *Journal of Agricultural and Food Chemistry* 66:11784–11796. <https://doi.org/10.1021/acs.jafc.8b02525>
20. Liu C, Zhang Z, Liu X, et al (2013) Gelatin-based hydrogels with β -cyclodextrin as a dual functional component for enhanced drug loading and controlled

- release. *RSC Advances* 3:25041–25049. <https://doi.org/10.1039/c3ra42532k>
21. Zhang Y, Ding N, Zhang T, et al (2019) A Tetra-PEG Hydrogel Based Aspirin Sustained Release System Exerts Beneficial Effects on Periodontal Ligament Stem Cells Mediated Bone Regeneration. *Frontiers in Chemistry* 7. <https://doi.org/10.3389/fchem.2019.00682>
 22. Shi Y, Wan A, Shi Y, et al (2014) Experimental and mathematical studies on the drug release properties of aspirin loaded chitosan nanoparticles. *BioMed Research International* 2014. <https://doi.org/10.1155/2014/613619>
 23. Xu X, Gu Z, Chen X, et al (2019) An injectable and thermosensitive hydrogel: Promoting periodontal regeneration by controlled-release of aspirin and erythropoietin. *Acta Biomaterialia* 86:235–246. <https://doi.org/10.1016/j.actbio.2019.01.001>
 24. Sethi S, Saruchi, Kaith BS, et al (2020) Cross-linked xanthan gum–starch hydrogels as promising materials for controlled drug delivery. *Cellulose* 27:4565–4589. <https://doi.org/10.1007/s10570-020-03082-0>
 25. Gholamali I, Asnaashariisfahani M, Alipour E, Sepahi AA (2020) In-situ synthesized carboxymethyl chitosan/poly(vinyl alcohol) bio-nanocomposite hydrogels containing nanoparticles with drug-delivery properties. *Bulletin of Materials Science* 43. <https://doi.org/10.1007/s12034-020-02231-2>
 26. Rahmani S, Olad A, Rahmani Z (2022) Preparation of self-healable nanocomposite hydrogel based on Gum Arabic/gelatin and graphene oxide: study of drug delivery behavior. *Polymer Bulletin* 80:4117–4138. <https://doi.org/10.1007/s00289-022-04247-6>
 27. Naeem F, Khan S, Jalil A, Ranjha NM, Riaz A, Haider MS, Sarwar S, Saher F, Afzal S (2017) pH Responsive cross-linked polymeric matrices based on natural polymers: Effect of process variables on swelling characterization and drug delivery properties. *BioImpacts* 7:177–192. <https://doi.org/10.15171/bi.2017.21>

28. Suhail M, Chiu IH, Hung MC, et al (2022) In Vitro Evaluation of Smart and pH-Sensitive Chondroitin Sulfate/Sodium Polystyrene Sulfonate Hydrogels for Controlled Drug Delivery. *Gels* 8:1–18. <https://doi.org/10.3390/gels8070406>
29. Kalantari K, Mostafavi E, Saleh B, et al (2020) Chitosan/PVA hydrogels incorporated with green synthesized cerium oxide nanoparticles for wound healing applications. *European Polymer Journal* 134:109853. <https://doi.org/10.1016/j.eurpolymj.2020.109853>
30. Hu Y, Dong X, Ke L, et al (2017) Polysaccharides/mesoporous silica nanoparticles hybrid composite hydrogel beads for sustained drug delivery. *Journal of Materials Science* 52:3095–3109. <https://doi.org/10.1007/s10853-016-0597-x>
31. Khushbu, Warkar SG, Thombare N (2022) Controlled release and release kinetics studies of boron through the functional formulation of carboxymethyl tamarind kernel gum-based superabsorbent hydrogel. *Polymer Bulletin* 79:2287–2303. <https://doi.org/10.1007/s00289-021-03634-9>
32. Jing Z, Xu A, Liang YQ, et al (2019) Biodegradable poly(acrylic acid-co-acrylamide)/ poly(vinyl alcohol) double network hydrogels with tunable mechanics and high self-healing performance. *Polymers* 11. <https://doi.org/10.3390/polym11060952>
33. Raza MA, Park SH (2020) Irradiated Ch/GG/PVP-based stimuli-responsive hydrogels for controlled drug release. *Journal of Applied Polymer Science* 137. <https://doi.org/10.1002/app.49041>
34. Jana S, Sharma R, Maiti S, Sen KK (2016) Interpenetrating hydrogels of O-carboxymethyl Tamarind gum and alginate for monitoring delivery of acyclovir. *International Journal of Biological Macromolecules* 92:1034–1039. <https://doi.org/10.1016/j.ijbiomac.2016.08.017>
35. Hao PY, Zhou HY, Ren LJ, et al (2023) Preparation and antibacterial properties of curcumin-loaded cyclodextrin-grafted chitosan hydrogel. *Journal of Sol-Gel*

- Science and Technology 106:877–894. <https://doi.org/10.1007/s10971-023-06097-8>
36. Elzayat EM, Abdel-Rahman AA, Ahmed SM, et al (2016) Studying the impact of formulation and processing parameters on the release characteristics from hydroxypropyl methylcellulose matrix tablets of diclofenac. *Acta Poloniae Pharmaceutica - Drug Research* 73:439–452.
 37. Piyakulawat P, Praphairaksit N, Chantarasiri N, Muangsin N (2007) Preparation and evaluation of chitosan/carrageenan beads for controlled release of sodium Diclofenac. *AAPS PharmSciTech* 8. <https://doi.org/10.1208/pt0804094>
 38. Suhail M, Khan A, Rosenholm JM, et al (2021) Fabrication and characterization of diclofenac sodium loaded hydrogels of sodium alginate as sustained release carrier. *Gels* 7:1–16. <https://doi.org/10.3390/gels7010010>
 39. Malik NS, Ahmad M, Minhas MU (2017) Cross-linked β -cyclodextrin and carboxymethyl cellulose hydrogels for controlled drug delivery of acyclovir. *PLoS ONE* 12:1–17. <https://doi.org/10.1371/journal.pone.0172727>
 40. Soltani B, Nabipour H, Ahmadi Nasab N (2018) Fabrication, controlled release, and kinetic studies of indomethacin—layered zinc hydroxide nanohybrid and its effect on the viability of HFFF2. *Journal of Dispersion Science and Technology* 39:1200–1207. <https://doi.org/10.1080/01932691.2017.1388178>
 41. Nayak AK, Pal D, Santra K (2016) Swelling and drug release behavior of metformin HCl-loaded tamarind seed polysaccharide-alginate beads. *International Journal of Biological Macromolecules* 82:1023–1027. <https://doi.org/10.1016/j.ijbiomac.2015.10.027>
 42. Rehman S, Ranjha NM, Raza MR, et al (2021) Enteric-coated Ca-alginate hydrogel beads: a promising tool for colon targeted drug delivery system. *Polymer Bulletin* 78:5103–5117. <https://doi.org/10.1007/s00289-020-03359-1>

43. Ghumman SA, Noreen S, Hameed H, et al (2022) Synthesis of pH-Sensitive Cross-Linked Basil Seed Gum/Acrylic Acid Hydrogels by Free Radical Copolymerization Technique for Sustained Delivery of Captopril. *Gels* 8. <https://doi.org/10.3390/gels8050291>
44. Das D, Das R, Mandal J, et al (2014) Dextrin crosslinked with poly(lactic acid): A novel hydrogel for controlled drug release application. *Journal of Applied Polymer Science* 131:1–12. <https://doi.org/10.1002/app.40039>
45. Goonoo N, Bhaw-Luximon A, Ujoodha R, et al (2014) Naltrexone: A review of existing sustained drug delivery systems and emerging nano-based systems. *Journal of Controlled Release* 183:154–166. <https://doi.org/10.1016/j.jconrel.2014.03.046>
46. Meena P, Singh P, Warkar SG (2023) Fabrication and evaluation of stimuli - sensitive xanthan gum - based hydrogel as a potential carrier for a hydrophobic drug ibuprofen. *Colloid and Polymer Science* 302:377-391. <https://doi.org/10.1007/s00396-023-05198-8>
47. Mouchati A, Yagoubi N (2023) Mechanical Performance and Cytotoxicity of an Alginate/Polyacrylamide Bipolymer Network Developed for Medical Applications. *Materials* 16. <https://doi.org/10.3390/ma16051789>
48. Hemmati K, Ghaemy M (2016) Synthesis of new thermo / pH sensitive drug delivery systems based on tragacanth gum polysaccharide. *International Journal of Biological Macromolecules* 87:415–425. <https://doi.org/10.1016/j.ijbiomac.2016.03.005>
49. Fan Z, Cheng P, Liu M, et al (2020) Dynamic crosslinked and injectable biohydrogels as extracellular matrix mimics for the delivery of antibiotics and 3D cell culture. *RSC Advances* 10:19587–19599. <https://doi.org/10.1039/d0ra02218g>
50. Meena P, Singh P, Warkar SG (2024) Tailoring pH-sensitive carboxymethyl tamarind kernel gum-based hydrogel for an efficient delivery of hydrophobic

drug indomethacin. *International Journal of Biological Macromolecules* 280:136029.
<https://doi.org/10.1016/j.ijbiomac.2024.136029>

51. Sarfraz RM, Ahmad M, Mahmood A, et al (2017) Development of β -cyclodextrin-based hydrogel microparticles for solubility enhancement of rosvastatin: An in vitro and in vivo evaluation. *Drug Design, Development and Therapy* 11:3083–3096. <https://doi.org/10.2147/DDDT.S143712>

CHAPTER 6

SYNTHESIS AND CHARACTERIZATION OF COPPER OXIDE NANOPARTICLE-INCORPORATED HYDROGEL MICROSPHERES PREPARED VIA IONOTROPIC GELATION TECHNIQUE FOR DELIVERY OF CURCUMIN

6.1 Introduction

Over the past few decades, biopolymers-based hydrogel microspheres have been extensively studied for their potential in drug delivery. Their remarkable properties, such as biodegradability, biocompatibility, non-toxicity, uniform release profile and targeted delivery, make them particularly suitable for this application [1-7]. One such example of a biopolymer utilized for the development of hydrogel is CMTKG, which possesses pH-sensitive properties that facilitate targeted delivery.

Moreover, sodium alginate (SA) is one of the most commonly used biopolymers for the synthesis of hydrogel microspheres intended for drug delivery applications [8]. However, these alginate beads faced significant challenges with rapid drug release due to their quick degradation in alkaline pH [9]. Consequently, nanoparticles have been currently incorporated into hydrogel microspheres to facilitate controlled release, thereby providing them with unique properties such as high swelling capacity,

enhanced drug loading efficiency and controlled drug release. These nanoparticles typically range in size from 1 to 100 nm. Recently, there has been considerable interest in developing a nanocomposite hydrogel microsphere that incorporates inorganic nanoparticles like silver, copper oxide and zinc oxide [2], [10].

Among these nanoparticles, copper oxide nanoparticles (CuO Nps) are currently being extensively studied in the field of biomedical. CuO Nps have shown great potential in numerous applications due to their high stability, cost-effectiveness, low toxicity, and excellent antiviral and antibacterial properties. Their antimicrobial action arises from the release of metal ions into the solution, which can damage cell structures by generating reactive oxygen species [11]. These CuO Nps have been investigated for their ability to deliver a range of hydrophobic and hydrophilic drugs, such as curcumin, naproxen, amoxicillin, and ibuprofen [11-13].

Curcumin is a natural yellow colour compound derived from the turmeric plant (*Curcuma longa*), renowned for its anti-bacterial properties. It is also known for its potent anti-inflammatory effects, which may help reduce inflammation in conditions like arthritis and other chronic inflammatory diseases. Despite its potential benefits, curcumin's bioavailability and poor solubility in water is a significant challenge. It is poorly absorbed when taken orally, and its rapid metabolism and elimination from the body limit its effectiveness [14]. Hence, the study focuses on the development of novel CMTKG/SA/CuO nanocomposite hydrogel microspheres for the prolonged and targeted release of curcumin. The synthesized hydrogel microspheres were characterized using ATR-FTIR, PXRD, and SEM techniques. Their swelling and drug

release behaviour were evaluated at pH 1.2 and 7.4 buffer solutions. The impact of CuO Nps on properties like sol-gel fraction, porosity, drug entrapment, and drug loading efficiency was assessed. The drug release mechanism was further investigated using mathematical models, including Hixson-Crowell, Korsmeyer-Peppas, First-Order, Zero-Order, and Higuchi. All experiments were performed thrice, and standard deviations were plotted as error bars in the graph.

6.2 Experimental Section

6.2.1 Materials

Copper chloride dihydrate (MW=170.48 g/mol, CDH, New Delhi, India), Calcium chloride (MW=110.98 g/mol, Fischer Scientific, Mumbai, India), Sodium alginate (MW= 1.65×10^5 g/mol, Qualikems Lifesciences Pvt. Ltd., Gujarat, India) were used as obtained. CMTKG (0.20° of substitution, MW= 9.14×10^5 g/mol) was courteously gifted by Hindustan Gum Pvt Ltd, Haryana, India MW= 8.4×10^5 g/mol, CDH, New Delhi, India).

6.2.2 Synthesis of CuO Nps

The CuO Nps was synthesized via co-precipitation approach. Initially, copper chloride was dissolved in 100 mL of deionised water. A 0.1 M NaOH solution was then gradually added dropwise under vigorous stirring until the pH of the solution reached 7. The resulting black precipitates were repeatedly washed with deionised water and absolute ethanol until the pH of the water reached 7. The cleaned precipitates were then filtered and dried at 110°C for 16 hours. Finally, the dried material was calcined at 500°C for 4 hours to obtain CuO Nps [15].

6.2.3 Synthesis of CMTKG/SA and CMTKG/SA/CuO nanocomposite hydrogel microspheres

A series of CMTKG/SA/CuO nanocomposite hydrogel microspheres (B-1 to B-4) with varying proportions of CuO Nps (0.01-0.07 g) and CMTKG/SA (B-5) hydrogel microsphere were synthesized via ion-gelation using CaCl_2 as a crosslinker, as shown in Table 6.1. For the synthesis of CMTKG/SA/CuO nanocomposite hydrogel microspheres (B-1 to B-4), a fixed amount of CuO Nps mixed in distilled water and stirred for 20 min. In another beaker, the required amounts of CMTKG and SA were dissolved in distilled water with continuous stirring for 30 min. An aqueous solution of CuO Nps was then added to the above CMTKG and SA solution and stirred for another 30 min. This solution was then introduced dropwise via syringe into an aqueous CaCl_2 solution. The CaCl_2 solution remained undisturbed overnight, and the developed microspheres were filtered and dried in an oven at 40°C for 48 hours, as illustrated in Fig. 6.1. Moreover, for the CMTKG/SA hydrogel (B-5), the similar steps were performed following the same procedure in absence of CuO Nps [18].

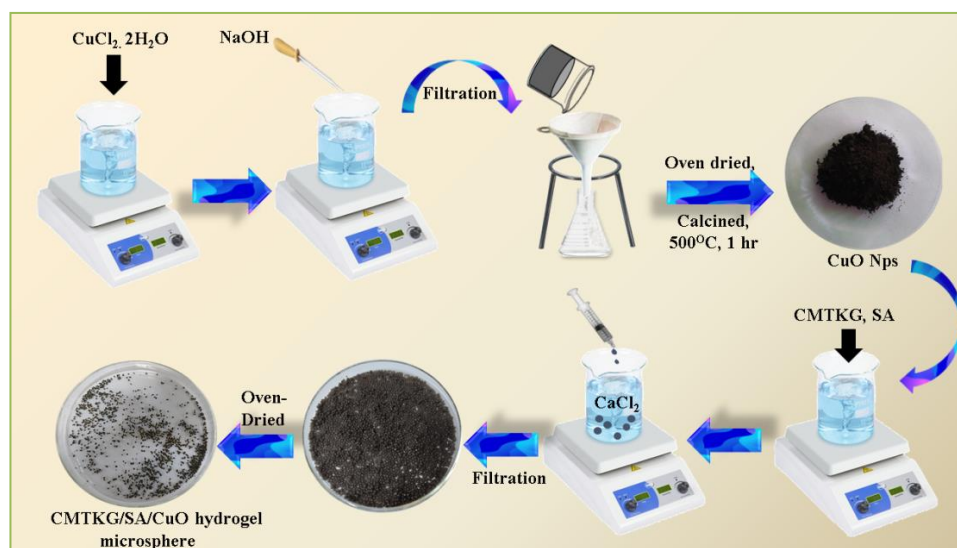


Fig. 6.1 Depiction of the synthesis of CMTKG/SA/CuO nanocomposite hydrogel microspheres

Table 6.1 Various TG-based nanocomposite hydrogel microspheres with varying compositions

Sample Code	CMTKG (g)	SA (g)	CuO Nps (g)
B-1	0.4	1	0.01
B-2	0.4	1	0.03
B-3	0.4	1	0.05
B-4	0.4	1	0.07
B-5	0.4	1	0

6.2.4 Characterization

PXRD was performed using a Bruker D8 Discover Diffractometer equipped with Cu $K\alpha$ radiation ($\lambda = 1.5418 \text{ \AA}$), scanning in the 2θ range from $5-70^\circ$. ATR-FTIR spectra

were obtained using a Nicolet iS50 FTIR Tri-detector spectrometer over a wavenumber range of 450–4000 cm^{-1} . TEM analysis was conducted using a TECNAI G20 operating at 200 kV. The surface morphology of the samples was examined using scanning electron microscopy (SEM) on a JEOL JSM 6610LV model.

6.2.5 Swelling studies

Swelling studies were conducted on all synthesized hydrogel microspheres in both simulated gastric fluid (pH 1.2) and simulated intestinal fluid (pH 7.4). A measured quantity (A_{DH}) of dried hydrogel microspheres was immersed in the respective buffer solutions. After a time interval of 1 hour, the hydrogel microspheres were removed, gently blotted with filter paper to remove excess liquid, and weighed again (A_{SH}). This procedure was repeated consistently for a duration of 8 hours [16-17]. The swelling (%) and equilibrium swelling (%) was calculated using the following Eqn. (6.1) and Eqn. (6.2).

$$\text{Swelling (\%)} = \frac{A_{\text{SH}} - A_{\text{DH}}}{A_{\text{DH}}} \times 100 \quad (6.1)$$

$$\text{Equilibrium Swelling (\%)} = \frac{A_{\text{EH}} - A_{\text{DH}}}{A_{\text{DH}}} \times 100 \quad (6.2)$$

where A_{EH} is the weight of the hydrogel microsphere at equilibrium (maximum swelling).

6.2.6 Sol-Gel analysis

A sol-gel analysis was conducted to determine the non-crosslinked (sol fraction) and crosslinked (gel fraction) components of the synthesized hydrogel microspheres. First, the dry weight of the hydrogel microspheres was recorded (A_i) and then immersed in distilled water for 8 hours to allow swelling to remove the soluble sol portion. The

swollen microspheres were then dried in an oven at 40°C until a constant weight (A_e) was reached [28], [29]. The sol-gel fractions were calculated using Eqn. (6.3) and Eqn. (6.4).

$$\text{Sol Fraction (\%)} = \frac{A_i - A_e}{A_e} \times 100 \quad (6.3)$$

$$\text{Gel fraction (\%)} = 100 - \text{Sol fraction} \quad (6.4)$$

6.2.7 Porosity

The solvent displacement technique was utilised to assess the porosity of the fabricated nanocomposite hydrogel microspheres. Initially, the dried hydrogel microsphere was weighed (M_i) and then submerged in 5 ml of hexane for 1 hr. Afterwards, the microsphere was gently dried with filter paper, and its weight (M_f) was measured. The Eqn. (6.5) was used to determine the porosity of the CMTKG/SA/CuO nanocomposite hydrogel microspheres.

$$\text{Porosity (\%)} = \frac{M_f - M_i}{\rho V} \times 100 \quad (6.5)$$

Here, ρ represent hexane density, and V is the volume of the nanocomposite hydrogel microsphere.

6.2.8 Curcumin Loading and Entrapment Efficiency

Among the various synthesized formulations, the nanocomposite hydrogel microsphere (B-4) exhibited the highest swelling capacity, making it the most suitable candidate for drug loading. The drug loading efficiency of hydrogel microspheres with CuO Nps (CMTKG/SA/CuO) was compared to those without CuO Nps

(CMTKG/SA). The drug loading was conducted using the swelling equilibrium method. A pre-measured quantity of hydrogel microspheres (A_{UH}) was immersed in 100 ml of a curcumin drug solution composed of a 30:70 mixture of ethanol and pH 7.4 buffer solution containing 50 mg of curcumin, which represent as A_{UH} . The mixture was left undisturbed for 8 hours. Afterwards, the hydrogel microspheres were removed and oven-dried at 40°C, and their weight (A_{UH}) was recorded. The Eqn. (6.6) and Eqn. (6.7) were used to determine the drug loading (DL%) and drug entrapment efficiency (DEE%) [18].

$$DL (\%) = \frac{A_{LH} - A_{UH}}{A_{UH}} \times 100 \quad (6.6)$$

$$DEE (\%) = \frac{A_{LH} - A_{UH}}{A_D} \times 100 \quad (6.7)$$

6.2.9 In vitro curcumin release analysis

To investigate the release of curcumin from the hydrogel microspheres, a measured amount of curcumin-loaded nanocomposite hydrogel microspheres was immersed in 100 ml buffer solutions with pH values of 7.4 and 1.2. These solutions were then placed in an orbital incubator shaker set to 37°C. To maintain a consistent volume of the medium during the experiment, 3 ml of the solution was withdrawn every hour for a total duration of 8 hours and replaced with 3 ml of fresh buffer. The collected solution was diluted with ethanol, and the absorbance of curcumin released into the solution was determined using a UV-Visible spectrophotometer (Model: Cary 300 UV-Vis) by measuring absorbance at λ_{max} 427. The drug quantity was calculated using a calibration curve. The drug release was calculated using Eqn. (6.8.)

$$\text{Cumulative drug release } \left(\frac{M_t}{M_\infty} \right) = \frac{V_t C_t + V_w \sum_1^{n-1} C_{t-1}}{M_\infty} \quad (6.8)$$

where, M_t indicates the quantity of drug released at a time, M_∞ is the total quantity of drug loaded, V_t is the overall volume of release medium, V_w is the volume of solution taken, C_t and C_{t-1} represent the concentration of drug solution at time t and $t-1$, respectively.

6.2.10 Kinetic Modelling

To better understand the mechanism of drug release, several mathematical models, including Hixson-Crowell, Korsmeyer-Peppas, First-Order, Zero-Order, and Higuchi, were applied to the drug release data. The corresponding regression coefficient (R^2) values for each model were evaluated. The model with the R^2 value closest to 1 was considered the most suitable for accurately describing the drug release process [19-20].

6.2.11 Anti-bacterial Assay

The antibacterial activity was assessed using the Zone Inhibition Method (Kirby-Bauer method). Mueller-Hinton Agar plates were prepared by spreading 100 μ l of *S. aureus* bacterial culture, which was adjusted to a 0.5 McFarland Unit (1.5×10^8 CFU/ml from Mueller-Hilton Broth). Discs containing varying concentrations (62.5 to 1000 μ g/disc) of the CuO Nps and curcumin-loaded CMTKG/SA/CuO nanocomposite hydrogel were then placed on the plates. The *S. aureus* plates were incubated at 37 °C for 24 hours in a Basil Scientific Corp. incubator. After incubation, the clear zones surrounding the discs were measured.

6.2.12 Cytotoxicity

The cytotoxic effects of curcumin-loaded CMTKG/SA/CuO nanocomposite hydrogel microspheres on the HCT 116 human colon cancer cell line, obtained from NCCS Pune, were assessed using the MTT assay. About 10,000 cells per well were seeded into a 96-well plate and cultured in DMEM medium, enriched with 10% fetal bovine serum (FBS) and 1% antibiotic solution at 37°C in a 5% CO₂ environment for 24 hours. Cells were then treated with various concentrations of the nanocomposite hydrogel microspheres (0.78, 1.56, 3.125, 6.25 µg/ml), while untreated wells were maintained as controls. After an additional 24-hour incubation, an MTT solution was introduced to each well, followed by a 2-hour incubation. The supernatant was subsequently removed, and the remaining cell layer was dissolved in 100 µl of dimethyl sulfoxide (DMSO). Absorbance measurements were taken at 540 and 660 nm using an Elisa plate reader (iMark, Biorad, USA) to evaluate cell viability. Microscopic images were also captured with an Olympus EK2 inverted microscope using a 10 MP Aptima CMOS digital camera (AmScope).

6.2.13 Degradation studies

Degradation studies were performed using a phosphate buffer solution (PBS) at pH 7.4 in an orbital incubator shaker set to 80 rpm and maintained at 37°C. The dried hydrogel disc was first immersed in PBS until it reached full swelling capacity, after which its weight (A_I) was recorded. Then, the disc was again dipped in buffer, and at regular intervals (1 hr), the hydrogel microsphere was taken out, gently blotted with filter paper to remove excess moisture, weighed (A_T), and then returned to the buffer.

This process was repeated until the hydrogel discs had degraded entirely [21-22]. The degradation (%) was determined using the given Eqn. (6.9).

$$\text{Degradation (\%)} = \frac{A_I - A_T}{A_T} \times 100 \quad (6.9)$$

6.3 Result and Discussion

6.3.1 Mechanism for the synthesis of CMTKG/SA/CuO and curcumin-loaded CMTKG/SA/CuO nanocomposite hydrogel microsphere

A range of CMTKG/SA/CuO hydrogel microspheres (B1 to B4) were fabricated using the ionotropic gelation technique. The stable cage-like structures are formed as the Ca^{2+} of CaCl_2 interacts with the O^- within the SA, resulting in ionic crosslinking [23]. Moreover, the $-\text{COO}^-$ group of SA interacts with CuO Nps via electrostatic attraction. Additionally, the -O atoms in CuO Nps form hydrogen bonds with the -OH groups of SA and -COOH of CMTKG, resulting in the development of a CMTKG/SA/CuO nanocomposite hydrogel microsphere. Furthermore, in the curcumin-loaded CMTKG/SA/CuO hydrogel microspheres, hydrogen bonding occurs between the -O atom of the CuO Nps and the -OH group of curcumin, facilitating the successful formation of the curcumin-loaded CMTKG/SA/CuO nanocomposite hydrogel microspheres [2], [24]. The probable mechanism for the development of curcumin-loaded CMTKG/SA/CuO nanocomposite hydrogel microspheres was depicted in Fig. 6.2.

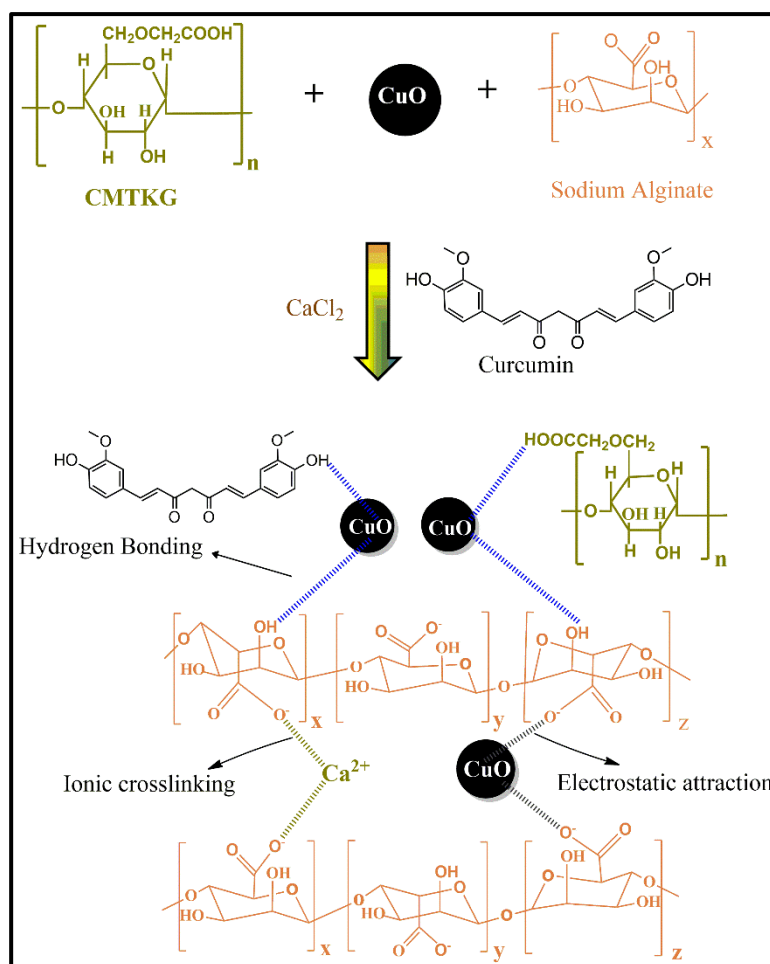


Fig. 6.2 Mechanism for curcumin-loaded CMTKG/SA/CuO nanocomposite hydrogel microsphere synthesis

6.3.2 Characterization

The ATR-FTIR spectra for the SA, curcumin, CuO Nps, CMTKG/SA/CuO nanocomposite hydrogel microspheres and curcumin-loaded CMTKG/SA/CuO nanocomposite hydrogel microspheres are illustrated in Fig. 6.3. In the FTIR spectra of curcumin, a characteristic peak corresponds to the C=C observed at 1628 cm^{-1} , while a peak at 3508 cm^{-1} indicates the O-H vibration. The C=O peak appears at 1509

cm^{-1} , whereas the peak at 1024 cm^{-1} corresponds to the C-O-C stretching vibration [25]. Moreover, in the FTIR spectrum for CuO Np, a peak centered at 528 cm^{-1} , 624 cm^{-1} and 784 cm^{-1} corresponds stretching vibration of the Cu-O bond. Due to the hygroscopic nature of CuO Nps, a broad band at 3441 cm^{-1} was noticed, corresponding to the -OH stretching, while the peak at 1632 cm^{-1} is related to the H-O-H bending vibrations [26]. The band corresponding to the -OH group of SA, initially at 3365 cm^{-1} , exhibited a downward shift to 3281 cm^{-1} and 3288 cm^{-1} in the CMTKG/SA/CuO nanocomposite hydrogel microspheres and curcumin-loaded CMTKG/SA/CuO nanocomposite hydrogel microspheres respectively. This shift signifies the formation of hydrogen bonds between the -OH group of SA and the -O atom of CuO Nps, thereby confirming physical crosslinking within the polymeric network of the nanocomposite hydrogel microspheres. Additionally, the carboxylate peak of SA, originally at 1594 cm^{-1} , shifted towards higher wavenumbers of 1606 cm^{-1} and 1608 cm^{-1} in the microspheres. The observed shift highlights a strong interaction between Ca^{2+} or Cu^{2+} and the carboxylate of SA, confirming the successful synthesis of the nanocomposite hydrogel microspheres [27]. In the FTIR spectrum of the curcumin-loaded CMTKG/SA/CuO nanocomposite hydrogel microspheres, the incorporation of curcumin did not result in any additional peaks, as all the peaks corresponding to curcumin overlapped with those of the hydrogel. However, a shift in the -OH peak was observed, indicating hydrogen bonding between curcumin and the hydrogel matrix. This

observation confirms the successful synthesis of the curcumin-loaded CMTKG/SA/CuO nanocomposite hydrogel microspheres [28]

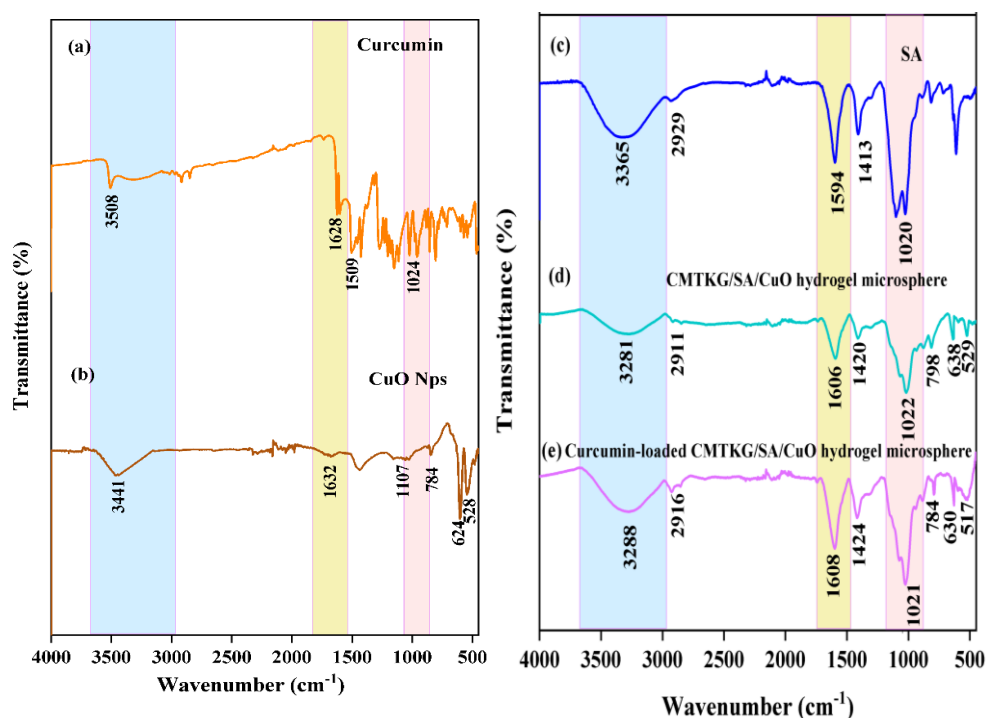


Fig. 6.3 ATR-FTIR spectra of curcumin, SA, CuO Nps, CMTKG/SA/CuO and curcumin-loaded CMTKG/SA/CuO nanocomposite hydrogel microspheres

PXRD analysis was conducted to investigate the crystalline or amorphous nature of synthesized CuO Nps and hydrogels, as displayed in Fig. 6.4. The PXRD pattern of CuO Nps comprise sharp crystalline peaks at 2θ values of 32.48° , 35.47° , 38.9° , 48.71° , 53.42° , 58.3° , 61.5° , 66.4° , 68.2° , and 68.11° . Moreover, the lattice parameters were found to be $a = 4.683 \text{ \AA}$, $b = 3.428 \text{ \AA}$, $c = 5.129 \text{ \AA}$ (JCPDS 80-1268). This revealed the successful synthesis of CuO Nps with monoclinic symmetry [26]. The absence of additional peaks indicates that the synthesized CuO Nps are pure.

Moreover, the Debye-Scherrer's Eqn. (6.10) was used to calculate the average particle size of the fabricated CuO Nps.

$$D = \frac{k\lambda}{\beta \cos \theta} \quad (6.10)$$

Here, λ is X-ray wavelength (0.154 nm), θ is Bragg's angle, D denotes the average particle size (nm), β represents the full-width half maxima, and k is constant (0.89) [26]. According to the above Eqn. 6.10, the average particle size of the CuO Nps measures around 19 nm. Moreover, the CMTKG/SA (B-5) nanocomposite hydrogel microspheres exhibit broad peaks, revealing their amorphous nature. However, CMTKG/SA/CuO (B-4) nanocomposite hydrogel microspheres exhibit some sharp crystalline peaks along with this broad peak. This sharp peak at 2θ values of 32.39° , 35.41° , 38.79° , 48.66° , 53.44° , 58.26° , 61.46° , 66.38° and 68.18° corresponds to the diffraction peaks of CuO Nps, confirming the successful incorporation of CuO Nps into the hydrogel matrix [2]. Additionally, the curcumin-loaded CMTKG/SA/CuO nanocomposite hydrogel microspheres do not display any additional peaks associated with curcumin as compared to the CMTKG/SA/CuO hydrogel, suggesting that curcumin is entrapped within the amorphous hydrogel network [29-30].

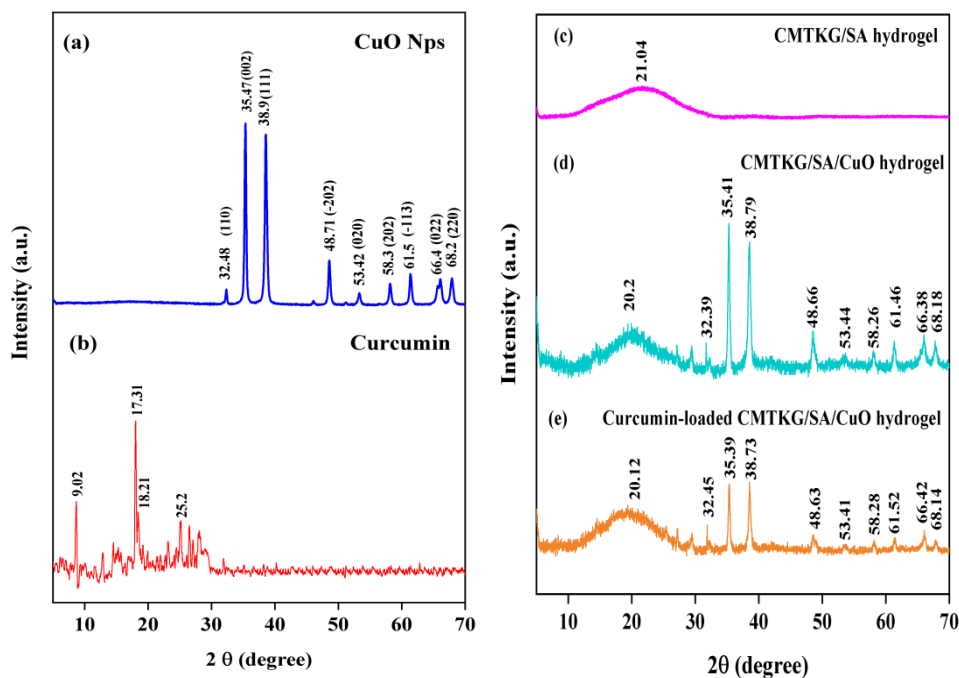


Fig. 6.4 XRD of (a) CuO Nps, (b) Curcumin, (c) CMTKG/SA (B-5), (d)

CMTKG/SA/CuO (B-4) and (e) Curcumin-loaded CMTKG/SA/CuO nanocomposite

The SEM images of the CuO Nps, CMTKG/SA/CuO (B-4) nanocomposite hydrogel and the curcumin-loaded CMTKG/SA/CuO nanocomposite hydrogel microsphere are illustrated in Fig. 6.5. The CuO Nps exhibits a granular rod-like structure with the average diameter of 15 nm, found using ImageJ software [31]. Additionally, SEM images of the CMTKG/SA/CuO and curcumin-loaded CMTKG/SA/CuO nanocomposite hydrogel microsphere exhibit a rough and spherical surface [32]. Moreover, diameter measurements from SEM images using ImageJ software revealed that the CMTKG/SA/CuO nanocomposite hydrogel microspheres had a diameter of 789 μm , and the curcumin-loaded CMTKG/SA/CuO nanocomposite measured 801 μm . These findings confirm the microspheric nature of the synthesized hydrogel

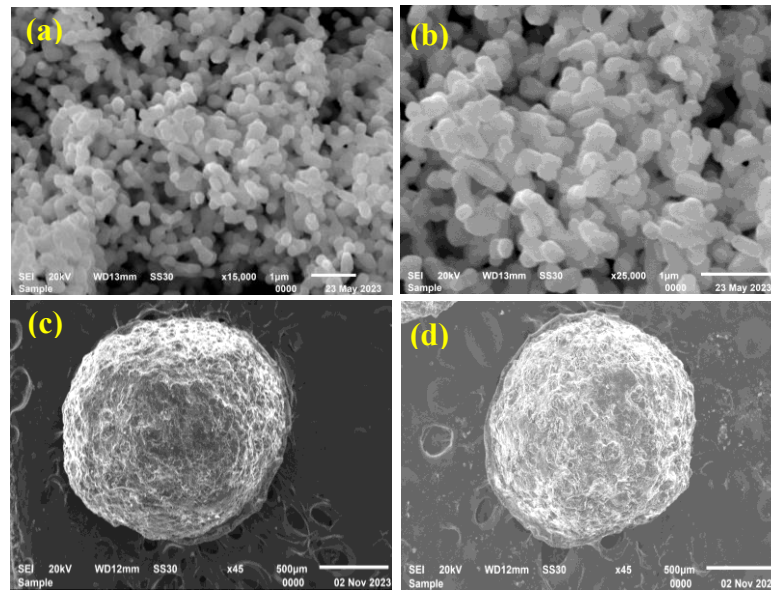


Fig. 6.5 SEM images of (a, b) CuO Nps at different magnifications, (c) CMTKG/SA/CuO and (d) curcumin-loaded CMTKG/SA/CuO hydrogel

The TEM images of the fabricated CuO NPs at various magnifications are shown in Fig. 6.6. The CuO Nps display a quasi-spherical or rod-shaped morphology and appear to be aggregated [33]. The diameter obtained using ImageJ software indicates that the CuO Nps have an average diameter of 18 nm, which aligns well with the results from PXRD and SEM analyses, confirming the successful synthesis of the CuO Nps.

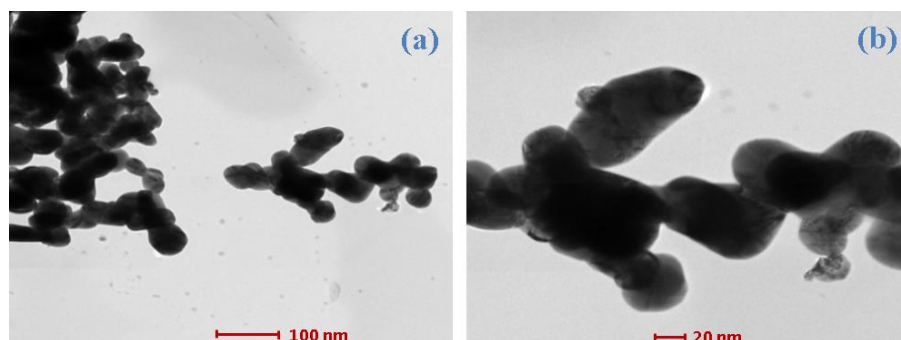


Fig. 6.6 TEM Images of CuO Nps at 100 nm and 20 nm magnification

6.3.3 Swelling studies

The impact of varying concentrations of CuO Nps (B-1 to B-4) on the swelling behavior of nanocomposite hydrogel microspheres is illustrated in Fig. 6.7. As the amount of CuO Nps increases (0.01- 0.07 g), the swelling of the nanocomposite hydrogel microspheres also increases. The increased swelling observed with higher amounts of CuO Nps is due to the greater availability of oxygen atoms present within the CuO Nps. These oxygen atoms facilitate hydrogen bonding with water molecules, leading to an increase in swelling [24]. Moreover, significant differences in swelling were observed between pH 7.4 and pH 1.2 for all nanocomposite hydrogel microspheres. At pH 7.4, the deprotonation of the carboxylic acid groups within CMTKG leads to electrostatic repulsion between the deprotonated COO^- ions, resulting in hydrogel microsphere expansion and increased swelling. Moreover, at pH 1.2, the carboxylic acid groups remain protonated, leading to reduced swelling [3]. Additionally, the CMTKG/SA/CuO nanocomposite hydrogel microsphere (B-4) microspheres show higher swelling as compared to CMTKG/SA (B-5), as illustrated in Fig. 6.8. This is linked to the presence of CuO Nps with hydrophilic moieties (-O), which enhance the swelling of CMTKG/SA/CuO hydrogel. The CMTKG/SA/CuO nanocomposite hydrogel revealed swelling of $1802 \pm 0.79\%$ at pH 7.4 and $160.71 \pm 0.84\%$ at pH 1.2. However, the CMTKG/SA hydrogel microsphere displays swelling of $1700.19 \pm 0.82\%$ and $140.36 \pm 0.86\%$ at pH 7.4 and 1.2.

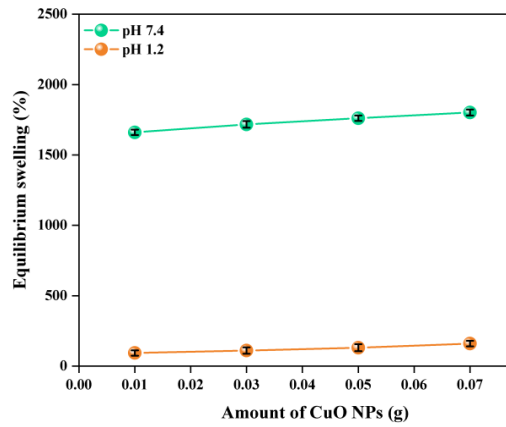


Fig. 6.7 Impact of the CuO Nps on the swelling of the CMTKG/SA/CuO nanocomposite hydrogel microspheres

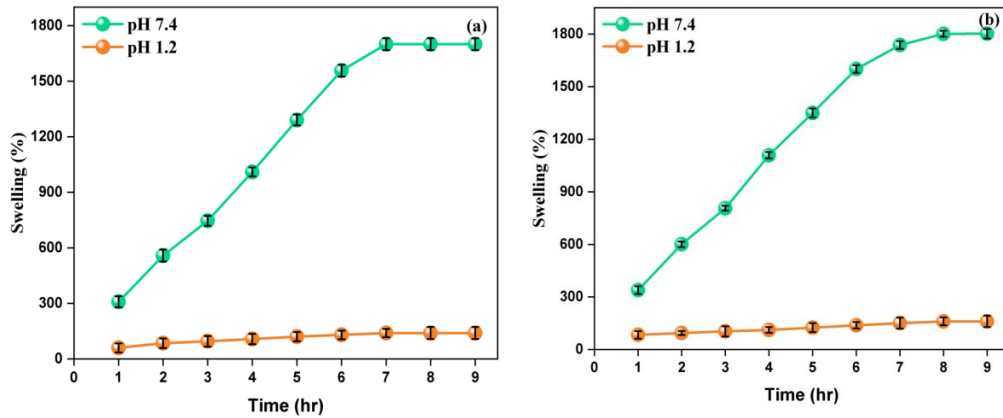


Fig. 6.8 Swelling studies of (a) CMTKG/SA and (b) CMTKG/SA/CuO nanocomposite hydrogel microsphere at pH 7.4 and pH 1.2

6.3.4 Sol-Gel analysis

The sol-gel fraction studies of the synthesized hydrogels are depicted in Fig. 6.9. An increase in CuO NP amount (B-1 to B-4) results in an increase in interaction between the polymeric network and CuO NPs. This causes the hydrogel network to become

more compact, thereby increasing the gel fraction of the nanocomposite hydrogel microsphere [34].

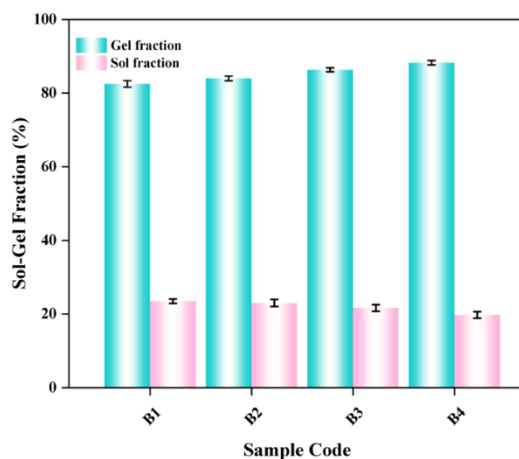


Fig. 6.9 Sol-Gel fraction studies of all CMTKG/SA/CuO hydrogel microsphere

6.3.5 Porosity

The porosity analysis of the fabricated hydrogel microspheres is shown in Fig. 6.10. As the concentration of CuO Nps increases from B-1 to B-4 formulation, there is a corresponding increase in electrostatic repulsion among the CuO Nps. This interaction causes the hydrogel network to expand, resulting in increased porosity of the CMTKG/SA/CuO nanocomposite hydrogel microspheres [35].

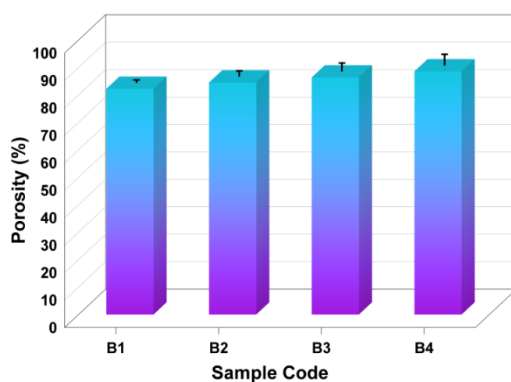


Fig. 6.10 Porosity analysis studies of all CMTKG/SA/CuO hydrogel microsphere

6.3.6 Curcumin Loading and Entrapment Efficiency

The drug loading and drug entrapment efficiency were determined for the CMTKG/SA and CMTKG/SA/CuO nanocomposite hydrogel microsphere, as shown in Table 6.2. The CMTKG/SA/CuO nanocomposite hydrogel demonstrates higher drug loading and entrapment efficiency in comparison to the CMTKG/SA hydrogel. This is due to CuO Nps acting as nano-reservoirs for curcumin, which increase loading and entrapment in the CMTKG/SA/CuO nanocomposite hydrogel. Additionally, hydrogen bonding and electrostatic interactions between curcumin and CuO Nps contribute to improved drug loading [2]. Additionally, the higher swelling observed in the CMTKG/SA/CuO nanocomposite hydrogel also correlates with its increased drug loading and entrapment.

Table 6.2 Drug loading and drug entrapment efficiency of CMTKG/SA and CMTKG/SA/CuO nanocomposite hydrogel

Sample Code	Hydrogel microsphere	Drug Loading (DL%)	Drug Entrapment Efficiency (DEE%)
B1	CMTKG/SA/CuO	25.69 \pm 0.85	69.84 \pm 0.49
B5	CMTKG/SA	16.37 \pm 0.66	61.32 \pm 0.55

6.3.7 In vitro curcumin release analysis

In vitro release studies were conducted for the CMTKG/SA hydrogel microsphere and the CMTKG/SA/CuO nanocomposite hydrogel microsphere. The CMTKG/SA/CuO nanocomposite hydrogel microsphere showed a lower and prolonged drug release in

comparison to the CMTKG/SA hydrogel microsphere, as illustrated in Fig. 6.11. The hydrogen bonds are formed between CuO Nps and curcumin, resulting in the slow curcumin release from the CMTKG/SA/CuO nanocomposite hydrogel microsphere. The maximum release of curcumin at pH 7.4 was determined as $60.97 \pm 0.56\%$ for CMTKG/SA hydrogel microsphere and $49.9 \pm 0.61\%$ for CMTKG/SA/CuO nanocomposite hydrogel microsphere. However, at pH 1.2, the drug releases were $20.18 \pm 0.61\%$ and $15.1 \pm 0.63\%$, respectively. In both formulations, curcumin release was higher at pH 7.4, which corresponded to increased swelling of the hydrogel microspheres, which facilitates greater curcumin diffusion from the hydrogel. While, at pH 1.2, due to reduced swelling, drug release lowered. Therefore, the fabricated CMTKG/SA/CuO nanocomposite hydrogel microsphere shows potential for achieving slow and prolonged release of the curcumin at pH 7.4 [2].

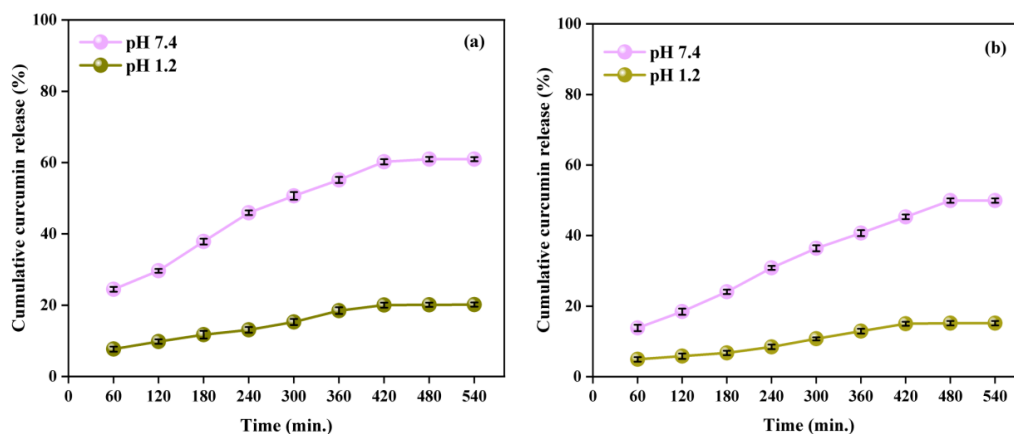


Fig. 6.11 Drug Release plot of curcumin-loaded (a) CMTKG/SA and (b) CMTKG/SA/CuO nanocomposite hydrogel microsphere

6.3.8 Kinetic Modelling

Various models, including Korsmeyer-Peppas, Zero-Order, Hixson-Crowell, First-Order, and Higuchi, were evaluated to identify the most suitable model for providing an explanation of the curcumin release mechanism from the CMTKG/SA/CuO nanocomposite hydrogel microsphere, as detailed in Table 6.3. The analysis revealed that the Higuchi model was the best-fitted model at both pH 7.4 and 1.2, as illustrated in Fig. 6.12. This suggests that the drug release from the CMTKG/SA/CuO nanocomposite hydrogel microsphere obeys a Fickian diffusion mechanism, where the drug diffuses from an area of higher concentration within the hydrogel to a lower concentration in the surrounding release buffer solution [36].

Table 6.3 Kinetic modelling data of CMTKG/SA/CuO nanocomposite hydrogel

Model	Equations	pH 7.4		pH 1.2		Ref.
		R ²	k	R ²	k	
Hixson-Crowell	$(M_t)^{1/3} - (M_\infty)^{1/3} = k_{HX} \cdot t$ k _{HX} =Hixson Crowell constant	0.963	0.085	0.972	0.086	[37]
First Order	$\text{Log } M_t = \text{Log } M_\infty + \frac{kt}{2.303}$ k=First order rate constant	0.953	0.085	0.948	0.053	[5]
Korsmeyer-Peppas	$M_t/M_\infty = kt^n$ k = kinetic constant n = diffusion exponent	0.975	0.053	0.979	0.074	[16]
Zero Order	$M_t = M_\infty + k_0t$	0.968	0.065	0.942	0.063	[37]
Higuchi	$M_t/M_\infty = k_H t^{1/2}$ k _H = kinetic constant	0.981	0.056	0.991	0.035	[37]

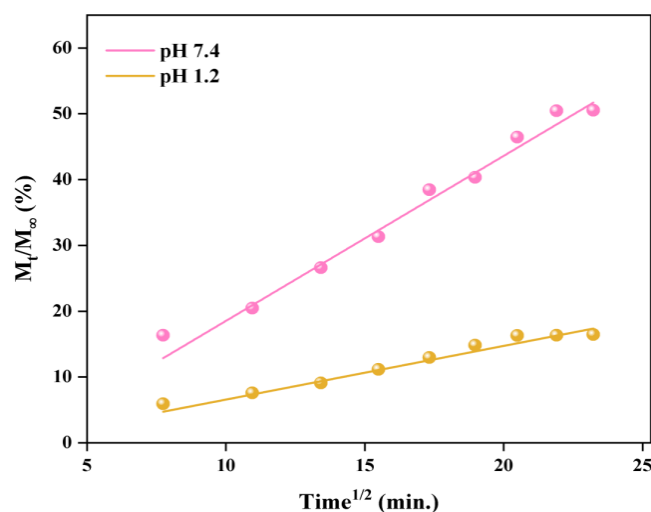


Fig. 6.12 Plot of Higuchi model for CMTKG/SA/CuO nanocomposite hydrogel microsphere

6.3.9 Anti-bacterial Assay

The antibacterial activity of CuO Nps and the curcumin-loaded CMTKG/SA/CuO nanocomposite hydrogel microspheres was evaluated using *Staphylococcus aureus* (*S. aureus*) bacteria. The inhibition zones for CuO NPs at various concentrations are illustrated in Fig. 6.13. At the highest concentrations (1000 $\mu\text{g}/\text{disc}$), the inhibition zone diameters measured 6 mm for CuO NPs and 10 mm for the curcumin-loaded CMTKG/SA/CuO nanocomposite hydrogel microspheres. The antibacterial activity of CuO Nps is due to the interaction of Cu^{2+} ions with bacteria, which disrupts the electrical balance of the bacterial cell wall. This membrane damage leads to the leakage of DNA and RNA into the extracellular matrix, resulting in cell death. Additionally, the small size of CuO Nps allows them to penetrate the cell membrane, where they can interact with and alter cytosolic structures through ions and free radicals, ultimately killing the bacteria [2]. Moreover, the CMTKG/SA/CuO

nanocomposite hydrogel exhibited a larger inhibition zone compared to CuO Nps. This enhanced antibacterial effect can be attributed to the combined action of CuO Nps and curcumin, which damages bacterial cells upon contact. The observed inhibitory action of the curcumin-loaded nanocomposite hydrogel microsphere provides evidence that the curcumin was released upon swelling from the hydrogel [38].

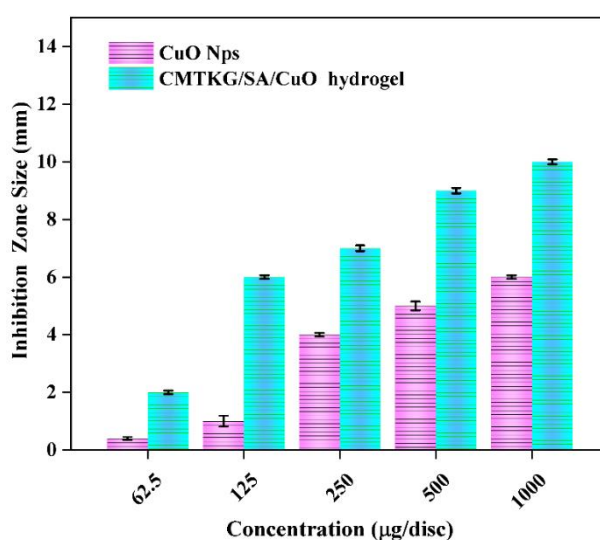


Fig. 6.13 Anti-bacterial profile of CuO Nps and Curcumin-loaded CMTKG/SA/CuO nanocomposite hydrogel microspheres

6.3.10 Cytotoxicity

The cytocompatibility of fabricated CMTKG/SA/CuO nanocomposite hydrogel microsphere was assessed across various concentrations (0.78, 1.56, 3.125, and 6.25 µg/ml) along with a control sample (without hydrogel microsphere) using the HCT-116 human colon cell line, as shown in Fig. 6.14. Remarkably, the CMTKG/SA/CuO nanocomposite hydrogel microsphere demonstrates 93% cell viability, attributed to the biocompatible properties of CMKTG and SA biopolymers present in the hydrogel

microspheres. Additionally, microscopic images revealed a polygonal-shaped cell in control and nanocomposite hydrogel microsphere-treated samples, suggesting no significant changes in cell shape due to the synthesized hydrogel, as depicted in Fig. 6.15 [37], [39-40].

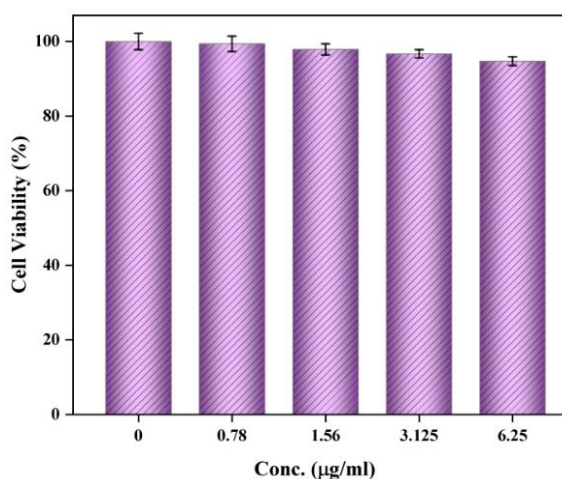


Fig. 6.14 Cytotoxicity plot of CMTKG/SA/CuO nanocomposite hydrogel

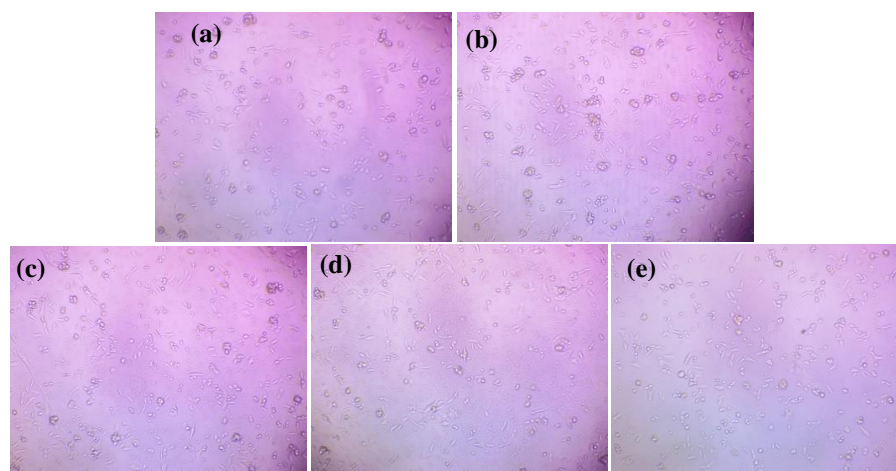


Fig. 6.15 Microscopic images of HCT-116 cells treated with (a) control (b) 0.78 µg/ml, (c) 1.56 µg/ml, (d) 3.125 µg/ml and (e) 6.25 µg/ml of CMTKG/SA/CuO nanocomposite hydrogel microsphere

6.3.11 Degradation

The degradation was studied for synthesized curcumin-loaded CMTKG/SA/CuO nanocomposite hydrogel microsphere, as displayed in Fig 6.16. The degradation took place in two phases: an initial rapid phase followed by a slower phase. The rapid degradation observed during the first 9 hr is attributed to the breakage of hydrogen bonds and electrostatic interaction between the CMKTG, SA, CuO Nps and curcumin in the nanocomposite hydrogel. After this initial period, a gradual degradation phase continued until 13 hr, attributed to the breaking of C-O-C or glycosidic linkages within the CMKTG. The synthesized curcumin-loaded CMTKG/SA/CuO nanocomposite hydrogel degraded fully in 13 hr. Thus, the developed curcumin-loaded CMTKG/SA/CuO nanocomposite hydrogel microsphere presents a promising safe delivery of curcumin [21] .

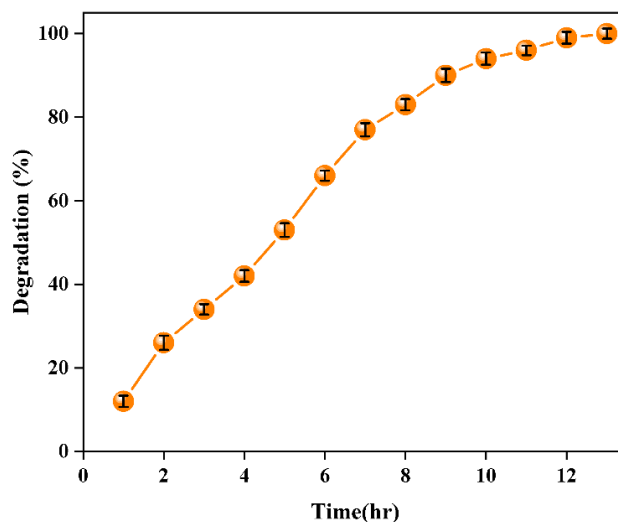


Fig. 6.16 Degradation curve of curcumin-loaded CMTKG/SA/CuO nanocomposite hydrogel microsphere

6.4 Conclusion

In this work, the CMTKG/SA/CuO nanocomposite hydrogel microsphere was successfully developed and investigated for the controlled release of the hydrophobic drug curcumin. The swelling, porosity and sol-gel fraction of the nanocomposite hydrogel microspheres increased with higher concentrations of CuO Nps. Additionally, the incorporation of CuO Nps into the hydrogel microspheres facilitated a slow and prolonged release of curcumin, which was characterized by the Fickian diffusion mechanism, as indicated by fitting the Higuchi model, at both pH 1.2 and 7.4. The CMTKG/SA/CuO nanocomposite hydrogel microspheres exhibited significantly higher drug release in an alkaline medium (pH 7.4), making them ideal for targeted colon drug delivery. Additionally, the CMTKG/SA/CuO nanocomposite hydrogel microspheres demonstrated complete degradation. They exhibited non-cytotoxicity towards HCT-116 human colon cell lines, highlighting their significant potential for the targeted and safe delivery of curcumin.

6.5. REFERENCE

1. Gholamali I, Yadollahi M (2021) Bio-nanocomposite Polymer Hydrogels Containing Nanoparticles for Drug Delivery: a Review. *Regenerative Engineering and Translational Medicine* 7:129–146. <https://doi.org/10.1007/s40883-021-00207-0>
2. Gholamali I, Hosseini SN, Alipour E (2021) Doxorubicin-loaded oxidized starch/poly (vinyl alcohol)/CuO bio-nanocomposite hydrogels as an anticancer drug carrier agent. *International Journal of Polymeric Materials and Polymeric Biomaterials* 70:967–980. <https://doi.org/10.1080/00914037.2020.1767616>

3. Meena P, Singh P, Warkar SG (2023) Development and assessment of carboxymethyl tamarind kernel gum-based pH-responsive hydrogel for release of diclofenac sodium. *European Polymer Journal* 197:112340. <https://doi.org/10.1016/j.eurpolymj.2023.112340>
4. Kajal, Kumar R, Meena P, Warkar SG (2023) Development and characterization of pH-responsive CMTKG/PAM/PEG hydrogel for oral administration of etophylline. *Colloid and Polymer Science* 301:1313–1323. <https://doi.org/10.1007/s00396-023-05152-8>
5. Anshul, Tomar G, Meena P, Warkar SG (2024) Synthesis and Assessment of Acacia Gum-Based Hydrogel as a Promising Novel Biopolymeric Matrix for Delivery of Ciprofloxacin. *ChemistrySelect* 9. <https://doi.org/10.1002/slct.202401639>
6. Lin F, Li Y, Cui W (2023) Injectable hydrogel microspheres in cartilage repair. *Biomedical Technology* 1:18–29. <https://doi.org/10.1016/j.bmt.2022.11.002>
7. Lengyel M, Kállai-Szabó N, Antal V, et al (2019) Microparticles, microspheres, and microcapsules for advanced drug delivery. *Scientia Pharmaceutica* 87:20. <https://doi.org/10.3390/scipharm87030020>
8. Li S, Xiaowen Y, Yang Y, et al (2023) Osteogenic and anti-inflammatory effect of the multifunctional bionic hydrogel scaffold loaded with aspirin and nano-hydroxyapatite. *Frontiers in Bioengineering and Biotechnology* 11:1–16. <https://doi.org/10.3389/fbioe.2023.1105248>
9. Nayak AK, Pal D, Santra K (2016) Swelling and drug release behavior of metformin HCl-loaded tamarind seed polysaccharide-alginate beads. *International Journal of Biological Macromolecules* 82:1023–1027. <https://doi.org/10.1016/j.ijbiomac.2015.10.027>
10. Kirubakaran D, Selvam K, Prakash P, et al (2023) In-vitro antioxidant, antidiabetic, anticholinergic activity of iron/copper nanoparticles

- synthesized using *Strobilanthes cordifolia* leaf extract. *OpenNano* 14:100188. <https://doi.org/10.1016/j.onano.2023.100188>
11. Namazi H, Pooresmaeil M, Hasani M (2021) Oxidized starch/CuO bio-nanocomposite hydrogels as an antibacterial and stimuli-responsive agent with potential colon-specific naproxen delivery. *International Journal of Polymeric Materials and Polymeric Biomaterials* 70:1296–1305. <https://doi.org/10.1080/00914037.2020.1798431>
 12. Gholamali I, Asnaashariisfahani M, Alipour E, Sepahi AA (2020) In-situ synthesized carboxymethyl chitosan/poly(vinyl alcohol) bio-nanocomposite hydrogels containing nanoparticles with drug-delivery properties. *Bulletin of Materials Science* 43:. <https://doi.org/10.1007/s12034-020-02231-2>
 13. Gholamali I, Alipour E (2020) Carboxymethyl Chitosan/Starch/CuO Nanocomposite Hydrogels for Controlled Release of Amoxicillin. *Regenerative Engineering and Translational Medicine* 6:398–406. <https://doi.org/10.1007/s40883-020-00173-z>
 14. Upadhyaya L, Singh J, Agarwal V, et al (2014) In situ grafted nanostructured ZnO/carboxymethyl cellulose nanocomposites for efficient delivery of curcumin to cancer. *Journal of Polymer Research* 21:550. <https://doi.org/10.1007/s10965-014-0550-0>
 15. Phiwdang K, Suphankij S, Mekprasart W, Pecharapa W (2013) Synthesis of CuO nanoparticles by precipitation method using different precursors. *Energy Procedia* 34:740–745. <https://doi.org/10.1016/j.egypro.2013.06.808>
 16. Shrila M, Ananya, Meena P, Warkar SG (2024) Preparation and Characterization of Sodium Alginate-Based Hydrogel for Delivery of Hydrophilic Drug Metformin Hydrochloride. *ChemistrySelect* 9:e202401773. <https://doi.org/10.1002/slct.202401773>
 17. Ahmed I, Mahmood A, Qureshi OS, et al (2024) Development of tamarind gum/ β -CD-co-poly (MAA) hydrogels for pH-driven controlled delivery of

capecitabine. Springer Berlin Heidelberg

18. Niu B, Jia J, Wang H, et al (2019) In vitro and in vivo release of diclofenac sodium-loaded sodium alginate/carboxymethyl chitosan-ZnO hydrogel beads. *International Journal of Biological Macromolecules* 141:1191–1198. <https://doi.org/10.1016/j.ijbiomac.2019.09.059>
19. Suhail M, Wu PC, Minhas MU (2021) Development and characterization of pH-sensitive chondroitin sulfate-co-poly(acrylic acid) hydrogels for controlled release of diclofenac sodium. *Journal of Saudi Chemical Society* 25:101212. <https://doi.org/10.1016/j.jscs.2021.101212>
20. Khushbu, Warkar SG, Thombare N (2022) Controlled release and release kinetics studies of boron through the functional formulation of carboxymethyl tamarind kernel gum-based superabsorbent hydrogel. *Polymer Bulletin* 79:2287–2303. <https://doi.org/10.1007/s00289-021-03634-9>
21. Jing Z, Xu A, Liang YQ, et al (2019) Biodegradable poly(acrylic acid-co-acrylamide)/ poly(vinyl alcohol) double network hydrogels with tunable mechanics and high self-healing performance. *Polymers* 11. <https://doi.org/10.3390/polym11060952>
22. Raza MA, Park SH (2020) Irradiated Ch/GG/PVP-based stimuli-responsive hydrogels for controlled drug release. *Journal of Applied Polymer Science* 137. <https://doi.org/10.1002/app.49041>
23. Erdal NB, Hakkarainen M, Blomqvist AG (2019) Polymers, Giant Molecules with Properties: An Entertaining Activity Introducing Polymers to Young Students. *Journal of Chemical Education* 96:1691–1695. <https://doi.org/10.1021/acs.jchemed.8b00918>
24. Rani I, Warkar SG, Kumar A (2023) Nano ZnO embedded poly (ethylene glycol) diacrylate cross-linked carboxymethyl tamarind kernel gum (CMTKG)/poly (sodium acrylate) composite hydrogels for oral delivery of

- ciprofloxacin drug and their antibacterial properties. *Materials Today Communications* 35:105635. <https://doi.org/10.1016/j.mtcomm.2023.105635>
25. Hao PY, Zhou HY, Ren LJ, et al (2023) Preparation and antibacterial properties of curcumin-loaded cyclodextrin-grafted chitosan hydrogel. *Journal of Sol-Gel Science and Technology* 106:877–894. <https://doi.org/10.1007/s10971-023-06097-8>
 26. Varughese A, Kaur R, Singh P (2020) Green Synthesis and Characterization of Copper Oxide Nanoparticles Using *Psidium guajava* Leaf Extract. *IOP Conference Series: Materials Science and Engineering* 961. <https://doi.org/10.1088/1757-899X/961/1/012011>
 27. Jana S, Sharma R, Maiti S, Sen KK (2016) Interpenetrating hydrogels of O-carboxymethyl Tamarind gum and alginate for monitoring delivery of acyclovir. *International Journal of Biological Macromolecules* 92:1034–1039. <https://doi.org/10.1016/j.ijbiomac.2016.08.017>
 28. Tan LS, Tan HL, Deekonda K, et al (2021) Fabrication of radiation cross-linked diclofenac sodium loaded carboxymethyl sago pulp/chitosan hydrogel for enteric and sustained drug delivery. *Carbohydrate Polymer Technologies and Applications* 2:100084. <https://doi.org/10.1016/j.carpta.2021.100084>
 29. Elzayat EM, Abdel-Rahman AA, Ahmed SM, et al (2016) Studying the impact of formulation and processing parameters on the release characteristics from hydroxypropyl methylcellulose matrix tablets of diclofenac. *Acta Poloniae Pharmaceutica - Drug Research* 73:439–452
 30. Kiran, Tiwari R, Singh VK, et al (2020) Synthesis, characterization of β -CD based novel hydrogels with dual objectives of drug release and dye removal. *Iranian Polymer Journal* 29:615–623. <https://doi.org/10.1007/s13726-020-00826-4>
 31. Mousali E, Zanjanchi MA (2019) Electrochemical synthesis of copper(II) oxide nanorods and their application in photocatalytic reactions. *Journal of Solid State*

- Electrochemistry 23:925–935. <https://doi.org/10.1007/s10008-019-04194-9>
32. Zakaria AF, Kamaruzaman S, Abdul Rahman N, Yahaya N (2022) Sodium Alginate/ β -Cyclodextrin Reinforced Carbon Nanotubes Hydrogel as Alternative Adsorbent for Nickel(II) Metal Ion Removal. *Polymers* 14:5524. <https://doi.org/10.3390/polym14245524>
 33. Sarkar J, Chakraborty N, Chatterjee A, Bhattacharjee A (2020) Green Synthesized Copper Oxide Nanoparticles Ameliorate Defence and Antioxidant Enzymes in *Lens culinaris*. *Nanomaterials* 10:1–27. [doi:10.3390/nano10020312](https://doi.org/10.3390/nano10020312)
 34. Suhail M, Khan A, Rosenholm JM, et al (2021) Fabrication and characterization of diclofenac sodium loaded hydrogels of sodium alginate as sustained release carrier. *Gels* 7:1–16. <https://doi.org/10.3390/gels7010010>
 35. George D, Maheswari PU, Sheriffa Begum KMM, Arthanareeswaran G (2019) Biomass-Derived Dialdehyde Cellulose Cross-linked Chitosan-Based Nanocomposite Hydrogel with Phytosynthesized Zinc Oxide Nanoparticles for Enhanced Curcumin Delivery and Bioactivity. *Journal of Agricultural and Food Chemistry* 67:10880–10890. <https://doi.org/10.1021/acs.jafc.9b01933>
 36. Suhail M, Chiu IH, Hung MC, et al (2022) In Vitro Evaluation of Smart and pH-Sensitive Chondroitin Sulfate/Sodium Polystyrene Sulfonate Hydrogels for Controlled Drug Delivery. *Gels* 8:1–18. <https://doi.org/10.3390/gels8070406>
 37. Meena P, Singh P, Warkar SG (2024) Tailoring pH-sensitive carboxymethyl tamarind kernel gum-based hydrogel for an efficient delivery of hydrophobic drug indomethacin. *International Journal of Biological Macromolecules* 280:136029. <https://doi.org/10.1016/j.ijbiomac.2024.136029>
 38. Gupta P, Purwar R (2021) Influence of cross-linkers on the properties of cotton grafted poly (acrylamide-co-acrylic acid) hydrogel composite: swelling and drug release kinetics. *Iranian Polymer Journal* 30:381–391.

<https://doi.org/10.1007/s13726-020-00897-3>

39. Mouchati A, Yagoubi N (2023) Mechanical Performance and Cytotoxicity of an Alginate/Polyacrylamide Bipolymer Network Developed for Medical Applications. *Materials* 16. <https://doi.org/10.3390/ma16051789>
40. Fan Z, Cheng P, Liu M, et al (2020) Dynamic crosslinked and injectable biohydrogels as extracellular matrix mimics for the delivery of antibiotics and 3D cell culture. *RSC Advances* 10:19587–19599. <https://doi.org/10.1039/d0ra02218g>

CHAPTER 7

CONCLUSION, FUTURE SCOPE AND SOCIAL IMPACT

7.1 Conclusion

Biopolymer-based hydrogels have emerged as highly effective carriers for drug delivery, owing to their tunable properties and stimuli-responsive behavior. In this work, several biopolymer-based hydrogels were successfully developed and evaluated for their potential in drug delivery. A smart CMTKG/PVP/PAM hydrogel was designed for the controlled release of sparingly soluble diclofenac sodium drug. The hydrogel's swelling properties were modulated by varying the concentrations of initiators, biopolymers, and cross-linkers. The synthesized hydrogel exhibited greater swelling and drug release in alkaline conditions (pH 7.4) due to electrostatic repulsion. Moreover, the drug release kinetics were consistent with the Korsmeyer-Peppas model, indicating a Fickian diffusion mechanism.

Additionally, XG/PAM/PVP hydrogels synthesized using another biopolymer, XG, showed excellent performance in the delivery of ibuprofen. The incorporation of PVP enhanced the hydrogel's drug loading and release efficiency, with significant improvements in swelling and porosity. This hydrogel demonstrated a

pH-responsive behavior suitable for targeted drug delivery in the gastrointestinal tract, with a non-Fickian release mechanism at both pH 7.4 and 1.2. Furthermore, the optimization of synthesized β -CD/PAM/CMTKG hydrogel suggested that varying concentrations of PEGDA affected key properties such as porosity, gel fraction, and swelling behavior of the hydrogel. These hydrogels exhibited complete degradation within 10 days and showed no cytotoxicity, indicating their suitability for safe delivery of indomethacin.

Moreover, the TG/SA/ β -CD hydrogel microspheres demonstrate that the addition of β -CD improved drug loading and entrapment efficiency. Additionally, the drug release followed a Zero-Order model, exhibiting high release rates at pH 7.4, which makes these microspheres well-suited for colon-targeted drug delivery of aspirin.

Lastly, the *in vitro* drug release studies demonstrated that the presence of CuO nanoparticles in the curcumin-loaded CMTKG/SA/CuO nanocomposite hydrogel microspheres resulted in a controlled and prolonged release of curcumin.

In conclusion, the evaluation of the synthesized biopolymer-based hydrogels confirms their potential as effective drug delivery systems. Their ability to provide controlled and pH-responsive drug release, along with their non-toxic nature, makes them ideal for various other biomedical applications.

7.2 Future Prospects

Physical crosslinking techniques, especially the Freeze-thaw method, present a promising alternative to chemical crosslinking for hydrogel synthesis. This environmentally friendly technique eliminates the need for potentially toxic chemicals, making it particularly suitable for biomedical applications. By fine-tuning parameters

like the number of cycles, freezing temperature, and thawing time, it is possible to achieve optimized hydrogels with better porosity and swelling, which is crucial for effective drug delivery. In addition to this physical method, the exploration of alternative crosslinking agents, such as citric acid, further improves the biocompatibility of hydrogel-based drug delivery systems. As citric acid is a natural and non-toxic crosslinking agent, it holds great potential for biomedical applications.

Furthermore, smart hydrogel systems that respond to dual stimuli, such as pH as well as temperature, offer an innovative pathway for achieving targeted drug release. These systems can be designed to release drugs in response to particular environmental conditions, such as the acidic pH of tumor sites and the elevated temperature of inflamed tissues. The development of such dual-stimuli-responsive hydrogels is aimed at enhancing drug delivery efficacy while minimizing side effects by restricting drug release to non-targeted sites of the body.

Moreover, injectable hydrogels and hydrogel films represent another promising area for exploration as efficient drug delivery systems. Injectable hydrogels provide a minimally invasive method for localized drug delivery, making them ideal for drug delivery applications. However, hydrogel films, with their flexible and conformable nature, could be employed in wound healing, offering sustained drug release.

7.3 Social Impact

The utilization of biopolymer-based hydrogels for drug delivery has a significant social impact across various fields, including healthcare and environmental sustainability. This research addresses a crucial need in drug delivery systems by focusing on the development of novel pH-responsive hydrogels based on biopolymers,

such as CMTKG, tragacanth gum, sodium alginate and xanthan gum, that effectively encapsulate and prolong the delivery of hydrophobic drugs, i.e., ibuprofen, diclofenac sodium, curcumin, aspirin and indomethacin, which are often challenging to administer due to their poor solubility and loading efficiency. This not only improves individual health outcomes but also contributes to a more efficient and cost-effective healthcare system by minimizing the cost associated with repeat doses. Moreover, from an environmental perspective, the use of biopolymers as one of the necessary components in hydrogel synthesis promotes sustainability by reducing complete reliance on synthetic polymeric materials. Hence, the development of biopolymer-based hydrogels for drug delivery has the potential to make a positive impact on public health and environmental sustainability.

LIST OF PUBLICATIONS AND THEIR PROOFS

Journal Articles:

1. Meena P, Singh P, Warkar SG (2023) Development and assessment of carboxymethyl tamarind kernel gum- based pH-responsive hydrogel for release of diclofenac sodium. *European Polymer Journal*. 197:112340. <https://doi.org/10.1016/j.eurpolymj.2023.112340>
2. Meena P, Singh P, Warkar SG (2023) Fabrication and evaluation of stimuli-sensitive xanthan gum-based hydrogel as a potential carrier for a hydrophobic drug ibuprofen. *Colloid and Polymer Science*. 302:377-391. <https://doi.org/10.1007/s00396-023-05198-8>
3. Meena P, Singh P, Warkar SG (2024) Tailoring pH-sensitive carboxymethyl tamarind kernel gum-based hydrogel for an efficient delivery of hydrophobic drug indomethacin. *International Journal of Biological Macromolecules*. 280:136029. <https://doi.org/10.1016/j.ijbiomac.2024.136029>
4. Meena P, Singh P, Warkar SG (2024) Degradable pH-sensitive calcium-crosslinked tragacanth gum/ β -cyclodextrin/sodium alginate hydrogel microspheres prepared via ionotropic gelation technique for hydrophobic drug delivery. *Journal of Polymers and Environment*. <https://doi.org/10.1007/s10924-024-03449-5>

Journal Articles:

Colloid and Polymer Science (2024) 302:377–391
<https://doi.org/10.1007/s00396-023-05198-8>

RESEARCH

Check for updates

Fabrication and evaluation of stimuli-sensitive xanthan gum-based hydrogel as a potential carrier for a hydrophobic drug ibuprofen

Priyanka Meena¹ · Poonam Singh¹ · Sudhir G. Warkar¹

Received: 26 September 2023 / Revised: 28 October 2023 / Accepted: 8 November 2023 / Published online: 29 November 2023
 © The Author(s), under exclusive licence to Springer-Verlag GmbH Germany, part of Springer Nature 2023

Abstract
 This research work aimed at the synthesis and characterization of novel xanthan gum/polyacrylamide/polyvinyl pyrrolidone (XG/PAM/PVP)-based hydrogels for the delivery of the hydrophobic drug ibuprofen. The influence of crosslinker, biopolymer, and initiator amount on the hydrogel's swelling ratio, porosity, and gel fraction was also investigated. Several techniques like Powder X-ray Diffraction (PXRD), Attenuated Total Reflection-Fourier Transform Infrared spectroscopy (ATR-FTIR), Scanning Electron Microscopy (SEM), and Thermogravimetry Analysis (TGA) were employed to characterize the synthesized hydrogels. Sol–gel analysis revealed an increase in the gel fraction with a rise in the concentration of MBA, XG, and KPS. Porosity measurements indicated a greater porosity with higher XG and KPS amounts, while porosity decreased as the MBA amount increased. Furthermore, the presence of PVP in the hydrogel was observed to greatly enhance various properties, including gel fraction, swelling ratio, porosity, drug loading, and drug release percent. Notably, under alkaline conditions (pH 7.4), the swelling ratio and release of ibuprofen were significantly increased, as compared to acidic (pH 1.2). The ibuprofen release from the XG/PAM/PVP hydrogel is governed by a Fickian diffusion mechanism, and the Korsmeyer-Peppas model serves as the most appropriate model for elucidating the drug release kinetic in both pH 1.2 and 7.4. The pH-responsive nature exhibited by the XG/PAM/PVP hydrogel highlights its potential as a drug delivery system.

Keywords Hydrogel · Biopolymer · Porosity · Drug release · Kinetic modeling

Introduction

Ibuprofen is one of the extensively used nonsteroidal anti-inflammatory drug (NSAID) having poor solubility, high permeability, and limited bioavailability [1]. It is chemically called as 2-(4-(2-methylpropyl)phenyl) propionic acid and is commonly prescribed for its analgesic, antipyretic, and anti-inflammatory properties, particularly in the treatment of rheumatoid arthritis and osteoarthritis [2]. However, owing to its shorter half-life and rapid elimination from the body, multiple dosages are required to maintain an extended pharmacological effect [3]. This frequent dosing regimen is associated with side effects, i.e., gastrointestinal problems, nausea, ulcers etc. [4]. To address these challenges,

the development of a novel biopolymer-based hydrogel is required to minimize adverse effects and achieve extended delivery, thereby enhancing therapeutic efficacy [5].

Xanthan gum (XG) is an anionic biopolymer derived from the microorganism *Xanthomonas campestris* [6–8]. The primary structure of this naturally occurring polysaccharide comprises the side chain of glucuronic acid and pyruvic acid [9]. XG-based hydrogels have emerged as a promising material for drug delivery systems due to their unique properties such as hydrophilicity, tunable release rate, and biocompatibility [10, 11].

Hydrogels are three-dimensional networks mainly composed of hydrophilic polymers that possess the capability to hold large amounts of fluid while maintaining their structural integrity [12]. Hydrogels exhibit high biocompatibility and biodegradability, ensuring compatibility with biological systems and minimizing adverse reactions [13, 14]. They also protect drugs from degradation, enzymatic activity, and harsh physiological conditions, leading to enhanced drug stability and bioavailability.

✉ Poonam Singh
 poonam@dtu.ac.in

✉ Sudhir G. Warkar
 sudhirwarkar@gmail.com

¹ Department of Applied Chemistry, Delhi Technological University, Delhi, India

Springer



Contents lists available at ScienceDirect

European Polymer Journal

journal homepage: www.elsevier.com/locate/europolj



Development and assessment of carboxymethyl tamarind kernel gum-based pH-responsive hydrogel for release of diclofenac sodium

Priyanka Meena, Poonam Singh^{*}, Sudhir G. Warkar^{*}

Department of Applied Chemistry, Delhi Technological University, Delhi, India

ARTICLE INFO

Keywords:
Smart hydrogel
CMTKG
Diclofenac sodium
Biopolymer
Sol-gel

ABSTRACT

The current research work focuses on the fabrication of carboxymethyl tamarind kernel gum/polyvinylpyrrolidone/polyacrylamide (CMTKG/PVP/PAM) based hydrogel and its loading was done with diclofenac sodium drug (DS) to obtain smart pH-responsive hydrogels. In addition, the effect of concentration of cross-linker- N, N-methylene bis(acrylamide) (MBA), biopolymer (CMTKG), as well as initiator- potassium persulfate (KPS) on the swelling behavior of smart hydrogel was also analyzed. The synthesized hydrogels were characterized using Scanning Electron Microscopy (SEM), Powder X-ray Diffraction (PXRD), Thermogravimetry Analysis (TGA), and Attenuated Total Reflection-Fourier Transform Infrared spectroscopy (ATR-FTIR). ATR-FTIR confirms the successful formation of hydrogels, while PXRD and SEM indicate the amorphous and porous nature of the polymeric network. The TGA results indicate higher thermal stability for DS-loaded hydrogel than unloaded hydrogel. However, sol-gel analysis shows a rise in gel fraction, with increased concentrations of CMTKG, MBA, and KPS. The swelling ratio as well as the release of DS were found to be higher under slightly alkaline conditions. The result of drug loading and release indicates that PVP increases drug loading (%) and release (%). The drug release behavior of DS-loaded hydrogel follows the Fickian mechanism of diffusion with the Korsmeyer-Peppas model as the best-fitted one. The synthesized DS-loaded CMTKG/PVP/PAM hydrogels could be a promising substitute for prolonged delivery of sparingly soluble DS in pH 7.4.

1. Introduction

A drug delivery system (DDS) acts as a sustained release system that can alter the pharmacokinetics and biodistribution of the drug by enhancing several crucial properties of drugs i.e. solubility, in vivo stability, specificity, efficacy, etc [1]. Till today numerous materials have been explored in the drug delivery field, including nano-scale materials (nano-capsules, dendrimers, nanotubes, nano gels, and so on) [2,3], and inorganic-based DDS (layer double hydroxide, graphene oxide, metal oxides etc) [1,4,5]. However, conventional drug delivery systems do possess certain limitations i.e. poor bioavailability, low biocompatibility, high toxicity, burst drug release, and lesser hydrophilicity, resulting in reduced drug delivery efficiency. To address the above-mentioned issues, drug delivery systems based on hydrogels have been focused in recent decades owing to their easily tunable properties during synthesis, followed by controlled release, degradation, and efficiency to protect labile drugs [6].

Basically, hydrogels are highly hydrated 3D networks, derived from natural, semi-synthetic, or synthetic polymers having physical or

covalent cross-linkage [7,8]. One of the most remarkable properties of hydrogel to be termed as smart or stimuli-sensitive hydrogels is their ability to adjust their volume in response to changes in physical and chemical stimuli such as pH, light, magnetic field, temperature, enzyme, ionic strength, etc [9,10,11,12]. The most notable among all are pH-responsive hydrogels, which provide an excellent drug administration system [11].

Polyacrylamide (PAM) is one of the most extensively used pH-sensitive polymers in drug delivery applications [13]. It is a synthetic, non-toxic polymer with excellent mechanical strength, and contains a cationic amine functional group that either protonates or deprotonates to show variation in swelling with a change in pH [14,15]. PAM has been widely combined with natural polymers such as gelatin, carboxymethyl tamarind kernel gum, collagen etc. to synthesize composite hydrogels [16,17]. The introduction of biopolymers imparts efficient drug release and also enhances the hydrophilicity, biodegradability, and biocompatibility of the hydrogel [11,18,19].

Tamarind kernel gum (TKG) is a biopolymer obtained from *Tamarindus indica* L., a typical African tree and carboxymethylation of TKG

^{*} Corresponding authors.

E-mail addresses: poonam@dtu.ac.in (P. Singh), sgwarkar@dtu.ac.in (S.G. Warkar).

<https://doi.org/10.1016/j.eurpolymj.2023.112340>

Received 30 April 2023; Received in revised form 27 July 2023; Accepted 30 July 2023

Available online 31 July 2023

0014-3057/© 2023 Elsevier Ltd. All rights reserved.



Research Paper

Tailoring pH-sensitive carboxymethyl tamarind kernel gum-based hydrogel for an efficient delivery of hydrophobic drug indomethacin

Priyanka Meena, Poonam Singh*, Sudhir G. Warkar*

Department of Applied Chemistry, Delhi Technological University, Delhi, India



ARTICLE INFO

Keywords:
Biopolymer
Drug release
Hydrogel

ABSTRACT

Polyacrylamide hydrogels have gained attention in the drug delivery field for their pH-dependent nature. Nevertheless, their limited degradability and lower entrapment efficiency for hydrophobic drugs hinder their utility in controlled drug release. This research aims to design a degradable pH-sensitive hydrogel for delivering the hydrophobic drug indomethacin to the colon. This work developed and optimized the hydrogels based on β -cyclodextrin, carboxymethyl tamarind kernel gum, and polyacrylamide with varying amounts of polyethylene glycol diacrylate. The optimized hydrogel exhibits 76.52 % gel fraction, 89.21 % porosity, 1000.27 % swelling, and 90.0 % equilibrium water content. The hydrogel was characterized using Attenuated Total Reflection-Fourier Transform Infrared spectroscopy, confirming the successful crosslinking of the synthesized hydrogel. Powder X-ray Diffraction revealed their amorphous nature while Scanning Electron Microscopy showed a porous surface morphology of the hydrogel. Moreover, rheology confirmed the hydrogel's elastic nature. Notably, the hydrogel demonstrated a drug release of 60.26 % at pH 7.4. Kinetic modelling of indomethacin release data indicated a Fickian diffusion release mechanism. Cytotoxicity tests on HCT-116 cells showed 79 % viability, and the hydrogel fully degraded within 10 days. These results confirmed the potential of synthesized β -CD/PAM/CMTKG hydrogel for controlled indomethacin delivery to the colon.

1. Introduction

The emergence of new-generation drugs has sparked increased interest in innovative controlled drug delivery systems [1]. Unlike conventional drug delivery systems, where the concentration of the drug in the blood rapidly rises after intake, followed by a decline over time, controlled drug delivery systems prioritize maintaining a consistent delivery rate. Hydrogels play a crucial role as a controlled drug delivery system due to their time-dependent swelling behavior and pH-dependent nature. Hydrogels are three-dimensional polymeric networks with hydrophilic functional groups such as -OH, -SO₃H, -CONH₂, etc., facilitating them to absorb bio-fluids [2].

Moreover, developing environment-sensitive delivery systems responsive to changes in external factors like pH, temperature, light, ionic strength, etc., is crucial for targeted and controlled drug delivery [3]. Among these, pH-sensitive hydrogels have been extensively investigated for their ability to respond to pH variations that occur in the gastrointestinal tract. The pH-sensitive hydrogels can shield drugs from enzymatic hydrolysis and stomach acid, making them ideal for drug-

delivery systems. Nowadays, natural biopolymer-based pH-sensitive hydrogels, particularly those derived from polysaccharides such as sodium alginate, chitosan, carboxymethyl tamarind kernel gum, gelatin, etc., have gained interest due to their low cost, good biodegradability, and biocompatibility [1,4]. For example, Akhlaq et al. synthesized a pH-sensitive methotrexate-loaded gelatin and polyvinyl alcohol hydrogel, which exhibited 94.3 % drug release at pH 1.2 and 83.21 % at pH 7.4 [5]. Patel et al. developed hydrogel using carboxyethyl xanthan gum and carboxymethyl xanthan gum for repaglinid drug delivery, showing approximately 80 % drug release in gastric fluids [6]. Additionally, Nawaz et al. reported gelatin/polyvinyl pyrrolidone hydrogels for oral captopril delivery, showing faster drug release at pH 1.2 compared to pH 7.4 (colon pH) [7]. However, the authors disclosed controlled oral drug delivery potential, but they did not focus on colon targeting, even the research on carboxymethyl tamarind kernel gum is limited. Moreover, they did not study with polyacrylamide combination.

Tamarind kernel gum (TKG), extracted from the seeds of the *Tamarindus indica* tree, is a natural, cost-effective, and biocompatible polysaccharide used in drug delivery [8,9]. For example, Pal et al. developed

* Corresponding authors.

E-mail addresses: poonam@dru.ac.in (P. Singh), sgwarkar@dru.ac.in (S.G. Warkar).<https://doi.org/10.1016/j.ijbiomac.2024.136029>

Received 24 April 2024; Received in revised form 17 September 2024; Accepted 24 September 2024

Available online 25 September 2024

0141-8130/© 2024 Elsevier B.V. All rights are reserved, including those for text and data mining, AI training, and similar technologies.



Degradable pH-Sensitive Calcium-Crosslinked Tragacanth Gum/ β -Cyclodextrin/Sodium Alginate Hydrogel Microspheres Prepared via Ionotropic Gelation Technique for Hydrophobic Drug Delivery

Priyanka Meena¹ · Poonam Singh¹ · Sudhir G. Warkar¹

Accepted: 11 November 2024

© The Author(s), under exclusive licence to Springer Science+Business Media, LLC, part of Springer Nature 2024

Abstract

Sodium alginate (SA) hydrogel microspheres are attracting interest in biomedical applications due to their easy degradation and non-toxic nature. However, their high swelling capacity and limited loading efficiency for hydrophobic drugs hinder their application in controlled drug release. The objective of the work is to develop smart vehicles that show effective loading and controlled release of hydrophobic drug. In this study, a series of tragacanth gum/ β -cyclodextrin/sodium alginate (TG/ β -CD/SA) hydrogel microspheres were designed via the ionotropic gelation method for delivery of hydrophobic drug aspirin. The effect of variation in TG, SA, and β -CD concentration on hydrogel microspheres swelling (%) was examined. The hydrogel microspheres were analyzed using Powder X-ray Diffraction (PXRD), Attenuated Total Reflection-Fourier Transform Infrared spectroscopy (ATR-FTIR), and Scanning Electron Microscopy (SEM) techniques. ATR-FTIR confirmed the successful synthesis of crosslinked TG/ β -CD/SA hydrogel microspheres. PXRD showed that the microspheres are amorphous and that the drug is uniformly dispersed within the hydrogel. SEM revealed that the polymeric network has a porous and spherical surface morphology. The drug loading (%), sol-gel fraction (%), degradation (%), and rheological studies were investigated. The in vitro analysis shows a controlled release pattern at pH 1.2 and 7.4 in the TG/ β -CD/SA hydrogel. The rheological analysis revealed that the elastic nature is dominant over the viscous one ($G' > G''$) in synthesized TG/ β -CD/SA hydrogel microspheres. The cytotoxicity evaluations conducted on the HCT-116 cell line indicate the excellent biocompatibility (87.9%) of the hydrogel. The degradation profile of the hydrogel microsphere in pH 7.4 demonstrates complete degradation (100%). Hence, the TG/ β -CD/SA hydrogel microsphere reflects its potential as a non-toxic, degradable, and pH-dependent drug delivery system.

✉ Poonam Singh
poonam@dtu.ac.in

✉ Sudhir G. Warkar
sudhirwarkar@gmail.com

¹ Delhi Technological University, New Delhi, India

Published online: 26 November 2024

Springer



DELHI TECHNOLOGICAL UNIVERSITY

(Formerly Delhi College of Engineering)

Shahbad Daultapur, Main Bawana Road, Delhi-42

PLAGIARISM VERIFICATION

Title of the Thesis “**Synthesis, Characterization and Application of Biopolymeric Hydrogels in Drug Delivery**”

Total Pages **212**, Name of the Scholar **Priyanka Meena**

Supervisor (s)

(1) Prof. Sudhir G. Warkar

(2) Dr. Poonam Singh

Department **Applied Chemistry**

This is to report that the above thesis was scanned for similarity detection. Process and outcome is given below:

Software used: **Turnitin**, Similarity Index: **8 %**, Total Word Count: **42991**

Date: **4-11-2024**

Candidate's Signature

Signature of Supervisor(s)

PAPER NAME

PhD Thesis of Ms Priyanka Meena (2k19
-PHDAC-02) DEPARTMENT OF APPLIED
CHEMISTRY8.pdf

WORD COUNT

42991 Words

CHARACTER COUNT

237385 Characters

PAGE COUNT

212 Pages

FILE SIZE

5.7MB

SUBMISSION DATE

Nov 4, 2024 5:30 PM GMT+5:30

REPORT DATE

Nov 4, 2024 5:33 PM GMT+5:30

● **8% Overall Similarity**

The combined total of all matches, including overlapping sources, for each database.

- 4% Internet database
- 7% Publications database
- Crossref database
- Crossref Posted Content database
- 3% Submitted Works database

● **Excluded from Similarity Report**

- Bibliographic material
- Cited material
- Small Matches (Less than 10 words)
- Manually excluded sources
- Manually excluded text blocks

CURRICULUM VITAE

PERSONAL INFORMATION



Priyanka Meena

Nationality: Indian

Date of Birth: 11th September 1996

📍 Sai Dham Colony, Kota, Rajasthan, India - 324001

📞 +918433060087

✉️ priyankameena.du2016@gmail.com

🌐 <https://scholar.google.com/citations?user=fjdUC LgAAAAJ&hl=en&oi=ao>

💬 Skype live:.cid.1637dcf014b3b744

DESIGNATION

Guest Faculty

Delhi Technological University, Delhi, India

AREAS OF INTEREST

Polymeric materials, Hydrogels, Drug delivery,
Dye removal

QUALIFICATION

- Bachelor of Science (Hons), Chemistry, 2017
Ramjas College, University of Delhi, Delhi, India.
- Master of Science, Chemistry, 2019
Indian Institute of Technology Roorkee, India
- Ph.D, Chemistry, 2024
Delhi Technological University, Delhi, India

EXPERIENCE

- Teaching assistant (2019-2024)
B.Tech Chemistry Laboratories
Delhi Technological University, Delhi, India.
- Chegg Subject Matter Expert (2021-till date)
Chegg India
Freelance Independent contractor.
- Guest Faculty (2024-till date)
Department of Applied Chemistry
Delhi Technological University, Delhi, India

